DANMARKS OG GRØNLANDS GEOLOGISKE UNDERSØGELSE RAPPORT 2006/27

Gold potential of the Nuuk region based on multi-parameter spatial modelling

Progress 2005

Bo Møller Stensgaard, Agnete Steenfelt
& Thorkild M. Rasmussen

GEOLOGICAL SURVEY OF DENMARK AND GREENLAND
MINISTRY OF THE ENVIRONMENT

G E U S

DANMARKS OG GRØNLANDS GEOLOGISKE UNDERSØGELSE RAPPORT 2006/27

Gold potential of the Nuuk region based on multi-parameter spatial modelling

Progress 2005

Bo Møller Stensgaard, Agnete Steenfelt
& Thorkild M. Rasmussen

GEOLOGICAL SURVEY OF DENMARK AND GREENLAND
MINISTRY OF THE ENVIRONMENT

G E U S

Contents

Abstract 5

Regional geology and known gold mineralisation 6

Summary of data and results of the first phase 7

Gold showings ... 7
Regional data ... 7
Regional stream sediment data ... 7
GEUS aeromagnetic data ... 8

Results of fieldwork and new sampling in areas outlined as favourable for gold 9

Description of favourable areas ... 11
Qangaatarssuakop Isukasia ... 11
Eastern Kangerssuaq ... 11
Western Kangerssuaq ... 12
North of the lake Tussaap Tasia, northeastern part of Ujarassuit Nunaat ... 14
Central Ujarassuit Nunaat – north of the fjord Ujarssuit Paavat ... 15
Qooqqut lake area ... 16
General remarks from follow-up observations ... 18

Data compiled during the second phase 19

Updated gold showings ... 19
Geochemistry data from exploration companies ... 19
Lineament data from exploration companies ... 22
Statistically defined lineaments in aeromagnetic data ... 24
Aeroradiometric data ... 26

Progress in multi-parameter modelling 29

Grouping of gold showings ... 29
Groups of gold showings ... 30
Data signatures of the groups ... 32
Method ... 32
Results ... 34
New gold potential maps ... 38
Favourability for the Isua gold showing group ... 39
Favourability for the Bjørneøen gold showing group ... 48
Favourability for the Storø gold showing group ... 56
Cross-validation ... 67
Method ... 67
Results of cross-validation ... 67

Discussion 72

Signatures of gold showings 72
Ni/Mg ratio 72
Concentration of LILE and aeroradiometric signature 76
Lithological and geochemical similarities, and the differences between gold hosting areas 78
Spatial distribution of favourable areas 80
Use of predictive gold potential maps 80

Conclusions and implications 81

Recommendations 82

Acknowledgements 83

References 84

Appendix A – Statistical identification of lineaments 87

Lineament analysis 88
Extraction of lineaments 89
Statistical characterisation of lineaments 94

Appendix B – Grid images of aeroradiometric data and statistical characterisations of lineaments in aeromagnetic data 95

Aeroradiometric data 96
Statistically defined lineaments from aeromagnetic data 99

Appendix C – Signatures 138

Signatures in regional fine fraction stream sediment geochemistry 139
Signatures in regional aeromagnetic data 162
Signatures in regional aeroradiometric data 166
Signatures in statistically defined lineaments from aeromagnetic data 172

Abstract

This report documents the progress made in the second phase of a multi-parameter spatial statistical modelling of gold showings in the *c.* 13,700 km^2 large Nuuk region, southern West Greenland. The project is jointly financed by the Geological Survey of Denmark and Greenland (GEUS) and the Bureau of Minerals and Petroleum (BMP), government of Greenland. In the first phase of the project, the signatures of a group of 45 gold showings expressed by 29 geochemical and geophysical parameters were used to produce a map of gold-favourable areas.

Fieldwork has been undertaken in several of the predicted gold-favourable areas in 2005. Lithologically, these new areas are similar to those with known gold mineralisation, but none of the rock samples analysed showed high gold values.

In the second phase of the study, the number of gold showings has been increased to 52 and the showings have been subdivided into three groups based on their ability to predict other showings and be predicted by other showings. New regional data sets, aeroradiometric data and aeromagnetic lineaments, have been compiled and evaluated with regard to their suitability as parameters in the modelling. New gold potential maps have been constructed for each gold-showing group using various combinations of the regional parameters. Beside a geological evaluation of the new gold potential maps, the predictions have been statistically cross-validated.

The areas outlined as gold-favourable using more showings, grouping of showings and more regional parameters are still largely confined to the NNE-trending zone that was recognised in the first phase of the spatial modelling. Common to these areas are metavolcanic rocks with signs of hydrothermal alteration in settings that can be interpreted to be subduction-related.

Based on experiences so far, it is recommended to refine the methodology and apply it to prediction of gold favourable areas in other parts of Greenland and to prediction of other kinds of mineral deposits or geological settings.

Regional geology and known gold mineralisation

New aspects of the regional geology of the Nuuk region, and of the supracrustal belts in particular, have recently been addressed in several reports and papers, e.g. Appel *et al.* 2005; Friend & Nutman, 2005; Hollis, 2005; Hollis *et al.* 2004, Hollis *et al.* 2006, Nielsen *et al.* 2004.

The Nuuk region (Figure 1) comprises a complex assemblage of early to late Archaean geochronologically distinct crustal blocks, referred to as terranes. Up to now, four small terranes have been recognised between the larger Akia terrane to the north and the Tasiusarsuaq terrane to the south (Friend & Nutman 2005; Hollis 2005). In general, the terranes have been amalgamated during NW-directed thrusting during continental collision along tectonic boundaries that in many cases underwent intense deformation during later movements.

Several supracrustal belts dominated by amphibolite facies metavolcanic rocks are intercalated with tonalitic to granodioritic gneisses. The most common rock types of the supracrustal belts are amphibolite of tholeiitic to komatiitic composition, but recently metavolcanic rocks of andesitic composition have been recognised locally. Metasedimentary rocks, mica-schists, are a significant component in parts of the belts. Bodies of mafic and ultramafic plutonic rocks are common within the amphibolites. Current studies have delineated three geological environments for the supracrustal belts; magmatic, oceanic, and continental volcanic arc environments (Appel *et al.* 2003; Garde 1997; Garde 2005; Hollis *et al.* 2006).

Gold mineralisation has been located at a number of sites within the supracrustal belts. Mineralised sites show evidence of hydrothermal alteration such as quartz veining, silicification, garnetisation, leaching and carbonatisation. Both syngenetic and epigenetic mineralisations have been identified and genetic models for all gold mineralisations within the region are currently being debated.

Gold occurrences at Qingaaq, Aappalaartoq and Qussuk (Fig. 1) are currently targets for commercial exploration by the company NunaMinerals A/S (lincense number 2002/07). The Qingaaq gold prospect has been drilled in 2004 and 2005.

Summary of data and results of the first phase

The statistical analysis operates with two kinds of data: gold showings and regional data. Both were represented by 200 × 200 m pixels in the statistical analysis.

Gold showings

Known gold occurrences have been compiled and localities, from which samples have yielded concentrations of 1 ppm Au or more, form the basis for defining a gold showing in the sense of the present statistical analysis. A showing has been defined as a 200 m × 200 m area containing one or more of such localities. Each gold showing, therefore, occupies one discrete pixel. Forty-five showings were defined and they were treated as one group in the first phase.

Regional data

Geochemical and geophysical data were treated as continuous data in the statistical analysis, in the sense that they are represented by a surface based on interpolated values in a regular grid using a cell size of 200 x 200 m.

Regional stream sediment data

Grids were produced using stream sediment geochemistry data selected from a compilation of data for the entire West and South Greenland (Steenfelt 1999; Steenfelt 2001a; Steenfelt 2001b).

Table 1. *Overview of the most indicative geochemical parameters for gold showings*

Geochemical element Regional stream sediment data from GEUS	**Range for data signature of gold showings (45 showings)**	**Range for data signature of background**	**Significance and remarks**
As	22– 42ppm As	Below 3 ppm As (modified As grid)	Highly significant
Au	40–100 ppb Au and 140–220 ppb Au	Below 20–30 ppb Au (modified Au grid)	Highly significant. A bi-modal distribution is observed.
Cs	3.5–5 ppm Cs and 5.8–6 ppm Cs	Below 2.3 ppm Cs (modified Cs grid)	Highly significant. A bi-modal distribution is observed with the higher range belonging to a small part of the gold showings.
Rb	60–75 ppm Rb	10–50 ppm Rb	Moderately significant. Some overlap with the background signature exists.
Th	15–17.5 ppm Th	3–13 ppm Th	Little significance. A bi-modal, or multi-modsl distribution is observed. Overlap with the background signature exists.
U	80–150 ppm U	0–25 ppm U	Highly significant. Some overlap with the background signature exists.
Ni/Mg ratio	Ratio 30–43	Ratio between 1–35	Moderately significant. Overlap with the background signature exists.

The geochemical parameters As, Au, Cs, Rb, Th and the Ni/Mg ratio were found to be indicative for the gold showings (Table 1).

Fifteen other geochemical parameters showed no distinct signature for the gold showings: Al_2O_3, CaO, Fe_2O_3, K_2O, La, MgO, Na_2O, P_2O_5, Sb, SiO_2, TiO_2, V, Zr, Zn and the Ni/Cr ratio.

GEUS aeromagnetic data

The magnetic parameters used in the first phase of the project were from a regional aeromagnetic survey, 'Aeromag 1998', jointly conducted by GEUS and BMP.

The total magnetic field intensity (TMI) was non-indicative for the gold showings, whereas the vertical gradient of TMI, the amplitude of the horizontal gradients of TMI and the horizontal gradients in four directions (N, NW, E, and SE) was found to have an indicative signature, clearly different from the background signature, for a limited number of the showings. The ranges of the indicative signatures for the gold showings in the aeromagnetic parameters are given in Table 2.

Table 2. *Overview over the variation in processed aeromagnetic data within and outside gold showings.*

Aeromagnetic data Regional aeromagnetic data from GEUS	**Range for data signatures found to be characteristic for Au showings**	**Range for background signature**	**Significance and remarks**
VG-TMI	-0.35 – -0.55 nT/m and 0.45 – 0.75 nT/m	-0.3 – 0.4 nT/m	Highly significant. Bi-modal distribution.
Amp-Hor-Grad_TMI	0.45 – 1.0 nT/m	0.0 – 0.4 nT/m	Highly significant
Hor-Grad-North	-3.6 – 2.9 nT/m and -1.2 – -0.7 nT/m	-0.5 – 0.5 nT/m	Highly significant
Hor-Grad-Northwest	-3.6 – -2.7 nT/m and -1.4 – -0.6 nT/m	-0.5 – 0.5 nT/m	Highly significant
Hor-Grad-East	0.4 – 0.7 nT/m	-0.3 – 0.4 nT/m	High significant – though the characteristic data signature only is for a limited number of the occurrences.
Hor-Grad-Southeast	-1.6 – -1.3 nT/m, -0.9 – -0.5 nT/m and 0.3 –0.6 nT/m	-0.4 – 0.4 nT/m	High significant – though the characteristic data signature is only for a limited number of the occurrences.

Results of fieldwork and new sampling in areas outlined as favourable for gold

The BMP and GEUS have initiated several projects to investigate the geology and economic potential of the supracrustal belts in the Nuuk region. Participants in the fieldwork summer of 2005 were asked, where feasible, to inspect and sample the areas outlined as most favourable for gold by the first phase of the multi-parameter modelling (Fig. 1). The samples were analysed to test if they hold the predicted geochemical characteristics. Unless references to published work are made, the descriptions in the following are based on personal communications with the geologists and edited citations from their field diaries and reproduced here with their approval.

The results of the chemical analyses of samples are treated in the section ‘Discussion’.

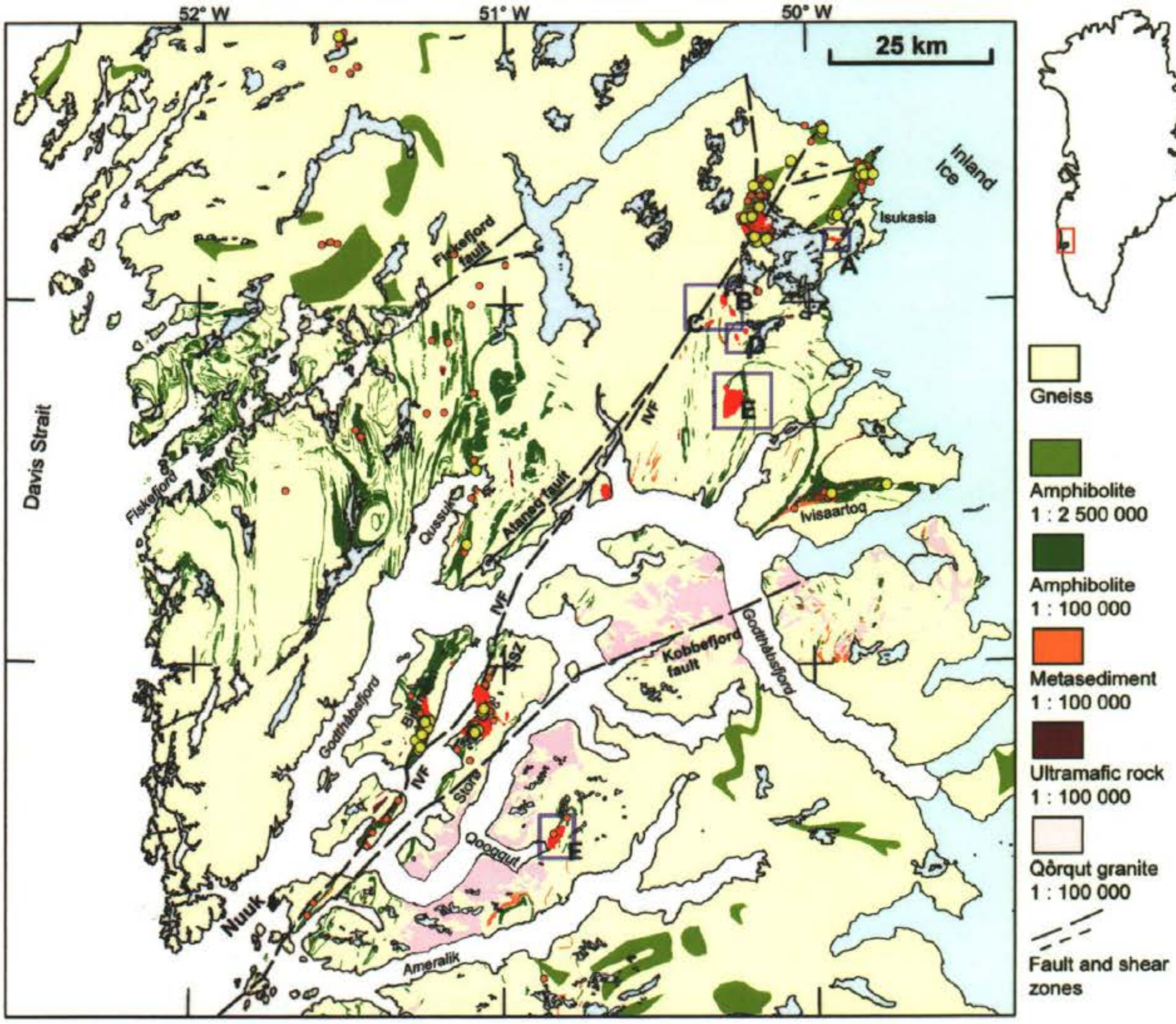

Figure 1. *Simplified geological map of the Nuuk region with red patches over areas predicted as favourable for gold in the first phase of multi-parameter modelling (Nielsen et al. 2004). Orange filled circles mark rock samples with more than 50 ppb Au; yellow circles for rock samples with above one ppm Au. The lithology is combined from geological maps at scales 1:100 000 and 1:2 500 000 (Chadwick & Coe 1988; Escher & Pulvertaft 1995; Garde 1989; McGregor 1983).*

Description of favourable areas

Qangaatarssuakop Isukasia

Peter Appel, GEUS, and Robert Willan, consultant, visited the area (A in Fig. 1) during a short helicopter reconnaissance stop.

Field observations: This area consists mainly of orthogneiss with many small enclaves of ultramafic bodies (up to tens of metres long and ten metres wide). Locally, cm-sized veins of a brown mineral rimmed by bright pargasite cut the bodies. The visitors to the area suggest that the area is predicted as favourable because of the ultramafic enclaves. The high concentration of ultramafic enclaves is in contrast to unpredicted neighbouring areas.

Eastern Kangerssuaq

Peter Appel, GEUS, and Wouter Heijlen, Leeds University, had a 3-day camp in the area (B in Fig. 1).

Field observations: Monotonous orthogneisses dominate this area, but the gneiss contains enclaves of ultrabasic rocks and of supracrustal amphibolite with calc-silicates and rust zones, the latter reflecting contents of pyrrhotite and chalcopyrite (Fig. 2). The observed supracrustal enclaves generally have exposed widths of 5 m and lengths of a few tens of metres. Small quartz veins are common in the amphibolite. A larger, c. one m wide, quartz vein containing pyrrhotite and chalcopyrite can be traced for over 100 metres. Boulders of heavily oxidised (reddish-orange to deep purple), quartz-veined and silicified amphibolite have been observed in an elongated trail (10 m long, 2 m wide, N10°E orientation) in a short gully, where the boulders are not transported over great distance. The medium-grained quartz contains abundant euhedral to subhedral chalcopyrite, pyrite and pyrrhotite (possibly also arsenopyrite).

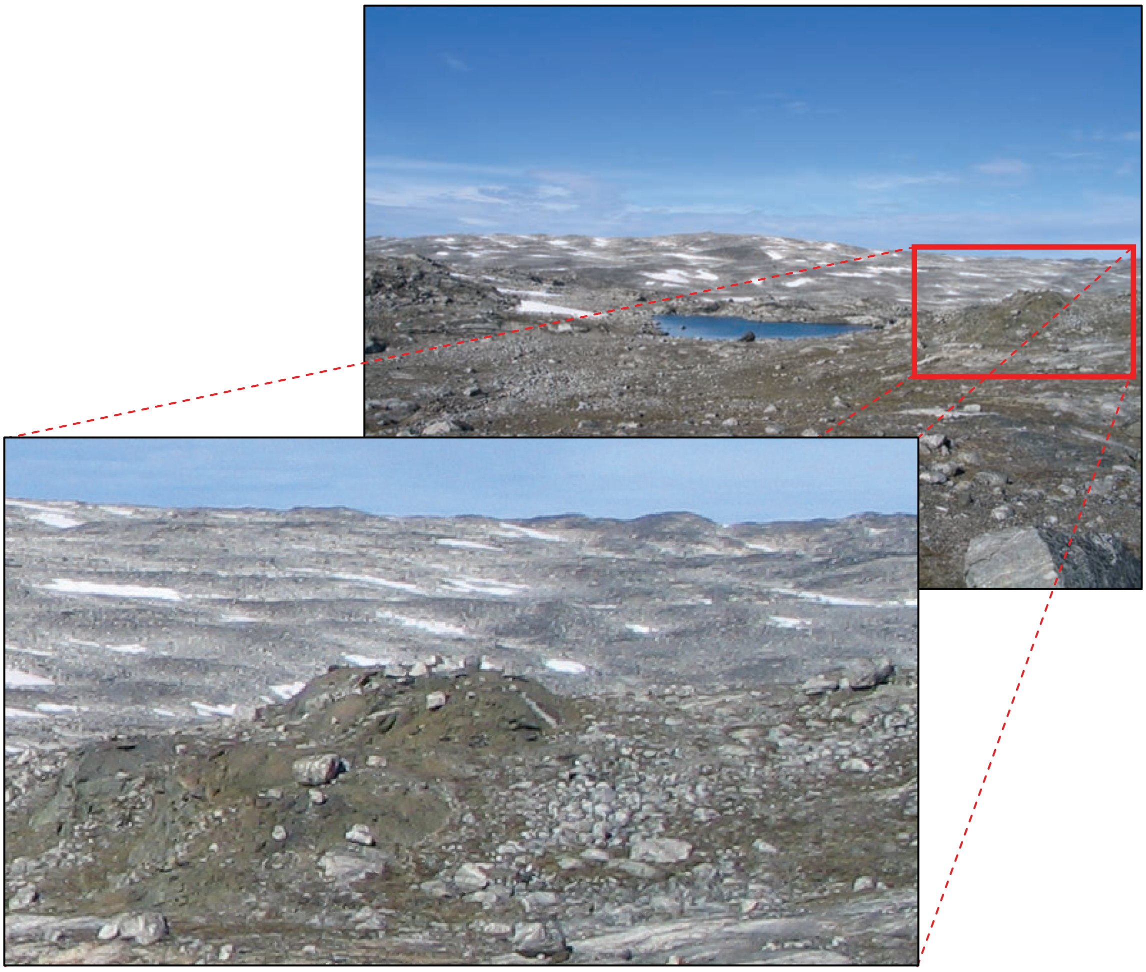

Figure 2. *Eastern Kangerssuaq area. Monotonous grey gneisses with enclaves of supracrustal sequences and ultrabasite. The enclaves often outcrop as hills or ridges in the area. Quartz veining and rust zones are observed within the supracrustal sequences. Photo: P. Appel, GEUS.*

Western Kangerssuaq

Peter Appel, GEUS, and Wouter Heijlen, Leeds University, had a short helicopter reconnaissance stop in the area (C in Fig. 1).

Field observations: The area comprises an extensive field of local, large-sized boulders with scattered outcrops of ultrabasites, supracrustal amphibolites and gneisses (Figure 3). The bedrock is dominated by gneisses, locally sheared and locally with rust zones containing small amounts of pyrrhotite. Thin hematised joints are frequently observed in the bedrock. In general, the bedrock is bleached in the area. The amphibolites are locally slightly rusty and cut by metre wide pegmatites. The amphibolites have been calc-silicate altered resulting in a diopside garnet rock locally with gash veins filled with quartz. The amphibolite shows a good foliation, in some cases almost slaty. Abundant deformed slightly rusty quartz veining parallel to the banding in the amphibolite is seen. Quartz-rich micaceous rocks are intercalated with banded amphibolites. Many of the micaceous rocks contain blebs or clasts of quartz. Some of the clasts contain fuchsite. Boudins of amphibolites are seen in the mica-schists. The boudins are 5 cm thick and 10-15 cm long and arranged parallel to the schistosity of the rock. An about 2 metre wide very rusty zone with 5 to 10 % pyrrhotite and chalcopyrite is also exposed in the boulder field. A fuchsite-stained, pyrrhotite-quartz vein occurring as a train of boulders was also observed. One stream sediment sample was collected in the area. P. Appel suggests that the predicted high favourability of the area is caused by a combination of ultramafic rocks and hydrothermal activity.

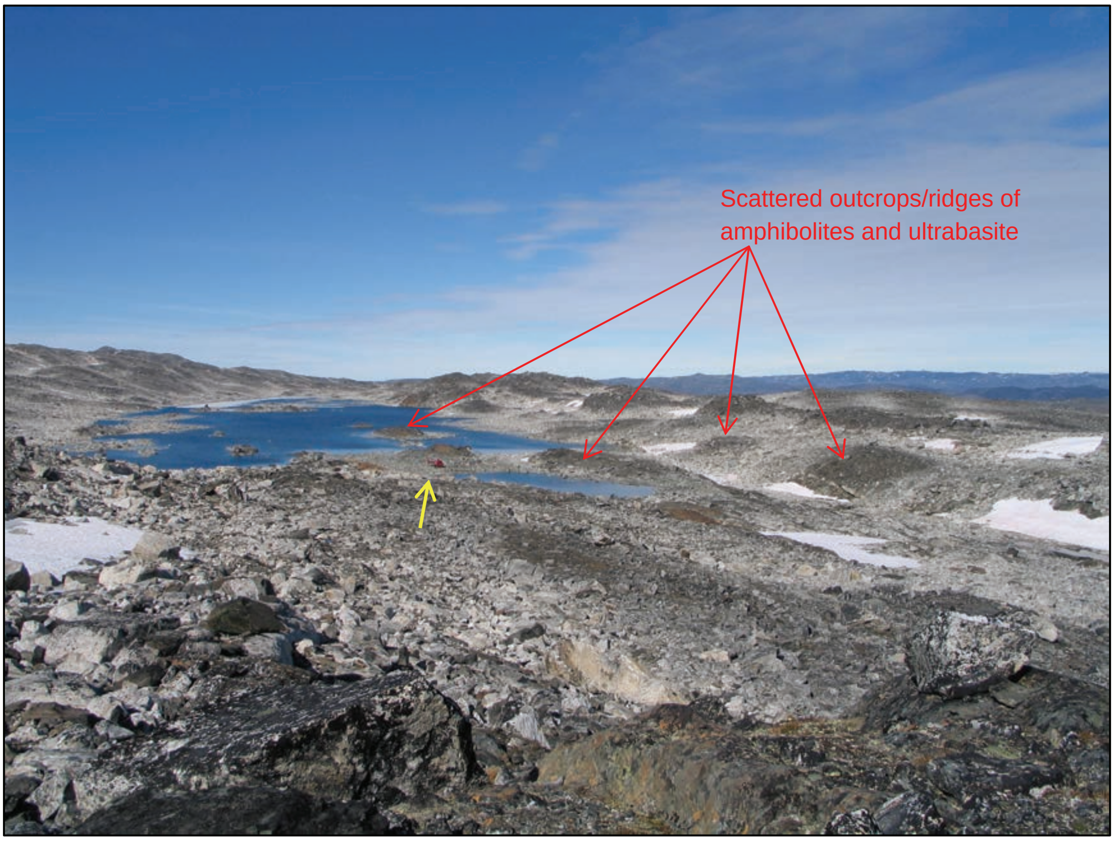

Figure 3. *The extensive boulder fields at western Kangerssuaq with outcrops of ultrabasite and amphibolites in scattered small hills or ridges. At the head of the yellow arrow, a red helicopter is standing for scale. Photo: P. Appel, GEUS.*

Figure 4. *A general feature of the bedrock in the area at Kangerssuaq: red-coloured (hematite) joints in bleached gneisses. White card in the middle of the photo is 10 cm high. Photo: P. Appel, GEUS.*

North of the lake Tussaap Tasia, northeastern part of Ujarassuit Nunaat

Peter Appel, GEUS, and Robert Willan, consultant, spent one week in the area (D in Fig. 1).

Field observations: Large bodies of ultrabasite are common in this area. The bodies are several tens of metres wide and can be traced for more than 100 metres. Several types of late alteration features are observed. The ultrabasites are either reddish weathering, serpentinized, massive, and highly altered, or light brownish dunite that weathers out more strongly than the other variety (Fig. 5).The country rock consists of gneisses with minor enclaves of amphibolite. Enclaves with successions similar to those of the Isua Greenstone Belt are also found in the area. These enclaves contain slightly rusty, banded iron formation, amphibolites, and ultrabasic rocks. The magnetite-banded metasediments occurs in metre wide bands. Rust zones occur within the enclaves. Voluminous red K-feldspar pegmatites crosscutting the gneisses and amphibolites are common in the area (Fig. 6).

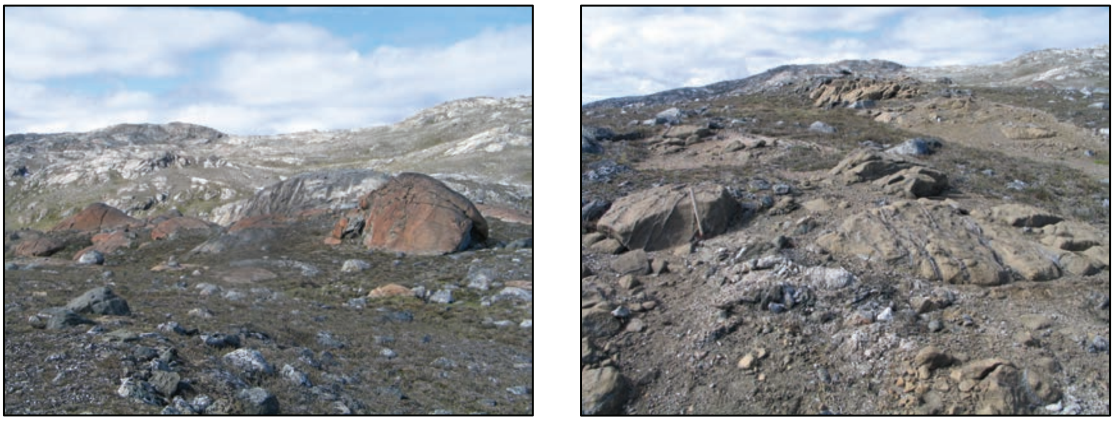

Figure 5. *Examples of ultrabasic bodies in the area north of lake Tussaap Tasia. Two types of ultrabasites were found in the area: to the left a red, massive, highly altered and serpentinised type, to the right a light brownish dunite type that weathers more strongly. Photos: P. Appel, GEUS.*

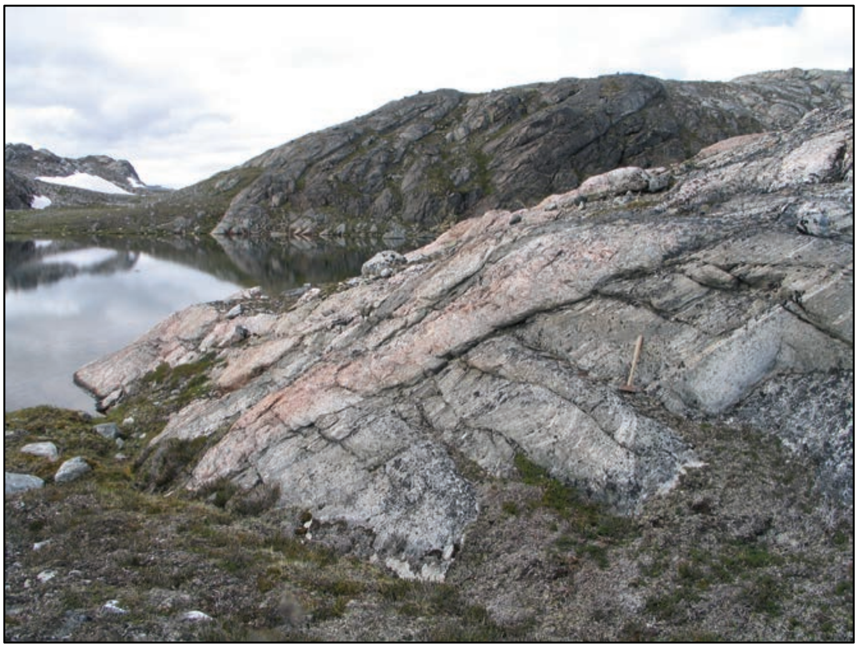

Figure 6. *Voluminous pink K-feldspar pegmatites crosscutting gneisses and amphibolites. Hammer for scale (c. 50 cm long). Photo: P. Appel, GEUS.*

Central Ujarassuit Nunaat – north of the fjord Ujarssuit Paavat

Johann Raith and Gernot Loidl, both University of Leoben, Austria, visited the area (E in Fig. 1). Also Jeroen van Gool and Ole Stecher (van Gool & Stecher 2006), both GEUS, and Juan Carlos Ordóñez-Calederón (Ordóñez-Calederón 2006), Windsor University, Canada, visited the area.

Field observations: This area contains the main supracrustal belt in this part of the Nuuk region. Most of the area outlined as favourable is situated, however, on the southern outskirts of the belt, within an area of tonalitic to granodioritic orthogneisses with enclaves of amphibolite and ultramafic rock. The supracrustal belt itself is dominated by homogeneous to banded amphibolites. Medium to coarse-grained metagabbroic bodies occur within the amphibolite. Ultramafic rocks occur as lenses, which are up to 1 km long. The contacts between the amphibolites and the orthogneisses to the south are intrusive and gradual. The transition zone contains up to 100 m long slivers of amphibolites (van Gool & Stecher 2006). Hydrothermal alteration is common according to Ordóñez-Calederón (2006). Two types of alterations are observed within the belt: calc-silicate alterations, and pyrite-bearing rust alterations. The former type is developed as a replacement of amphibolites, whereas the latter type is found within pyrite-bearing quartzite.

Qooqqut lake area

Previous mapping and mineral exploration have sustained that this area (F in Fig. 1) is lithologically similar to Bjørneøen and Storø. It hosts a 100-metre wide belt of mafic volcanic rocks, from which pegmatites and ultramafic rocks, as well as sulphide mineralisation, silicification, calc-silicate alteration have been reported. Three gold-bearing samples have been acquired from the area (200–380 ppb Au) as referred to in our previous report (Nielsen et al. 2004).

Geological observations: H. Stendal, GEUS, and his assistant Tove Nielsen, paid a visit in 2005. Twenty-nine rock and three stream sediment samples were collected and analysed chemically. The findings are described briefly and analytical data are documented in Hollis et al. 2006. New observations include pillow structures, magnetite-rich layers and garnet-quartz rocks interpreted as metamorphosed volcanic exhalites. Numerous granite veins (Qôrqut granite) and pegmatites crosscut the area. A rusty high strained zone, tens of meters wide, is observed in the cliff wall at the north-eastern side of the valley (Fig. 7). Comprises rock types within the zone are dubious; it is either high strained gneisses or silicified amphibolite. Several rust zones and iron-sulphide bearing horizons in the amphibolites are observed in the area (Fig. 8).

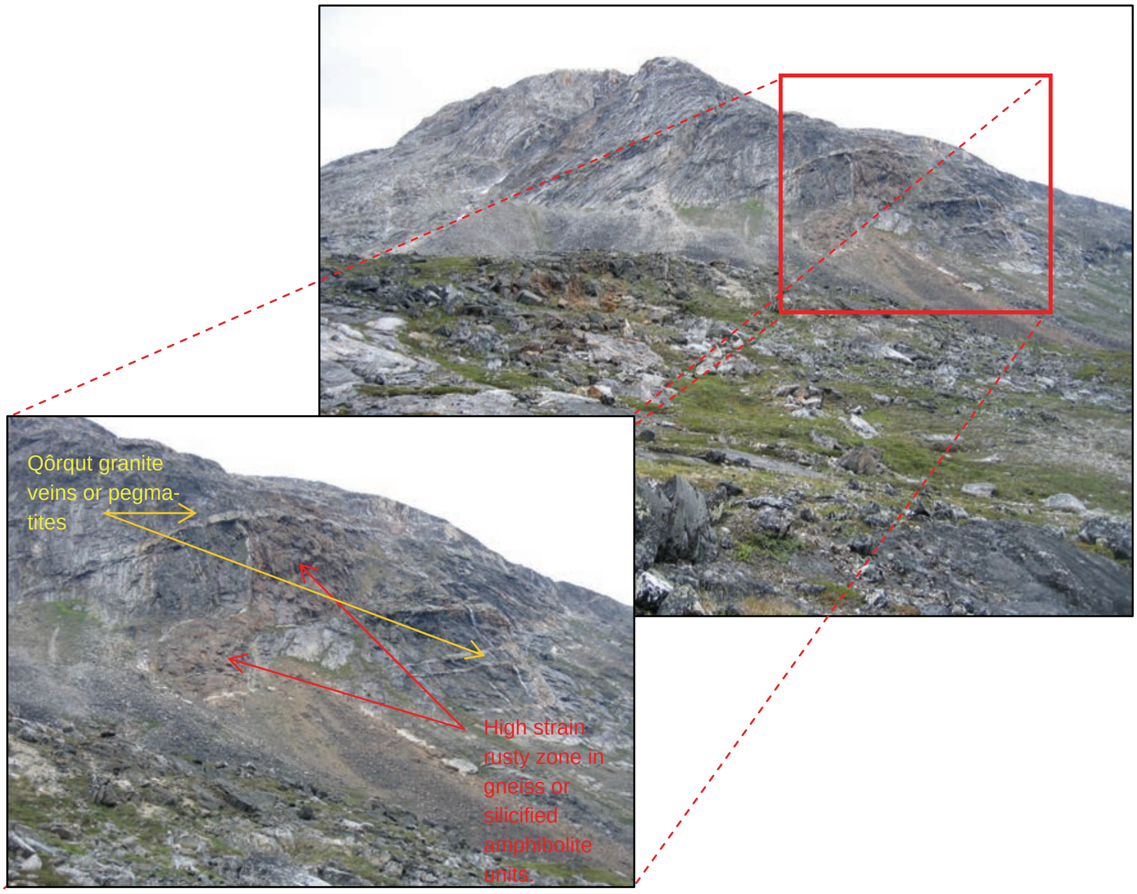

Figure 7. *Rusty high-strain zone in the cliff wall at the northwestern side of the Qooqqut lake in the area predicted as favourable. Photo: H. Stendal, GEUS.*

Figure 8. *Examples of rust zones found within amphibolite units in the valley east of Qooqqut fjord. Photo: H. Stendal.*

Geochemical results: None of the samples shows elevated gold concentrations; samples of meta-exhalites display variable to strong Cu, Ni and Zn enrichment and high Ni/Mg ratio.

One of the ultramafic rock samples, a pyroxenite with mica, has unexpectedly high concentrations of Cs (30 ppm), K (4.24 %) and Rb (298 ppm), in addition to the expected high Ni and Cr. The high concentration of lithophile elements suggests infiltration by material with a presumed granitic origin.

The new stream sediment samples display fairly high U (16–17 ppm) and Cs and Ni/Mg ratio, thereby confirming the characteristics of the regional samples.

General remarks from follow-up observations

The areas visited present many similarities in terms of lithology and alteration phenomena. Almost all areas comprise ultrabasite and amphibolite units; either as enclaves or as bodies floating in orthogneisses, or as continuous belts surrounded by gneisses. The sizes of the enclaves and bodies vary from tens of metres to hundreds of metres. Signs of hydrothermal activity are observed in many of the areas, such as bleaching of rocks and oxidation of joint surfaces, calc-silicate alteration and rust zones in amphibolites, in addition to quartz veining and quartz filling of gash fractures.

Data compiled during the second phase

Updated gold showings

Based on data collected by GEUS during the 2004 fieldwork, seven new gold showings were identified and added to the existing showings, making 52 presently identified gold showings. For the localities of gold bearing samples recorded previously, see Nielsen *et al.* 2004.

Geochemistry data from exploration companies

One essential way of improving the resolution of stream sediment data for the region would be to collect and analyse more samples using the same methods as previously applied by GEUS. In the absence of plans to carry out such activity, we have compiled geochemical datasets obtained by exploration companies to see if they are, or can be made, suitable for statistical spatial analysis.

NunaMinerals A/S sediment geochemistry data

NunaMinerals A/S, former NunaOil A/S, has been very active during the last decade in mineral exploration in the Nuuk region. However, the company has not compiled geochemical data that have already been reported individually by each campaign. Although much of the data have been archived in digital form by the company, the sample localities have in many cases not been digitised and had to be read off copies of sample maps included with the reports submitted to BMP and GEUS. In a time-consuming joint effort with geologists from NunaMinerals compiled the necessary information about sample locality, sample type, treatment and analysis (Figs 9 and 10).

The amount of geochemical information represented by NunaMinerals' samples could constitute a future valuable supplement to presently available geochemical data. What remains is a thorough quality control of the analytical data before selected elements in the data can be made consistent with GEUS data and become part of the overall statistical analysis.

Even if the company data cannot be made internally consistent, or calibrated with GEUS data, they still present additional information about areas predicted as favourable for gold mineralisation. For now, the compilation carried out here documents results that have not been publicly available before. The data will be made accessible by GEUS for future investigations of the Nuuk region.

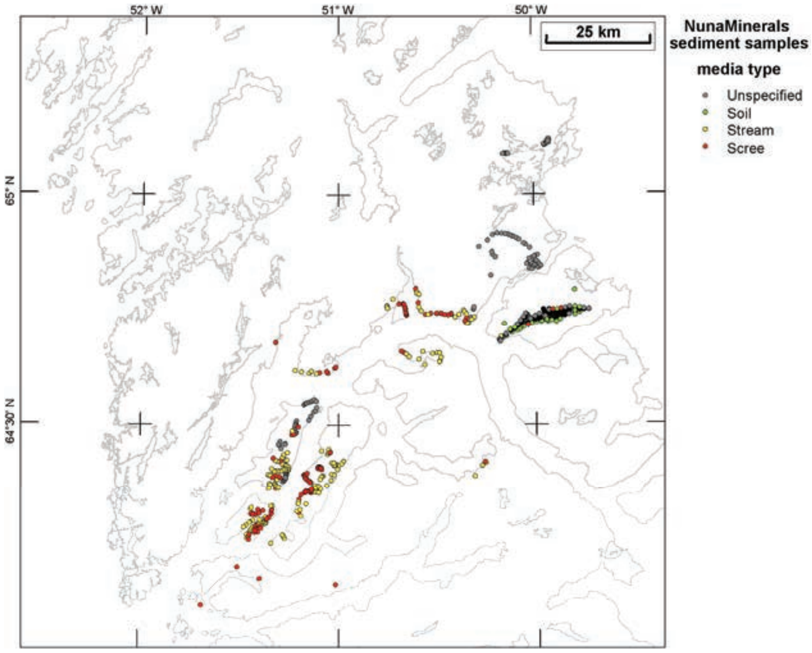

Figure 9. *Location of samples of different surface material from compiled NunaMinerals A/S data.*

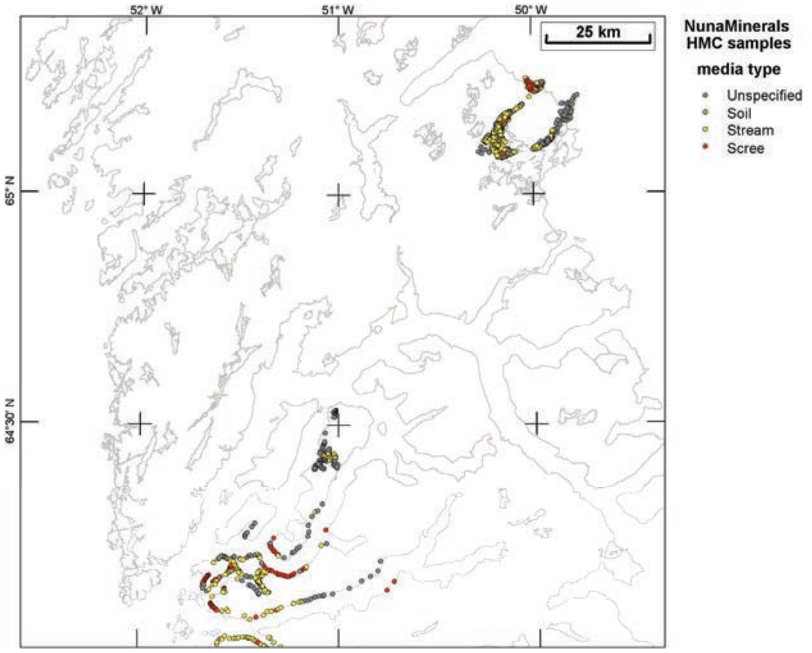

Figure 10. *Location of surface samples collected by NunaMinerals A/S and processed for heavy mineral concentrates.*

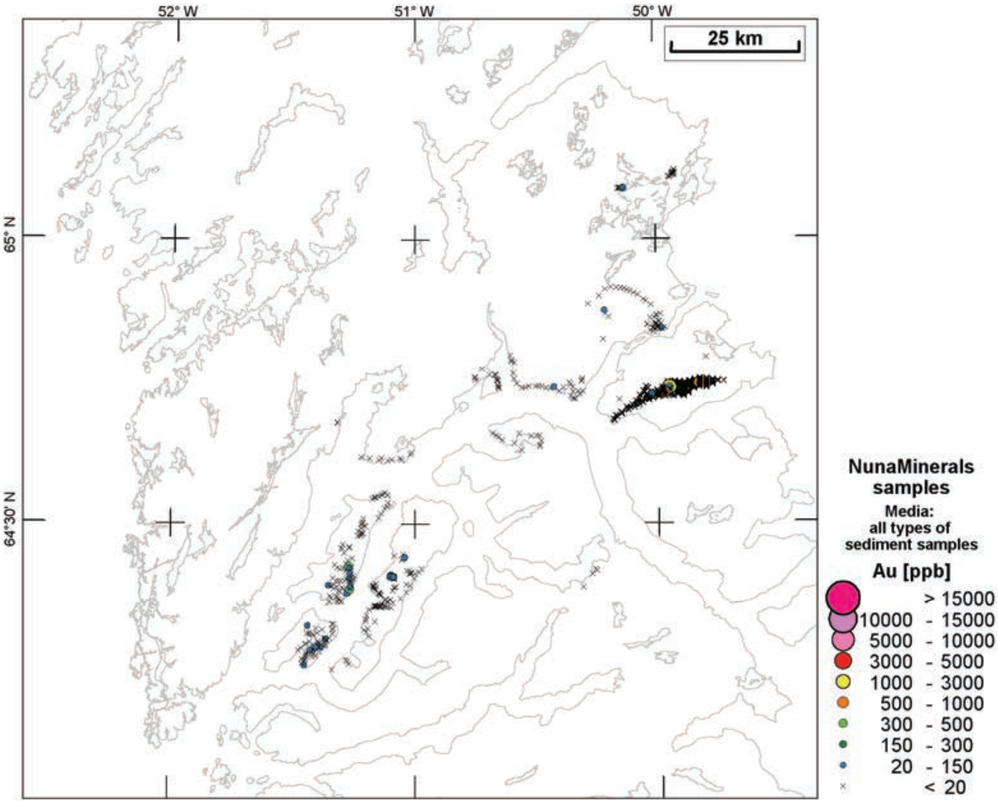

Figure 11. *Gold content in sediment samples from compiled NunaMinerals A/S data.*

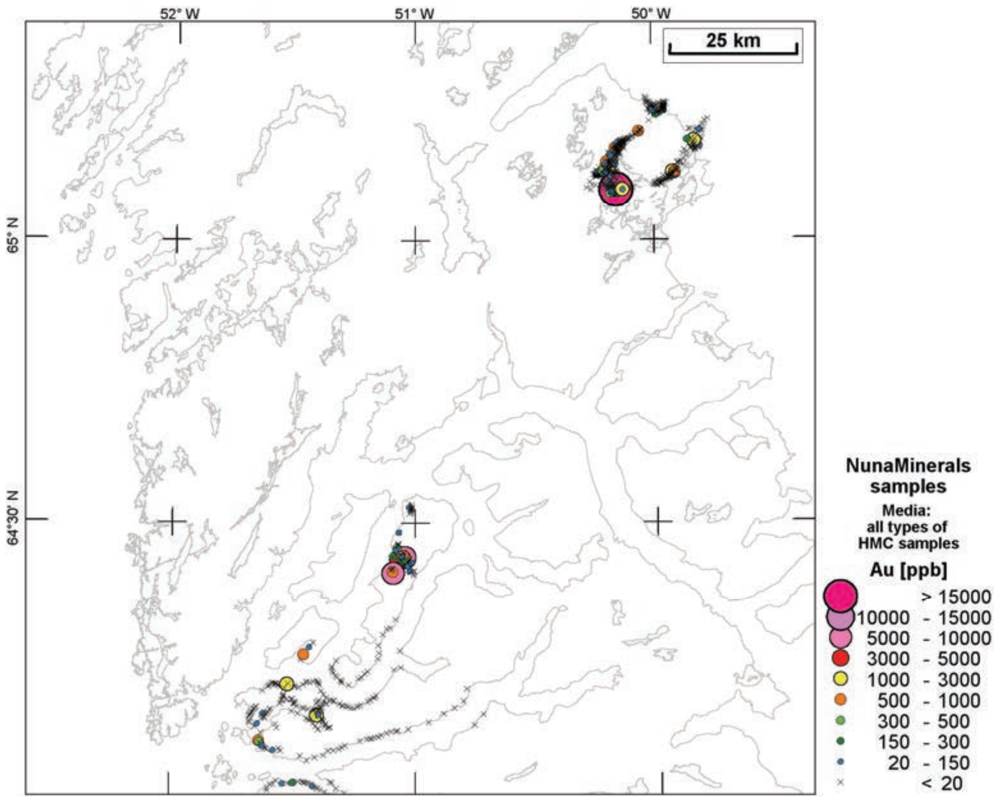

Figure 12. *Gold content in the heavy mineral concentrates of samples from compiled NunaMinerals A/S data.*

Diamond exploration data

Till and stream sediment samples from large parts of the Archaean West Greenland have been acquired by exploration companies with the purpose of identifying mantle-derived minerals (so-called kimberlite indicator minerals) in them. A number of such samples were also analysed for trace elements (Jensen *et al.* 2004). Their distribution is shown in Fig. 13.

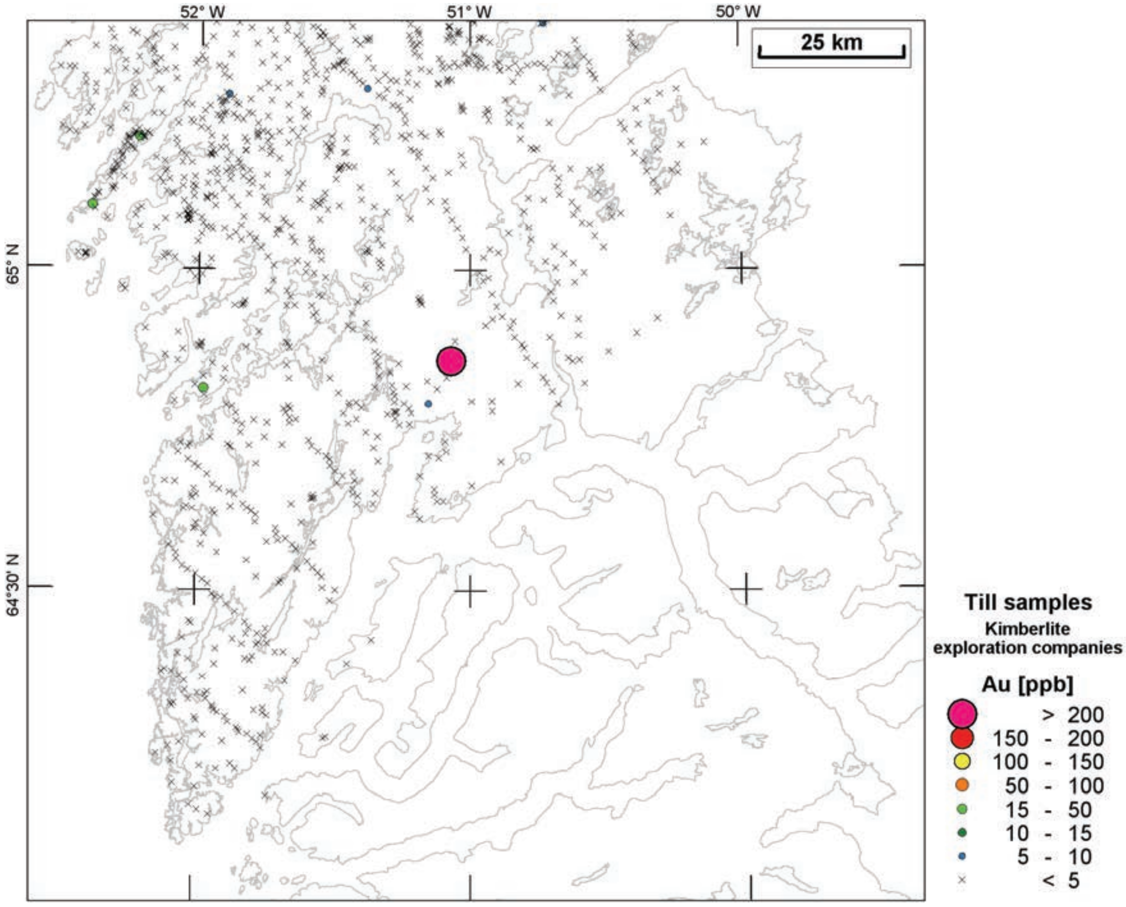

Figure 13. *Distribution of till samples and their gold content.*

Lineament data from exploration companies

A photo-geological interpretation of the entire Precambrian shield of West Greenland (more than 950 km in length) has been made by J. Grootenboer as a part of the exploration company Quadrant Resources Pty. Ltd.s activities in 1997 (Ferguson 1998). Besides identifying circular to ovoid structures in the attempt to target possible kimberlite pipes, this work included a relatively detailed identification of topographic lineaments. The interpretation of the aerial photographs, was mostly based on 1:150 000 scale vertical photographs and, where available, 1:40 000 scale photographs. The results of the interpretation was reduced and transferred into 1:500 000 scale maps, which are available in paper format in the report by Ferguson (1998).

These data are potentially valuable for a linking between gold mineralisation and lineaments in the Nuuk region (Fig. 14). Consequently, a digitisation and evaluation of the lineaments were pursued during the second phase of the project.

The region of interest in the map was scanned as a tiff-file. Afterwards, the map was vectorised and geo-referenced (using the software Vextractor 2.90) by means of the geographical coordinates indicated on the map. Due to the resolution it was not possible to extract marked circular to ovoid targets, hence these were omitted. Neither was it possible to distinguish signatures of lineaments for dykes, faults, or shear zones, hence all lineaments were treated as on group.

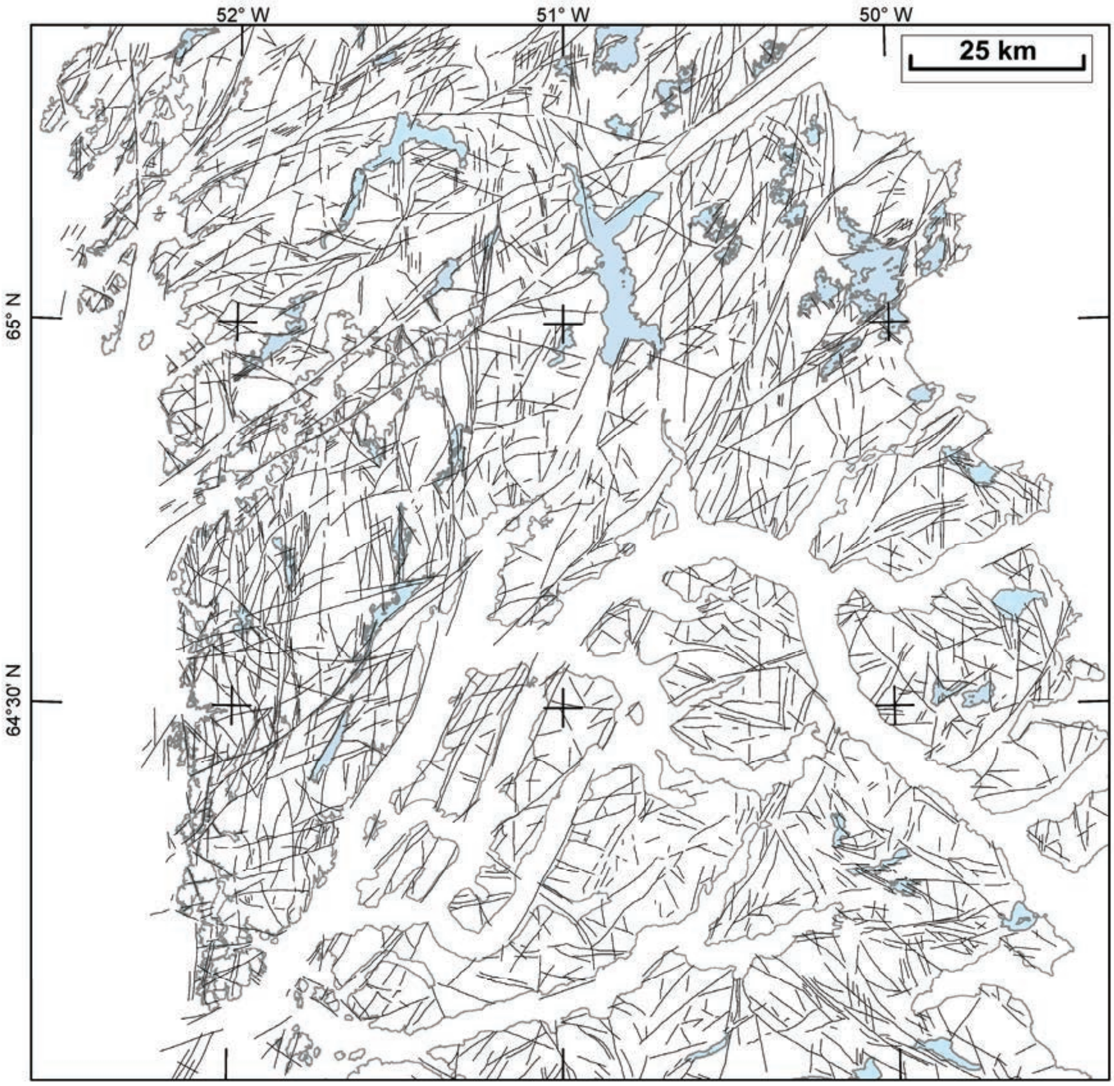

Figure 14. *Recovered lineaments from the photo-geological interpretation made by the consultant J. Grootenboer for the exploration company Quadrant Resources Pty. Ltd.*

The coastline on the scanned map was also digitised to examine the magnitude of the differences between the former topographic base used in Ferguson (1998) and the current topographic map base (in scale 1:100 000) for the region. Rather small differences of c. 100–200 m between coastlines were observed in most parts of the digitised map. This difference was, however, very variable and locally amounts to as much as 1 km. In regional scale investigation, such differences may be acceptable, but they were considered unsuitable for the current statistical analysis, which is based on 200 × 200 m pixels. Consequently, it was decided not to make use of the digitised lineament data in the current statistical analysis. Nevertheless, the new digital lineament data have been produced and may be very useful for larger scaled interpretations and analysis.

Statistically defined lineaments in aeromagnetic data

A procedure and mathematical algorithm for defining lineaments in spatial data have been developed during the second phase of the project. The procedure has been applied to the aeromagnetic data, but it can also be applied to other types of data, e.g. digital elevation data.

Lineaments defined in the aeromagnetic data are shown in Figure 15, and details of the method are given in Appendix A. If the lineaments based on aeromagnetic data can be taken to reflect structures in the bedrock, statistical methods can be applied to check if and how the gold showings are related to the linear features. For example, it has been shown in some gold mining districts that gold mineralisation tends to occur in 2^{nd} or 3^{rd} order splays away from a main structure.

Each lineament can be defined by its location, orientation and length, and these quantitative parameters can be statistically processed to determine e.g. their mean orientation, their density, or their mean length within a certain search radius from each observation point.

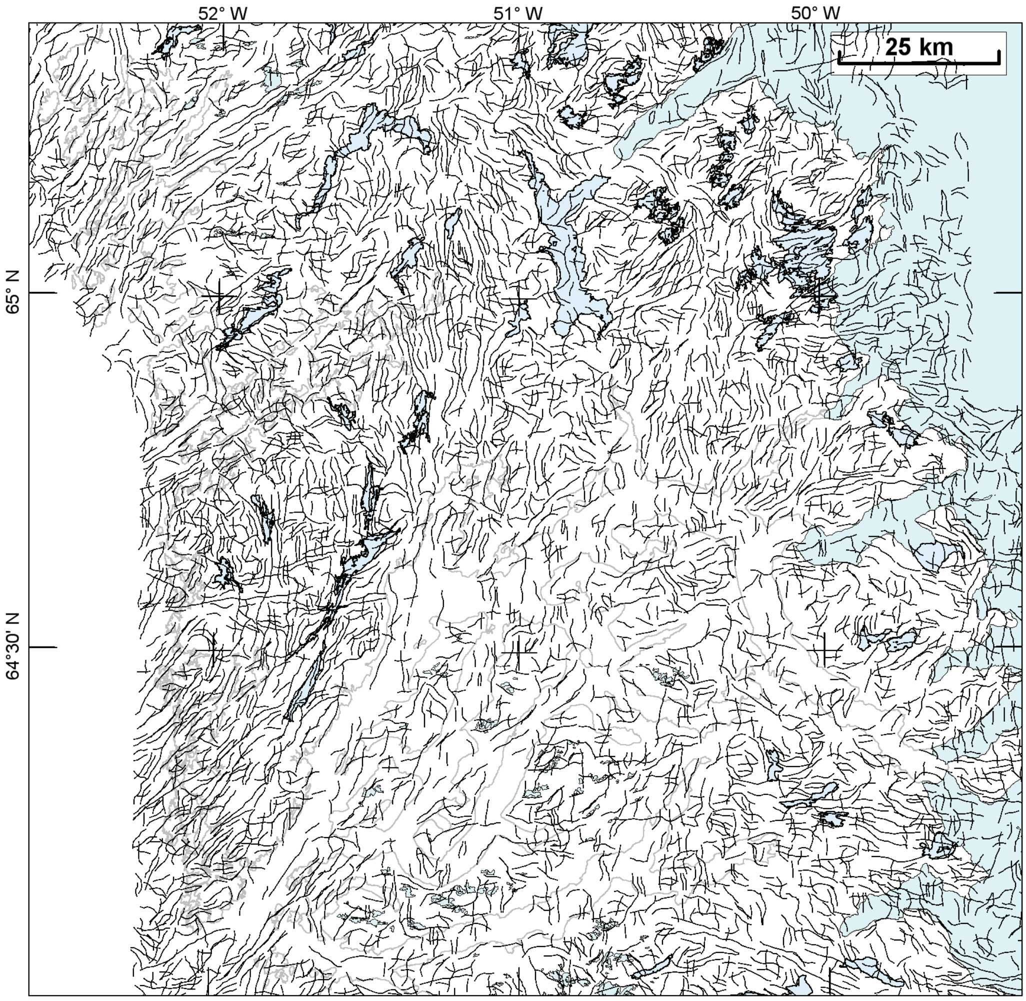

Figure 15. *Mathematically defined lineaments in aeromagnetic data from the Nuuk region. Statistical parameters describing the spatial distribution and properties of the lineaments are used as input to the multi-parameter modelling of gold showings.*

In this study, the following statistical parameters have been calculated:

- Mean direction of lineaments within a search radius (values from 0 to 180°)
- Minimum distance to nearest lineament within a search radius (values in metres)
- Number of crossing lineaments – the density of lineaments – within a search radius (a number)
- Total length of lineaments within a search radius (in metres)
- 'Complexity factor', uniformity of orientation angles within a search radius (values from 0 to 1; a value of 1 implies that all lineaments have the same orientation (less complex lineament patterns) whereas a value of 0 implies orthogonal orientations (complex lineament patterns))

The first four parameters are straightforward, whereas the calculation of fifth parameter needs detailed explanation, see Appendix A.

Further statistical parameters can be obtained if the lineament population is subdivided according to lineament length. In this study, parameters have been determined for each of the following intervals:

all lines	All lineaments irrespective of their length.
0–10%	Only lineaments with a length of 0–10% (2000–2100 m) of the maximum length.
0–25%	Only lineaments with a length of 0–25% (2000–2450 m) of the maximum length.
25–50%	Only lineaments with a length of 25–50% (2450–3100 m) of the maximum length.
50–75%	Only lineaments with a length of 50–75% (3100–4250 m) of the maximum length.
75–100%	Only lineaments with a length of 75–100% (4250–23600 m) of the maximum length.
90–100%	Only lineaments with a length of 90–100% (6030–23600 m) of the maximum length.

Parameters have been determined for each group with search radii of 1, 2, 3, and 5 km, respectively. The results for search radii of 1 and 5 km are shown in Appendix B.

A full multi-parameter modelling and identification of signatures for the gold showings have been carried out for a search radius of 1 km. The resulting signatures can be seen in Appendix C, and they are discussed in the section ‘Data signatures of the groups’.

Aeroradiometric data

In maps of airborne gamma-ray spectrometry over West Greenland, a pronounced radioactive zone with a north-north-east orientation stands out in the Nuuk region (Steenfelt 2001b). This zone also covers the clusters of gold showings. It was therefore obvious to try to include these data in the statistical analysis to see how high radioactivity or specific concentrations of one or more of the radioactive elements (K, Th and U) are spatially related to areas with gold showings.

Regional-scale, four-channel, gamma-ray spectrometry has been conducted from fixed-wing aircraft over a large part of West Greenland (Secher 1976; Secher 1977) by the Geological Survey of Greenland (now GEUS) in collaboration with Research Establishment Risø (now Risø National Laboratory). The measurements were made during contour-flying at an average ground clearance of 90 m. Spectrometric data and readings from a radar altimeter were recorded every second, and flight routes were drawn on topographical maps and later digitised. The obtained counts per second in each channel were corrected for instrumental drift and background radiation and further processed (stripped) and recalculated to represent ground concentrations of K, Th and U. Over the years, some data were lost due to deterioration of the magnetic tapes used for storage. Most of the data, however, has later been restored (Tukiainen *et al.* 2003).

The accuracy and precision of airborne gamma-ray spectrometry is dependent on a range of factors, the main being flight altitude, topography, background radiation (cosmic radiation) and air pressure. In practice, it was at the time not possible to correct the data for variations in topography, if flying along straight lines. Instead, it was attempted to fly along mountain slopes to maintain similar terrain geometry ("contour flying").

The dataset available for the present project consisted of records containing flight altitude, total radiation in counts per second, and equivalent ground concentrations of K (%), Th (eTh ppm) and U (eU ppm). In order to reduce noise, the data were screened to include only those recorded from heights between 75 and 105 metres above terrain, and to include only records with positive values in all channels. Negative values are invalid and probably result from the stripping procedure typically in situations where the radiation is very low, e.g. above humid or vegetated ground.

Figure 16 illustrates the spatial distribution of the remaining c. 31000 readings. The irregular coverage is illustrated, and the scarcity of data in certain areas is a disadvantage for a spatial analysis covering the entire Nuuk region. Another problem is that the flight routes were originally traced on old topographic maps at 1:250 000 scale. When the data are plotted on the new topographical maps at 1:100 000 scale used in this project, the data points deviate invariably from the correct position. Correcting the position of the flight routes would require a new digitisation, and this was not possible within the frame of the present phase of the project. We chose to include the data in the spatial analysis, realising that the position of the radioactive anomalies may be displaced.

Grids were produced using the screened data for total radiation, K, eTh, eU and the ratio eU/eTh. The gridding method 'minimum curvature' was applied with a pixel size of 200 m and blanking distance of 5000 m. As the track of the flight line is variably displaced from the true position, the large blanking distance ensures that the land surfaces that were actually flown are covered by data, and the pixel values for the gold showings will be approximately correct. Outside the blanking distance from the flight line, pixels have been given arbitrary values close to the mean of the data variation, so that they do not skew the distribution function for the background. The contoured grids for total radiation, K, eqU, eqTh and eqU/eqTh are shown in Appendix B.

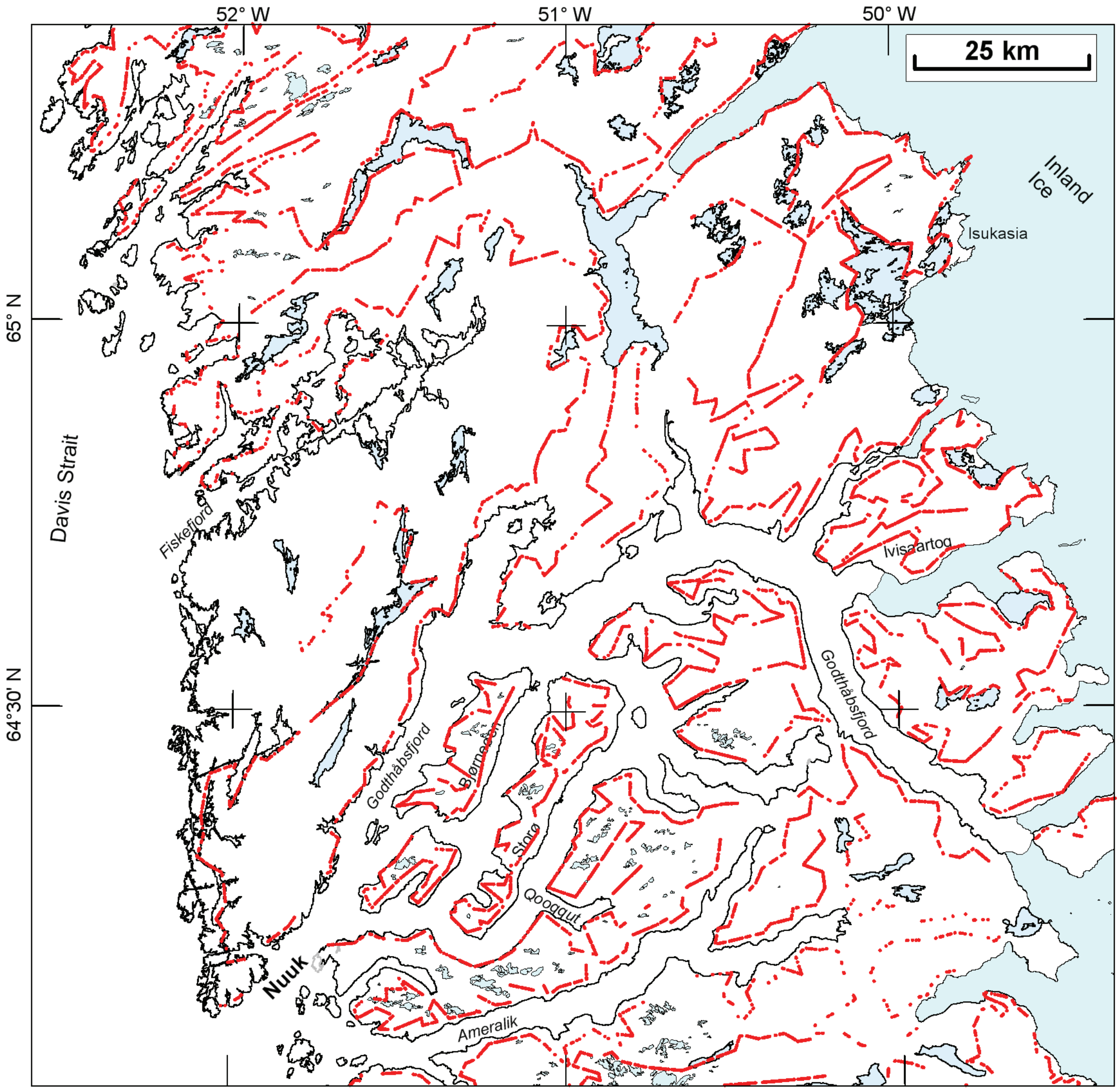

Figure 16. *Distribution of screened aeroradiometric data in the Nuuk region. The line segments are composed of red dots, each representing one of the available c. 31000 valid measurements. The flight lines were originally tracked on older topographic maps, so that their positions on the new topographic base used in this study are variably displaced (hardly seen at the scale of this map).*

Progress in multi-parameter modelling

In the second phase of the project, seven gold showings have been added to the training set, the gold showings have been divided into subgroups, and prediction maps have been made for each group. New regional datasets have been prepared and frequency distributions for background and showings have been constructed.

Grouping of gold showings

For reasons of simplicity, the known gold showings in the Nuuk region were at first treated as one group. In the present phase, the multi-parameter signatures of the showings have been investigated to see if there are statistically significant differences among them to justify a division into subgroups.

The grouping of the gold showings has been based on their ability to predict other showings within the same group. A prediction map was constructed for each gold showing and its capability to predict the remaining showings was examined. A two-dimensional matrix with numbered showings along the axes displays the result of the examination (Fig. 17). Red fields mark a high probability of the prediction. The rows of the matrix contain showings predicted by the showing of the row; the columns contain showings that predict the showing of the column. Gold showings that are mutually predicted (i.e. are able to predict each other, and show similarities in their prediction of other showings) are grouped.

In contrast, gold showings that predict and are themselves predicted by an insignificant number or none of the other showings are considered insufficiently characterised to qualify as input data. These are excluded from further analysis. Likewise, sets of very few mutually predicting showings are also excluded from further analysis.

Considering the low resolution of the regional data and the way characteristic signatures of showings are extracted, it lies implicitly in the statistical method that showings situated closely together in space will be grouped, even if they appear different on a local scale.

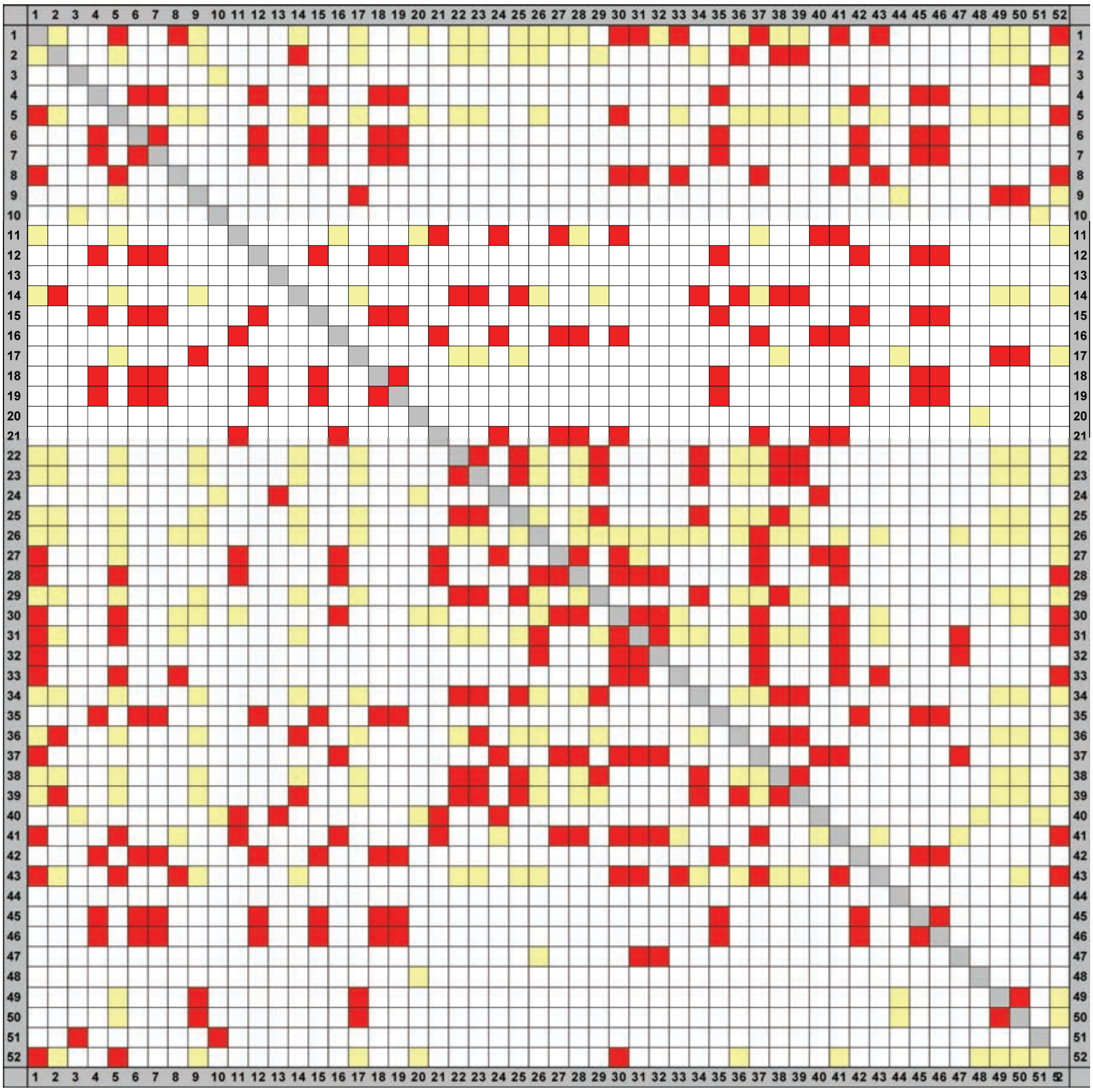

Figure 17. *Prediction matrix illustrating the prediction capabilities of fifty-two gold showings within the Nuuk region. Red squares indicate a prediction probability of above or equal to 99.5%. Yellow squares indicate a prediction probability from 90.0 to 99.4%. Thus, showing no. 18 predicts showings in row 18, i.e. no. 4,6,7,12, 15, 19 etc., and is itself predicted by showings in column 18, i.e. no. 4,6,7, etc. The prediction was based on signatures including As, Au, Ca, Rb, Th, U, and Ni/Mg ratio in stream sediment data, together with the vertical gradient and amplitude of the horizontal gradients of aero-magnetic data. These datasets were found to be indicative of gold showings in the first phase of the project (see Nielsen et al. 2004).*

Groups of gold showings

Based on a visual inspection of the prediction matrix (Fig. 17), three groups of gold showings are identified. One additional set of showings, the Qangaatarssuakop Isuakasia set, is also identified, but this set only contains four showings, which is regarded as statistically insufficient to form a proper group. Consequently, this set of showings is excluded from further analysis in this work. Eight showings are predicted by and themselves predict only a very small number of the other showings, or none at all. These are also excluded from further analysis. The members of the identified groups Figure 17 are listed in Table 3 and their spatial distribution is shown in Figure 18. It is noteworthy that the grouping based mainly on geochemical results in a geographical grouping.

The Isua group contains 19 showings, of which one is located in supracrustal belt at Ivisaartoq, and the remaining within the Isua supracrustal greenstone belt. The Bjørneøen group contains 10 showings all situated within the supracrustal belt in the central part of Bjørneøen. The final proper group is the Storø group, which contains 11 showings, all within the supracrustal rocks in the areas at and around the Qingaaq and Aappalaartoq gold prospects.

Table 3. *Identified groups of gold showings. Showing no. refers to the row and column numbers in the prediction matrix. Red, blue and green are used here and in the following tables and figures to mark the three main groups.*

Name of group	Gold showings no.	Number of showings
Isua group	1, 5, 8, 11, 16, 21, 26, 27, 28, 30, 31, 32, 33, 37, 40, 41, 43, 47, 52	19
Bjørneøen group	2, 14, 22, 23, 25, 29, 34, 36, 38, 39	10
Storø group	4, 6, 7, 12, 15, 18, 19, 35, 42, 45, 46	11
Showings excluded from further analysis:		
Qangaatarssuakop Isuakasia set	9, 17, 49, 50	4
No predictions	3, 10, 13, 20, 24, 44, 48, 51	8

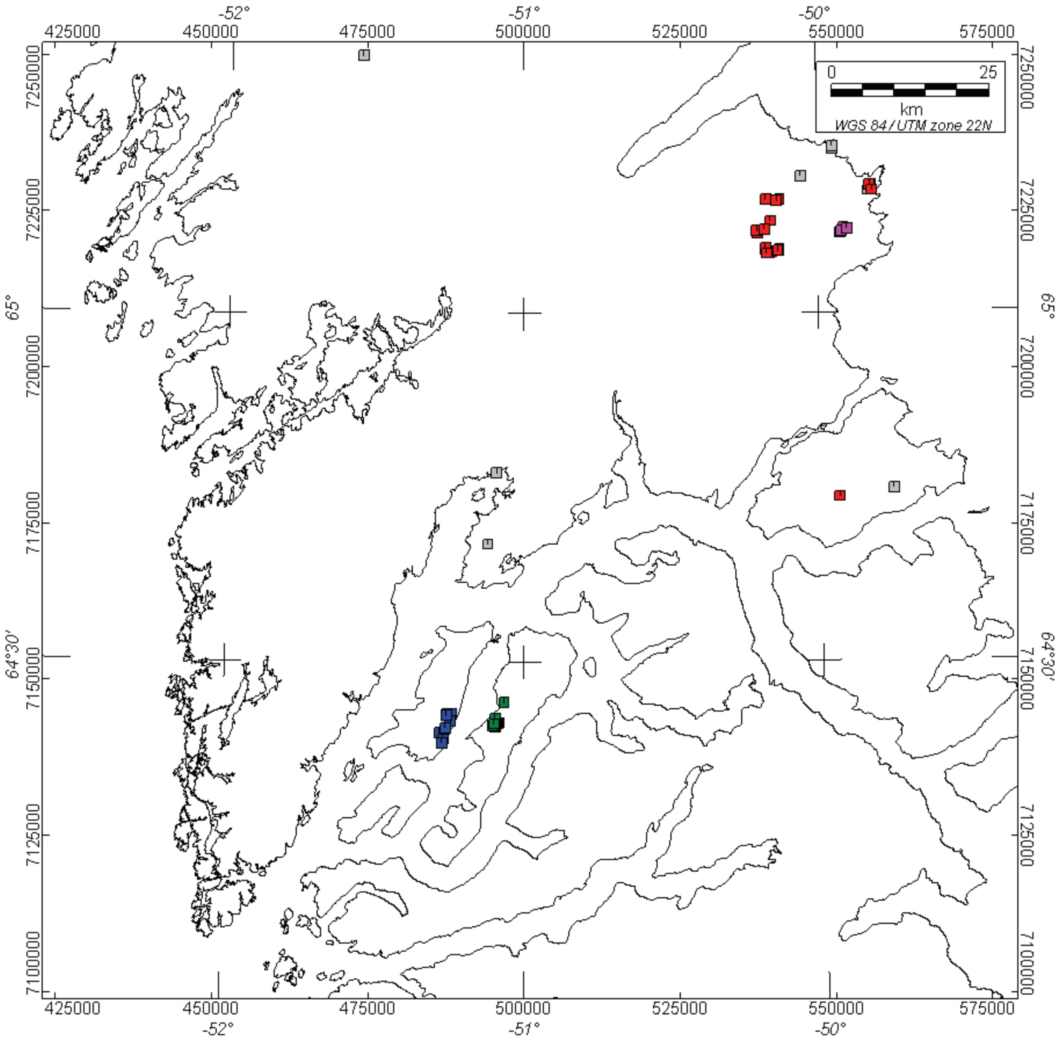

Figure 18. *Location of showings belonging to the groups defined. Red symbols belong to the Isua group, blue to the Bjørneøen group, and green to the Storø group. Pink symbols mark showings of the Qangaatarssuakop Isuakasia set of showings. Grey symbols mark showings, which could not be grouped. The grey and pink showings are not included in the calculation of prediction maps.*

Data signatures of the groups

Method

Empirical distribution functions describe the signature of the gold showings in each dataset. The determination of the empirical distribution functions is explained in detail in Nielsen *et al.* (2004). For each variable, four functions are calculated, one for pixels belonging to each of the three gold showing groups, and one for remaining pixels, defined as the background distribution. Because of the high number of pixels assigned to background compared to the number of pixels assigned to a group, the variations of the background signature for different groups will be infinitesimal. The empirical distribution functions are constructed using a smoothed kernel function.

The ratio between the distribution function for a group and for the background – the individual likelihood ratio – can be used to evaluate the significance of the data signature. The ratio ranges from 0 to infinite. To display and discuss the likelihood ratios, they have been normalised using the following function: ratio / (1 + ratio). The normalised ratio ranges from 0 to 1, and is equal to 0.5, when the two distribution functions have the same value. If the empirical likelihood ratio is above 0.7, the data signature is said to be significant. Examples of data signatures are shown in Figure 19. Signatures for all analysed datasets are given in Appendix C.

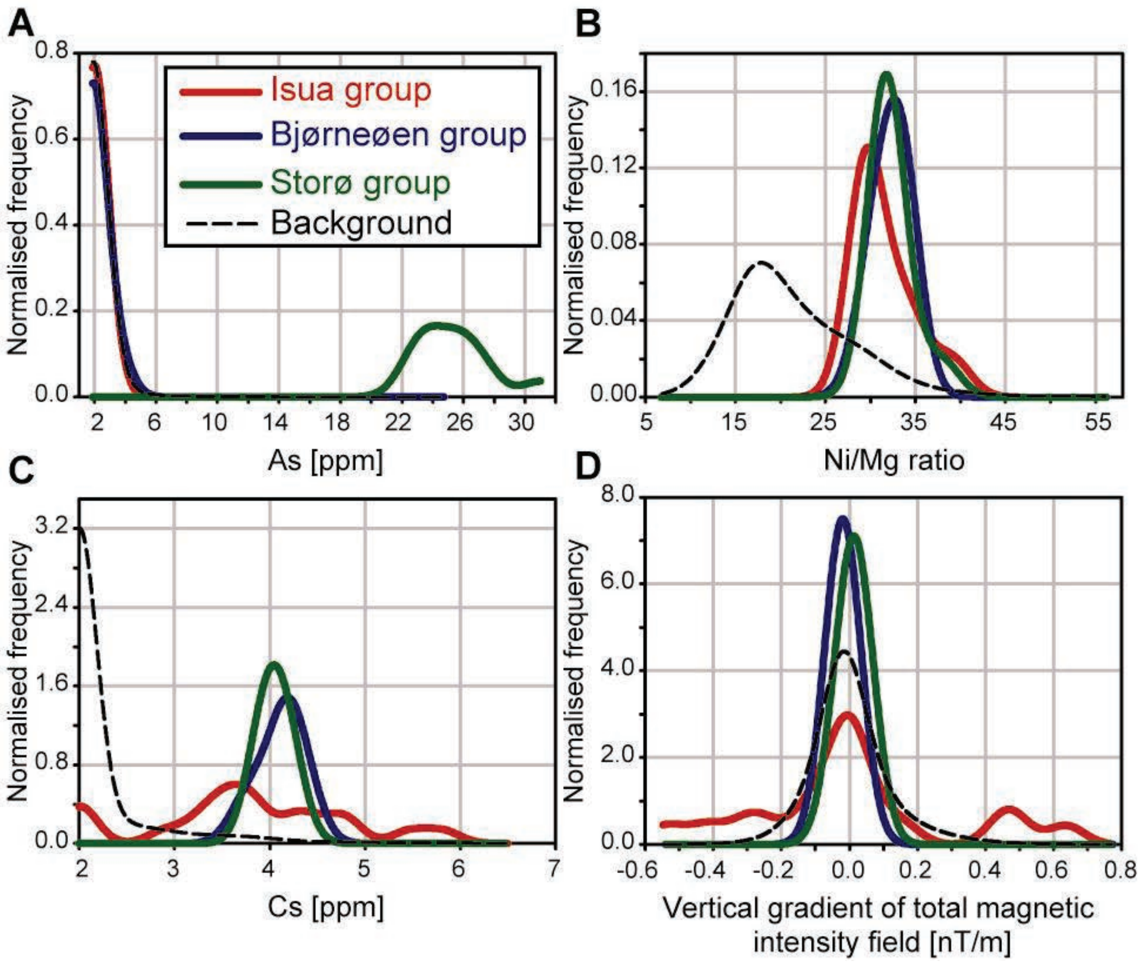

Figure 19. *Examples of empirical distribution functions for the three groups of gold showings and for the background. As, Ni/Mg ratio, and Cs stream sediment geochemistry signatures are given in the diagrams A., B. and C. The signatures in the vertical gradient of the total magnetic field intensity is given in D.*

Results

The contoured grids of the GEUS stream sediment geochemistry and the aeromagnetic data are available in Nielsen *et al.* (2004). The contoured grids of the aeroradiometric and the statistically defined lineaments in aeromagnetic data are available in Appendix B. The most significant signatures for the gold showing groups are summarised in Table 5. An overview of all datasets included so far in the project is shown in Table 4.

Table 4. *The datasets for which signatures of the gold showing groups have been determined.*

Type of data	Parameters	Number
GEUS fine fraction stream sediment geochemistry	Al_2O_3, As, Au, CaO, Cs, Fe_2O_3 K_2O, La, MgO, Na_2O, Ni+Cr, Ni/Mg ratio, P_2O_5, Rb, Sb, SiO_2, TiO_2, Th, U, V, Zr, Zn	22
GEUS aeromagnetic survey	Total magnetic intensity field (TMI), Vertical gradient of TMI, Amplitude of the horizontal gradients of TMI, Horizontal gradients of TMI (in four directions)	7
GEUS aeroradiometric survey	Total gamma-radiation, K, eTh, eU and eU/eTh ratio	5
Statistically defined lineaments in aero-magnetic data	For search radius 1000m and 7 classes of lineaments lengths: ❑ Mean direction of lineaments within the search radius ❑ Minimum distance to nearest lineament within the search radius ❑ Number of lineaments crossing the search radius ❑ The total length of lineaments crossing the search radius ❑ Length of vector sum of unit vectors divided by number of vectors within the search radius – a complexity factor	35
	In total	69

GEUS stream sediment geochemistry data

The geochemical signatures for the three groups do not exhibit characteristic contrasts from background in the following chemical components: CaO, K_2O, P_2O_5, Sb, SiO_2, TiO_2, V, Zr, and Zn.

The three groups have high Ni/MgO and high Cs as common features, but they are different in the remaining part of their signatures. Medium to high Rb, La, U and Th characterise the Storø and Bjørneøen groups, while the Isua group has low values in these elements. The Bjørneøen and Isua groups have medium to high MgO, Fe_2O_3, Ni and Cr in common, while the Storø group is characterised by high Al_2O_3. The Isua group has low Na_2O compared to the other groups. Gold in the stream sediment geochemistry is only found to be indicative for the Isua group. An important observation, as high gold concentrations are relatively rare in stream sediment. The regional stream sediments do not reflect even the gold prospects at Storø – probably the sampling site is too far away from rich mineralisation. Arsenic is indicative for the Storø group only.

GEUS aeromagnetic data

Though a modestly significant signature is observed for the Storø group, no clearly significant signature is obtained for any of the groups in the total magnetic field intensity (TMI). Only the Isua group has a significant signature in the aeromagnetic datasets; characteristically very low and very high values are obtained in the vertical gradient of TMI (VG-TMI) and likewise, very high values are obtained in the amplitude of the horizontal gradients of the TMI (Amp.-HG-TMI). However, these signatures are weakly defined and a considerable portion of the showings within the group falls within the range of the background values.

GEUS aeroradiometric data

Aeroradiometric signatures are found to be indicative, especially for the Storø group. This group shows distinct high values in K, Th, Total gamma, U and U/Th ratio signature, which, for the K, Th, and Total gamma radiation, is different from the signatures of the other groups and the background. Moderate values in U and moderate to high values in the U/Th ratio distribution are found for the Isua group. Showings of the Bjørneøen group are not different from the background in the aeroradiometric data.

Statistically defined lineaments in GEUS aeromagnetic data

Only parameters representing a search radius of 1000 m have been included in the spatial analysis during the second phase. An indicative minimum distance between 1600–3000 m to nearest lineament, when all lengths of lineaments are considered, is found to be characteristic for the Bjørneøen group. When lineament lengths between 4250–23600 m (75–100%) are considered, an indicative minimum distance between 2000–3250 m is found for this group. For the Storø group an indicative mean direction between 0–25° is found when lineament lengths between 2450–3100 m (25–50%) are considered. When lineament lengths between 3100–4250 m (50–75%) are considered an indicative mean direction of 30° is established for this group. Several other parameters derived from statistically defined lineaments are found to be moderately indicative.

Table 5. *Schematic presentation of signatures in grid values of geochemical and geophysical parameters for gold showing groups against the background. Low, medium, high, highest refer to values relative to background. A full coloured cell marks where a signature is regarded indicative for the group (the likelihood ratio is above 0.7 to 0.8, preferably well above – see diagrams in Appendix C). A hatched cell refers to a signature, which is found to be moderately indicative. Non-coloured cells are non-indicative. Abbreviations used: TMI, total magnetic field intensity; VG, vertical gradient of TMI; Amp.-HG-TMI, amplitude of horizontal gradients of TMI. Minimum distance refers to the minimum distance to the nearest lineament within the search radius.*

Data	Storø group	Bjørneøen group	Isua group	Background
GEUS stream sediment geochemistry:				
Au	Low (as backg., 0-40 ppb)	Low (as backg., 0 – 40 ppb)	**High (> 60 ppb, bimodal)**	Low (0 – 40 ppb)
As	**High (> 20 ppm)**	Low (as backg., < 4 ppm)	Low (as backg., < 4 ppm)	Low (< 4 ppm)
Cs	**High (3.5 – 5 ppm)**	**High (3.5 – 5 ppm)**	**Highest (wide range, 3 – 6.5 ppm, multimodal)**	Low (< 2.5 ppm)
Rb	**High (40 – 80 ppm)**	**High (40 – 80 ppm)**	**High* (slightly lower than the two other groups, 30 – 70 ppm)**	Low (10 – 50 ppm)
La	**High (50 – 70 ppm)**	**Medium (35 – 55 ppm)**	**Low (30 – 10 ppm)**	Medium (wide range, 15 – 50 ppm)
U	**Highest (>80 ppm)**	**Medium (17 – 35 ppm, bimodal)**	Low (as backg., <15 ppm)	Low (< 15 ppm)
Th	**Highest (12.5 – 20 ppm)**	**High (10 – 15 ppm)**	Low (as backg., <8 ppm)	Low (< 12.5 ppm)
Ni/Mg ratio	**High (ratio 30 – 40)**	**High (ratio 30 – 37)**	**High (ratio 30 – 45)**	Low (wide range, ratio 10 – 35)
MgO	Low (2-3%)	**High (3.5 – 4.0%)**	**Medium – High (rel. wide range, 3.0 –-7.0%, bimodal)**	Low (wide range,1.5 – 4.5%)
Ni+Cr	Low (200 – 400 ppm)	**High (400 – 800 ppm)**	**Medium – High (rel. wide range, 300 – 800 ppm)**	Low (150 – 400 ppm)
Al_2O_3	**Highest (15.5 – 16.5 %)**	Low (as backg., 13.5 – 15.0 %)	Low (as backg., 14.0 – 15.5 %)	Low (wide range, 13.5 – 15.5 %)
Fe_2O_3	Low (as backg., 4 – 6 %)	**Medium (as backg., 6 – 7.5 %)**	**Highest (wide range, 7 – 12.5 %, bimodal)**	Low (wide range, 3 – 9 %)
Na_2O	High (as backg., 3.00 – 3.75 %)	**Medium (2.75 – 3.50 %)**	**Low (2.50 – 3.50 %)**	High (3.00 – 4.75 %)
V	Low (60 – 90 ppm)	**High (85 – 105 ppm)**	**High (70** – 150 ppm, multimodal)	Low – Medium (50 – 100 ppm)
Zn	**High (60 – 90 ppm)**	**High (55 – 85 ppm)**	**High (50 – 110 ppm, bimodal)**	Low – Medium (wide 20 – 100 ppm)
Zr	**Low (200 – 450 ppm)**	**Low (200 – 450 ppm)**	**Low (< 300 ppm)**	Medium – High (wide 150 – 900 ppm)

Table 5 (continued)

GEUS aeromagnetic data:				
TMI	**Low (-450 – -150 nT)**	Medium (-300 – 0 nT)	High (-400 – 400 nT)	Low (wide range, -400 – 700 nT)
VG-TMI	Medium (-0.2 – 0.2 nT/m)	Medium (-0.2 – 0.2 nT/m)	**Lowest and Highest (-0.5 – -0.25 nT/m and 0.4 to 0.75 nT/m)**	Medium (-0.3 – 0.4 nT/m)
Amp.-HG-TMI	Low (0 – 0.1 nT/m)	Low (0 – 0.1 nT/m)	**Highest (wide range, 0.1 – 1.0 nT/m)**	Low (0 – 0.25 nT/m)
GEUS aeroradiometric data:				
K	**High (1.75 – 2.5%)**	Medium (as backg., 0.25 – 1.5%, bimodal)	Medium (slightly lower than main backg., 0.50 – 1.25%)	Medium (0.25 – 2.5%l)
Th	**High (8 – 14 ppm)**	Low (as backg., 1 – 8 ppm, bimodal)	Low (4 – 8 ppm)	Low (1 – 10 ppm)
Total gamma	**High (main 10 – 13 Ur, bimodal)**	Low (as backg., 3 – 7Ur, bimodal)	Low (as backg., 5 – 8 Ur)	Low (1 – 10 Ur)
U	**High (2.5 – 5.5ppm, multimodal)**	Medium (0.5 – 1.5%)	**Medium (1 – 4 ppm, multimodal)**	Low (0 – 3 ppm, main <1.5 ppm)
U/Th ratio	**Medium – High (0.25 – 0.55)**	Medium – Low (0.5 – 0.30)	**Medium – High (0.10 – 0.65, multimodal)**	Low (0.00 – 0.30)
Distance to lineaments derived from aeromagnetic data within a search radius of 1 km:				
Minimum distance, all lines	**Medium (1200 – 2300 m)**	**High (1600 – 3000 m)**	Low (0 – 1200 m, as main backg.)	Low (wide, 0 – 3600 m)
Minimum distance, 0 – 25%	Low (1000 – 2200 m)	**Medium** (1st peak at 2000 – 2500 m, 2nd peak at 3000 – 4000 m, bimodal)	Medium – **High** (trimodal, **significant peak at 2500 m – 3500 m)**	Low – High (0 – 4500 m)
Minimum distance, 75 – 100%	**Medium – High (1250 – 3000 m)**	**High (2000 – 3250 m)**	Low (0 – 1500 m)	Low – High (0 – 3000 m)
Minimum distance, 90 – 100%	**Medium (1500 – 2250 m)**	**Medium (2500 – 3500 m)**	Low – Medium (bimodal, 500 – 1500 m and 3500 – 4500 m)	Low – High (0 – 6000 m)
Mean direction, 25 – 50% lines	**Low (0 – 25°)**	**Low and High (bimodal, significant peak 0 – 35°**, 2nd smaller peak 130 – 180°)	Low and High (bimodal, 10 – 30° and 150 – 180°)	Low – High (0 – 180°)
Mean direction, 50 – 75% lines	**Low (0 – 30°)**	**Medium – High (bimodal, significant peak 95 – 175°**, 2nd smaller peak 30 – 80°)	Medium – High (wide, 70 – 180°, bimodal)	Low – High (0 – 180°)
Total length, all lines	**Low < 5000 m**	Low (2500 – 3500 m)	Low– High (trimodal, 5000 – 22500 m)	Low – High (2500 – 25000 m)
Data	**Storø group**	**Bjørneøen group**	**Isua group**	**Background**

New gold potential maps

Gold potential maps for the three groups with different combinations of datasets have been produced, and they are shown and commented in the following.

The maps are constructed so that the top 1% most favourable area refers to the one percent of the pixels that has the highest favourability for gold showings. In this project, the study area encompass 342 182 pixels equal to 13 687 km^2. In this way, the 1% most favourable pixels correspond to a favourable area covering 137 km^2.

The colour scales of the potential maps are not linear and vary a little between prediction maps with respect to the intervals in favourability. Furthermore, the favourability given as percentage (e.g. top 0.5% most favourable) does not always match the percentage area of the total study area (0.5% of the study area equals 68.5 km^2). These circumstances are to be expected as the predictions are based on empirical estimations. The method of constructing a gold potential map is described in Nielsen *et al*. (2004).

It is evident that low resolution in geochemical data as well as the problem of accuracy in location due to changing topographical base must have resulted in variable displacements of features influencing the signatures of the pixels. Therefore, it is, advisable to consider the nature of the data used to construct the maps when interpreting the significance and exact location of gold favourable areas. The sample locations of stream sediments are shown in many of the following maps to help the reader in this respect. More information about the regional data is given in Nielsen *et al.* (2004) and in the present report, and literature references are given to the data sources.

Favourability for the Isua gold showing group

Map based on stream sediment geochemistry data – Isua group

A gold potential map based on the indicative stream sediment geochemical parameters, Au, Cs, La, MgO, Fe2O, Na_2O, Ni+Cr and Ni/Mg-ratio is shown in Figure 20.

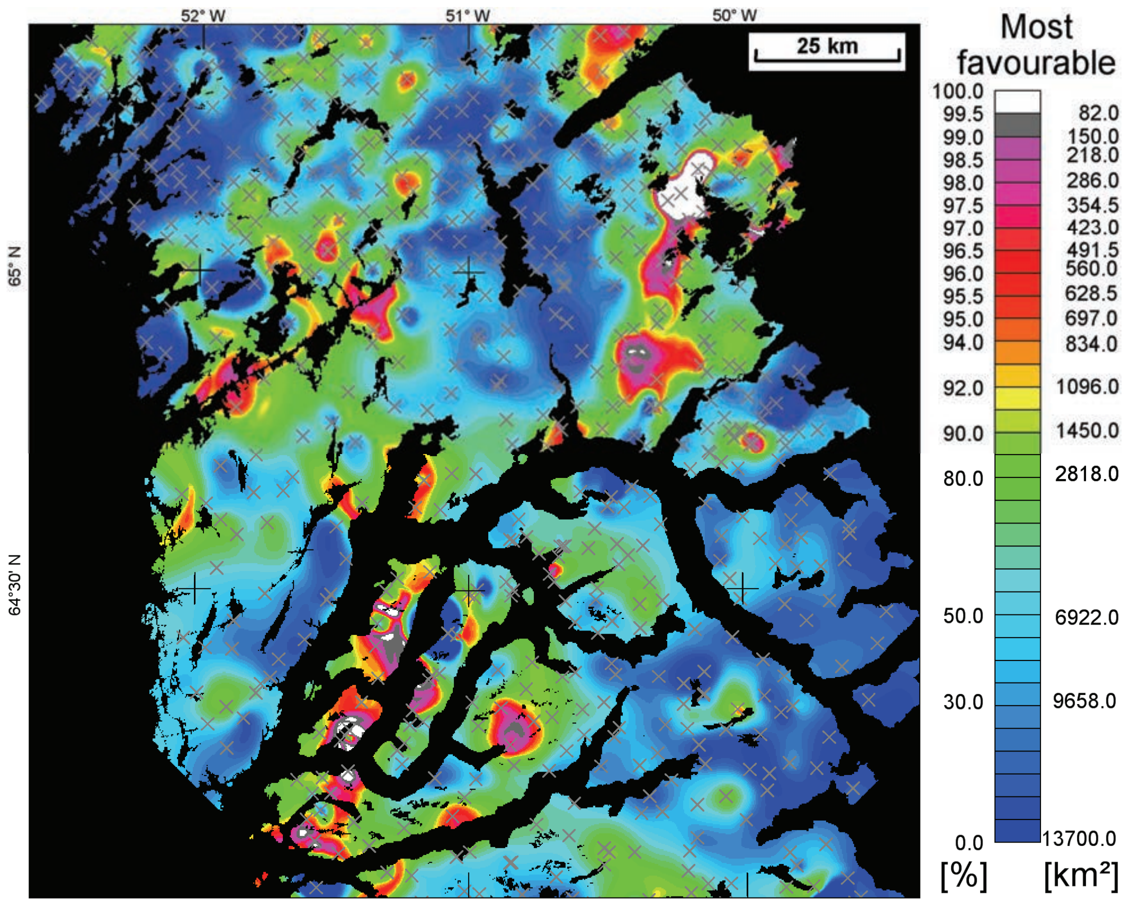

Figure 20. *Gold potential map for the Isua group based on indicative parameters of fine fraction stream sediment geochemistry: Au, Cs, La, MgO, Fe_2O_3, Na_2O, Ni+Cr and Ni/Mg-ratio distribution. The top 0.5 % most favourable area is shown in white.*

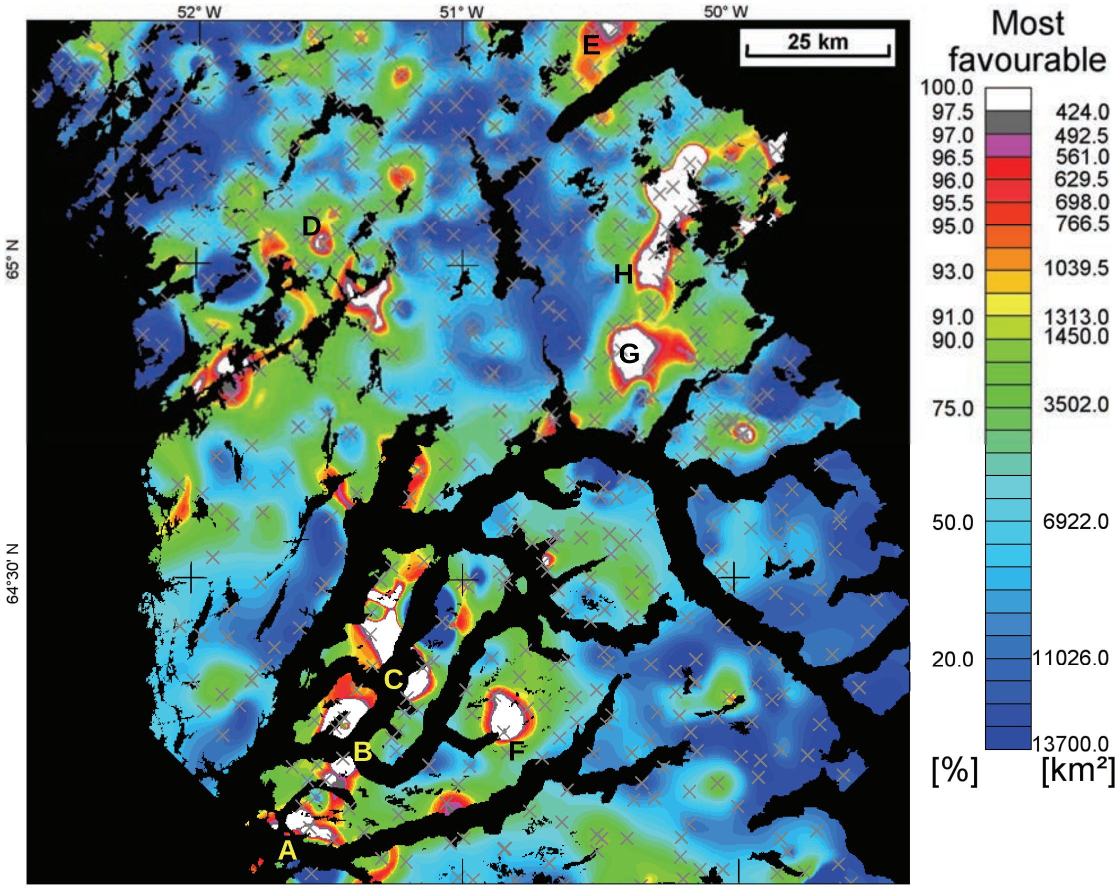

Figure 21. *The top 2.5% most favourable area in white, otherwise as in Figure 20.*

Areas with known gold mineralised sites:
Not surprisingly, areas immediately surrounding the showings at Isua are outlined as being within the top 0.5% most favourable area (Fig. 20). One of the showings of the Isua group is located in the Ivisaartoq supracrustal belt; an belt known to contain several gold mineralised localities in mafic metavolcanic rocks (Appel *et al.* 2003; Downes & Gardinev 1986). This area is also outlined as being within the top 0.5% most favourable area. Other top 0.5% areas are located on the south-eastern part of Sermitsiaq. Gold concentrations in the range of 0.1 ppm have been recorded from these areas (Dunnells 1995, and pers. com, H. Stendal, GEUS).

Areas outside known gold mineralised sites:
A couple of small areas in the outer and inner part of Fiskefjord are within the top 2.5% most favourable areas (Fig. 21). These areas comprise amphibolite units, in some locations with neighbouring or intercalated ultrabasic and noritic rocks.

The most interesting top 2.5% most favourable areas outside known gold mineralisation in Figure 21 coincide with supracrustal rocks south of Kobbefjord (A in Fig. 21), with supracrustal rocks west of at Serfarssuit (B in Fig. 21), with supracrustal rocks at the western part of central Storø (C in Fig. 21), and occur north of inner Tasiussarssuaq (D in Fig. 21), and north of the inner part of the glacier Serpaq Sermia (E in Fig. 21).

The Isua group gold potential map outlines areas that were already outlined in the first phase of the project and were visited during the 2005 field season. These areas are located east of the fjord Qooqqut (F in Fig. 21), in the central part of Ujarassuit Nunaat, north of the fjord Ujarassuit Paavat (G in Fig. 21) and north of the lake Tussaap Tasia, north-eastern part of Ujarassuit Nunaat (H in Fig. 21). Fieldwork in these areas has so far been unable to return any elevated gold contents in rock samples.

Map based on stream sediment geochemistry and aeromagnetic data – Isua group

A gold potential map based on geochemical as well as geophysical parameters found to be characteristic of the Isua group is presented in Figure 22. The parameters VG-TMI and Amp.-HG-TMI from regional aeromagnetic data were used.

Areas with known gold mineralised sites:

The top 0.5% areas with known gold showings (Fig. 22), are the same as those outlined in the gold potential map based only on stream sediment data (Fig. 21).

Favourable areas outside known gold mineralised sites:

Small favourable areas in the outer and inner part of Fiskefjord, which were predicted as being part of the top 2.5% area in the map based on indicative stream sediment geochemistry only (Fig. 21), are now outlined as being within the top 0.5% most favourable area for showings similar to Isua groups (Figs 22 and 23). However, small differences in the location of the most favourable areas in the Fiskefjord are observed. These areas are located within amphibolite units, in some cases with neighbouring or intercalated ultrabasic and noritic rocks. Other favourable areas, without known gold showings, discussed for the top 2.5% in the potential map based only on indicative stream sediment data, are still predicted when including the aeromagnetic data. However, changes in the shape and sizes of the different top 2.5% most favourable areas are observed.

An area just northwest of Nuua (A in Fig. 24), which was not predicted as a part of the top 2.5% area in the map based on stream sediment geochemistry alone, is now included.

Another previously unpredicted top 2.5% area occurs within and adjacent to supracrustal units in the western part of the Qussuk peninsula (B in Fig. 24). This area was not outlined as being within the top 2.5% in the potential map based only on stream sediment geochemistry (Fig. 24). The favourable area is adjacent to the sites where 2004 and 2005 fieldwork have collected rock and soil samples with gold contents in the range of 1 – 8 ppm (Hollis 2005; Hollis *et al.* 2006; Hollis *et al.* 2004).

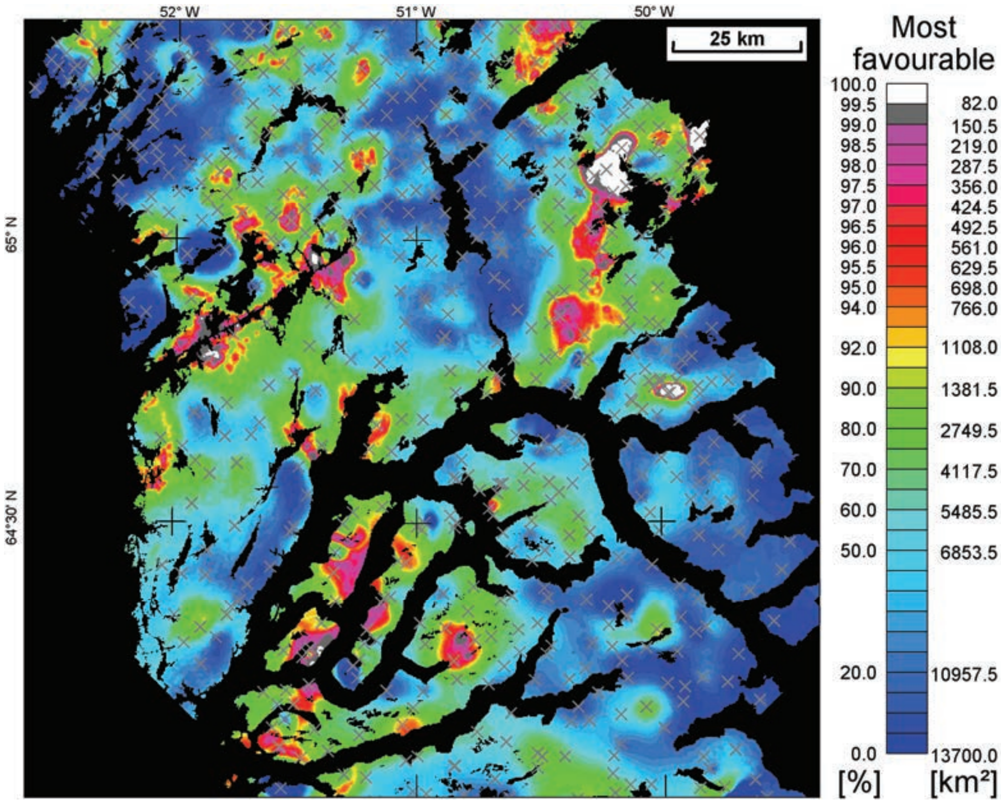

Figure 22. *Prediction map for the Isua group of gold showings. White areas depict the top 0.5% (68.5 km^2) most favourable area for showings similar to the Isua showings. Second most favourable 0.5% area is shown in grey. The map is based on the 19 showings of the group, and Au, Cs, La, MgO, Fe2O, Na2O, Ni+Cr and Ni/Mg-ratio from fine fraction stream sediment geochemistry, and VG-TMI and Amp.-HG-TMI from regional aeromagnetic data.*

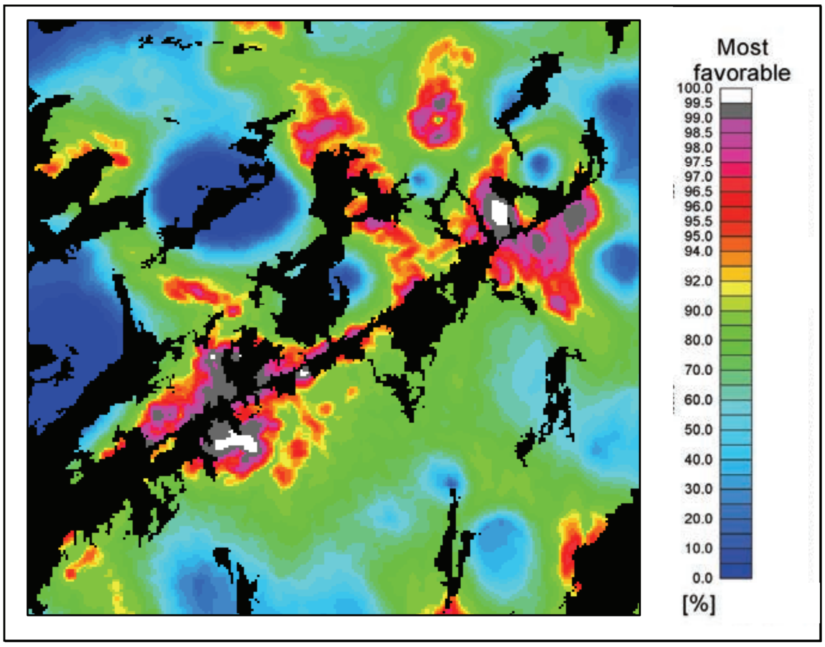

Figure 23. *Areas in Fiskefjord outlined as being within the most favourable 0.5% area in the gold potential map for the Isua group. The map is an enlarged part of the map in Figure 22.*

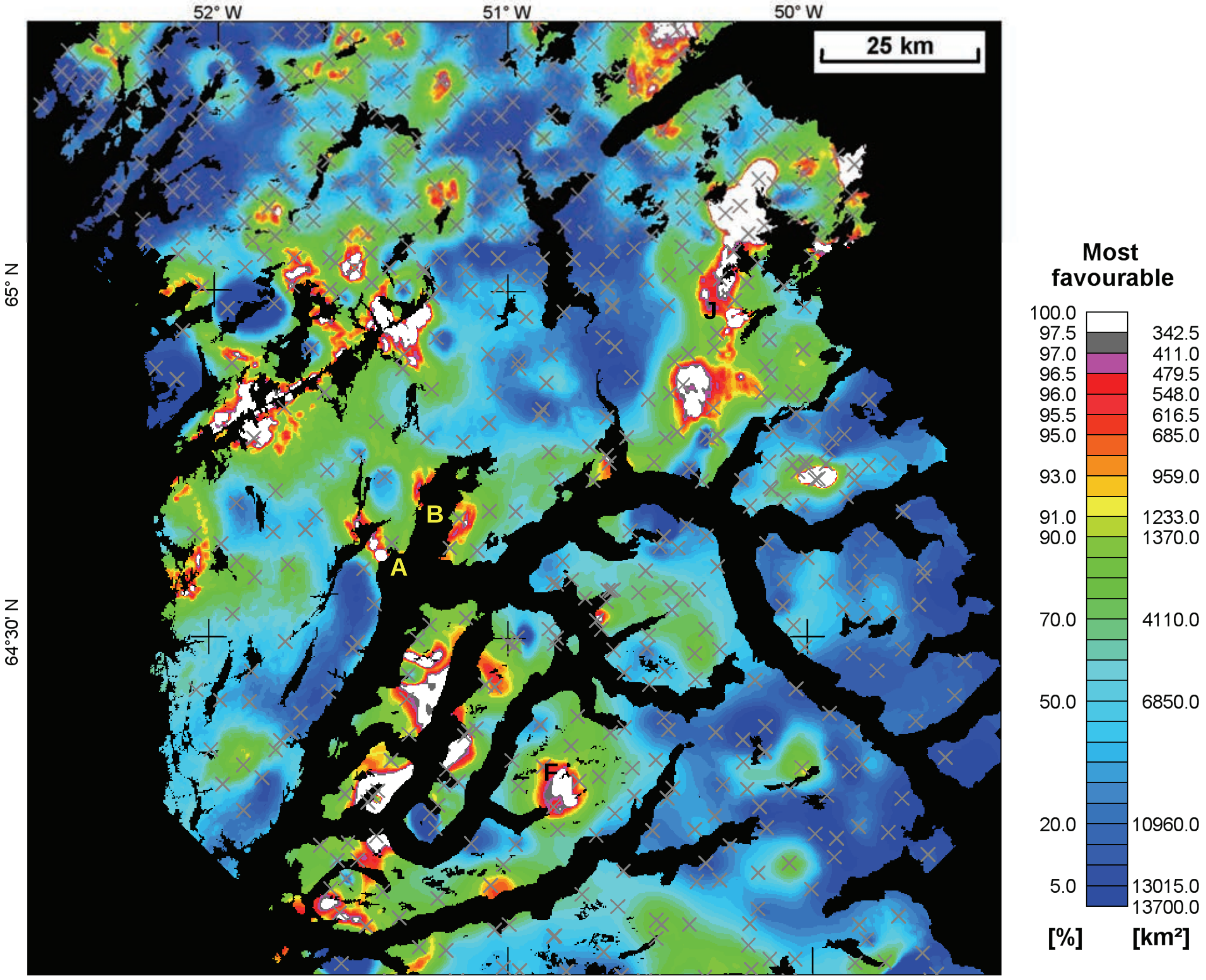

Figure 24. *Top 2.5% most favourable area in white for Isua group showing. The map is based on the 19 showings of the group, and Au, Cs, La, MgO, Fe2O, Na2O, Ni+Cr and Ni/Mg-ratio from fine fraction stream sediment geochemistry, and VG-TMI and Amp.-HG-TMI from regional aeromagnetic data. Crosses indicate locations of stream sediment samples. Letter labels are referred in text.*

It is interesting that the area at Qussuk peninsula is designated as favourable in the statistical analysis (Fig. 25.A). The top 2.5% most favourable pixel values are situated approximately 800 m west of the site where gold bearing samples have been taken but when the top 5.5% most favourable area is considered (Fig. 25.B), the gold bearing site is fully included in the favourable area. The reason why the pixels with favourable signatures are displaced from the recorded gold mineralisation is related to the fact that the pixel values are determined by interpolation of data from stream sediment samples collected away from the sites, where gold was found. In a regional scale, the stream sediment samples are picking up the chemical characteristics of the metavolcanic rocks, but the interpolated distribution pattern does not necessarily coincide with the narrow belts in which these rocks occur (Figures 25.A and 25.B).

Likewise, the scarcity of stream sediment samples north of the head of the Qussuk bay explains why the continuation of the supracrustal belt with one gold mineralised site could not be identified as favourable. Additional samples are needed towards Qussuk to the north and Godthaabsfjord to the south in order to produce a more accurate mapping of the gold-favourable structure by this method. Furthermore, the grids of aeromagnetic data used as input in the statistical analysis show that the trend of the 5.5% most favourable area to a large degree is determined by a trend of negative gradient values in the vertical gradient of TMI and the amplitude of the horizontal gradients of the TMI (see e.g. Figure 25.D).

The case at the Qussuk peninsula illustrates the complexity of merged data patterns, which is the prerequisite for the predictions. It also illustrates why a detailed investigation of the underlying data is necessary to judge the validity of the predicted areas, and how additional and more closely spaced samples are likely to increase the resolution of the prediction results.

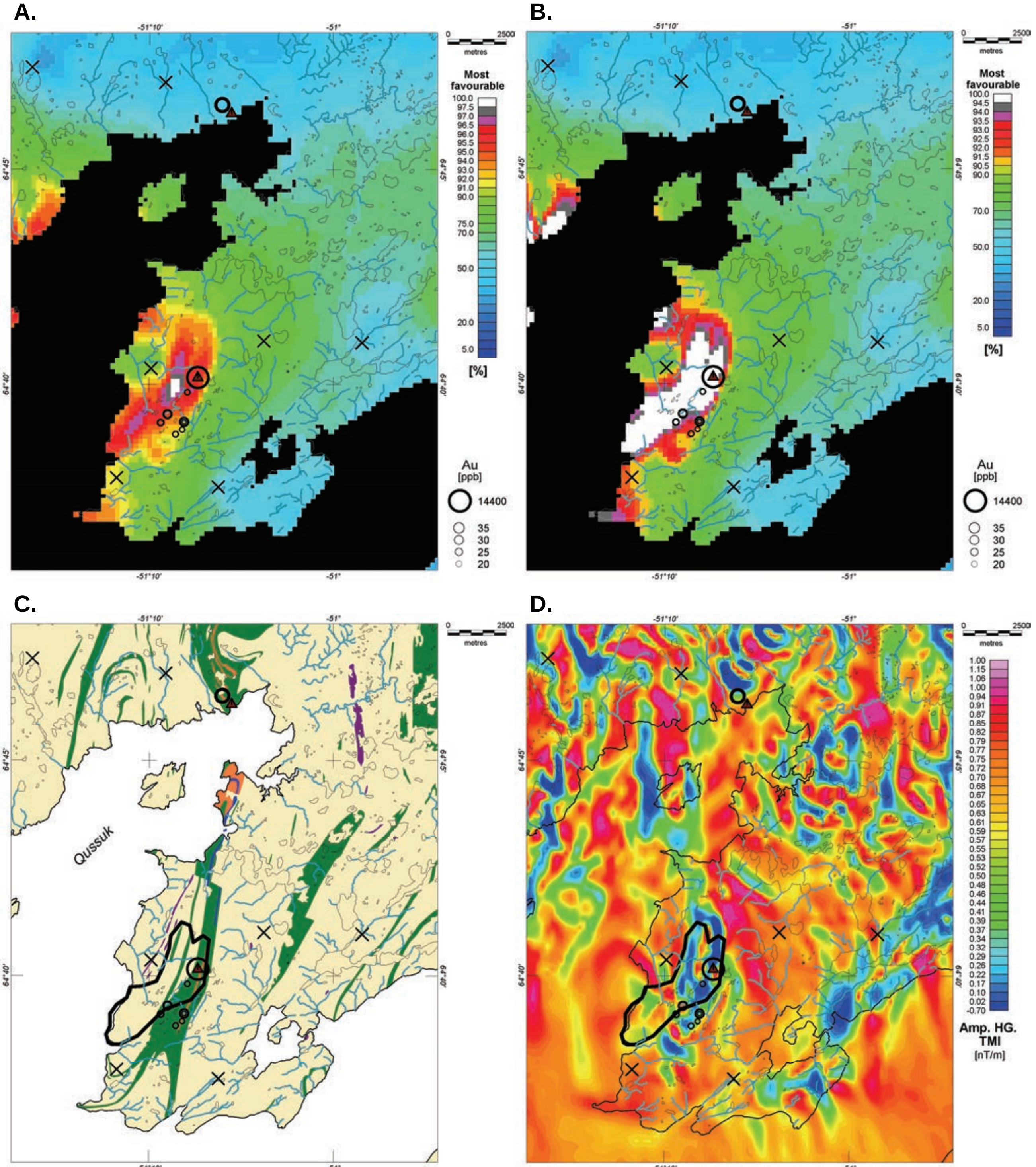

Figure 25. *Potential map for Isua group gold showings for the peninsula east of Qussuk. Enlarged part of map in Figure 24. **A** shows the top 2.5% most favourable area, **B** the top 5.5.% area. Crosses mark regional stream sediment sample sites. Filled triangles mark sites with more than 1 ppm Au in rock samples. **C** Simplified geological map of the Qussuk area (1: 100 000). Colour codes: amphibolites in green, metasediments in orange, ultrabasic rocks in purple, metagabbros in blue. Orthogneiss and granite in moccasin. Rivers and streams are given in greenish blue. **D** Grid image of the amplitude of horizontal gradient of the TMI. Other symbols as in A and B. The top 5.5% area is outlined in black in the two lower figures.*

Map based on stream sediment geochemistry, aeromagnetic, and aeroradiometric data – Isua group

A map including stream sediment geochemical, aeromagnetic and aeroradiometric parameters characteristic of the Isua group is presented in Figures 26 and 27.

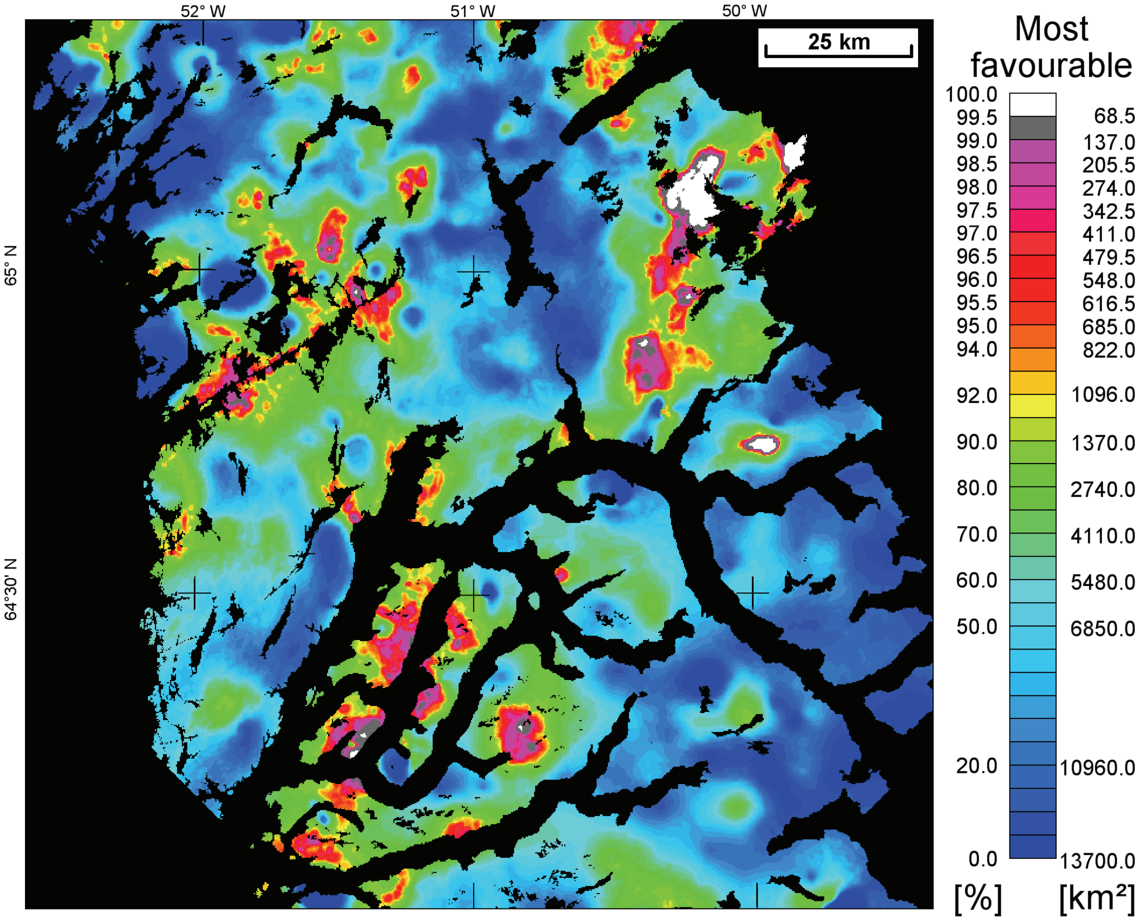

Figure 26. *Gold potential map for the Isua groups based on the datasets: Au, Cs, La, MgO, Fe2O, Na2O, Ni+Cr and Ni/Mg-ratio from fine fraction stream sediment geochemistry, VG-TMI and Amp.-HG-TMI from regional aeromagnetic data, and U/Th ratio from regional aeroradiometric data. The top 0.5% most favourable area is shown in white.*

When the aeroradiometric datasets are added to the statistical analysis, the prediction results will change again. A comparison of the gold potential maps in Figures 27 and 24 reveals that some favourable areas remain almost unchanged (J and K in Fig. 27), some grow (B, C and H in Fig. 27) or shrink (E in Fig. 27) in extent, and some new areas emerge (A in Fig. 27), when the aeroradiometric data are included in the analyse. The aeroradiometric U/Th ratio can be seen in **Figure 57**. As described in a previous section, the irregular distribution and resolution of these data has made it necessary to give some areas an artificial background value, where the distance to nearest measurement is too great. Unfortunately, this is the case a large area at Fiskefjord. However, the favourable areas outlined in the analysis based on stream sediment geochemistry and aeromagnetic data are still present (F in Fig. 27), and are not distorted by the inclusion of the aeroradiometric data. A likely explanation for this is that the resemblance of the geochemical and aeromagnetic signatures characteristic for the Isua group is so strong in this area that the aeroradiometric data only to a small degree changes the prediction patterns.

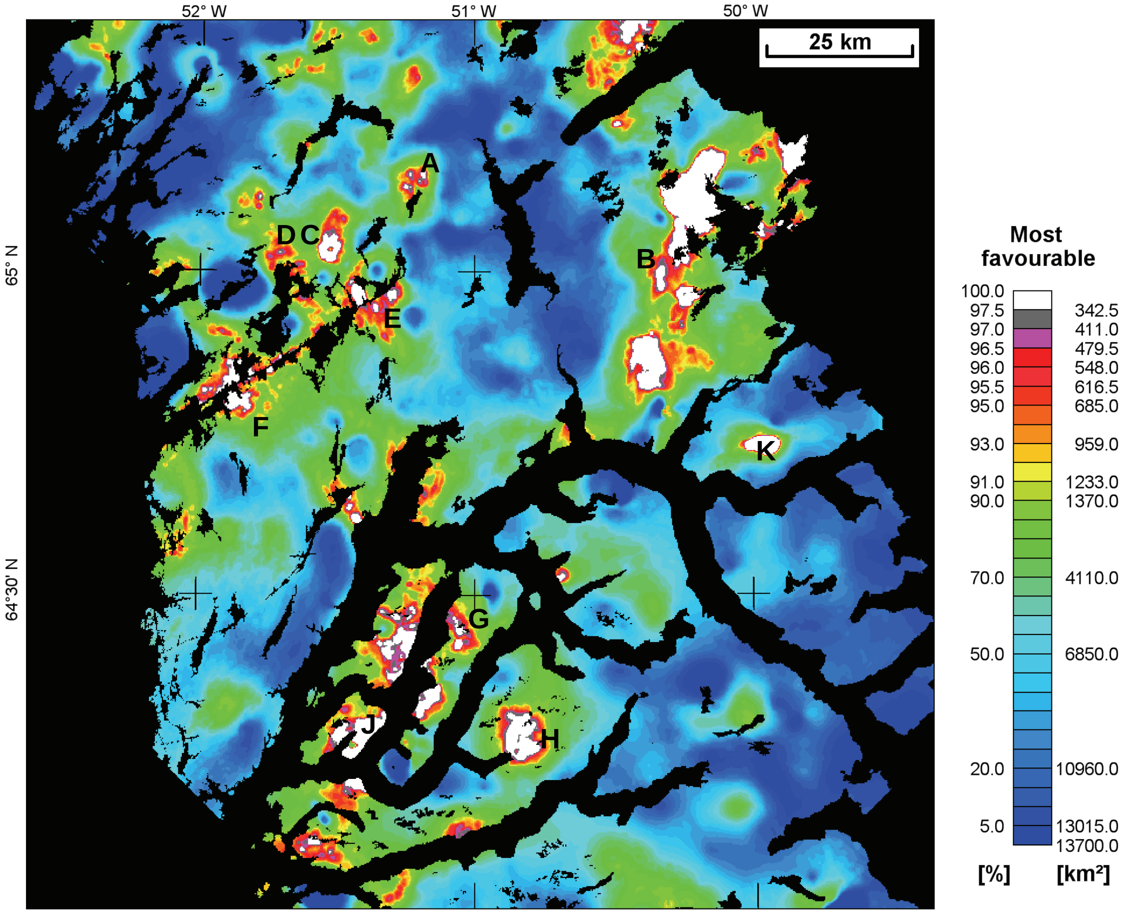

Figure 27. *Gold potential map for the Isua groups based on the datasets: Au, Cs, La, MgO, Fe2O, Na2O, Ni+Cr and Ni/Mg-ratio from fine fraction stream sediment geochemistry, VG-TMI and Amp.-HG-TMI from regional aeromagnetic data, and U/Th ratio from regional aeroradiometric data. The top 2.5% most favourable area is shown in white.*

Favourability for the Bjørneøen gold showing group

Map based on stream sediment geochemistry data – Bjørneøen group

The most favourable 0.5% and 2.5% areas for the Bjørneøen group are shown in Figures 28 and 29. The indicative data for the group analysed are: Cs, Rb, U, Th, Mg, Ni+Cr and Ni/Mg-ratio distribution from the fine fraction stream sediment geochemistry. That the resulting gold potential only is based on gridded stream sediment geochemistry is clearly seen in the prediction patterns, which reflects the circular anomaly patterns of the gridded data.

A major problem with these data is that no stream sediments samples have been collected within the areas adjacent to the Bjørneøen gold showings. Judged from the topography and courses of rivers only one, maximum two sampling sites, west of the showings at Bjørneøen can be said to represent the geochemical signature of the showings and no samples are located east of the site or within the supracrustal rocks (Fig. 30). This means that stream sediment samples on Storø can influence the geochemical patterns on eastern Bjørneøen, as the gridding in the current datasets are carried out over the entire surface. It seems, however, that the supracrustal rocks hosting the showings are partly covered by pixels with high favourability.

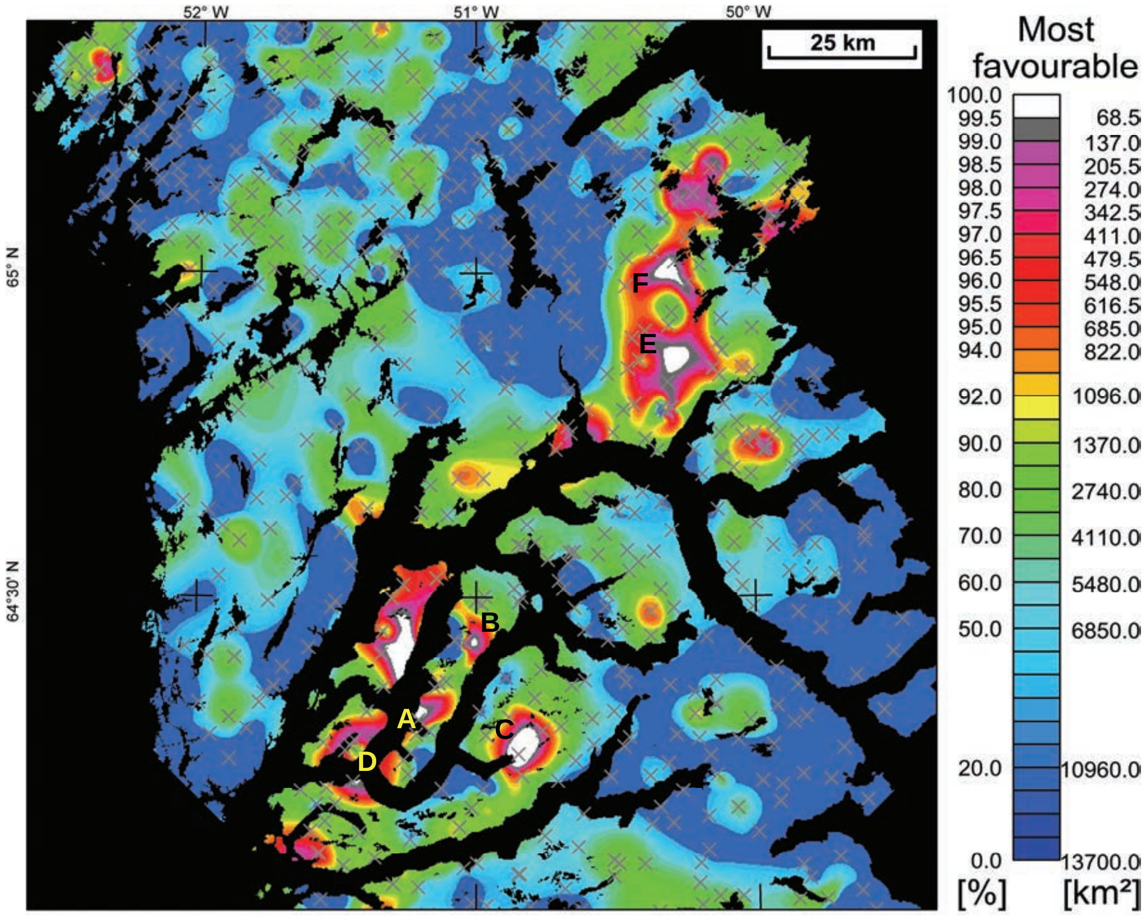

Figure 28. *Gold potential map based on the 10 showings of the Bjørneøen group and Cs, Rb, U, Th, Mg, Ni+Cr and Ni/Mg-ratio distribution from the fine fraction stream sediment geochemistry. The predicted top 0.5% most favourable areas are shown in white.*

Areas with known gold mineralised sites:

As for the Isua group, it is not surprising that areas immediately surrounding the showings at Bjørneøen are outlined as being within the top 0.5% most favourable area. It seems that the top 0.5% most favourable area to some degree mimics the distribution of the supracrustal rocks (Fig. 30). It is obvious, though, that the shape of the high-favourability area is determined by the interpolation patterns in the gridded stream sediment data (Fig. 31).

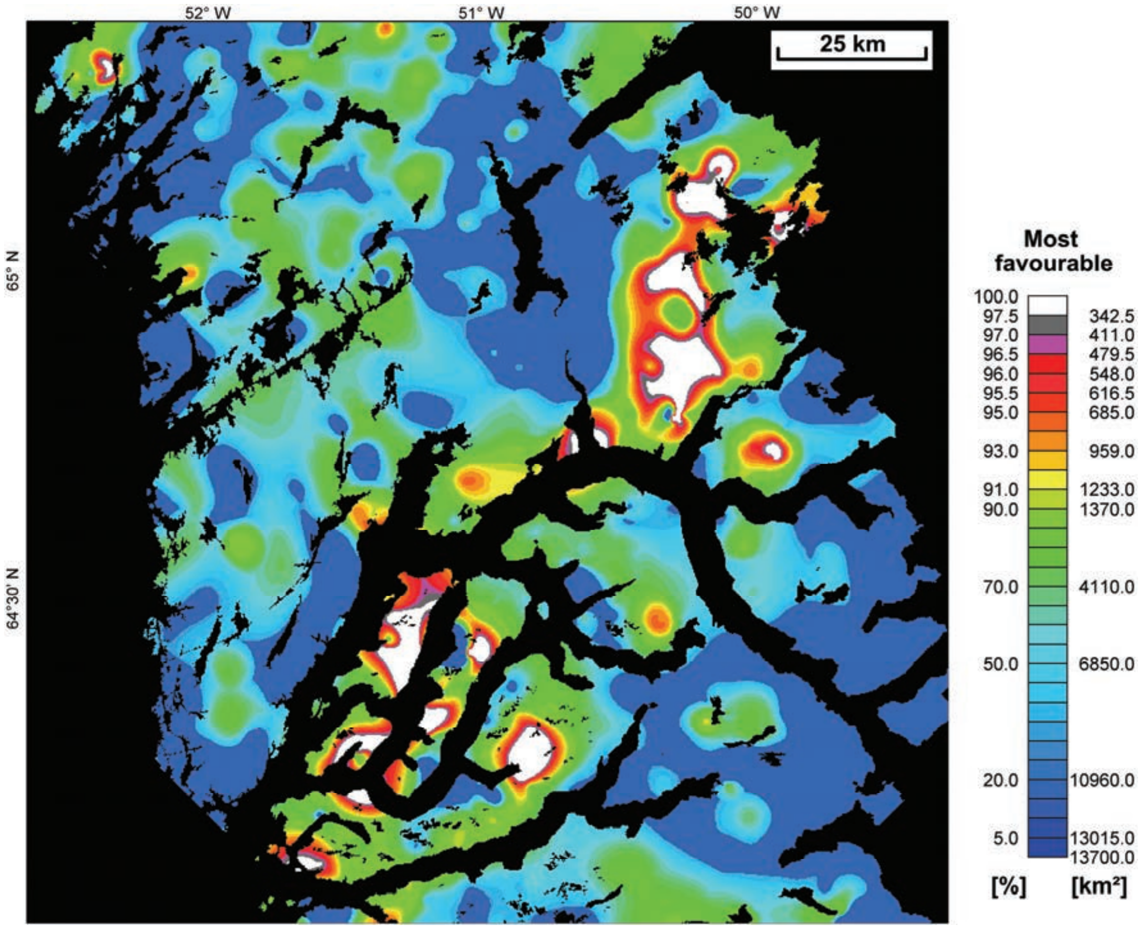

Figure 29. *Gold potential map based on the 10 showings of the Bjørneøen group and Cs, Rb, U, Th, Mg, Ni+Cr and Ni/Mg-ratio distribution from the fine fraction stream sediment geochemistry. The predicted top 2.5% most favourable areas are shown in white.*

Areas with no known gold mineralised sites:

An area at Nuukutdlak, central western Storø, and an area in the northeast of central Storø (A in Fig. 28) are predicted as being within the top 0.5% most favourable area (B in Fig. 28). It is interesting, that both areas are within the southwest and eastward extension of the supracrustal sequences (see Fig. 30) hosting the Qingaaq and Aappalaartoq gold prospects. An area is also outlined with the top 0.5% east of the fjord Qooqqut (C in Figs 28 and 30), also predicted in the first phase of the project. Again, this area coincides with supracrustal rocks (McGregor 1983). Follow-up by GEUS during the field season 2005 in this area did not reveal any elevated gold content (see earlier sections). However, the commercial exploration company NunaMinerals A/S has reported gold in the range of 200–300 ppb in rock samples from this area. At Serfarssuit (D in Figs 28 and 30), a small area is also outlined as having a top 0.5% favourability. This area was also predicted as being within the top 2.5% area for the Isua group. As the two groups have common indicative datasets this is possible. The area at Serfarssuit intersects also supracrustal rock units (McGregor 1983). Stream sediment samples taken by GEUS during the 2005 field season in this area yields elevated gold content in the range of 21-50 ppb Au (Hollis *et al.* 2004). Two other large top 0.5% favourable areas are predicted in the inner part of the Godthaabsfjord (E and F in Fig. 28). These were also predicted being part of the 2.5% most favourable area for the Isua group (I and J in Fig. 21) but as mentioned, follow up in these areas has so far not returned any notable gold content.

Map based on stream sediment geochemistry and lineaments in aeromagnetic data – Bjørneøen group

The minimum distance to nearest lineament (for a search radius of 1000 m) for all lengths of lineaments defined in regional aeromagnetic data, have been found to be indicative for the Bjørneøen group. An analysis including both this dataset and the indicative stream sediment geochemistry datasets have been carried out. The resulting gold potential map is presented in Figure 32. Only minor changes in the prediction patterns are observed (Fig. 33), when comparing the results of the analysis excluding (Fig. 28) and including the minimum distance to nearest lineament (Fig. 32). This is probably because the indicative signatures in the stream sediments geochemistry data are so strong that they dominate the signatures in the lineament data.

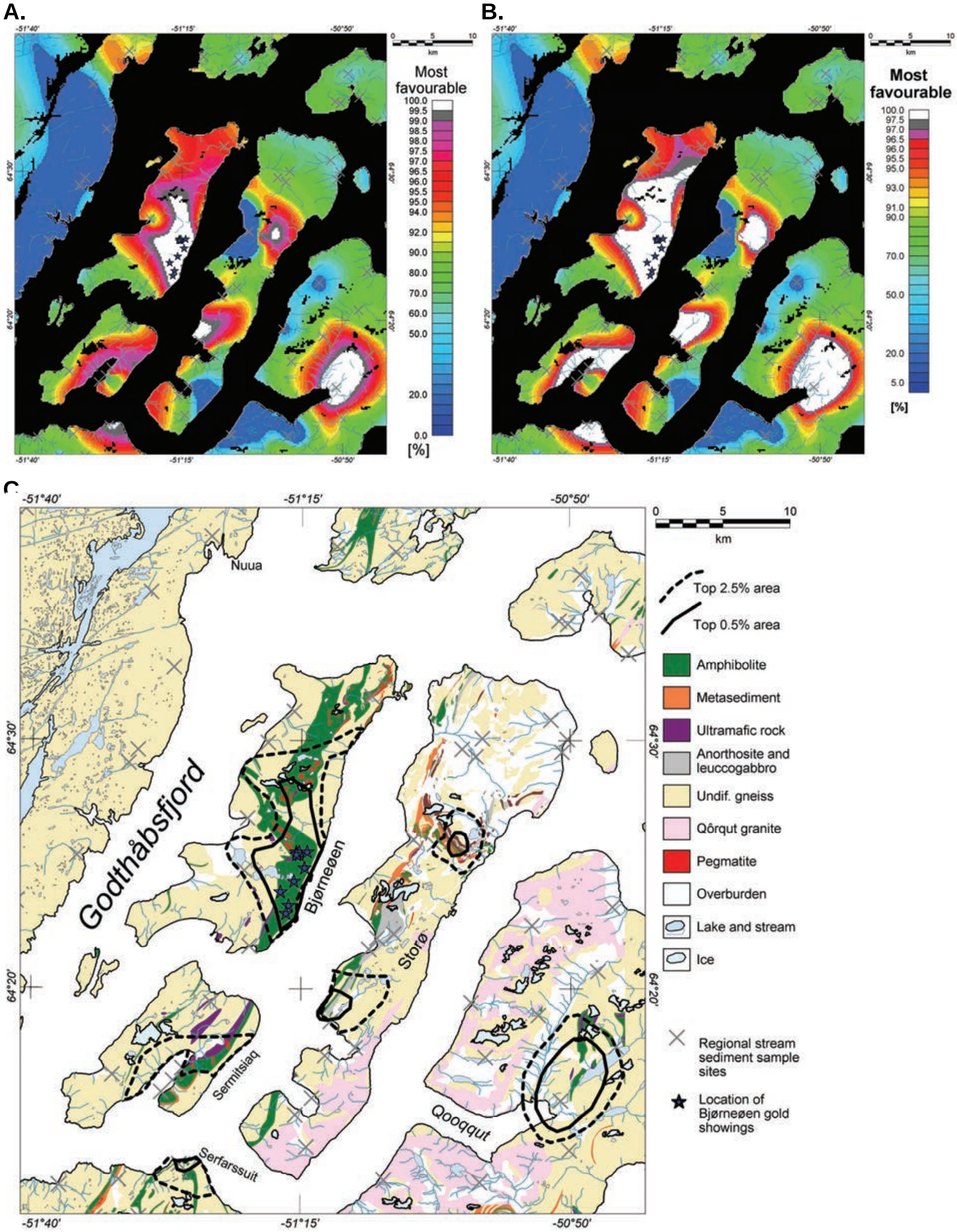

Figure 30. *Gold favourable areas in central Godthåbsfjord region. The potential maps are based on the same datasets as in Figure 28. A. Top 0.5% most favourable areas, B. top 2.5% most favourable areas. Crosses mark regional stream sediment sampling sites. C. Lithological map with outline of the top 0.5% and 2.5% most favourable areas for gold.*

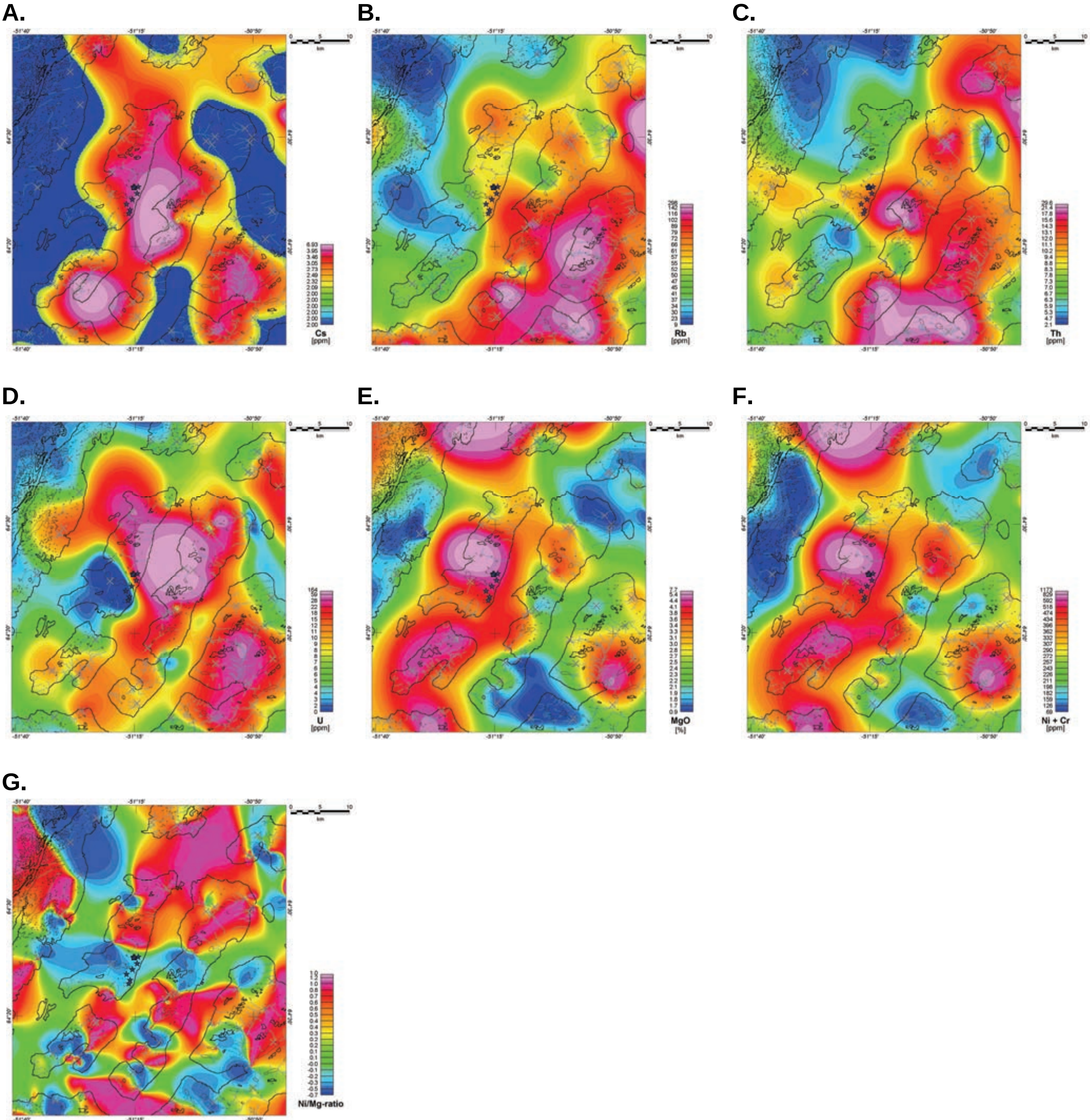

Figure 31. *Grid images of seven stream sediment geochemical parameters indicative for the Bjørneøen gold showings (marked with dark blue stars) that have been used as input in the construction of gold potential maps. The grid maps only cover the central part of the study area. Grey crosses mark stream sediment sample sites.*

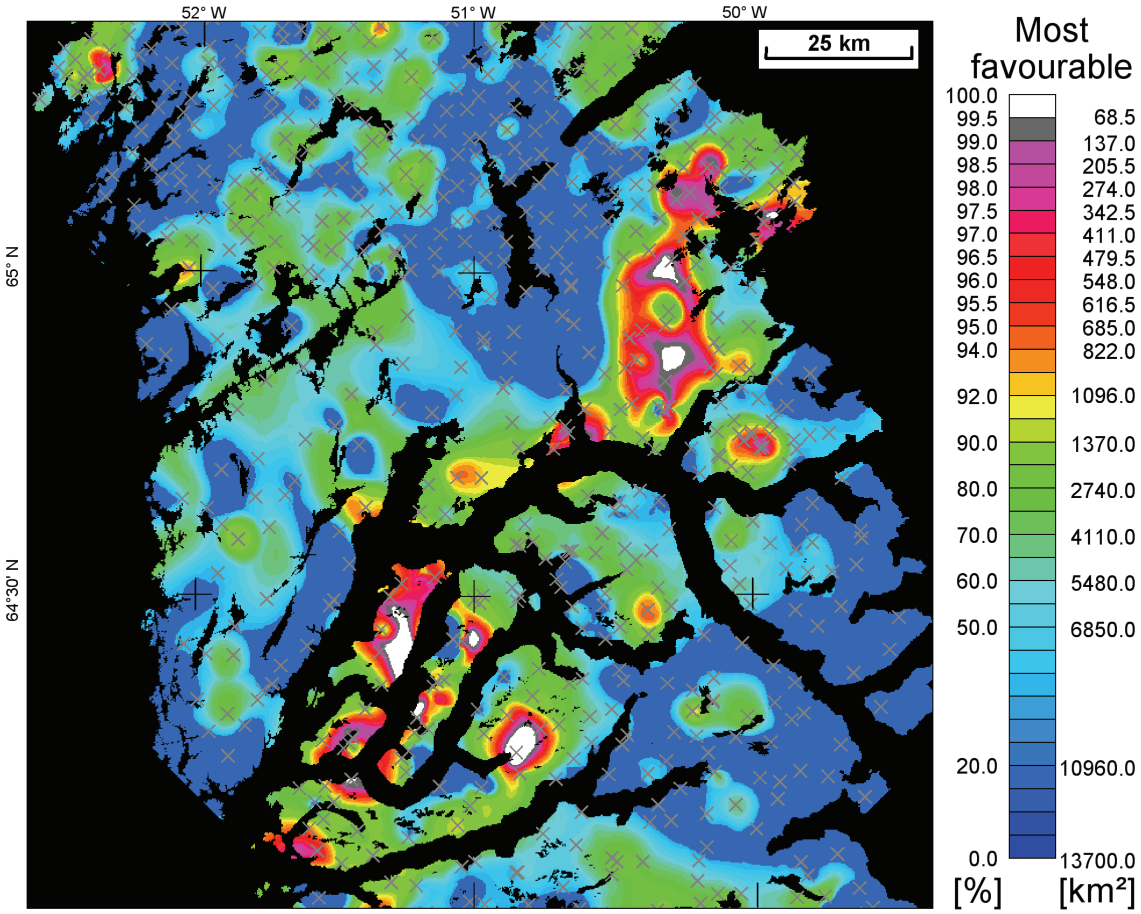

Figure 32. *Predicted favourable areas for Bjørneøen gold showings based on indicative stream sediment geochemistry (as in Fig. 28) and minimum distance to nearest lineament (within a search radius of 1000m) for all lineament lengths derived from aeromagnetic data (Fig. 60). The top 0.5% most favourable area is shown in white.*

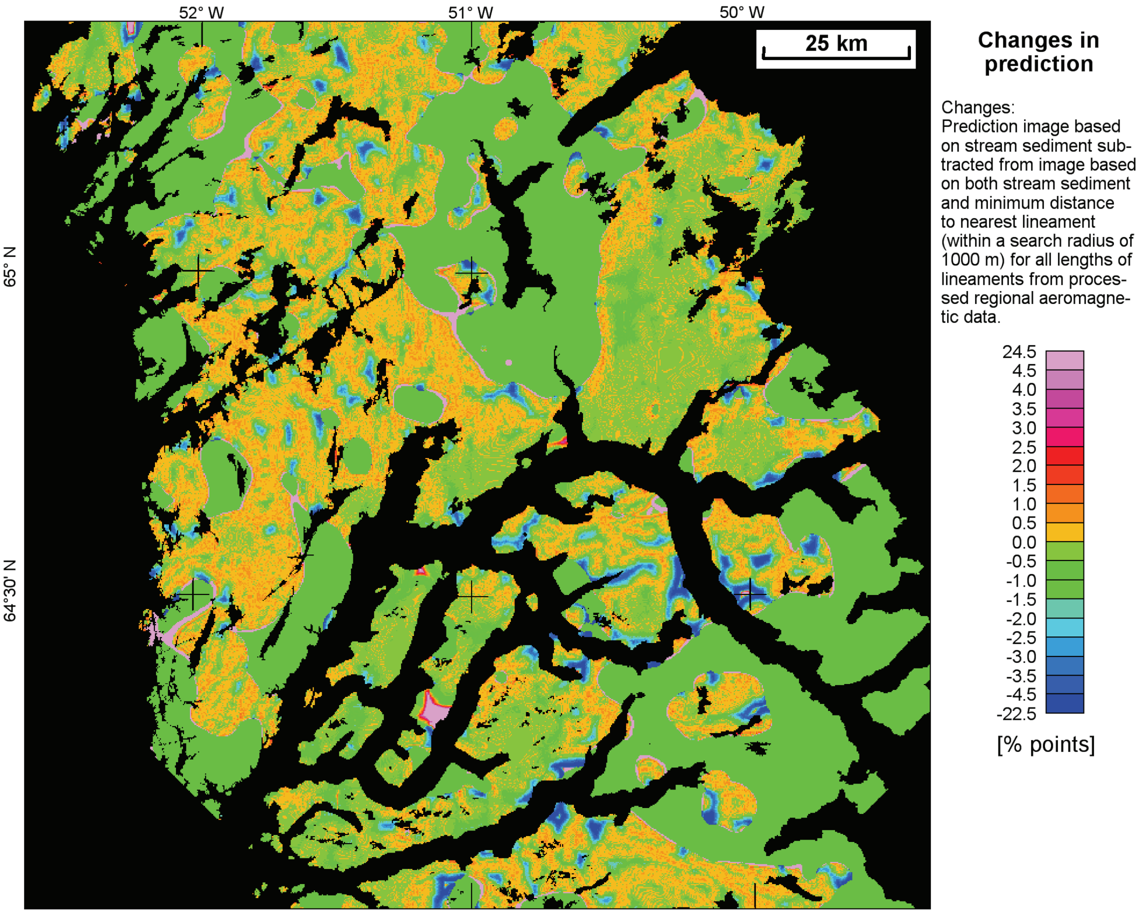

Figure 33. *Differences in percent points between the predictions based on stream sediment geochemistry, and stream sediment geochemistry and minimum distance to nearest lineament from regional aeromagnetic data.*

Favourability for the Storø gold showing group

Map based on stream sediment geochemistry – Storø group

A data analysis based on the 11 showings of the Storø group and the distribution of indicative parameters Al_2O3, As, Cs, La, Rb, Th, U, and Ni/Mg-ratio, the top 0.5% most favourable area only identify a small area at Storø adjacent to the showings. All other areas are predicted as being within the same prediction class. This happens because of a unique signature of the Storø group. Firstly, the showings of the Storø group are situated closely to each other, which imply that the signature of the group is confined to a very small area making the signature very distinct. Furthermore, the high level of As (above 20 ppm) in stream sediment geochemistry is a unique signature of the Storø group (Fig. 35). Although the high-As signature is very indicative for the gold showings at Storø, it is possibly not useful to use it in an attempt to identify areas similar to the Storø showings in other signatures. Consequently, the statistical analysis has been performed without taking the As signature into account. The results are shown in Figure 36. The prediction patterns are still governed by the very distinct and unique signature for the Storø group, but new favourable areas for the Storø group are predicted.

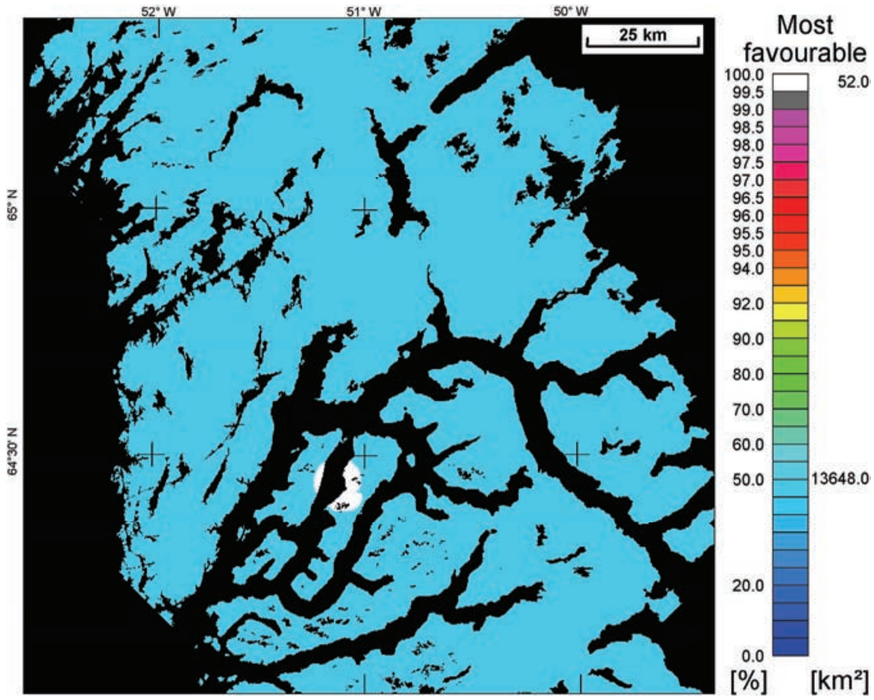

Figure 34. *Gold potential map for the gold showings of the Storø group based on the distribution of Al_2O3, As, Cs, La, Rb, Th, U, and Ni/Mg-ratio in fine fraction regional stream sediment geochemistry.*

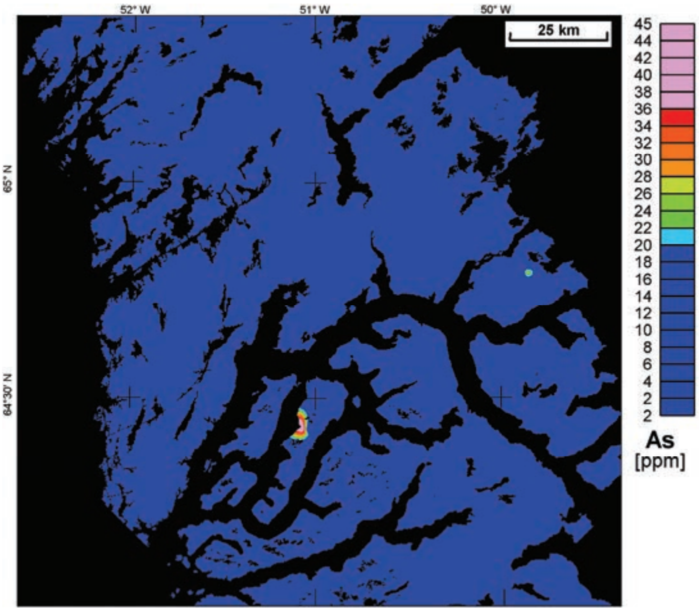

Figure 35. *Distribution of As in fine fraction stream sediment geochemistry. Values above 20 ppm are only encountered at central Storø close to the Qingaaq and Aappalaartoq gold prospects.*

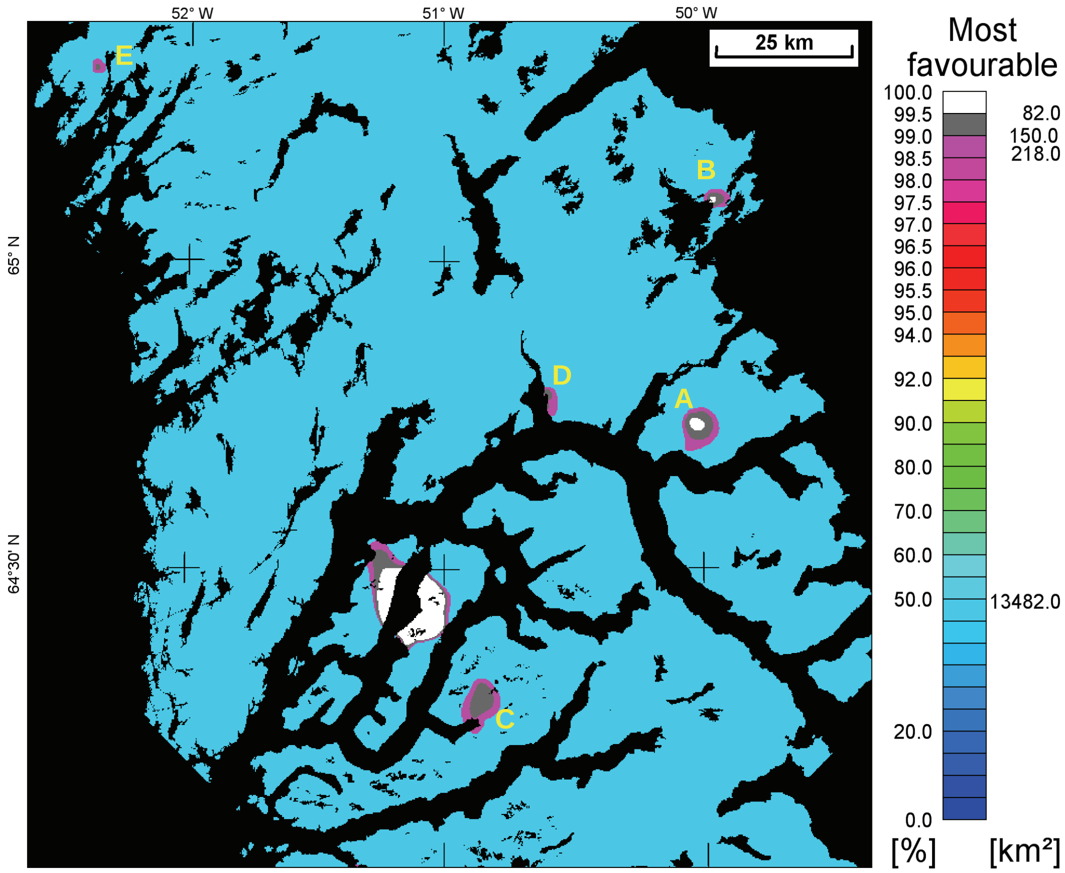

Figure 36. *Gold potential map for the gold showings of the Storø group based on the distribution of Al_2O_3, Cs, La, Rb, Th, U, and Ni/Mg-ratio in fine fraction regional stream sediment geochemistry, i.e. As is not included. Compare with Figure 34).*

Areas with known gold mineralised sites:

Beside the favourable area around the showings at Storø, an area at western Ivisaartoq (A in Fig. 36) appears from the prediction analysis to be within the top 0.5% most favourable area, when As is excluded from the prediction analysis. The area falls within the Ivisaartoq supracrustal belt, which is known to host several mineralised sites (Appel *et al.* 2003; Downes & Gardinev 1986; NunaMinerals 2006). Another area, though much smaller, is located southwest of Isukasia (B in Fig. 36). A relative large numbers of gold mineralised sites within this belt are well documented (e.g., Appel *et al.* 2003; Bliss 1996; Olsen & Grahl-Madsen 1994). However, the favourable area falls just south of the Isua supracrustal belt. This was also outlined in the first phase of the project and GEUS geologists made a very short visit to the area during the 2005 field season (see above). The few samples from the area did not return elevated gold contents. The Qooqqut lake area (C in Fig. 36) is covered by the next favourability class, and it has been assigned favourable in the gold potential maps for some of the other groups. Though follow-up has failed to return any elevated gold contents, the area is still considered an interesting target for gold exploration.

Areas outside known gold mineralised sites:

An area at Ilulialik (D in Fig. 36) and a small area northeast of the fjord Alaangua (E in Fig. 36) are covered by the second highest favourability class. The area at Ilulialik falls within an area without any supracrustal and a large amount of Quaternary deposits (Chadwick & Coe 1988). The small area northeast of the fjord Alaangua (E in Fig. 36) lies close to small amphibolite units in the 500 000 scale geological map (Allaart 1982).

Map based on stream sediment geochemistry and aeroradiometric data – Storø group

The U/Th ratio and the K radiation were found to be very indicative for the showings at Storø. These datasets are used as input in the statistical prediction analysis together with the indicative stream sediment geochemistry. The resulting gold potential map is shown in Figure 37.

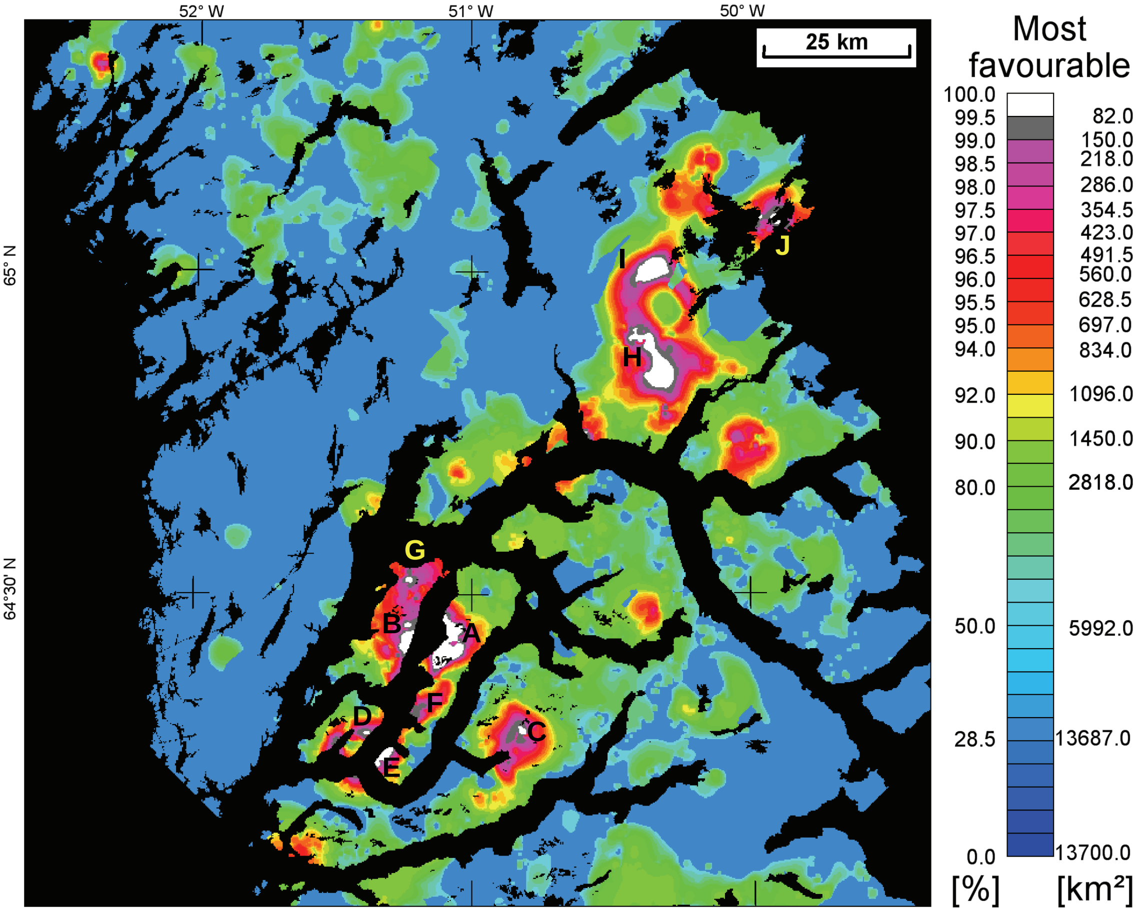

Figure 37. *Gold potential map for Storø group gold showings. The map is based on on the distribution of Al_2O_3, Cs, La, Rb, Th, U, and Ni/Mg-ratio in fine fraction regional stream sediment geochemistry and the aeroradiometric K radiation and U/Th ratio. The top 0.5 most favourable area is show in white.*

Considerable changes from the map based solely on geochemistry (Fig. 36) can be seen when aeroradiometric data are included. This reflects that the aeroradiometric data have a very strong indicative nature for the Storø group. Several interesting features can be seen in the map. The favourable zone for the Storø showings define an NNE-trending tract, which is common to the general orientation of supracrustal belts in this area and to the regional faults. The distribution patterns in many of the individual geochemical, aeromagnetic and aeroradiometric data are similar. At Storø, favourable areas have a westward-extension of the supracrustal belt hosting the Qingaaq and Aappalaartoq gold prospects.

Areas with known gold mineralised sites:

Not surprisingly, the areas of the Qingaaq and Aappalaartoq gold prospects are still outlined as favourable (A in Fig. 37). An area in the central part of eastern Bjørneøen is also outlined as favourable (B in Fig. 37). Only the northernmost gold showings at Bjørneøen lie within the outlined 0.5% favourable area for the Storø group. As discussed earlier, it is also highly likely that sediment samples at western Storø affect the prediction patterns at Bjørneøen (Fig. 30), which makes the favourable area at central eastern Bjørneøen uncertain. The area east of the fjord Qooqqut (C in Figs 37 and 38) is still identified as a favourable area. However, the addition of the aeroradiometric data has sharpened the resolution and a much smaller area is now targeted. The top 0.5% most favourable area is located in the middle of the north-western-most supracrustal rocks east of the fjord Qooqqut (Fig. 38). As mentioned before, this follow-up based on the prediction results from the first phase of the project was undertaken in this area during the 2005 field season. However, NunaMinerals A/S has obtained rock samples from the area with gold in the range of 210–240 ppb. The prediction seems to be a reflection of interfering data patterns, which is shown in Figure 39. The location of the 0.5% and 1.5% most favourable area seems to be controlled or affected by two to three stream sediment samples which have yielded high values of Cs, La, Ni/Mg ratio, Rb, Th, and aeroradiometric K and U/Th ratio. Especially the last dataset is believed to have a profound effect on the exact location of the favourable area.

Another favourable area that has been identified in earlier gold potential maps, but with the addition of aeroradiometeric data has shrunk in size, is an area on the eastern side of Sermitsiaq (D in Fig. 37). The area falls partly within the supracrustal package there.

Areas outside known gold mineralised sites:
As mentioned earlier, areas covering the southwestward extension of the supracrustal rocks in the central Storø are outlined as favourable (E and F in Fig. 38). An interesting area is also located within the supracrustal rocks in the north-western Bjørneøen (G in Fig. 38). These rocks are interpreted to be an extension of the supracrustal rocks at Qussuk peninsula – an area where gold mineralised sites have been discovered recently by GEUS (Hollis 2005; Hollis *et al.* 2005).

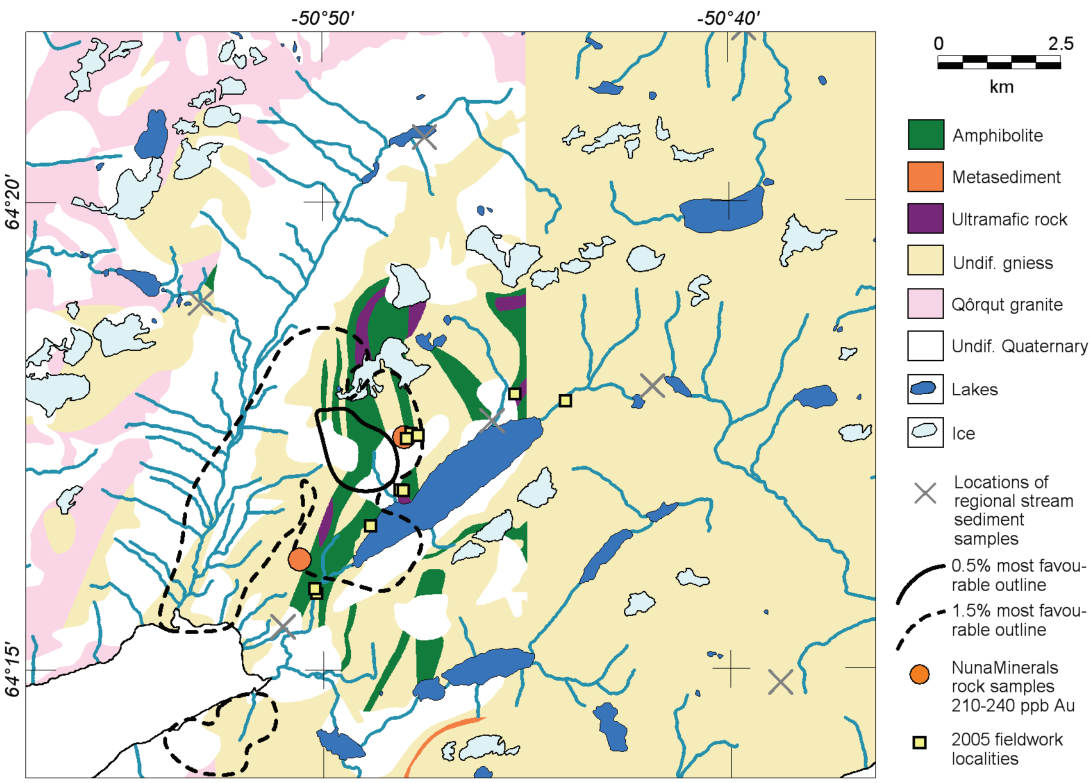

Figure 38. *Geological map of the Qooqqut area with the location of regional stream sediment samples, rock samples with 210 and 240 ppb Au collected by NunaMinerals A/S and localities from 2005 fieldwork conducted by GEUS. The predicted top 0.5% and 1.5% most favourable*

areas, based on stream sediment geochemistry and aeroradiometric data, are outlined. The discontinuity in the geology at 50°45' marks the eastern limit of available digital 1:100 000 scale geology.

Two large areas located at Ujarassuit Nunaat and Kangerssuaq (H and I in Figs. 38 and 40) are predicted as favourable. In this part of the study area, areas were also predicted as favourable for the Bjørneøen and partly also for the Isua group (Fig. 40). The areas are located in a northeast-directed zone between the showings at Isua and Storø, and are crossed by or flanking the Ivinnguit fault zone. This makes them interesting. However, as seen in Figure 40, this area is only very poorly represented in stream sediment samples and a strong influence of interpolation patterns can be expected. The fieldwork in 2005 by GEUS in the areas (Hollis *et al.* 2006) did not return any notable gold content in rock or stream sediment samples from the area. The highest value was 40 ppb Au in a rusty amphibolite. An unambiguous evaluation of the areas outlined as favourable is difficult to accomplish. New stream sediment data have been collected in the areas and when these are compiled with the existing data, a more definite evaluation is perhaps possible. In spite of these circumstances, it is intriguing that some of the characteristics of the known gold showings seem to be present in the data analysed from a poorly explored part of the Nuuk region and that the data, and the corresponding prediction patterns, define a northeast directed zone between known showings and large-scale tectonic structures. South of Isuakasia a couple of small areas are also predicted favourable for Storø gold. These areas were also predicted in the first phase of the project, and a short follow up investigation was completed (see former sections), but failed to return any elevated gold in samples from the areas.

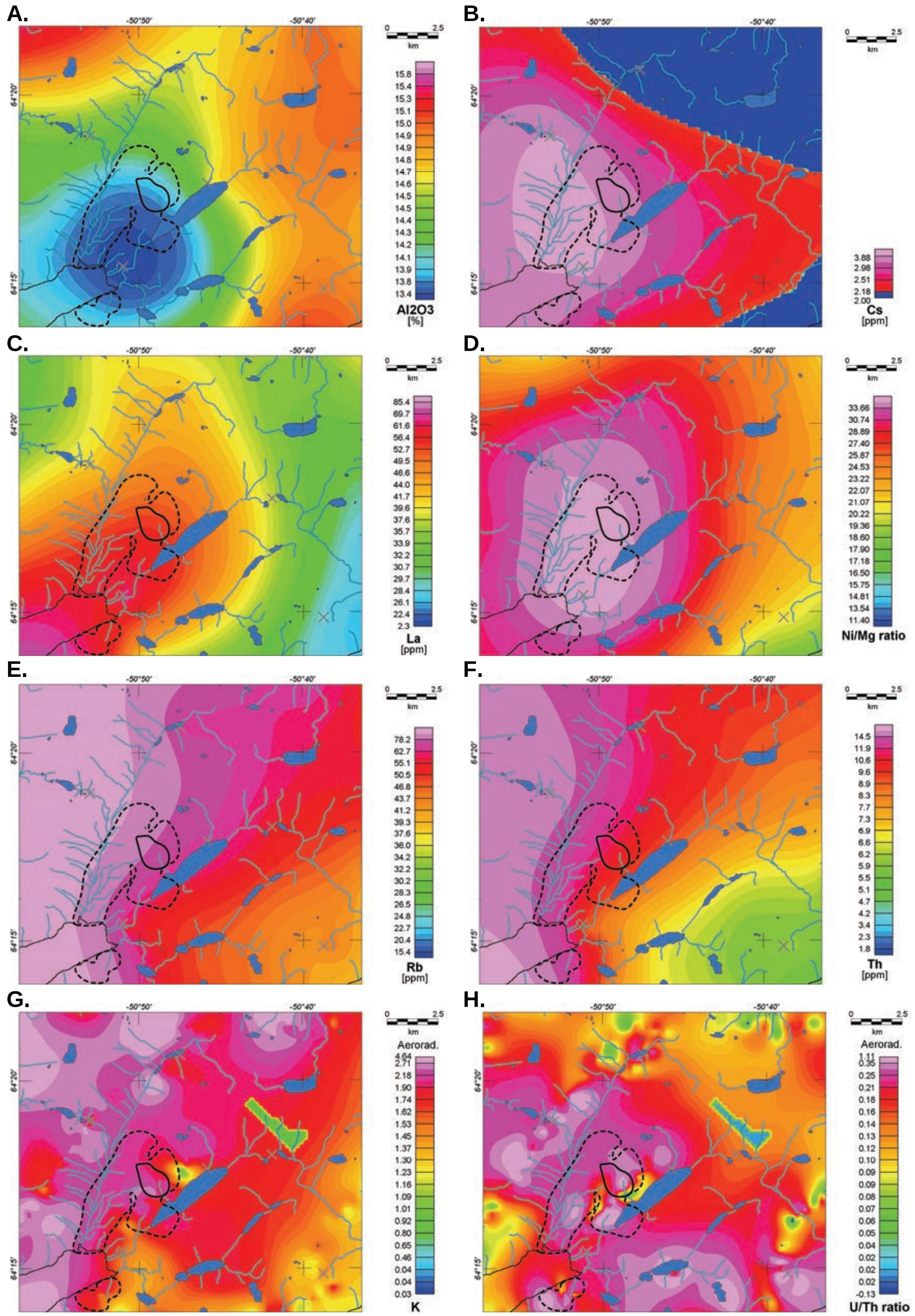

Figure 39. *Gridded stream sediment geochemistry and aeroradiometric data used in the gold potential map for Storø gold showings (see Fig. 37). Locations of stream sediment samples are indicated with grey crosses.*

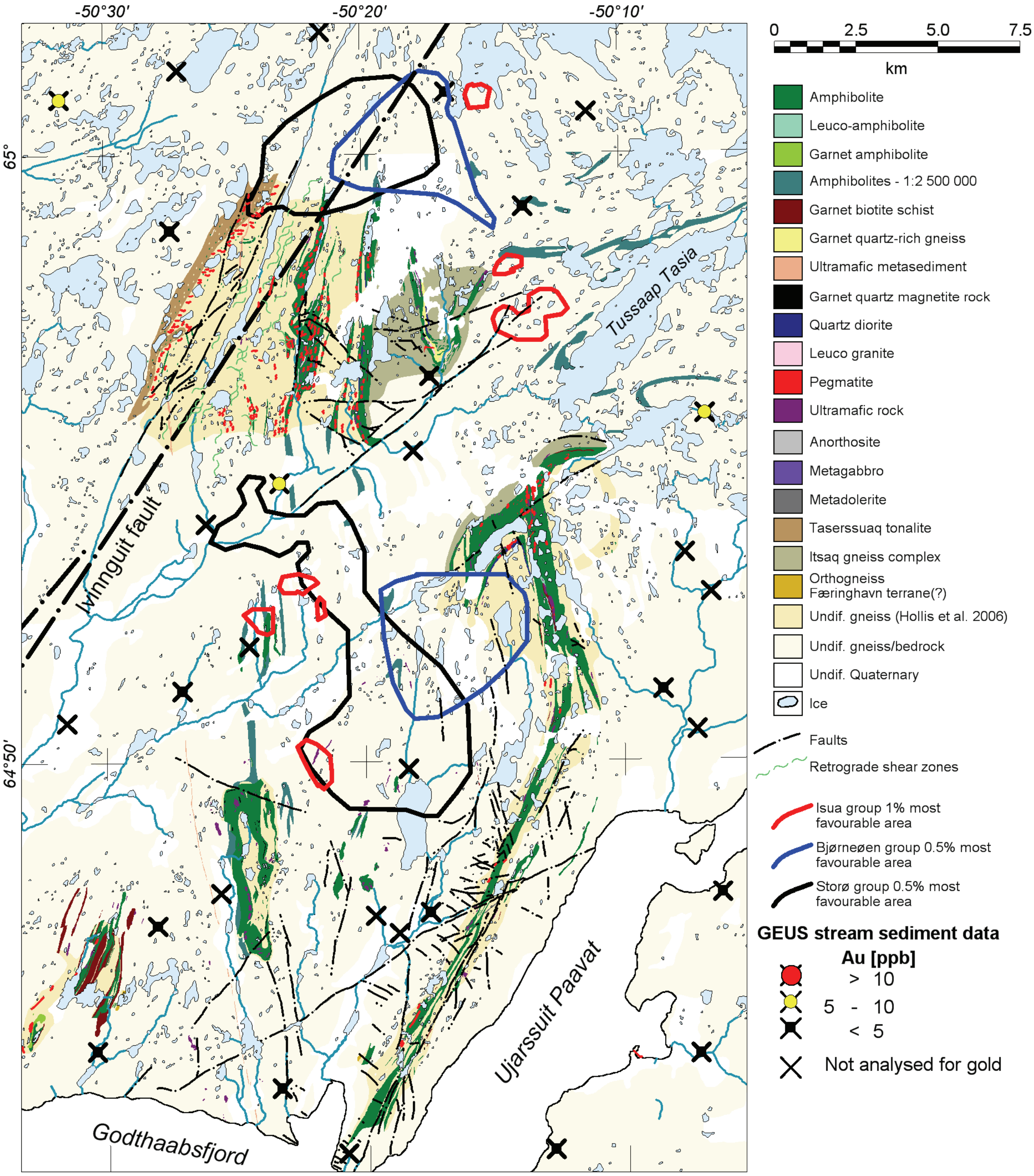

Figure 40. *Geological map of the Ujarassuit Nunaat area with outline of the predicted favourable areas for all three defined groups of showings. Unless stated otherwise in the legend, the geology is from detailed digital geology map of the area compiled from fieldwork in 2005 (Hollis et al. 2006).The location of regional stream sediment samples from the GEUS database and their gold content (if analysed for gold) is also shown.*

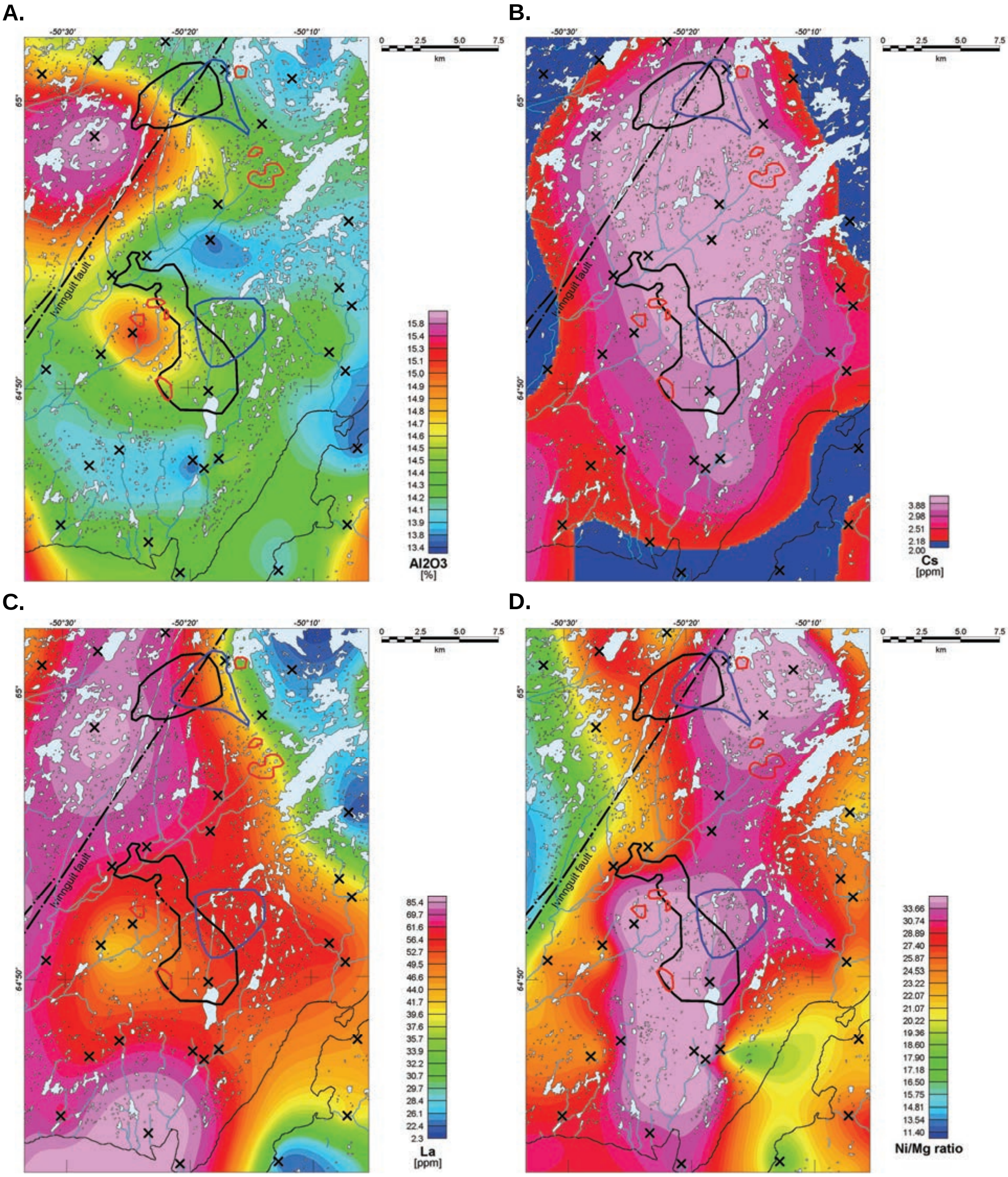
A.
B.
C.
D.
-50°30'
-50°20'
-50°10'
65°
64°50'
Ivinnguit fault
0 2.5 5.0 7.5
km
15.8
15.4
15.3
15.1
15.0
14.9
14.9
14.8
14.7
14.6
14.5
14.5
14.4
14.3
14.2
14.1
13.9
13.8
13.4
Al2O3
[%]
3.88
2.98
2.51
2.18
2.00
Cs
[ppm]
85.4
69.7
61.6
56.4
52.7
49.5
46.6
44.0
41.7
39.6
37.6
35.7
33.9
32.2
30.7
29.7
28.4
26.1
22.4
2.3
La
[ppm]
33.66
30.74
28.89
27.40
25.87
24.53
23.22
22.07
21.07
20.22
19.36
18.60
17.90
17.18
16.50
15.75
14.81
13.54
11.40
Ni/Mg ratio

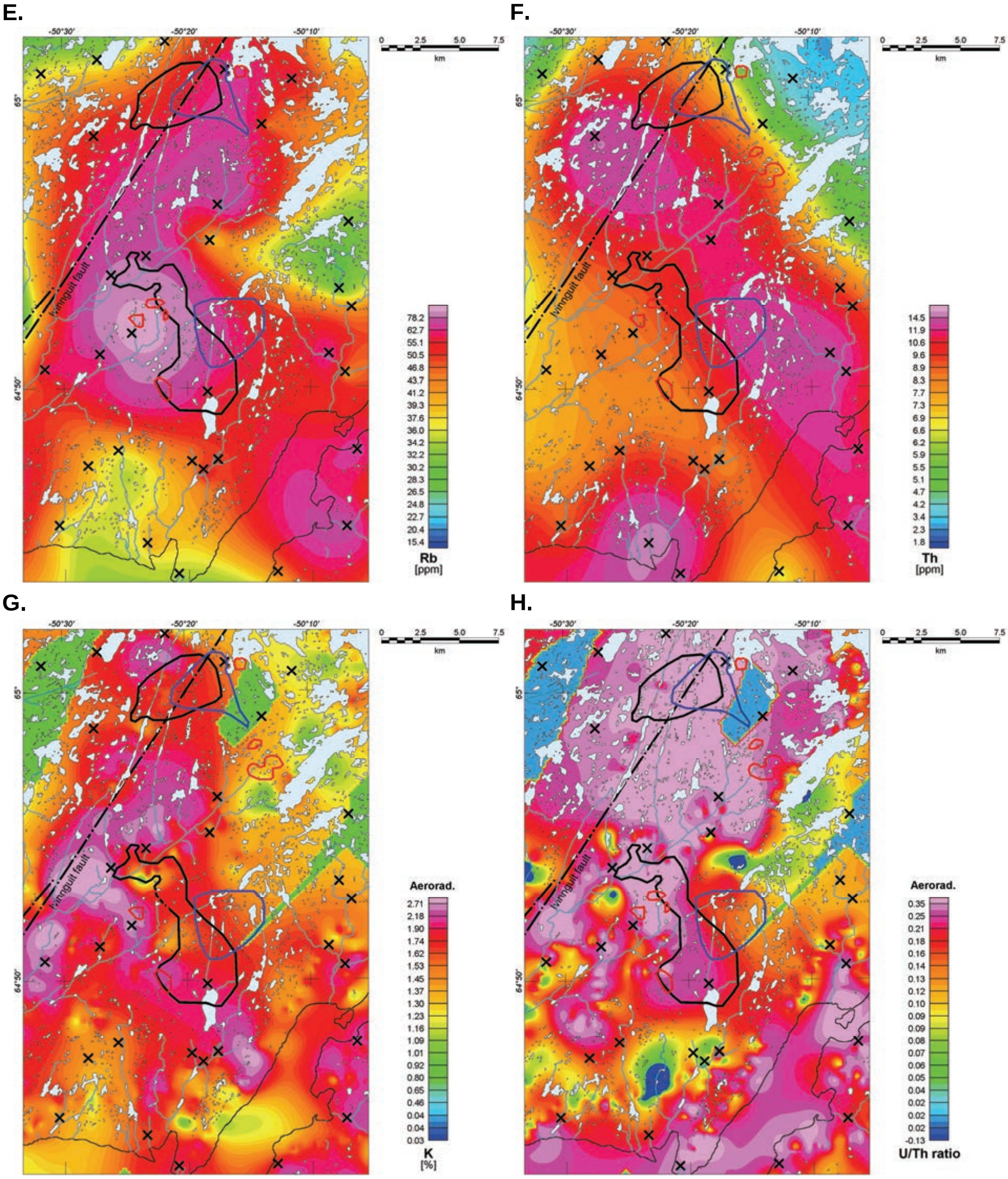

Figure 41. *The Ujarassuit Nunaat area.* ***A*** *–* ***F****: The gridded stream sediment geochemistry which is found to be indicative for the Storø group is shown and used in the gold potential map in Figure 37.* ***G*** *–* ***H****: Gridded aeroradiometric K and U/Th ratio; also found to be indicative for the Storø group. Crosses indicate locations of regional stream sediment samples. Areas outlined in black are top 0.5% most favourable areas for the Storø group (Fig. 37), areas outlined in blue are top 0.5% most favourable areas for the Bjørneøen group (Fig. 28), and areas outlined in black are top 1.0% most favourable areas for the Isua group (Fig. 22).*

Map based on stream sediment geochemistry, aeroradiometric data and processed lineaments from aeromagnetic data – Storø group

The minimum distance to nearest lineament (in a search radius of 1000 m for lengths of lineaments extracted from the aeromagnetic data), have also been found to be indicative for the Storø group (Fig. 60). Consequently, a gold potential map for the Storø group based on this dataset, the indicative stream sediment geochemistry datasets (however excluding the As dataset) and indicative aeroradiometric datasets has been constructed (Fig. 42). If this map is compared with the map only based on the stream sediment geochemistry and aeroradiometric datasets (Fig. 37), only minor changes can be observed, mostly as small modifications in the shape of the areas predicted to be most favourable. This is a reflection of the directional information stored in the added dataset.

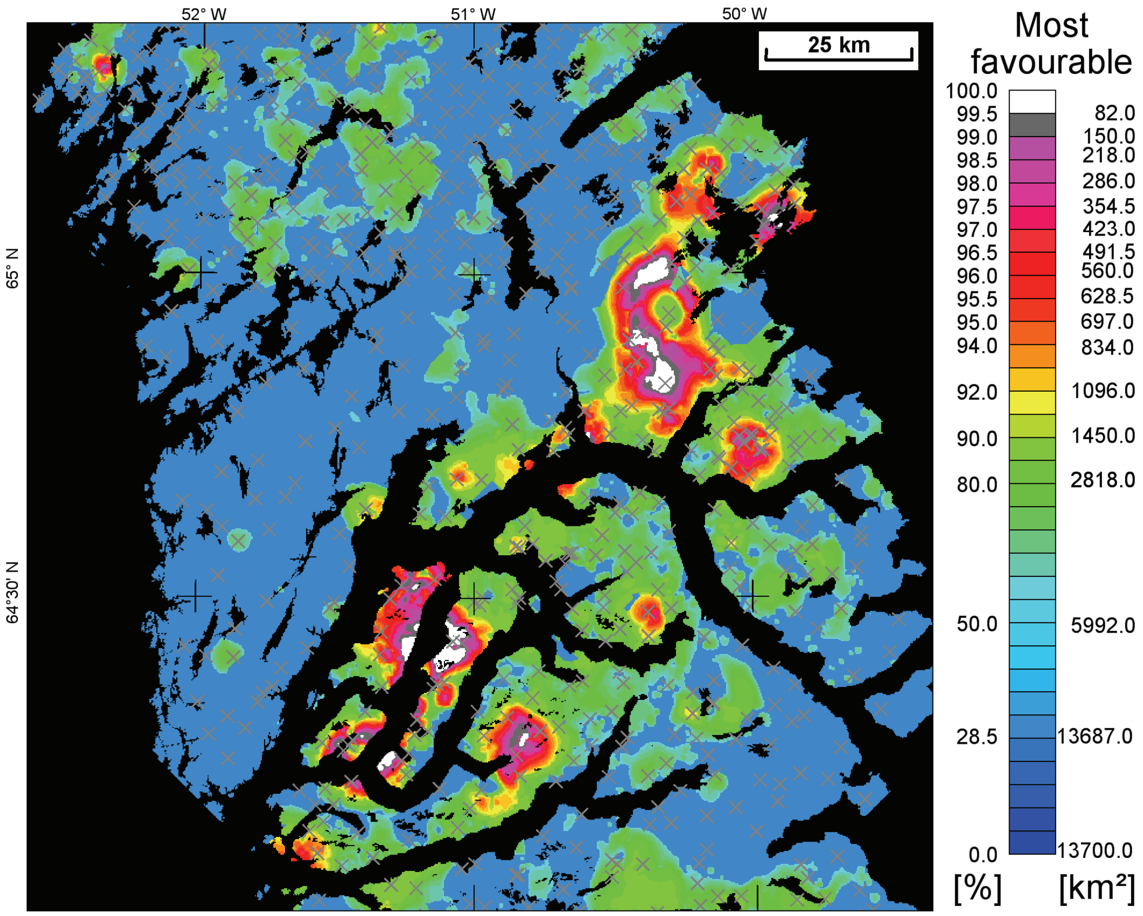

Figure 42. *Gold potential map for the Storø group based on indicative Cs, Al_2O_3, La, Rb, Th and Ni/Mg-ratio from stream sediment geochemistry data, K and U/Th-ratio from aeroradiometric data and the representation of minimum distance to nearest lineament in a search radius of 1000 m for all lengths of lineaments extracted from the aeromagnetic data. The top 0.5% most favourable area is shown in white.*

Cross-validation

Whenever results from a prediction are used, these should be scrutinised qualitatively by the user, the geologist, to validate how geologically reasonable the results are. Furthermore, the reliability or predictive ability of the prediction models for a mineral potential map should also be tested quantitatively by statistical cross-validation.

Method

A gold showing is selected from a group, and its location is pretended to be unknown. A gold potential map is then constructed based on the remaining showings of the group. The pixels occupied by the selected showing are then assessed in the mineral potential map in order to evaluate the ability to predict the "unknown" showing. If the prediction indices in the pixels representing the unknown are higher than 99.5%, then a discovery of the unknown showing is highly likely if the top 0.5% most favourable area of the entire study area is explored. Prediction indices can be seen as an expression of the success of a prediction, reflecting how well the group predicts the potential for other similar occurrences. The process is carried out for each gold showing in a group.

When the process has been carried out for each showing in a group, a prediction curves is constructed from the results. This curve describes the cumulative distribution of that portion of mineral occurrences, which would be discovered if a certain area was assigned for exploration. The quality of the prediction can be judged from the slope of the prediction rate curve: the steeper the slope, the more reliable the prediction.

The x-axis for the prediction curves (Fig. 43) represents the areas assigned for exploration; presented by the portion of the entire study area (in this study 13700 km^2). The percentage (e.g. top 0.5% most favourable) does not always match exactly the percentage area of the total study area (0.5% of the study area equals 68.5 km^2). E.g. in the case of our present study, 0.5% area corresponds to 82 km^2 and 1% corresponds to 150 km^2 in the prediction curves for the Storø group. This is to be expected as the predictions, from which the predictions curves are made, are based on empirical estimation. These conditions are also taken into account, when the prediction rate curves are evaluated (the next section) and the given numbers will always consider this.

The y-axis represents the portion of occurrences being included in the assigned area for exploration. However, because of the way in which the cross-validation was carried out (each time an potential map was made was it assumed that a selected showing was undiscovered), the y-axis can also be interpreted as the "estimated probability for the next discovery" within the assigned area for exploration.

Results of cross-validation

A cross-validation procedure, first exclusively for gold potential maps based on stream sediment geochemistry data alone, and then with additional types of datasets, has been carried out for all groups. The resulting prediction curves are shown in Figure 43. The prediction curves corresponding to the situation when areas were selected randomly for exploration and the 52 gold showings were treated as one group (Nielsen *et al.* 2004), are also shown.

Isua group

The Isua group contains 19 showings. A discovery of c. four showings would be made if the most favourable 0.1% (~16.5 km^2) area from the gold potential map based solely on stream sediment geochemistry was assigned for exploration. This means that the estimated probability for the next discovery within the c. 16.5 km^2 would be c. 21% (four showings discovered out of a total of 19). If other data types are added to the prediction, the portion of gold showings discovered in fact gets smaller if the same area were assigned for exploration. However, this changes if the 0.2% (~33 km^2) most favourable area was assigned for exploration. In this case c. six showings will be discovered if the areas are selected from the potential map based on geochemistry alone, whereas c. 10 showings would be discovered if the areas were selected from the maps where aeromagnetic and aeroradiometric data were included (estimated probabilities for the next discovery c. 32% and 53%, respectively). Differences in the number of discovered showings between the map based on geochemistry and aeromagnetic data and the map based on these two data types and aeroradiometric data are indicated, if the 0.3% (~49.5 km^2) most favourable area were assigned for exploration. Approximately 17 showings would be discovered if this area were selected from the potential map based on all three types of data, whereas only 14 showings were discovered if the map was based only on stream sediment geochemistry and aeromagnetic data.

In order to discover all of the Storø showings the potential map based on stream sediment geochemistry and aeromagnetic data provide the best scenario. Based on this, the top 1% most favourable area (150 km^2) should be assigned for exploration in order to discover all 19 showings of the Storø group. Eighteen showings would be discovered, if the area were selected from the map based on all three data types; only 14 showings would be discovered, if the map were based on stream sediment geochemistry only.

Storø group

The gold potential map based on all indicative stream sediment geochemistry, including the very indicative high As signature (which is very distinct compared with the regional distribution) are evaluated first. In order to discover all 11 showings of the Storø group, the most favourable 33 km^2 (top 0.2% area) would have to be assigned for exploration. If only the 16.5 km^2 most favourable area (top 0.1% area) is assigned then ten showings would be discovered. If As is excluded from the datasets, the prediction rate for the potential map based on the remaining stream sediment geochemistry datasets decreases. Thus, the 164 km^2 most favourable area (top 1.2% area) should be assigned for exploration if a discovery of all showings is desired. If indicative aeroradiometric data are included, the area, which should be assigned for exploration if all showings are to be found, drops to 89 km^2. In contrast, when also the minimum distance to nearest lineament for all lengths of lineaments extracted from the aeromagnetic dataset is included, the area increases to 120 km^2.

Bjørneøen group

If the 0.1% most favourable area based on stream sediment geochemistry were assigned for exploration seven out of the ten showings of the Bjørneøen group would be discovered (equals an estimated probability for the next discovery of 70%). In order to discover all ten showings, the c. 66 km^2 most favourable area should be assigned for exploration. If the minimum distance to nearest lineament for all lengths of lineaments extracted from the aeromagnetic dataset is included, the area for full discovery increases to c. 82 km^2

In general

Sensible prediction rate curves could be obtained for all three groups of showings. In general, the importance of the stream sediment geochemistry data for the prediction of favourable areas for gold showings is clearly seen from the prediction rate curves. None of the other types of data would be able to affect the predictions so clearly as the stream sediment geochemistry. The prediction rate curves also allow an evaluation of the effect of different data types. However, a general trend for all groups cannot be established. For example, the addition of aeroradiometric datasets to the Storø group predictions increases the prediction rate, whereas the addition of an aeroradiometric dataset to the Isua group predictions actually decreases the prediction rate.

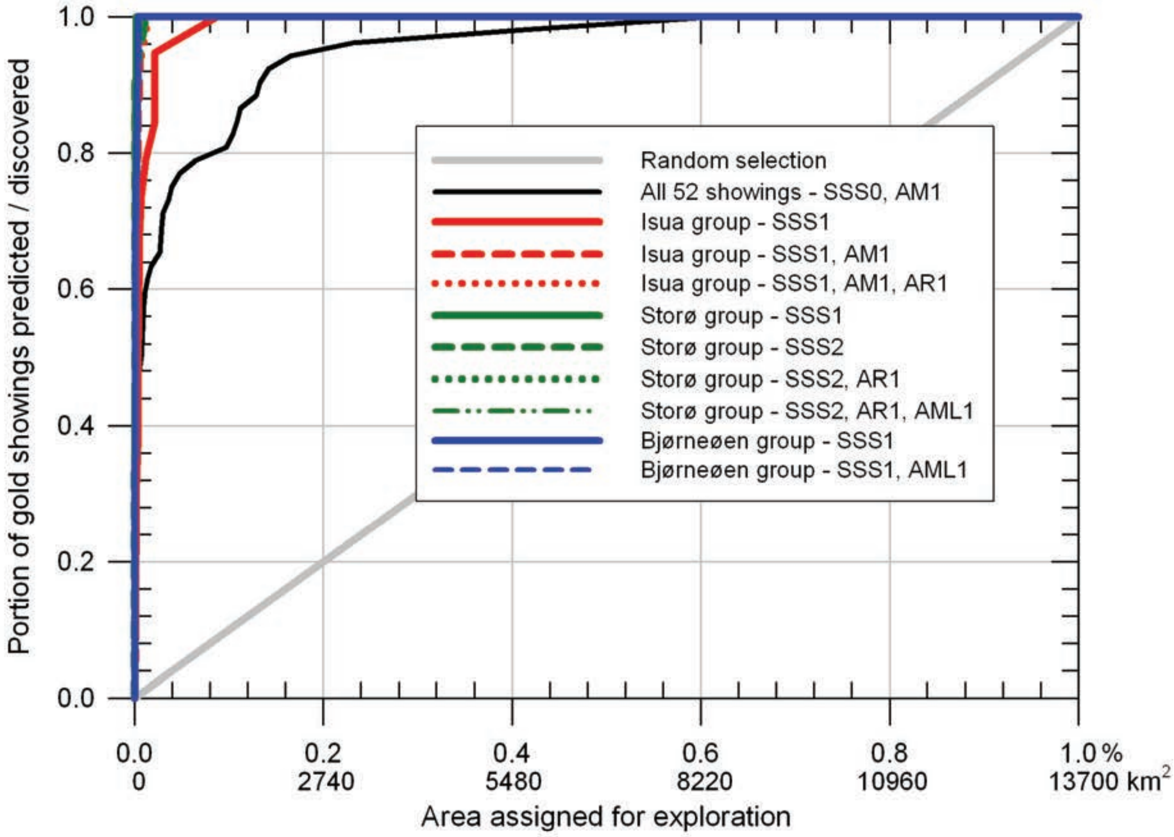

1.0
0.8
0.6
0.4
0.2
0.0
Portion of gold showings predicted / discovered
0.0
0
0.2
2740
0.4
5480
0.6
8220
0.8
10960
1.0 %
13700 km²
Area assigned for exploration
Random selection
All 52 showings - SSS0, AM1
Isua group - SSS1
Isua group - SSS1, AM1
Isua group - SSS1, AM1, AR1
Storø group - SSS1
Storø group - SSS2
Storø group - SSS2, AR1
Storø group - SSS2, AR1, AML1
Bjørneøen group - SSS1
Bjørneøen group - SSS1, AML1

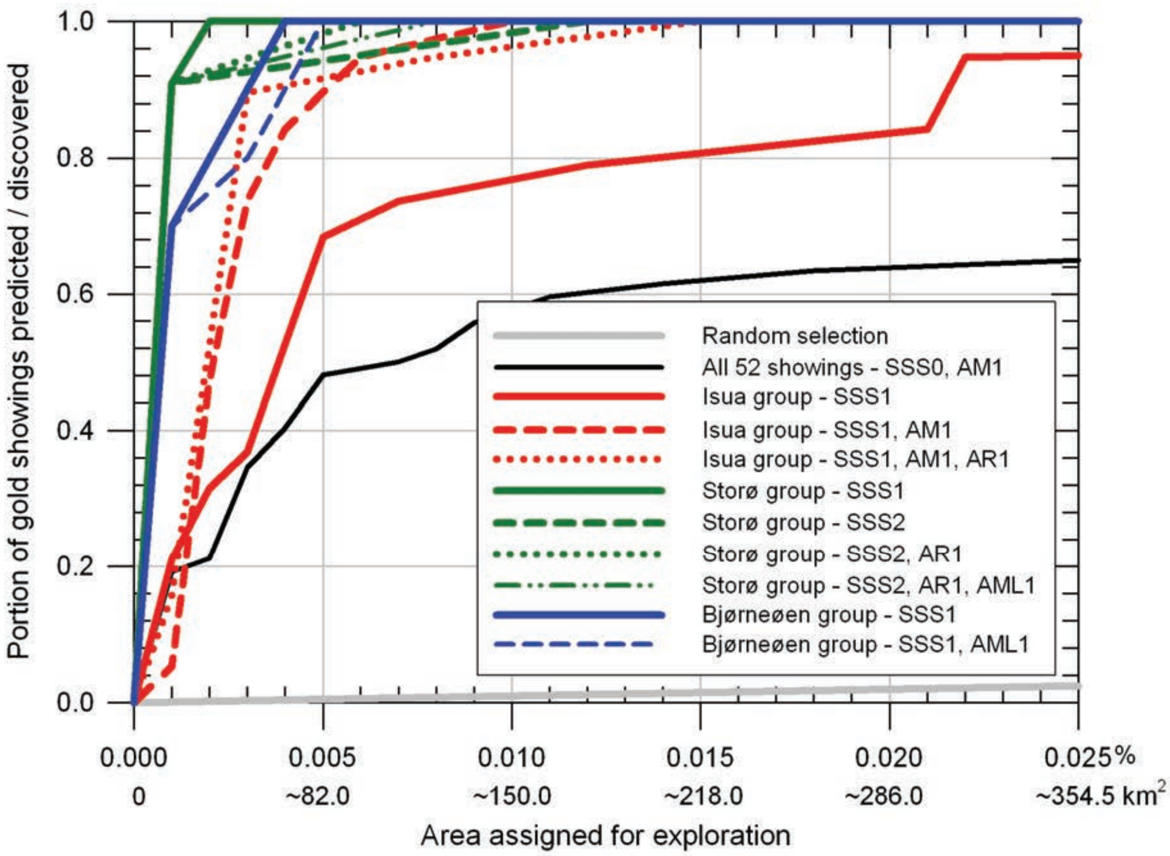

1.0
0.8
0.6
0.4
0.2
0.0
Portion of gold showings predicted / discovered
0.000
0
0.005
~82.0
0.010
~150.0
0.015
~218.0
0.020
~286.0
0.025%
~354.5 km²
Area assigned for exploration
Random selection
All 52 showings - SSS0, AM1
Isua group - SSS1
Isua group - SSS1, AM1
Isua group - SSS1, AM1, AR1
Storø group - SSS1
Storø group - SSS2
Storø group - SSS2, AR1
Storø group - SSS2, AR1, AML1
Bjørneøen group - SSS1
Bjørneøen group - SSS1, AML1

Figure 43. *Prediction rate curves for the three identified groups of gold showings in the Nuuk region. Isua group contains 19 showings, Bjørneøen contains 10 and Storø group contains 10. In addition, the prediction rate curve if areas were randomly selected for exploration is shown and the curve for all 52 gold showings treated as one group. For the* ***Isua group 'SSS1'*** *refers to the data Au, Cs, La, MgO, Fe2O3, Ni+Cr and Ni/Mg-ratio distribution in fine fraction regional stream sediment geochemistry and* ***'AM1'*** *for the Isua group refers to the datasets vertical gradient of TMI (total magnetic field intensity) and the amplitude of horizontal gradients of TMI.* ***'AR1'*** *refers to the radiometric U/Th-ratio. For the* ***Bjørneøen group 'SSS1'*** *refers to Cs, Rb, U, Th, Mg, Ni+Cr and Ni/Mg-ratio distribution in fine fraction regional stream sediment geochemistry and* ***'AML1'*** *refers to the minimum distance to nearest lineament within a search radius of 1000 m for lineaments of all lengths extracted from the aeromagnetic data. For the* ***Storø group 'SSS1'*** *refers to Al_2O3, As, Cs, La, Rb, Th, U, and Ni/Mg-ratio distribution in fine fraction regional stream sediment geochemistry,* ***'SSS2'*** *refers also to these element distribution, with the exclusion of As,* ***'AR1'*** *refers to the aeroradiometric K and U/Th distribution, and* ***'AML1'*** *refers to the minimum distance to nearest lineament within a search radius of 1000 m for lineaments of all lengths extracted from the aeromagnetic data. For the prediction rate curves for* ***All 52 showings*** *treated as one group* ***'SSS0'*** *refers to As, Au, Cs, Rb, Th, U, Ni/Mg-ratio distribution in fine fraction regional stream sediment geochemistry and* ***'AM0'*** *refers to the datasets vertical gradient of TMI (total magnetic field intensity) and the amplitude of horizontal gradients of TMI.*

Discussion

Signatures of gold showings

Given the open spacing of the stream sediment data and the fact that stream sediments represent a mixture of material from the drainage basin, it is obvious that the geochemical parameters cannot characterise a small target like the gold mineralisation itself. Mafic supracrustal rocks are very different geochemically from tonalitic to granodioritic orthogneisses, and as the known gold is hosted within supracrustal sequences dominated by mafic metavolcanic rocks, it is implicit that the geochemical signature of the areas with gold occurrences contains features such as high Mg, Ni, Cr.

However, it is interesting that the statistical analysis indicates 1) a significance of high Ni/Mg ratio, 2) the presence of high concentrations of large ion lithophile elements (LILE), and 3) that the three main gold hosting areas (Isua, Bjørneøen and Storø) display significant differences in their geochemical signature (see distribution functions in Appendix C, and Tables 5 and 6). These observations have prompted us to look at the lithology and the geochemistry of rock samples collected at the three gold hosting areas as well as in areas predicted favourable for gold, to see if the stream sediment based signatures express properties of the rocks themselves.

All chemical data produced for rock samples by GEUS and BMP projects in the Nuuk region 2003 – 2006 have been compiled. In total, c. 800 samples were analysed for the elements discussed below.

Ni/Mg ratio

Mafic meta-igneous rocks, both lavas and plutonic bodies, vary in composition from basic to ultrabasic and have a large range in MgO (3 to 30 %) and Ni (50 to 1000 ppm). In fresh basic to ultrabasic igneous rocks there is a correlation between Mg and Ni, see Figure 44. Obviously, increased values of the Ni/Mg ratio in a rock reflect either a gain in Ni or a loss in Mg. The possible association between elevated Ni/Mg ratio and gold mineralised sites was addressed in Hollis *et al.* (2004), where it was shown that rocks with elevated Ni/Mg ratios occur at Storø, Bjørneø, Ivisaartoq and Qussuk. Since then, chemical data have been acquired for the predicted gold favourable areas in Ujarassuit Nunaat and Qooqqut Lake (Hollis *et al.* 2006). They confirm that rocks with elevated Ni/Mg ratio also occur in the predicted areas (Fig. 46).

In Figure 45 we have plotted Ni against Mg and marked all samples exhibiting excess Ni in relation to the main group of rocks for which a linear correlation between Ni and Mg is seen. When these Ni-enriched samples are plotted in diagrams of S against Mg and Ca against Mg, it appears that high Ni correlates with high S in some samples and with high Ca (relative to Mg) in other samples. In summary, Ni-enriched samples suggest that some

Ni-enrichment is tied to sulphide mineralisation and other to calc-silicate alteration whereby Ca replaces Mg (and Fe). Thus, the increase in Ni/Mg ratio may be taken as a sign of alteration/mineralisation, and it has been sufficiently widespread to leave an imprint on the chemistry of the stream sediment.

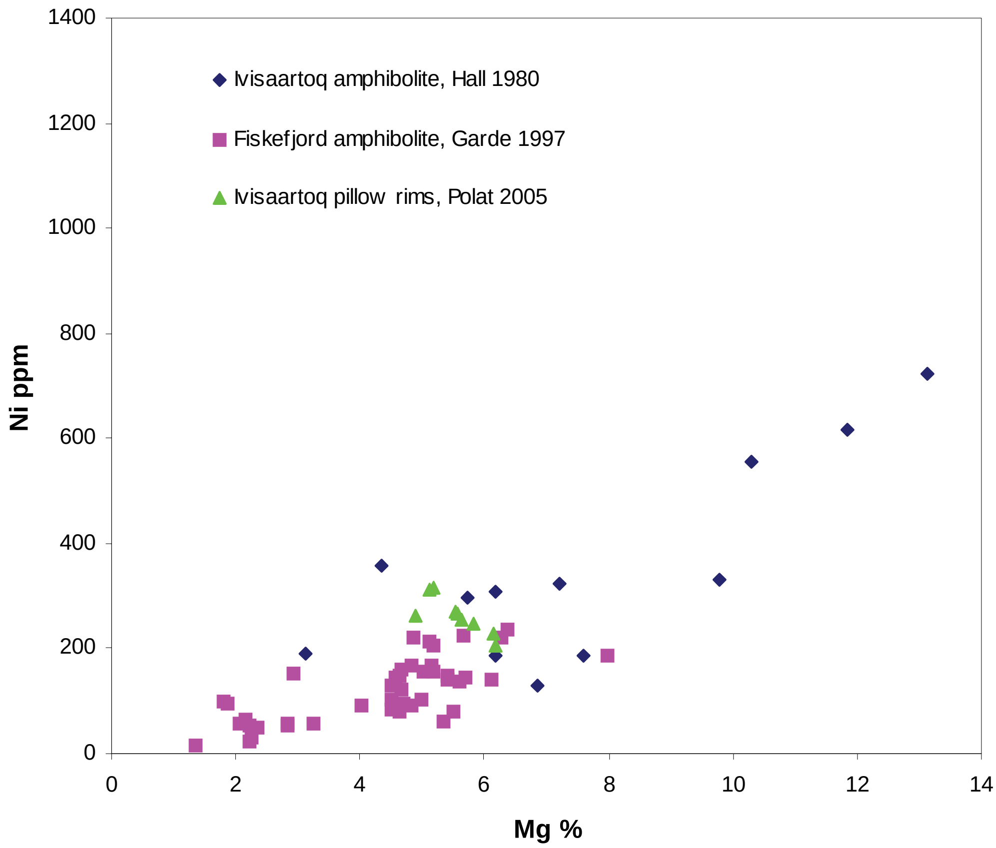

Figure 44. *Correlation between concentrations of Mg and Ni in unaltered mafic to ultramafic metavolcanic amphibolites.*

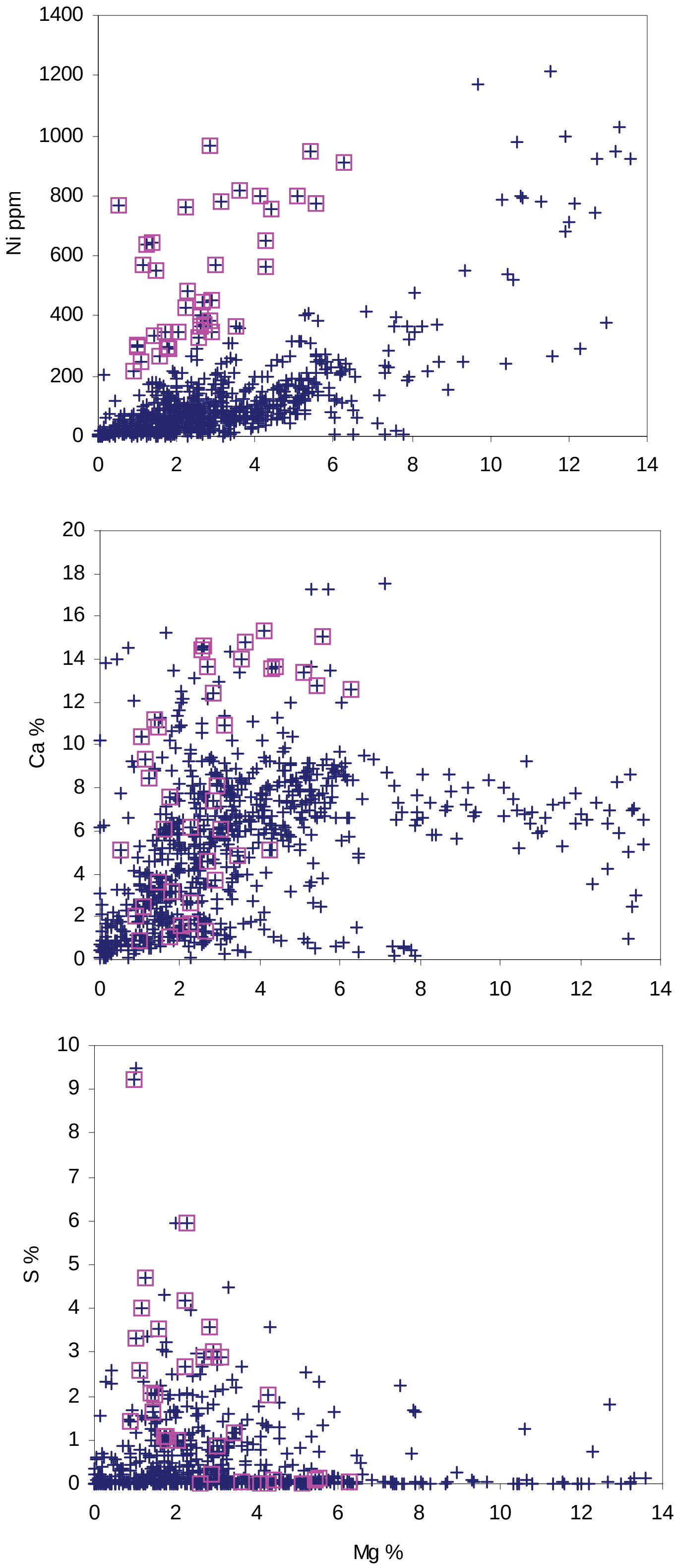

Figure 45. *All rock samples collected 2003 to 2005 in the Nuuk region and analysed for Ni, Mg, Ca and S by X-ray fluorescence or inductively coupled plasma emission spectrometry. Rock samples with excess Ni are framed.*

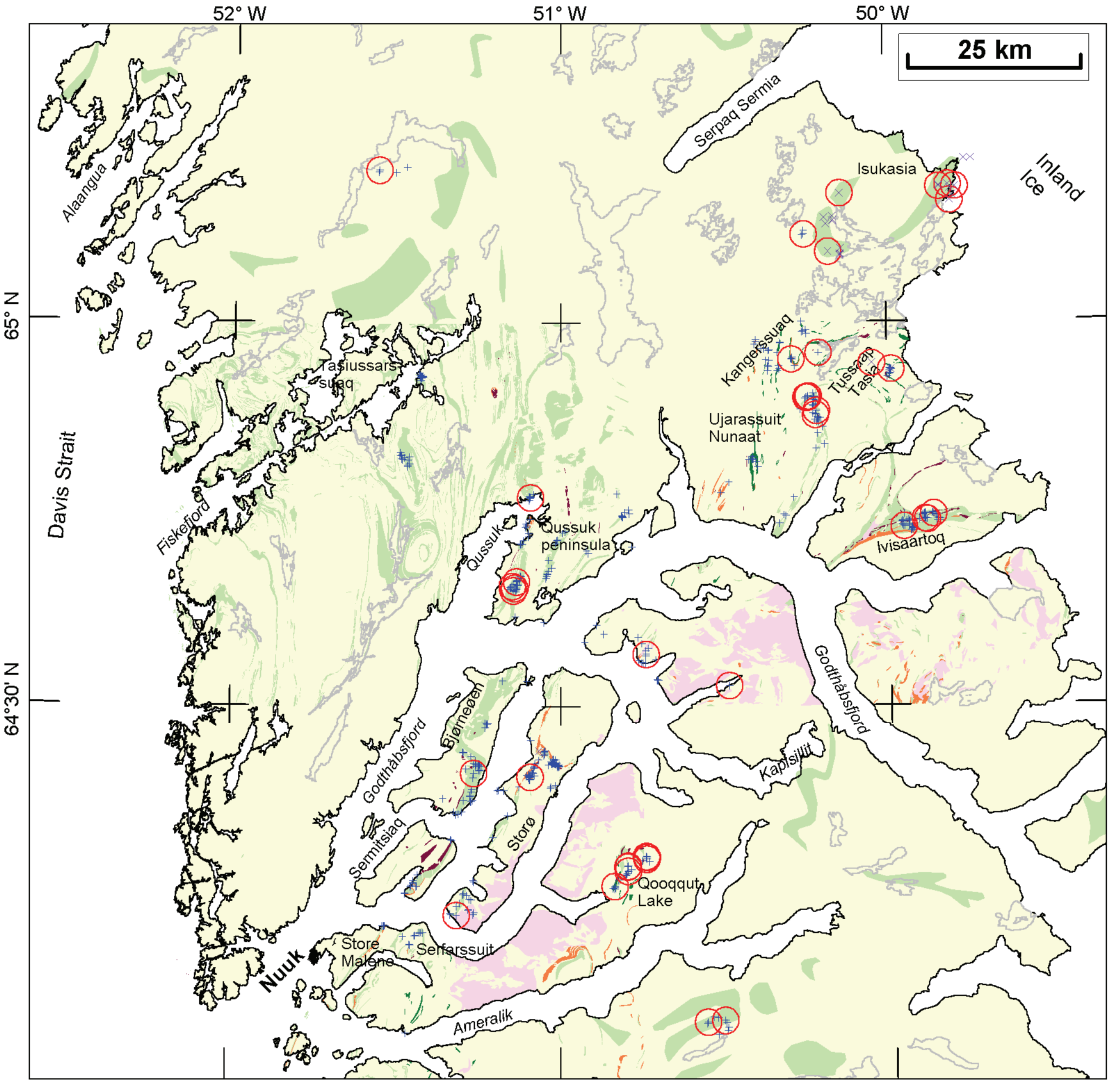

Figure 46. *Simplified lithological map of the Nuuk region with mafic meta-igneous rocks in light green, metasediments in orange and Qôrqut granite in pink. Location of rock samples (blue crosses) and red rings marking samples with excess Ni relative to Mg (framed samples in Figure 45).*

Polat (2005) interprets calc-silicate mineral assemblages as metamorphosed syndepositional sea-floor alteration, and suggests that environments characterised by this kind of alteration, in addition to massive sulphides, chert, iron formation and other types of chemical sediments (e.g. with tourmaline and scheelite), and ultramafic rocks represent supra-subduction settings. REE systematics of metavolcanic rocks from Isua and Ivisaartoq support this interpretation. As shown in previous reports, massive sulphides, ultramafic rocks, and various types of chemical sediments occur at Qussuk, Bjørneøen, Sermitsiaq, Store Malene and Qooqqut Lake. With the additional chemical evidence of sea-floor alteration discussed here, the supracrustal sequences at these sites could all be considered formed in a subduction environment. Samples of mafic metavolcanic rocks from the Fiskefjord area (Garde 1997) and from the eastern part of Qussuk peninsula do not show signs of chemical alteration, so the phenomenon does not apply to all mafic igneous rocks in amphibolite facies.

Although we now feel confident that the high Ni/Mg signature observed in stream sediment data reflects syn-depositional sea-floor exhalations and alteration, we do not have enough evidence to decide if such processes necessarily lead to gold mineralisation. Some gold may have been introduced to the sea-floor environment by hot aqueous solutions, as argued by Garde (2005) in the discussion of data from the syngenetically altered meta-andesites in the Qussuk area, but elsewhere in the Nuuk region high gold values (> 1 ppm) are typically recorded in samples from late veins or shear zones, i.e. the gold is epigenetic.

Concentration of LILE and aeroradiometric signature

The high concentrations of large ion lithophile elements (LILE, K, Rb, Cs, U) in stream sediments close to or at the gold mineralised sites reflect the occurrence of granitic material in the form of applitic or pegmatitic veins or possibly in the form of granite-related hydrothermal alteration within the supracrustal rocks. The questions are if the two kinds of sources can be discriminated from each other, and if hydrothermal alteration has affected a sufficiently large area to leave an imprint in the stream sediment data.

An examination of the Cs concentration in rock samples reveal that high Cs is generally not correlated with low Sc and high SiO_2 (Fig. 47), as would be expected if the Cs were concentrated in granites and pegmatites. In fact, there are several samples of amphibolite and even ultramafic rocks with elevated to high Cs, suggesting that granite-related hydrothermal alteration has taken place. The samples with introduced Cs occur in all of the areas with known and predicted gold showings (Fig. 48).

Pegmatites (and small granites) have been generated a number of times in the Nuuk region throughout its geological history. Early pegmatites are dated at 2840 Ma, while widespread pegmatite emplacement takes place between 2750 Ma and 2600 Ma, and the latest is associated with the intrusion of the c. 2550 Ma Qôrqut granite complex. This is evidence for the existence of long or recurrent high-level granite magmatism capable of generating and maintaining hydrothermal circulation. It has been argued that HHP (high heat producing) granites have particularly strong power to generate, drive and sustain hydrothermal circulation in surrounding rocks, which then favour the effect of hydrothermal alteration and mineralisation.

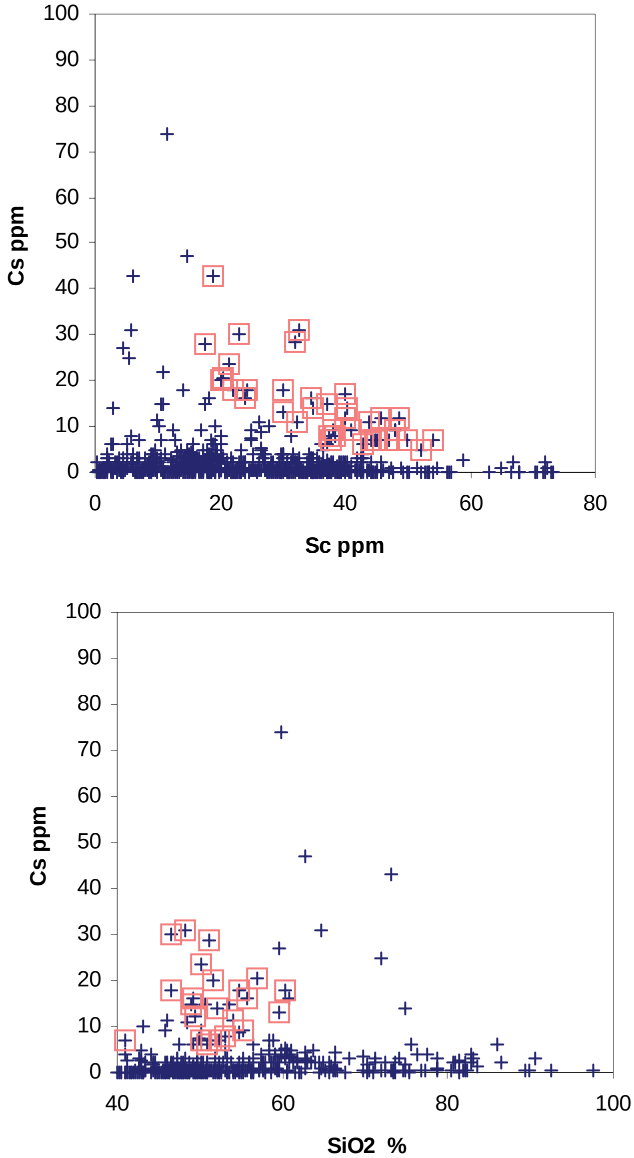

Figure 47. All rock samples collected 2003 to 2005 in the Nuuk region and analysed for Cs, Sc, and SiO_2 by X-ray fluorescence or inductively coupled plasma emission spectrometry. Rock samples, with excess Cs in samples with medium to high Sc, are framed. These samples have relatively low SiO_2.

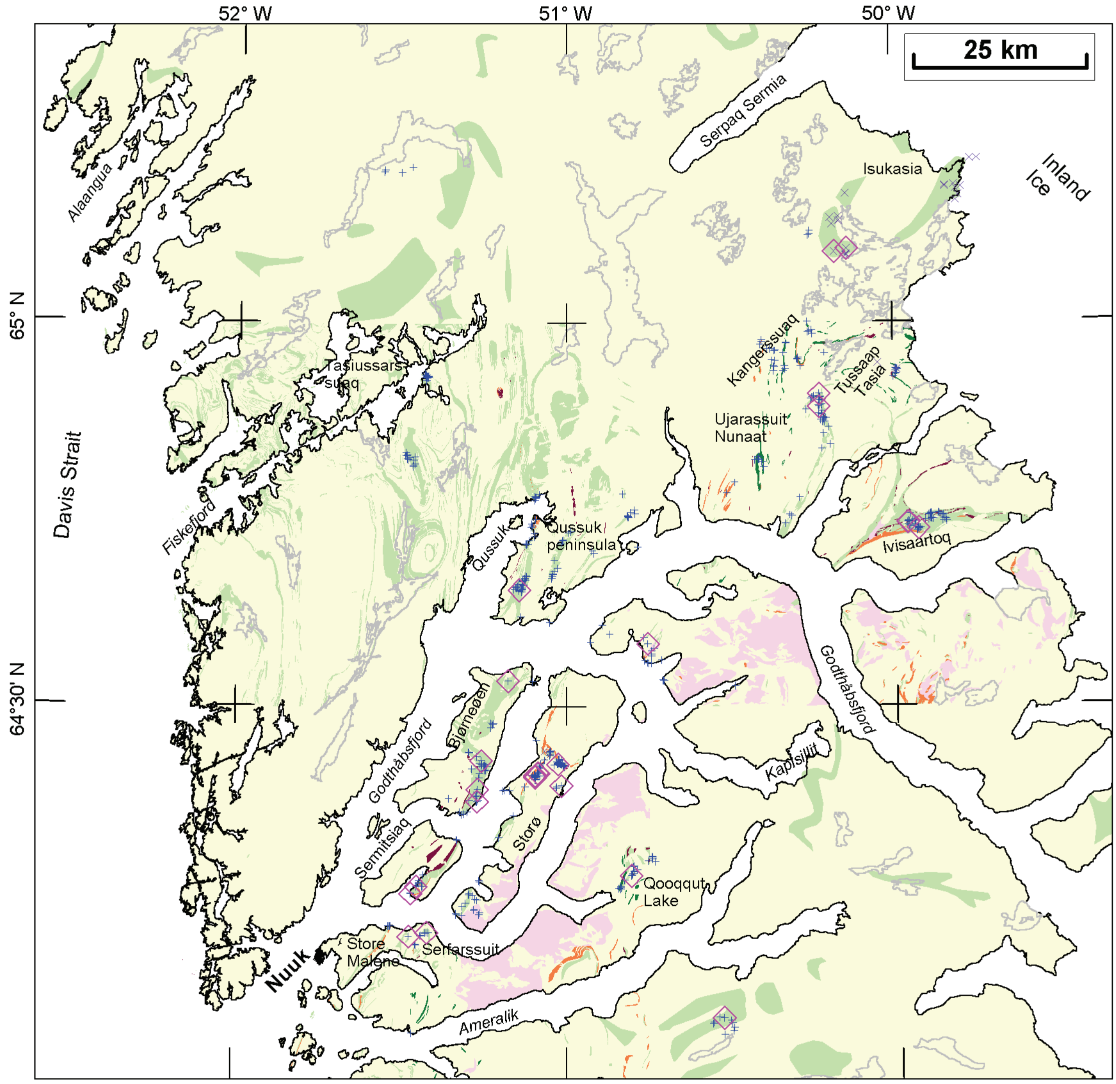

Figure 48. *Simplified lithological map of the Nuuk region with location of rock samples collected 2003 to 2005. Samples of mafic rocks (high Sc and low SiO_2, see Figure) with elevated Cs are framed.*

The high-radioelement zone in the Nuuk region documented by the aeroradiometric data testifies to the existence of a source along this zone, from which HHP pegmatites and granites have been generated several times.

Lithological and geochemical similarities, and the differences between gold hosting areas

All gold hosting and predicted areas are similar in the sense that they are dominated by mafic supracrustal rocks, and have variable proportions of ultramafic rocks and felsic metavolcanic and metasedimentary rocks in the supracrustal packages (Table 6).

Regarding the differences, Storø has the highest proportion of metasediments (garnet-biotite-sillimanite schists), Isua has the highest proportion of iron formation, and judged by presently available geological maps, Bjørneøen, Sermitsiaq and Ivisaartoq have the largest volumes of ultramafic rocks. Pegmatites are abundant, particularly on either side of Godthåbsfjord, i.e. on Sermitsiaq and Bjørneøen to the west, and Storø to the east. In addition, Store Malene, the proposed continuation of the Bjørneøen-Sermitsiaq belt has abundant and large pegmatites, and large pegmatites were observed during this year's fieldwork in Ujarassuit Nunaat. Pegmatites are scarce, on the other hand, at Isukasia. Storø alone has large bodies of anorthosite in contact with the supracrustal rocks.

The larger volumes of andesitic metavolcanic rocks at Qussuk peninsula and their temporal close relation with large granodioritic intrusions suggest that this area represent a continental margin, where the settings of the Palaeoarchaean supracrustal rocks at Isua and the Mesoarchaean Ivisaartoq, Bjørneøen-Sermitsiaq-Store Malene belts more likely represent oceanic plate margins.

The supracrustal rocks at Storø are lithologically and geochemically distinct from those of the other supracrustal belts. The amount of aluminous metasediment is larger (high Al_2O_3) and the high-As signature is unique. The significance of the anorthosite is not known and its presence has not been discussed in terms of the plate-tectonic setting in recent publications. The anorthosite intrudes metavolcanic rocks and is itself intruded by an orthogneiss with a protolith age of c. 3050 Ma. Thus these metavolcanic rocks are Mesoarchaean or older.

Table 6. *Overview of lithology and alteration observed in areas with gold showings (Isua, Bjørneøen, Storø) and predicted gold-favourable areas within the Nuuk region.*

	Isua	Bjøne-øen	Storø	Ujaras-suit North	Ujaras-suit South	Ivisaar-toq	Sermit-siaq	Qoor-quut	Qussuk
Lithology:									
Basalt	x	x	x	x	x	x	x	x	x
Andesite		x	x						x
Metasediment		x	xx	(x)			x		
Ultrabasic	xx	xx	(x)	x	(x)	xx	xx	x	(x)
Iron formation	x	x	x	x		x	x	x	
Pegmatites		x	x	x	x	x	x	x	x
Anorthosite			x						
Alteration:									
Epidotisation	x	x	x			x	x		x
Garnetisation			x	x				x	x
As-pyrite	(x)		x		(x)				
Quartz veining	x	x	x	x	x	x	x	x	
Massive sulphide		x	x			x	x	x	

However, age data (Hollis 2004, 2005, Hollis and Persson, GEUS, pers.comm. 2006) suggest that the aluminous metasediments at Qingaaq are younger (Neoarchaean), tectonically intercalated with Mesoarchaean rocks. The gold mineralised rocks at Qingaaq are rich in arsenopyrite, but the source of the As and the timing the mineralisation have not yet been established. Our observation that the signature of the Storø showings is different in several parameters from those of the other showing groups is worth noticing and is considered important for the modelling of the gold mineralisation. The combination of a high-As supracrustal environment and high-level granite magmatism is reminiscent of the situation in South Greenland, where gold mineralised areas have combined high-As and high-Cs stream sediment geochemical signatures (Steenfelt 2000).

Altogether, it appears that the geochemical signatures of known and predicted gold showings reflect properties of the supracrustal rock assemblages and their hydrothermal alteration, and may therefore be interpreted to outline favourable environments for gold mineralisation.

Spatial distribution of favourable areas

As argued in the first phase of the project (Nielsen *et al.* 2004), the spatial distribution of favourable areas suggest the existence of a regional tract with areas favourable for gold and gold mineralising environments. The work carried out in the second phase of the project supports the existence of such a favourable tract. Most of the predicted areas for the different group are situated within a NNE-trending tract from the town of Nuuk to Isukasia. The tract embraces all known gold showings as well as geochemical gold anomalies, and the zone has previously been suggested as being prospective for gold showings (e.g. Appel *et al.* 2003; Hollis *et al.* 2004; NunaMinerals 2003). A notable exception is however, the favourable areas situated in the Fiskefjord region.

As mentioned in Nielsen *et al.* (2004), the NNE-directed tract is common to the general orientation of the greenstone belts in this area and to the regional large-scale faults as well as to the patterns in many of the geochemical and geophysical datasets with indicative signatures of the gold showings. However, in general, greenstone units outside the tract constitute similar proportions but these are not indicated as being within the most favourable areas. This could indicate, that the greenstone units within the tract deviate from those outside and/or that other events/processes has affected the areas within the tract making the environment favourable for gold.

Use of predictive gold potential maps

The established datasets and their characteristics make it possible and feasible to construct potential maps for gold showings in the Nuuk region based on desired combination of datasets. The maps can be used constructively in the search for at better understanding of the ore-forming processes and their results in the form of mineralisations.

As illustrated, it is of greatest importance that the gold potential maps not are used uncritically. The potential maps should be used in conjunction with other methods and results. The analysed data and the results of the statistical predictions should be critically reviewed in order to catch misleading effects of interpolation and other ways of standardising parameters. Moreover, the results should always be judged and scrutinised according to qualitative geological knowledge.

Conclusions and implications

In the second phase of the multi-parameter spatial modelling, it has been demonstrated that gold showings in different parts of the Nuuk region have some common, but also some distinct signatures in the geochemical and geophysical data. The implication is that the local lithological setting at the gold mineralised sites varies. They are all, however, characterised by lithological diversity and signs of hydrothermal alteration, of both syngenetic and epigenetic nature. Most of the areas predicted by the statistical analysis to be favourable for gold mineralisation appear to comprise subduction-related supracrustal sequences that have been subjected to veining by granitic magmas.

Fieldwork in areas predicted to be favourable for gold mineralisation in the first phase of the project confirmed that these areas comprise mafic supracrustal rocks, ultramafic bodies, pegmatites and signs of syn- and epigenetic hydrothermal alteration. However, none of the rock samples analysed contained high gold concentrations.

A statistical cross-validation for all three groups of showings testifies that the grouping is reliable. The cross-validation also allows an assessment of the importance and effect of different data types in the prediction of favourable areas for gold showings. In general, the stream sediment geochemistry is the most important.

The areas outlined as gold-favourable using more showings, grouping of showings and more regional parameters are still largely confined to the NNE-trending zone that was recognised in the first phase of the spatial modelling. This encourages gold exploration within the zone, but also calls for more data from areas outside the zone to improve the documentation of the diagnostic features of the gold mineralised environments.

The statistical approach has been successful in outlining areas, which on field inspection turned out to have many lithological features in common with gold mineralised sites. However, working in detail with the method has revealed shortcomings in the data processing that justify more work being spent on optimising procedures and improving products.

Recommendations

Refinement of methodology and more data
The use of a small pixel size in relation to the resolution of the regional data demands a very reliable gridding method. Experiments are warranted with gridding methods, gridding parameters (cell sizes and blanking), and screening to refine the grids and thereby to avoid grid-artifacts. It is recommended that sediment geochemical data acquired by exploration companies be merged with the Survey data if possible to increase the resolution.

Other models should be applied than the empirical likelihood ratio model used until now, and the results from different models should be compared. Furthermore, methods of addressing the uncertainty related to the different data and their representation should be pursued. Though it would be complicated, a map showing the uncertainties in each pixel should be produced for each generated mineral potential map.

Follow-up and collection of additional data
Several of the areas outlined as favourable occur outside known gold mineralised sites and they are considered interesting targets for exploration. More lithological and geochemical data, particularly stream sediment and soil sample data, from these areas are warranted. However, owing to the possible displacements of indicative features, it is recommended that the underlying regional geochemical and geophysical data as well as new rock chemical data be consulted carefully before fieldwork is undertaken.

Comparison with gold fields elsewhere
It would be very interesting to compare the geochemical and geophysical regional features and lithogeochemical data with similar data from greenstone belts hosting gold fields elsewhere, e.g. Abitibi in Canada.

Mapping other kinds of mineralisation and geological environments
We have used the spatial modelling method to outline areas favourable for gold mineralisation. We have shown that owing to the low resolution of some of the regional data, we are likely to identify certain (and important) properties that relate to the depositional environment of the supracrustal rocks. Thus, the method and the experience gained could be used to characterise supracrustal belts elsewhere in Greenland. The same method and the same data can also be used to predict other kinds of mineralisation and identify other geological environments in West and South Greenland.

Acknowledgements

GEUS geologists and guests providing observations and analytical results from their field-work in 2005 for this project are greatly acknowledged for their contribution.

The study reported here is the result of a second phase of a project jointly financed by the Bureau of Minerals and Petroleum (BMP) and the Geological Survey of Denmark and Greenland (GEUS). The staff at BMP is thanked for constructive discussion of the method and results.

References

Allaart, J.H. 1982: Geological map of Greenland, 1:500 000, Frederikshåb Isblink - Søndre Strømfjord, sheet 2. Copenhagen: Geological Survey of Greenland.

Appel, P.W.U., Coller, D., Coller, V., Heijlen, W., Moberg, E., Polat, A., Raith, J., Schjøth, F., Stendal, H. & Thomassen, B. 2005: Is there a gold province in the Nuuk region? Danmarks og Grønlands Geologiske Undersøgelse Rapport **2005/27**, 79 pp., 1 CD-Rom.

Appel, P.W.U., Garde, A.A., Jørgensen, M.S., Moberg, E., Rasmussen, T.M., Schjøth, F. & Steenfelt, A. 2003: Preliminary evaluation of the economic potential of the greenstone belts in the Nuuk region. Danmarks og Grønlands Geologiske Undersøgelse Rapport **2003/94**, 137 pp., 1 DVD.

Bliss, I. 1996: Mapping and prospecting in the Isua supracrustals southern West Greenland 1995. Internal report, Nunaoil A/S, 21 pp., 1 app., 9 plates. Nunaoil A/S (in archives of the Geological Survey of Denmark and Greenland, GEUS Report file 21453).

Chadwick, B. & Coe, K. 1988: Geological map of Greenland, 1:100 000, Ivisârtoq 64 V.2 Nord. Copenhagen: Geological Survey of Greenland.

Downes, M.J. & Gardinev, W.W. 1986: Report of field work - 1985: Greenland tungsten project, 32 pp., 6 app., 25 plates. Kidd Creek Mines Ltd. Exploration division (in archives of the Geological Survey of Denmark and Greenland, GEUS Report file 20036).

Dunnells, D. 1995: Mineral exploration in the Malene concession and Nuuk Fjord region, southern West Greenland: July-August 1995, 30 pp., 5 app., 10 plates. NunaOil A/S (in archives of the Geological Survey of Denmark and Greenland, GEUS Report file 21457).

Escher, J.C. & Pulvertaft, T.C.R. 1995: Geological map of Greenland, 1:2 500 000. Copenhagen: Geological Survey of Greenland.

Ferguson, J. 1998: Report on prospecting lincence No. 29/95 for West Greenland held by Quadrant Resources Pty. Ltd., 2 pp., 2 plates. Unpublished report, Quadrant Resources Pty. Ltd., Queanbeyan, NSW, Australia: Quadrant Resources Pty. Ltd. (in archives of the Geological Survey of Denmark and Greenland, GEUS Report file 21624).

Friend, C.R.L. & Nutman, A.P. 2005: New pieces to the Archaean terrane jigsaw puzzle in the Nuuk region, southern West Greenland: steps in transforming a simple insight into a complex regional tectonothermal model. Journal Geological Society, London **162**, 147–162.

Garde, A.A. 1989: Geological map of Greenland, 1:100 000, Fiskefjord 64 V.1 Nord. Copenhagen: Geological Survey of Greenland.

Garde, A.A. 1997: Accretion and evolution of an Archaean high-grade grey gneiss - amphibolite complex: the Fiskefjord area, southern West Greenland. Geology of Greenland Survey Bulletin **177**, 115 pp.

Garde, A.A. 2005: A mid-Archaean island arc complex with gold mineralisation at Qussuk, Akia terrane, southern West Greenland. In: Hollis, J.A. (ed.): Greenstone belts in the central Godthåbsfjord region, southern West Greenland. Geochemistry, geochronology and petrography arisning from 2004 field work, and digital map data. Danmarks og Grønlands Geologiske Undersøgelse Rapport **2005/42**, 179–213.

Hall, R.P. 1980: The tholeiitic and komatiitic affinities of the Malene metavolcanic amphibolites from Ivisârtoq, southern West Greenland. Rapport Grønlands Geologiske Undersøgelse **97**, 20 pp.

Hollis, J.A. (ed.) 2005: Greenstone belts in the central Godthåbsfjord region, southern West Greenland. Geochemistry, geochronlogy and petrography arising from 2004 field work, and digital map data. Danmarks og Grønlands Geologiske Undersøgelse Rapport. **2005/42**, 213 pp., 1 DVD.

Hollis, J.A., Garde, A.A., Frei, D. & van Gool, J. 2005: Geochronology. In: Hollis, J.A. (ed.): Greenstone belts in the central Godthåbsfjord region, southern West Greenland. Geochemistry, geochronlogy and petrography arising from 2004 field work, and digital map data **2005/42**, 12–79.

Hollis, J.A., Schmid, S., Stendal, H., van Gool, J.A.M. & Weng, W.L. 2006: Supracrustal belts in Godthåbsfjord region, southern West Greenland. Progress report on 2005 field work: geological mapping, regional hydrothermal alteration and tectonic sections. Danmarks og Grønlands Geologiske Undersøgelse Rapport **2006/7**, 171 pp., 1 DVD.

Hollis, J.A., van Gool, J.A.M., Steenfelt, A. & Garde, A.A. 2004: Greenstone belts in the central Godthåbsfjord region, southern West Greenland. Danmark og Grønlands Geologiske Undersøgelse Rapport **2004/110**, 110 pp., 1 DVD.

Jensen, S.M., Secher, K., Rasmussen, T.M. & Schjøth, F. 2004: Diamond exploration data from West Greenland: 2004 update and revision. Danmark og Grønlands Geologiske Undersøgelse Rapport **2004/117**, 90 pp., 1 DVD.

McGregor, V.R. 1983: Geological map of Greenland, 1:100 000, Qôrqut 64 V.1 Syd. Copenhagen: Geological Survey of Greenland.

Nielsen, B.M., Rasmussen, T.M. & Steenfelt, A. 2004: Gold potential of the Nuuk region based on multi-parameter spatial modelling of known gold showings. Danmarks og Grønlands Geologiske Undersøgelse Rapport **2004/121**, 155 pp.

NunaMinerals 2003: Nuuk Fjord. A gold province in West Greenland, NunaMinerals A/S. Internal report. NunaMinerals A/S (available from NunaMinerals A/S, P.O. Box 790, DK-3900 Nuuk, Greenland).

NunaMinerals 2006: Ivisaartoq. License No. 2002/07 (Subarea 3). NunaMinerals A/S, GEO-meeting (internal meeting for NunaMinerals A/S geologists and different invited geologist), Copenhagen, Denmark 2006, 1 pp.

Olsen, H.K.O. & Grahl-Madsen, L. 1994: Prospecting in the early Archean Isua supracrustals. Exploration licence no 01/93. Internal report. Nunaoil A/S, 21 pp., 4 app., 8 plates. Nunaoil A/S (in archives of the Geological Survey of Denmark and Greenland, GEUS Report file 21329).

Ordóñez-Calederón, J.C. 2006: Appendix 5: Field report 2005 - Ujarassuit Nunat Region - East, and Ivisaartoq. In: Hollis, J.A., Schmid, S., Stendal, H., van Gool, J.A.M. & Weng, W.L. (eds): Supracrustal belts in Godthåbsfjord region, southern West Greenland. Progress report on 2005 field work: geological mapping, regional hydrothermal alteration and tectonic sections. Danmarks og Grønlands Geologiske Undersøgelse Rapport **2006/7**, 112–118.

Polat, A. 2005: Geochemical and petrographic characteristics of the Ivisaartoq and Storø greenstone belts, southern West Greenland: progress report. In Hollis, J.A. (ed.): Greenstone belts in the central Godthåbsfjord region, southern West Greenland. Geochemistry, geochronlogy and petrography arising from 2004 field work, and digital map data. Danmarks og Grønlands Geologiske Undersøgelse Rapport. **2005/42**, 80–112.

Polat, A. & Kerrich, R. 1999: Formation of an Archean tectonic melange in the Schreiber-Hemlo greenstone belt, Superior Province, Canada: Implications for Archean subduction-accretion processes. Tectonics **18**, 733–755.

Secher, K. 1976: Airborne radiometric survey between 66º and 69º N, southern and central West Greenland. Rapport Grønlands Geologiske Undersøgelse **80**, 65–67.

Secher, K. 1977: Airborne radiometric survey between 63º and 66º N, southern West Greenland. Rapport Grønlands Geologiske Undersøgelse **85**, 49–50.

Steenfelt, A. 1999: Compilation of data sets for a geochemical atlas of West and South Greenland based on stream sediment surveys 1977 to 1997. Danmarks og Grønlands Geologiske Undersøgelse Rapport **1999/41**, 33 pp.

Steenfelt, A. 2000: Geochemical signatures of gold provinces in South Greenland. Transactions Institution of Mining and Metallurgy (Section B: Applied earth sciences) **109**, B14–B22.

Steenfelt, A. 2001a: Calibration of stream sediment data from West and South Greenland. A supplement to GEUS report 1999/41. Danmarks og Grønlands Geologiske Undersøgelse Rapport **2001/47**, 43 pp.

Steenfelt, A. 2001b: Geochemical atlas of Greenland - West and South Greenland. Danmarks og Grønlands Geologiske Undersøgelse Rapport **2001/46**, 39 pp., 1 CD-ROM.

Tukiainen, T., Rasmussen, T.M., Secher, K. & Steenfelt, A. 2003: Restored digital airborne radiometric data from surveys flown in 1975 and 1976 by GGU between 63° and 69°N. Danmarks og Grønlands Geologiske Undersøgelse Rapport **2003/37**, 9 pp., 5 maps.

van Gool, J. & Stecher, O. 2006: Appendix 2: Field report 2005 - Ujarassuit Nunaat Region / North. In: Hollis, J.A., Schmid, S., Stendal, H., van Gool, J.A.M. & Weng, W.L. (eds): Supracrustal belts in Godthåbsfjord region, southern West Greenland. Progress report on 2005 field work: geological mapping, regional hydrothermal alteration and tectonic sections. Danmarks og Grønlands Geologiske Undersøgelse Rapport **2006/7**, 58–77.

Appendix A – Statistical identification of lineaments

Lineament analysis

A lineament can be described by its location, orientation and length. The presence of linear features or lineaments is often used in the characterisation of a ground surface, where the lineaments often represent the surface expression of a sheet-like structure, e.g. a dyke or a fault plane. In this case, the lineament is the intersection between two planar surfaces, namely the structure and the topographic surface. In order to characterise the appearance of the lineaments, statistical quantities such as mean orientation, mean length and density are often used.

In a similar manner, the appearance of magnetic anomalies can be characterised in terms of the presence and statistical nature of linear features. The main difference is that the magnetic field varies smoothly across the surface of observations, whereas geological features can be sharp, as e.g. a lithological boundary. Well-determined magnetic anomaly peaks, either minima or maxima, are often used to define the location of the lineaments, and often derivatives of the magnetic field are used. The term magnetic lineament is usually restricted to describe narrow anomalies although the definition of “narrow” is somewhat arbitrary. The often seen association of narrow geological dyke-like features with narrow magnetic anomalies seems to be the rationale for this use of terms.

For these types of lineaments, it must be remembered that for standard map projections, deviations of lineaments from a straight linear will occur, if the lineament plane cutting an uneven observation surface has a dip different from vertical. Dependent on the roughness of the topography and the dip angle of the plane of the lineament, the surface expression of that lineament will be curved to a variable extent. Therefore, the use of lineaments in a description of surface observations often presumes an acceptance of the concept of an “almost straight lineament”. Once again, some arbitrariness is evident in the definition.

Identification of lineaments by visual inspection of a surface can usually be done very fast and often with great confidence. However, to quantify the observed linear features is often a tedious, manual procedure for large data sets. Unfortunately, most algorithms for automatic lineament detection based on digital data often perform badly compared with the visual observation. We have tested a number of commercial and public domain software and found that the results were not satisfactory. Therefore, a new algorithm was developed and used to produce the results presented in this paper.

For this report, the data entered into the algorithm was the first vertical derivative of the vertical component of the total magnetic field intensity. The main reason for this particular choice of source data is that differentiation of the magnetic field will enhance anomaly features corresponding to near-surface features, and thus detect features that most likely correlate to mineral showings of certain types. A short description of the algorithm used to extract the lineaments and of the statistical analysis performed on the lineaments is given below.

Extraction of lineaments

The algorithm for linear feature extraction can be applied to any digitally sampled function of two variables, e.g. digital elevation models, geophysical data, and images. Although very general, some parameters are needed to describe the input data and to define a number of selection criteria to control the output. The description below is based on the assumption that airborne magnetic data are used as input.

The basic principles of the method are illustrated by use of an example with synthetic data (Figs 44 and 45). The example (Fig. 44) includes the magnetic total field response from ellipsoids of variable dimensions and depth to the top, with principal axes vertical and horizontal. The ellipsoids in the leftmost half of the area are uniformly distributed with orientation of the longest axis between 85° and 95° and the ellipsoids in the right part are uniformly distributed with orientation of the longest axis between 45° and 135°. The longest axis varies uniformly between 1000 m and 2500 m. The orthogonal horizontal axis and the vertical axis are 100 m and 200 m respectively.

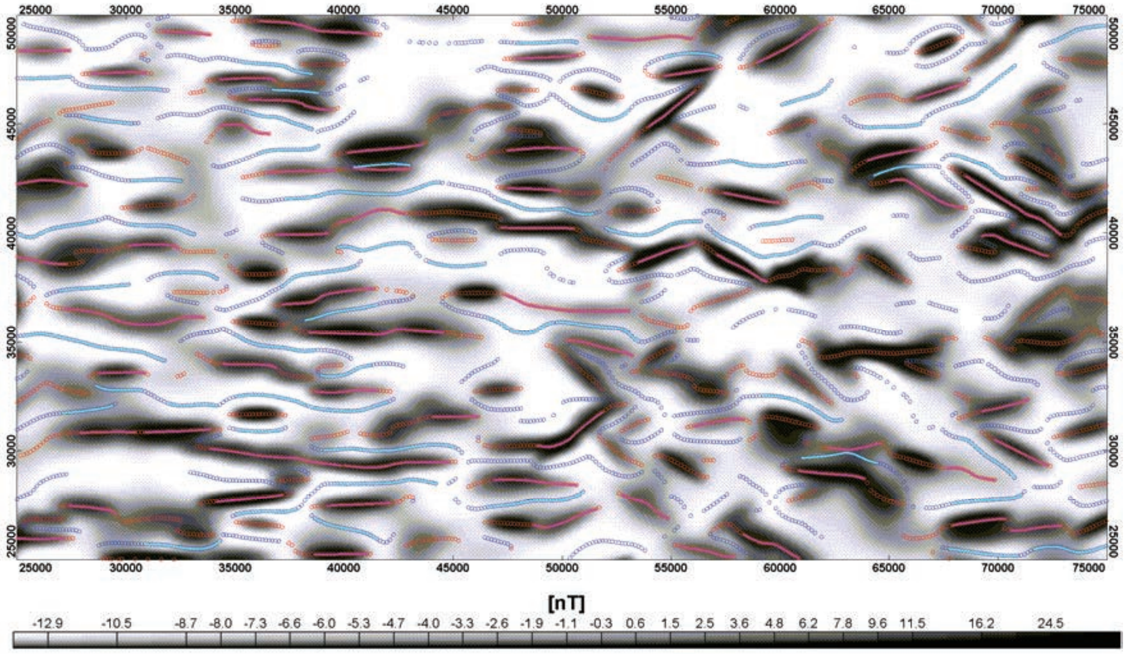

Figure 49. *Synthetic magnetic total field data generated from ellipsoids with their longest axis horizontal. The red circles mark the locations of maxima and the blue the locations of minima that are selected and entered to the algorithm for lineament extraction. The lines in cyan and light blue colours mark the lineaments obtained. The ellipsoids in the left half of the area are aligned uniformly with orientations between 85° and 95° and the ellipsoids in the right half have orientations uniformly distributed between 45° and 135°.*

Simultaneously, we will consider the case of an airborne survey, where the magnetic field is densely sampled along flight lines. Each flight line is characterised by an almost uniform sampling distance. The flight lines may have partially random orientation and may be crocked. In the synthetic example, we have used straight north–south oriented flight lines with a line distance of 150 m, in the real data case the line spacing is 500 meters. Comparison between the two may help understanding of the consequences of the choice of parameters.

The first step in the analysis is to determine the locations of all extremes of the field for each flight line, e.i. the maxima and minima determined in the synthetic case (circles in Fig. 44) and in the aeromagnetic data from the Nuuk region (Fig. 45). Clearly, although certain patterns may be discernible, there is really too much data to use sensibly.

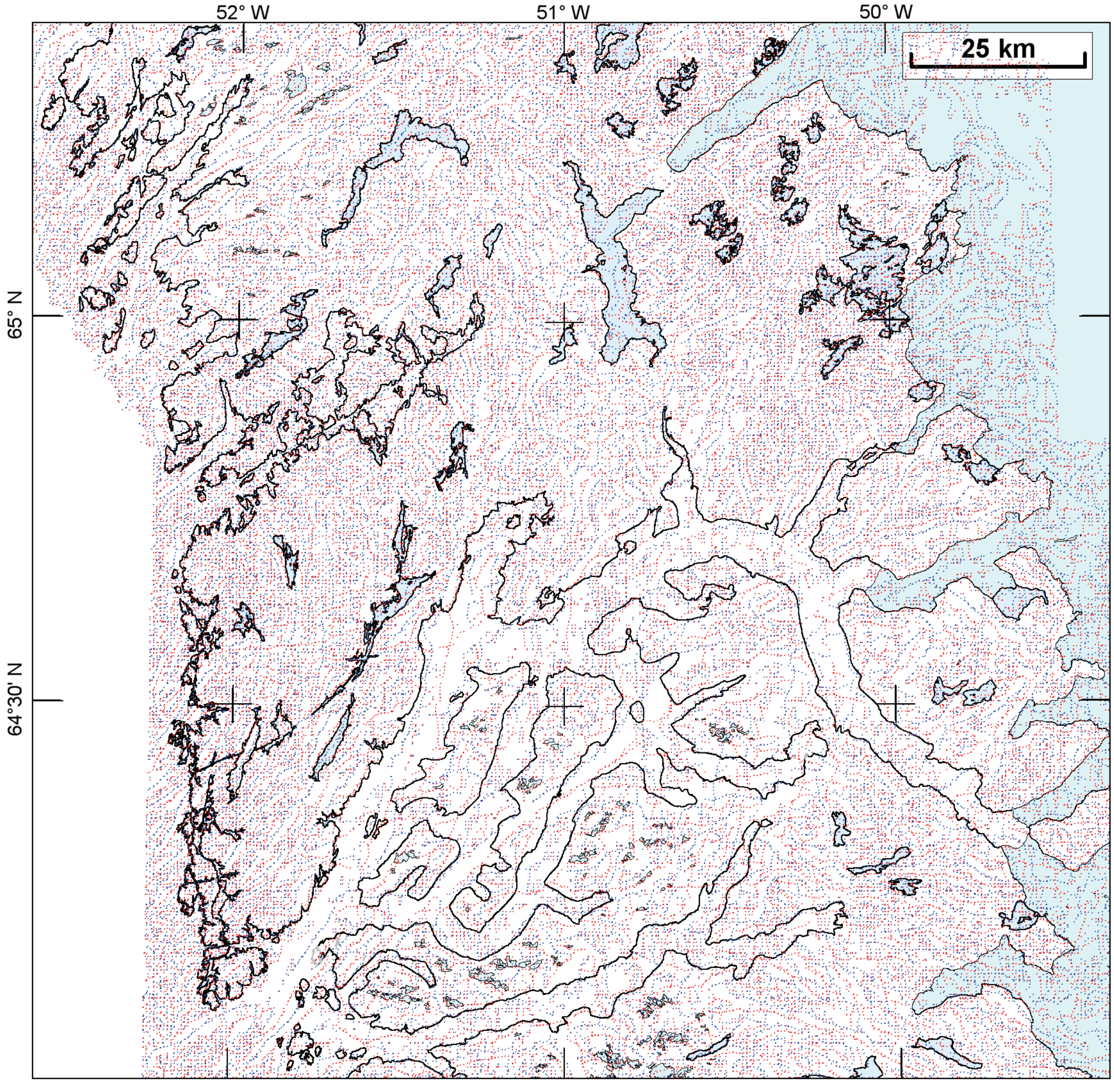

Figure 50. *All locations of maxima (red dots) and locations of minima (blue dots) extracted from the aeromagnetic data from the Nuuk region.*

As the next step, we define a lineament as straight-line segments that connect either maxima or minima across flight lines subject to the following requirements:

1. The extremes are located along an almost straight line
2. An extreme belongs to only one lineament
3. A lineament can only cross a flight line if this flight line contains an extreme point at the intersection of the two

4. The field variation perpendicular to the lineament must be similar at different positions along the lineament
5. The distance between two adjacent extremes on a straight-line segment must be smaller than a specified threshold distance
6. A lineament must contain a specified minimum number of extremes that fulfils requirements 1–5

The first requirement that the extreme occur along an almost straight line, is easily implemented by requiring that the angle between connecting straight-line segments are smaller than a specified threshold value. An extreme may fulfil this requirement along several possible combinations of extremes along various directions (see Fig. 46).

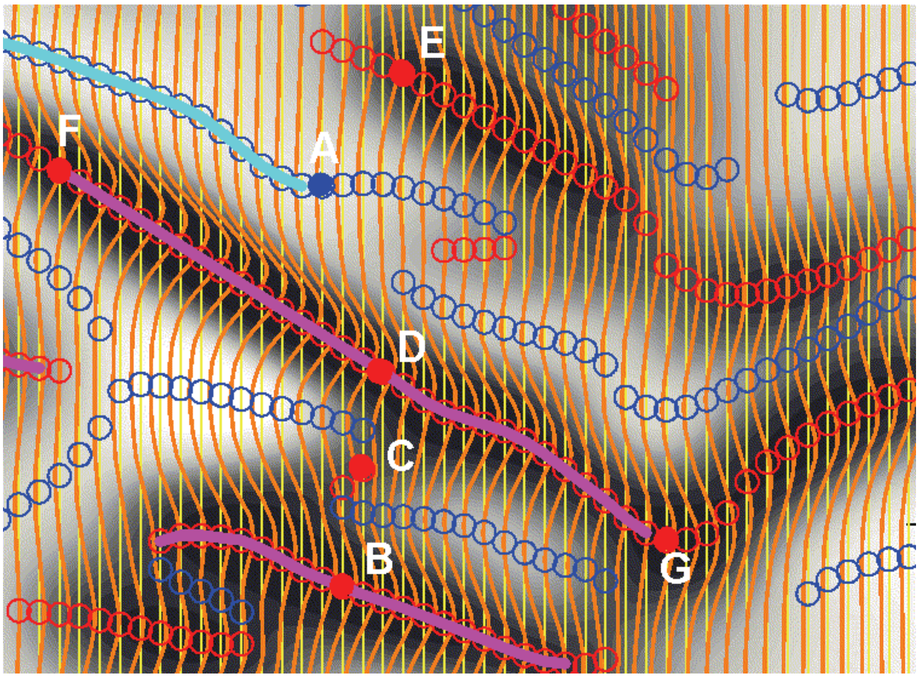

Figure 51. *A subset set of the data shown in Figure 49. Circles mark the extremes. The filled circles are discussed below and are referenced by labels A–G. Straight yellow lines mark the flight lines and the deviation of the curved orange lines from the yellow lines is proportional to the field value at the flight line. The distance between flight lines is 150 m. The minimum marked A is not included as part of the adjacent lineament because the angle of the segment connecting to the nearest minimum exceeds the threshold for angle differences (requirement 1 is not fulfilled). The maxima marked B, C, D and E define an almost straight line but this lineament is rightly excluded because of high rms values (requirement 4 is not fulfilled). In most applications of the algorithm, the threshold value for requirement 5 also excludes this lineament. Points F and G are also excluded because of high rms values.*

The third requirement is an implicit requirement related to the basic definition of a linear feature. However, it should be kept in mind that the magnetic field is a superposition of contributions from several sources and a break in the position of extremes along a particular direction does not necessarily imply a discontinuity in terms of structure.

The fourth requirement can be implemented in different ways. We have chosen to evaluate the root mean square (rms) difference between data along adjacent flight lines within windows surrounding the corresponding extreme. The line segment or width of the anomaly defined by the location of maximum/minimum gradient on each side of an extreme point is used to define the window length in the rms difference calculation. The average field value within each window is subtracted before calculation of the rms difference. Furthermore, normalisation of the data is done by dividing the measured values by the absolute difference between the maximum and minimum field values observed within one of the windows. If the rms difference is less than a specified threshold value, the extreme is considered a possible continuation of the lineament. If more than one extreme are possible connections, the one that gives the smallest rms value is selected if the other requirements are also fulfilled.

The purpose of the fifth requirement is to ensure that a possible connection between two points is excluded, if the distance is very large, i.e. when no data are available in order to judge whether a connection is likely. This criterion is implemented so that the distance threshold depends on the angle between the flight line and the line orientation for the potential connection.

The result of a similar process for the real data from the Nuuk region is shown in Figure 52.

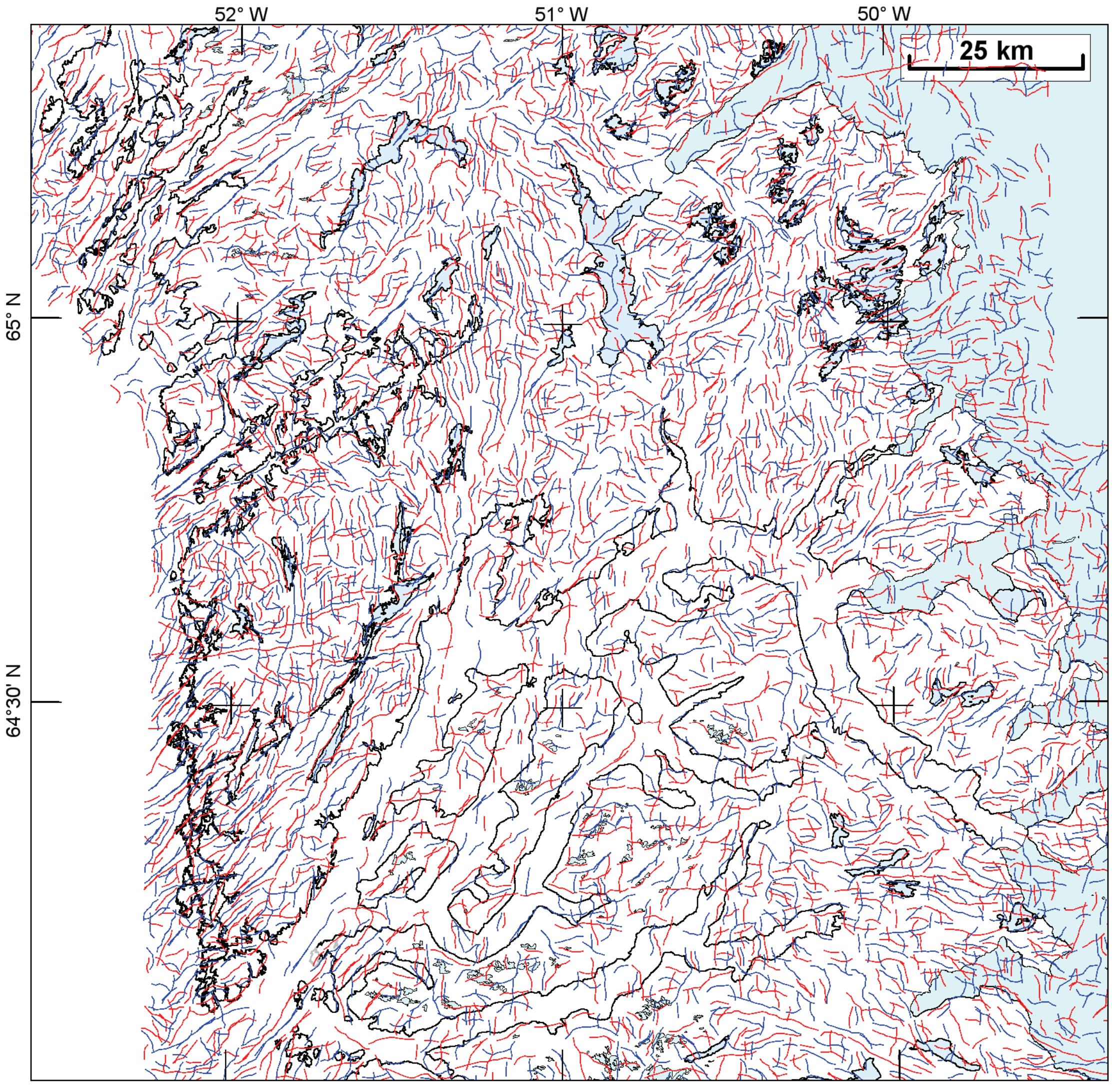

Figure 52. *Established lineaments from the extremes extracted from the aeromagnetic data from the Nuuk region.*

The above-mentioned requirements or rules are not alone sufficient for the constructing of a computer algorithm to locate lineaments from real data. The program must also be able to handle noise features that may resemble local extremes in the source magnetic field. Certain filters take care of this, disregarding an extreme if the difference between the source field values at the extreme location and at the closest position of maximum/minimum gradient is smaller than some predefined threshold. Furthermore, a criterion is implemented to select field variations for which the width of the anomalies is within a prescribed range.

The input data to the algorithm used in this report from the Nuuk region is the vertical gradient of the vertical component of the magnetic field. The derivatives are calculated by applying a linear filter to the total magnetic field data. Application of this technique requires that the total field data be represented on a regular grid, i.e. the original line data are interpolated and resampled in two directions at equidistant locations. The linear feature extraction algorithm is applied to grid-lines in two orthogonal directions, and the extracted lineaments with angles larger than 45° to the grid-lines are subsequently unified into one merged dataset of extracted lineaments. The unified dataset of lineaments is shown in Figure 15. This dataset is used in the subsequent statistical characterisations of lineaments (see next section).

Statistical characterisation of lineaments

The use of the results from the linear feature extraction in the statistical modelling of gold showings, demand a further parameterisation. Several options exist. Most of these involve minimum and maximum values or mean values for localised spatial averages within a predetermined area (the area is referred to as the *window or search radius*). Running mean calculations are used for the spatial averaging.

As presently implemented, some of the parameter options are:

- The mean, minimum and maximum length of lineaments within or crossing a window
- Minimum distance to nearest lineament within a window
- Density of lineaments in a window
- 'Complexity factor', uniformity of orientation angles within a window (values from 0 to 1; a value of 1 implies that all lineaments have the same orientation (less complex lineament patterns) whereas a value of 0 implies orthogonal orientations (complex lineament patterns))

The analysis can be sub-divided further by partitioning the lineaments into classes according to their length or width of the corresponding anomalies.

Calculations of the first mentioned quantities are self-explaining. However, the calculation of the complexity factor, the uniformity of orientations, needs some explanation. The first step in the calculation is to obtain a unit vector along each lineament and afterwards perform a rotation of these vectors by multiplying the rotation angle (the angle in the range 0 to 180 degrees measured from north towards east) by a factor of 2. The uniformity is then calculated as the Euclidean norm of the normalised vector sum of the rotated unit vectors. A value of 1 implies that all lineaments have the same orientation whereas a value of 0 implies orthogonal orientations. Values in the range between 0 and 1 indicate varying degree of uniformity. In the example with synthetic data, values of 0.97 are obtained for the leftmost part and 0.87 for the rightmost part when using circles of radius 10000 metres for the averaging windows. In general, this quantity can be regarded as a factor reflecting the complexity of the lineament patterns in an area.

The representations of the lineament extractions of the regional aeromagnetic data are available in Appendix B. The statistical characterisation of identified lineaments from the aeromagnetic data has so far been run for windows (search radiuses) of 1, 2, 3, and 5 km. However, only the results of the smallest and largest search radius are given in Appendix B, and only the search radius of 1000 m have been used so far as input to the statistical multiparameter modelling for gold showings (see Appendix C).

Appendix B – Grid images of aeroradiometric data and statistical characterisations of lineaments in aeromagnetic data

Aeroradiometric data

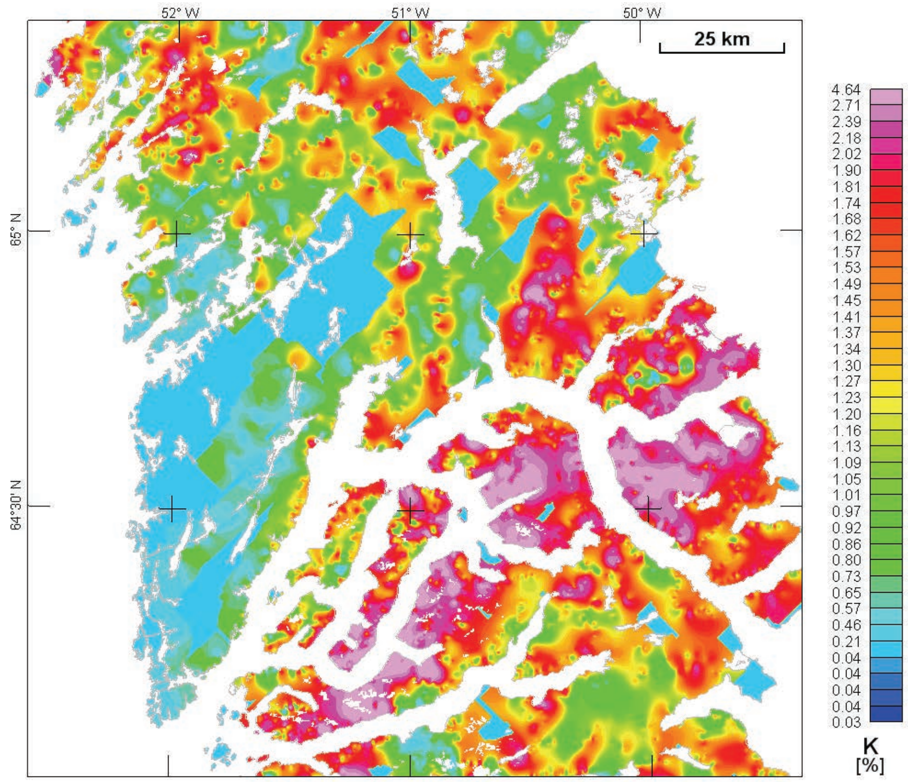

Figure 53. *Grid image of surface concentrations of K based on aeroradiometric measurements.*

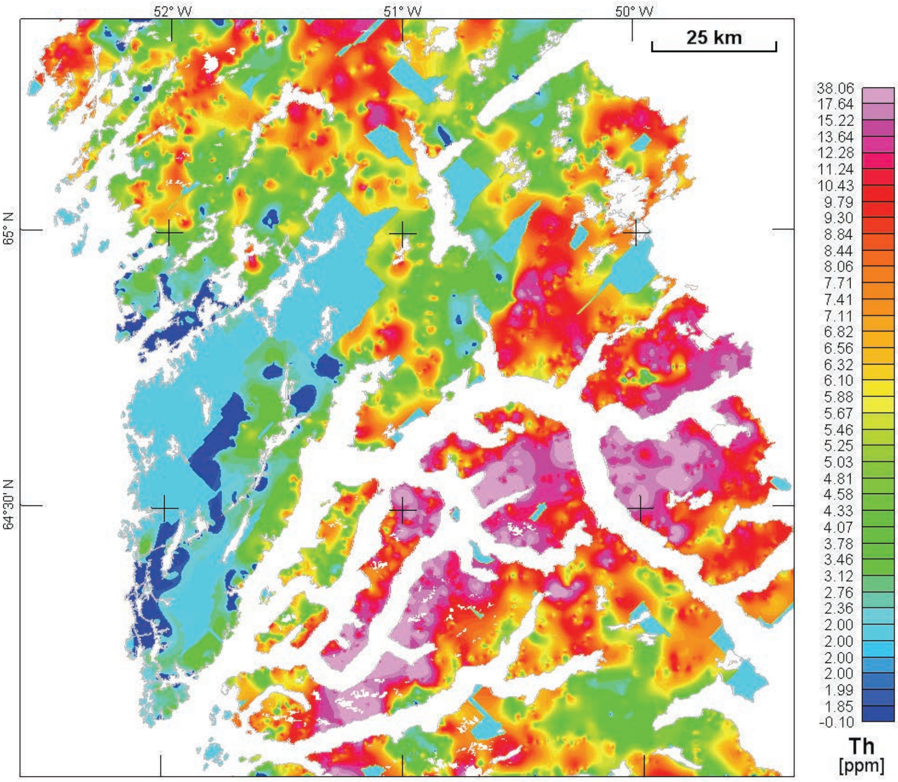

Figure 54. *Grid image of surface concentrations of eTh based on aeroradiometric measurements.*

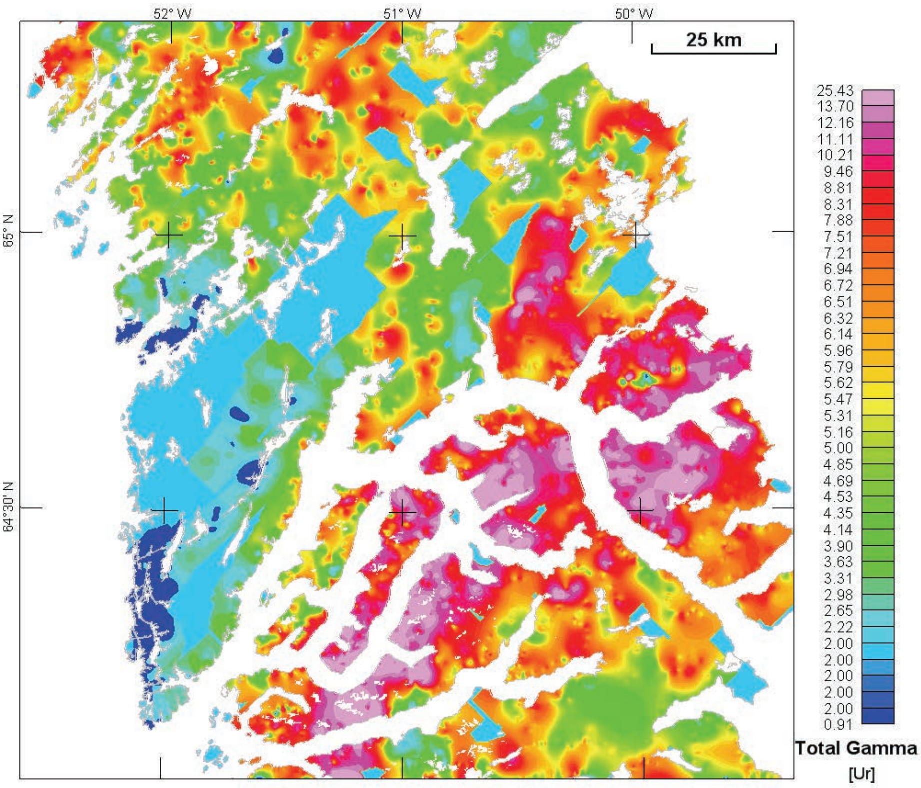

Figure 55. *Grid image of Total Gamma radiation based on aeroradiometric measurements.*

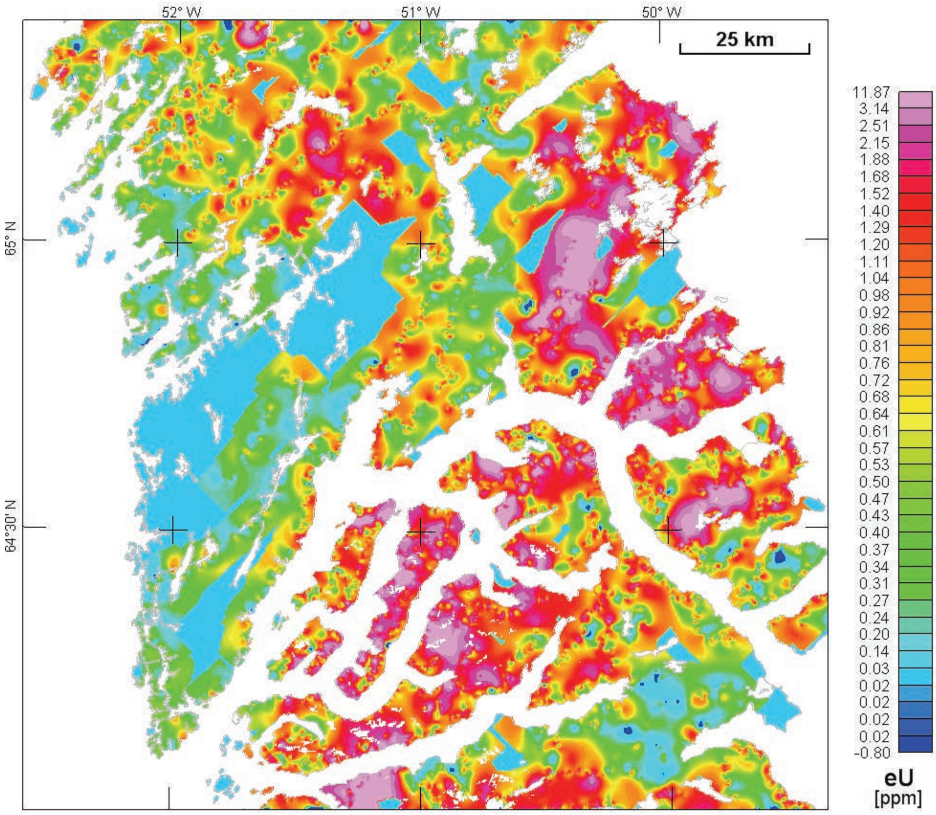

Figure 56. *Grid image of surface concentrations of eU based on aeroradiometric measurements.*

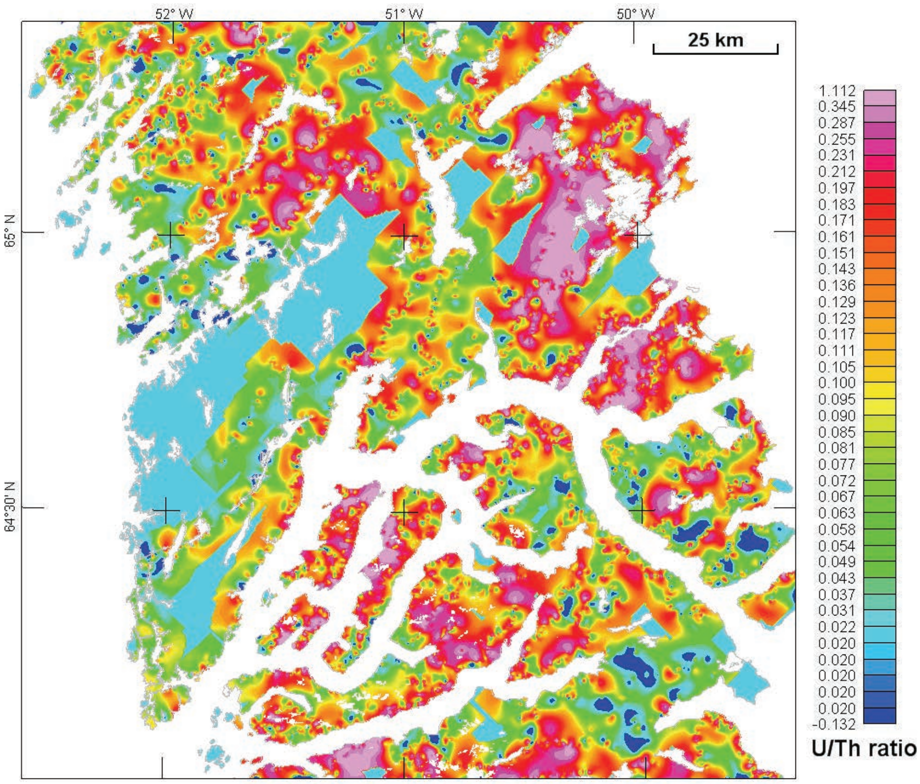

Figure 57. *Grid image of surface eU/eTh ratio based on aeroradiometric measurements.*

Statistically defined lineaments from aeromagnetic data

Locations of the identified gold showings are indicated by black filled squares. A linear colour scale is used unless stated otherwise in the figure captions.

Abbreviations in figure captions:

all lines	All lineaments, without considering their length, have been analysed.
0–10%	Only lineaments with a length which are 0–10% (2000–2100 m) of the maximum length of all lineaments have been analysed.
0–25%	Only lineaments with a length which are 0–25% (2000–2450 m) of the maximum length of all lineaments have been analysed.
25–50%	Only lineaments with a length which are 25–50% (2450–3100 m) of the maximum length of all lineaments have been analysed.
50–75%	Only lineaments with a length which are 50–75% (3100–4250 m) of the maximum length of all lineaments have been analysed.
75–100%	Only lineaments with a length which are 75–100% (4250–23600 m) of the maximum length of all lineaments have been analysed.
90–100%	Only lineaments with a length which are 90–100% (6030–23600 m) of the maximum length of all lineaments have been analysed.

mean direction	Mean direction of lineaments within the search radius (from 0 to 180°).
minimum distance	Minimum distance to nearest lineament within the search radius (in meters).
nlcross	Number of lineaments crossing the search radius (a number).
total length	The total length of the lineaments crossing the search radius (in meters).
unit vector sum	Uniformity – a complexity factor – length of vector sum of unit vectors divided by number of vectors within the search radius (from 0 to 1).

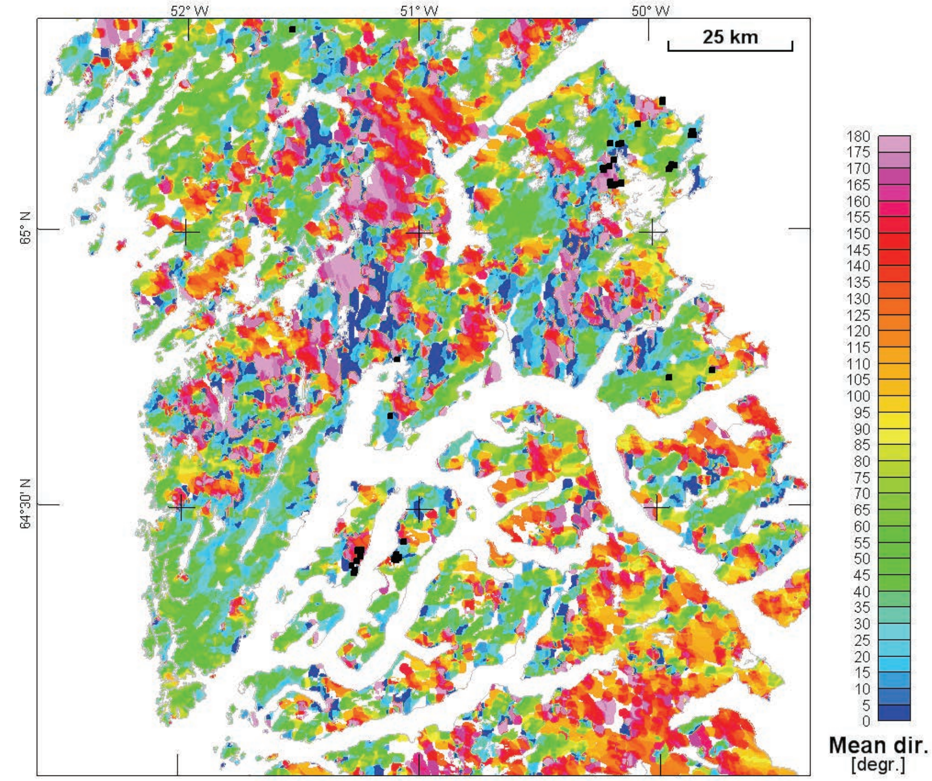

Figure 58. *Lineament statistics, mean direction, search radius 1000 m, all lineament lengths.*

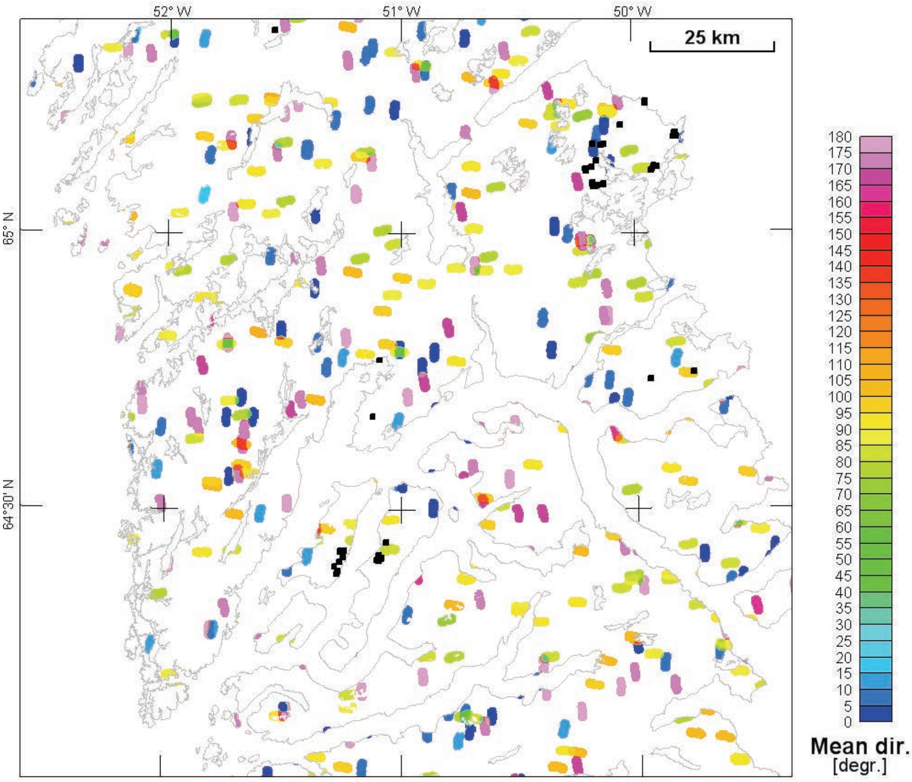

Figure 59. *Lineament statistics, mean direction, search radius 1000 m, for lineaments lengths 2000–2100m (0–10%).*

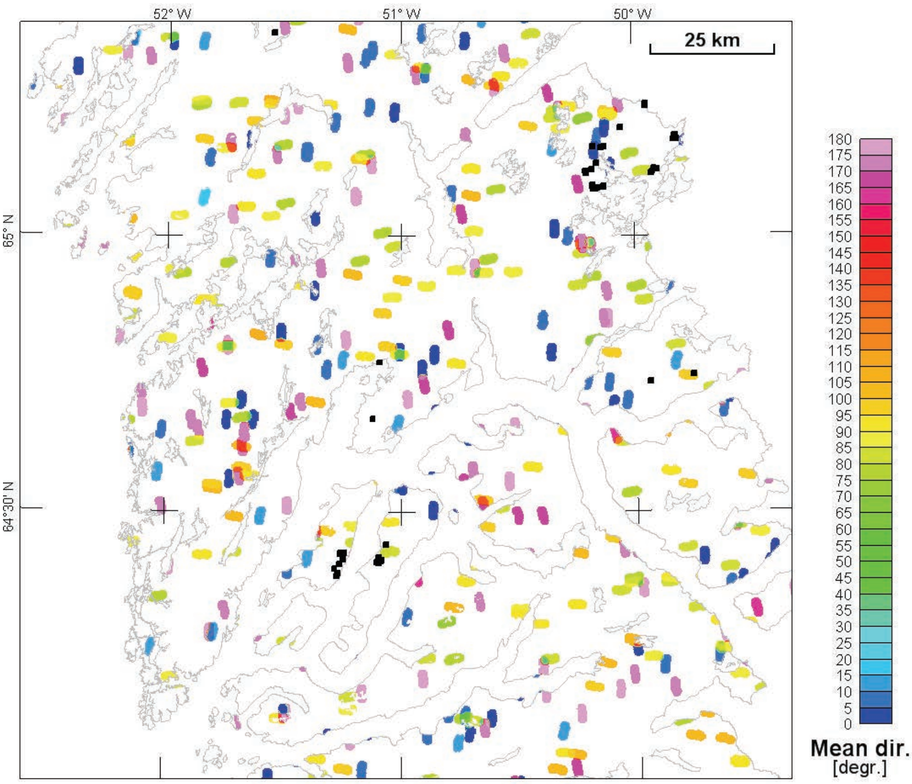

Figure 60. *Lineament statistics, mean direction, search radius 1000 m, for lineaments lengths 2000–2450m (0–25%).*

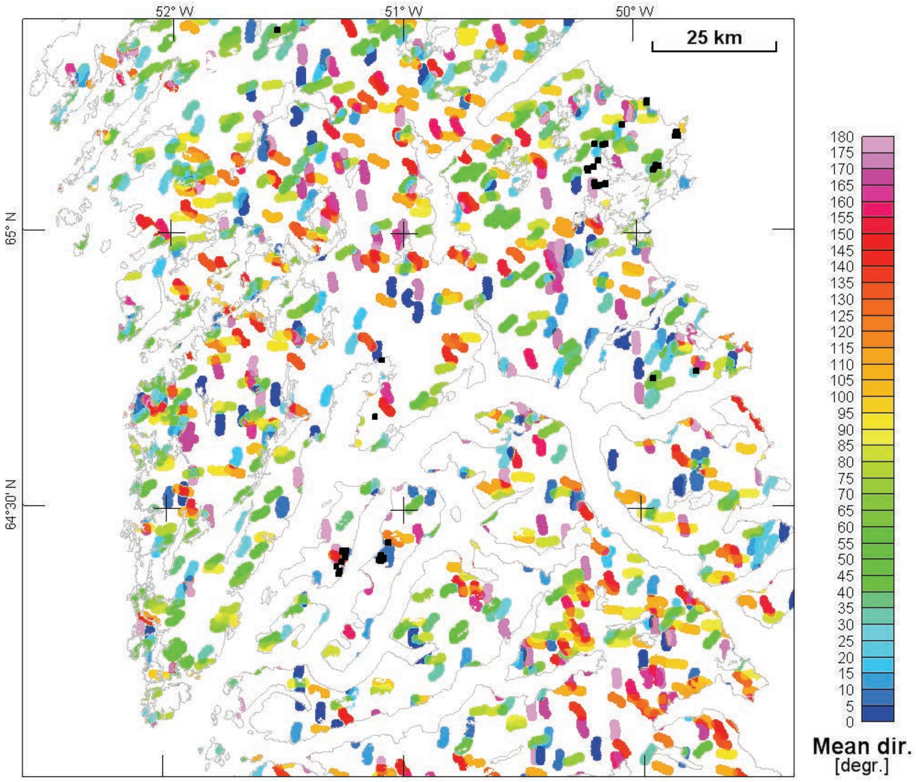

Figure 61. *Lineament statistics, mean direction, search radius 1000 m, for lineaments lengths 2450–3100 m (25–50%).*

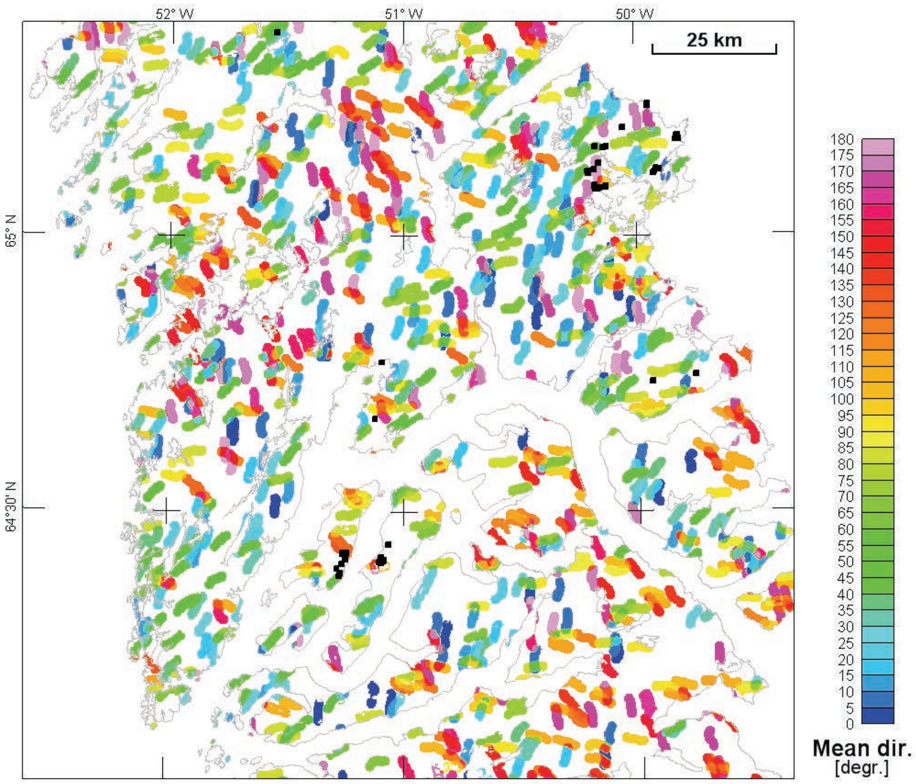

Figure 62. *Lineament statistics, mean direction, search radius 1000 m, for lineament lengths 3100–4250 m (50–75%).*

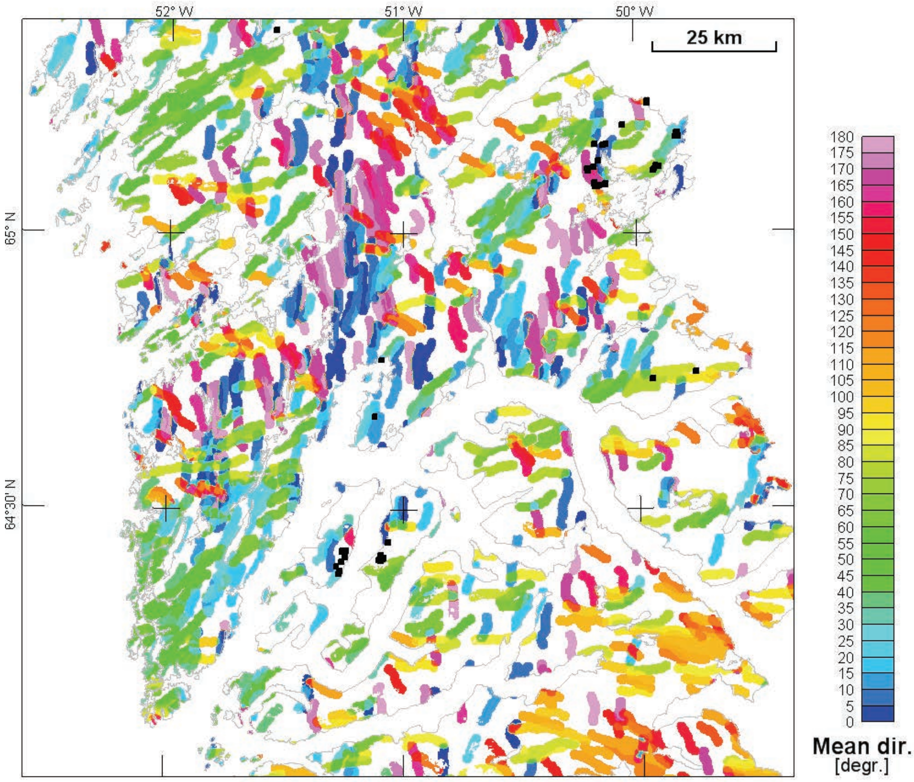

Figure 63. *Lineament statistics, mean direction, search radius 1000 m, for lineament lengths 4250–23600 m (75–100%).*

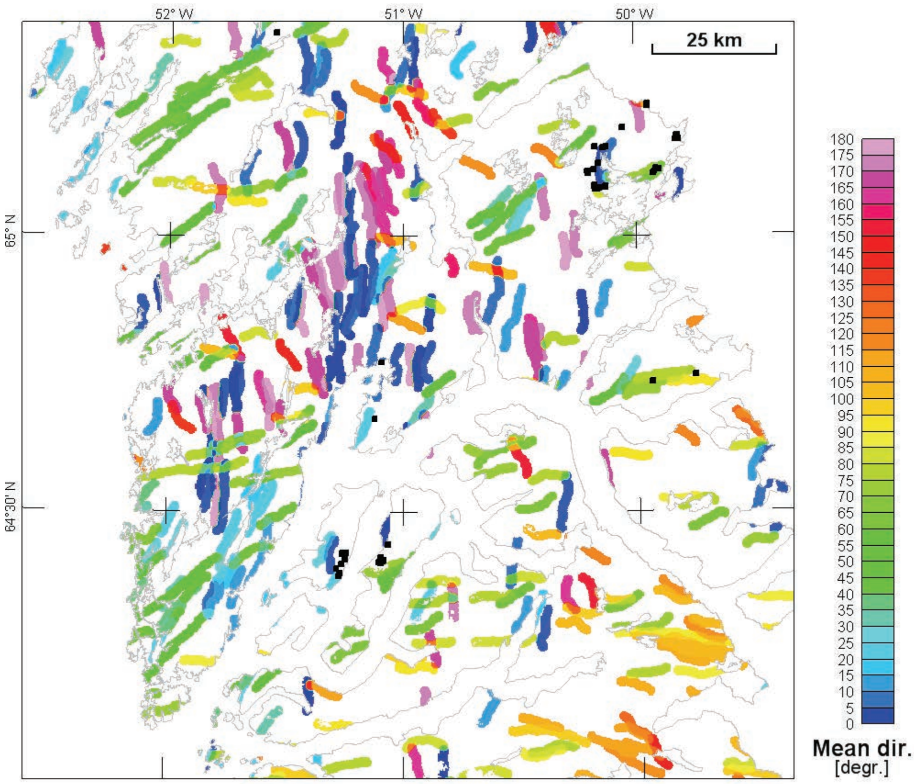

Figure 64. *Lineament statistics, mean direction, search radius 1000 m, for lineament lengths 6030–23600 m (90–100%).*

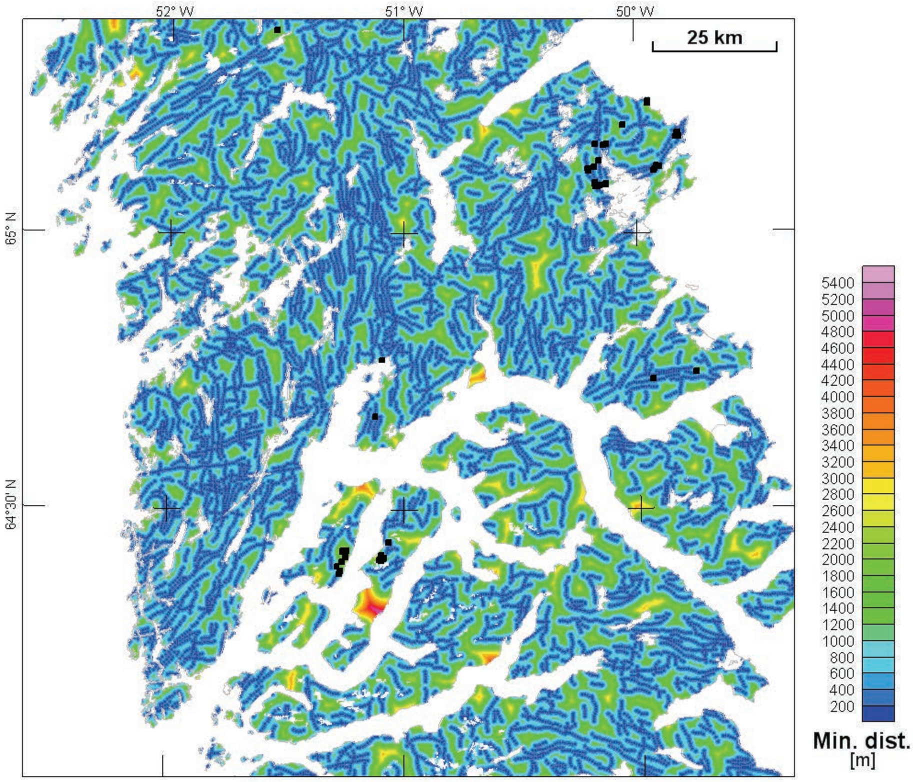

Figure 65. *Lineament statistics, minimum distance, search radius 1000 m, all lineament lengths.*

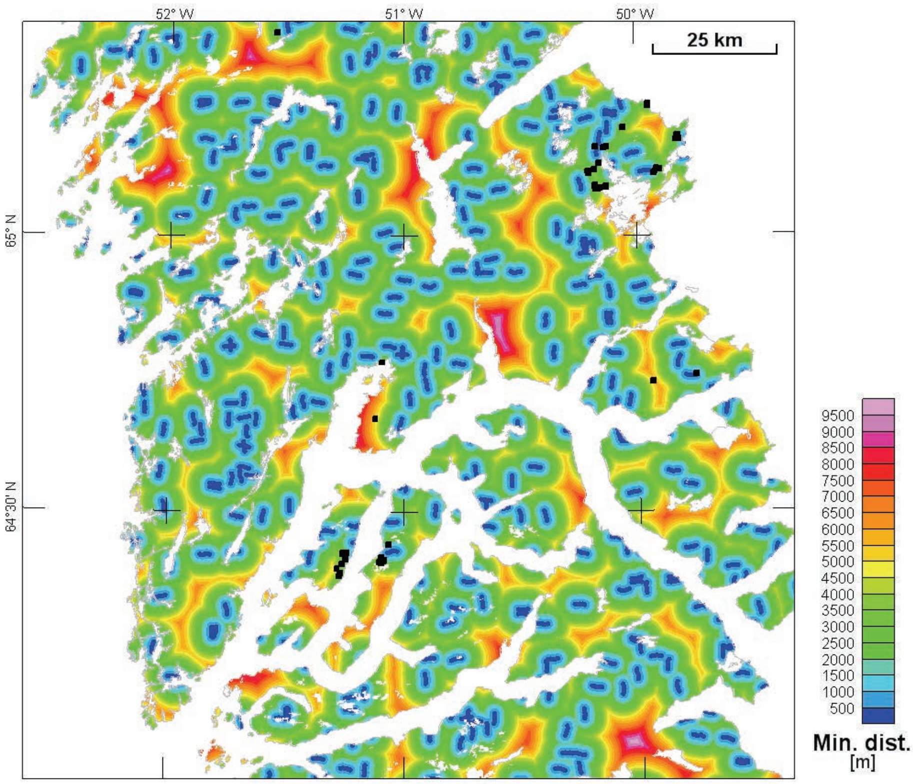

Figure 66. *Lineament statistics, minimum distance, search radius 1000 m, for lineaments lengths 2000–2100m (0–10%).*

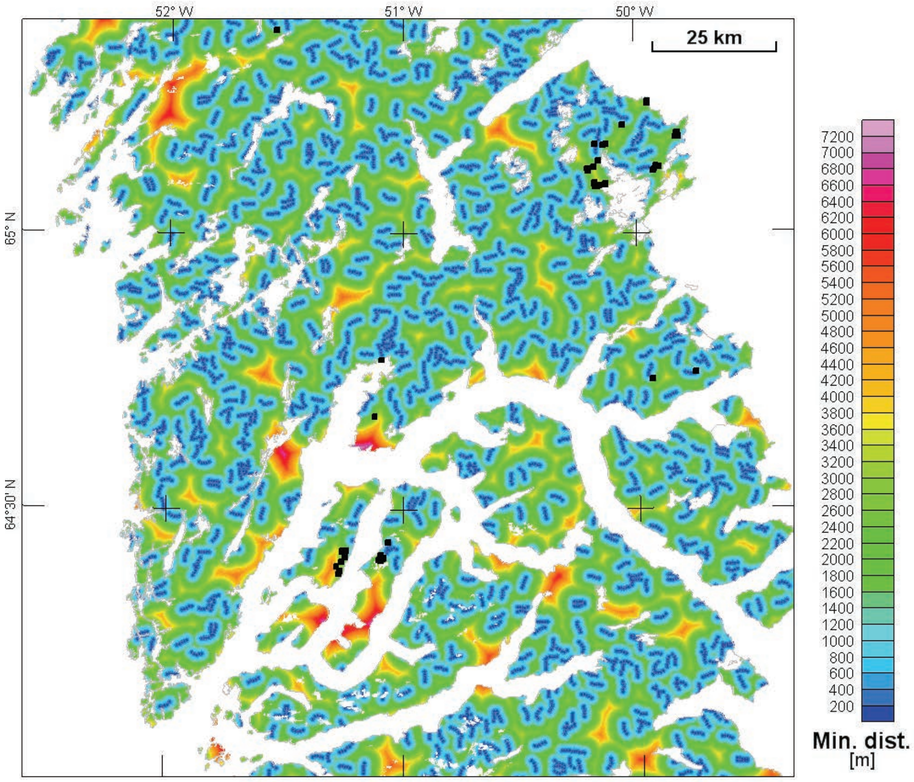

Figure 67. *Lineament statistics, minimum distance, search radius 1000 m, for lineaments lengths 2000–2450m (0–25%).*

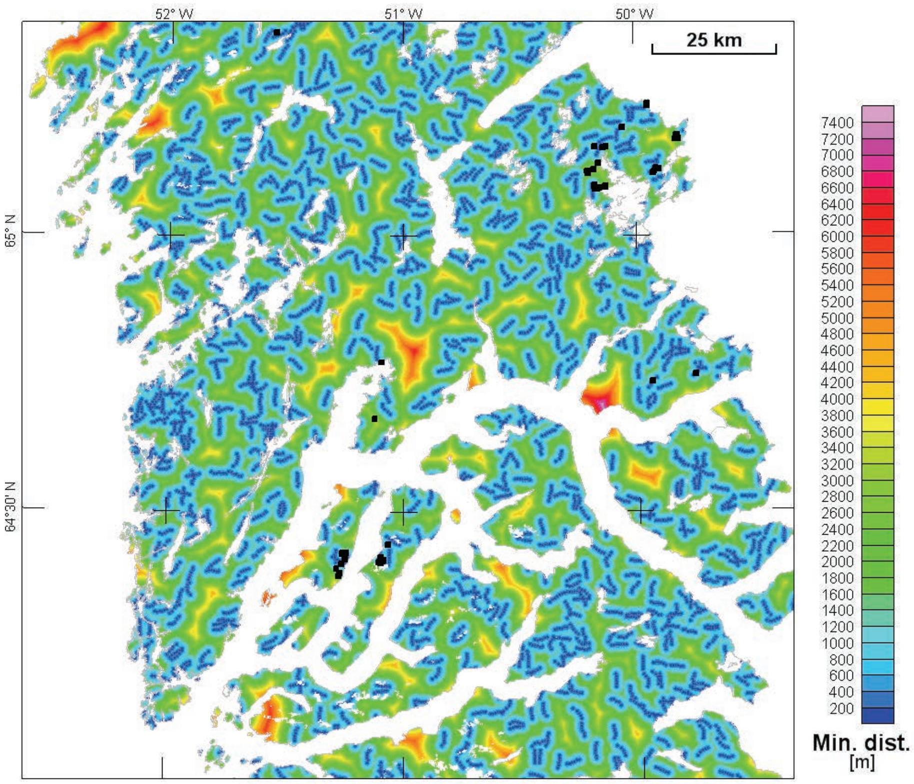

Figure 68. *Lineament statistics, minimum distance, search radius 1000 m, for lineaments lengths 2450–3100 m (25–50%).*

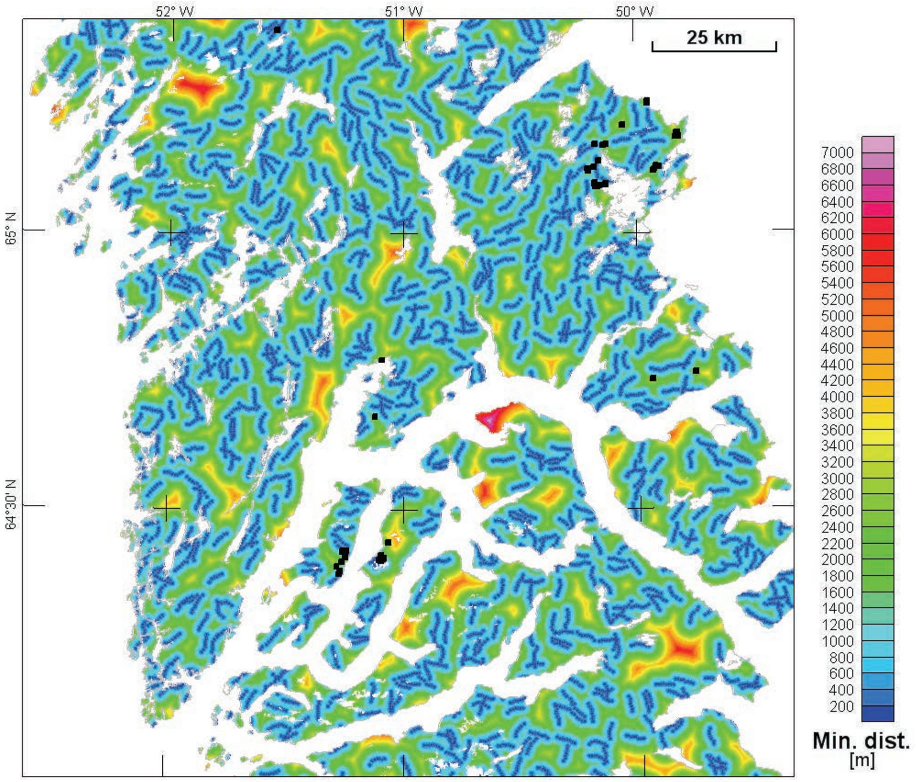

Figure 69. *Lineament statistics, minimum distance, search radius 1000 m, for lineament lengths 3100–4250 m (50–75%).*

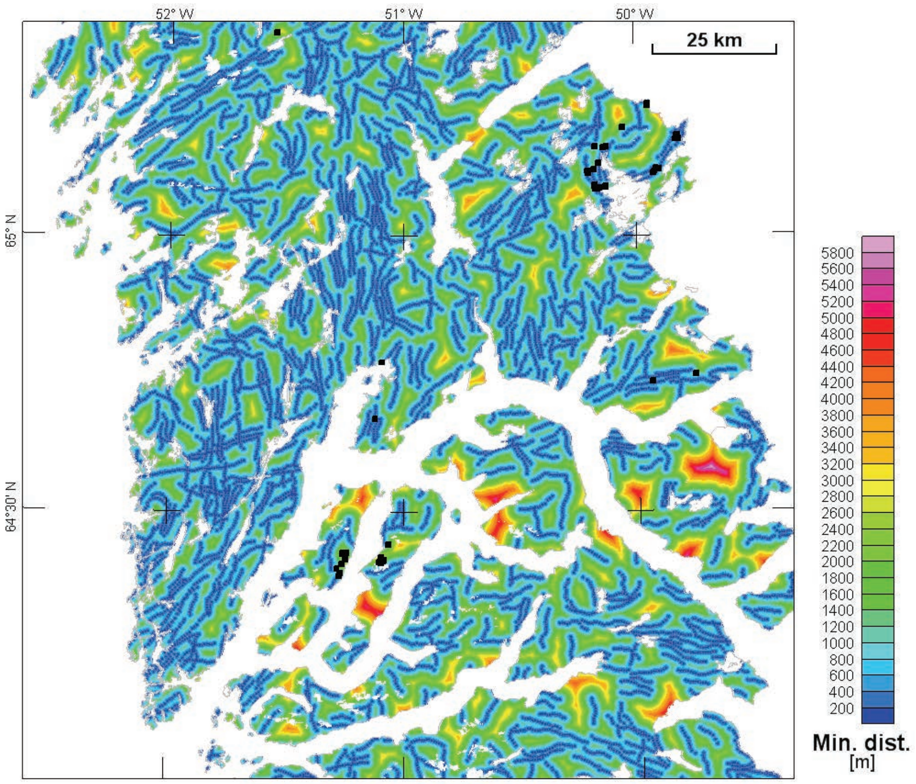

Figure 70. *Lineament statistics, minimum distance, search radius 1000 m, for lineament lengths 4250–23600 m (75–100%).*

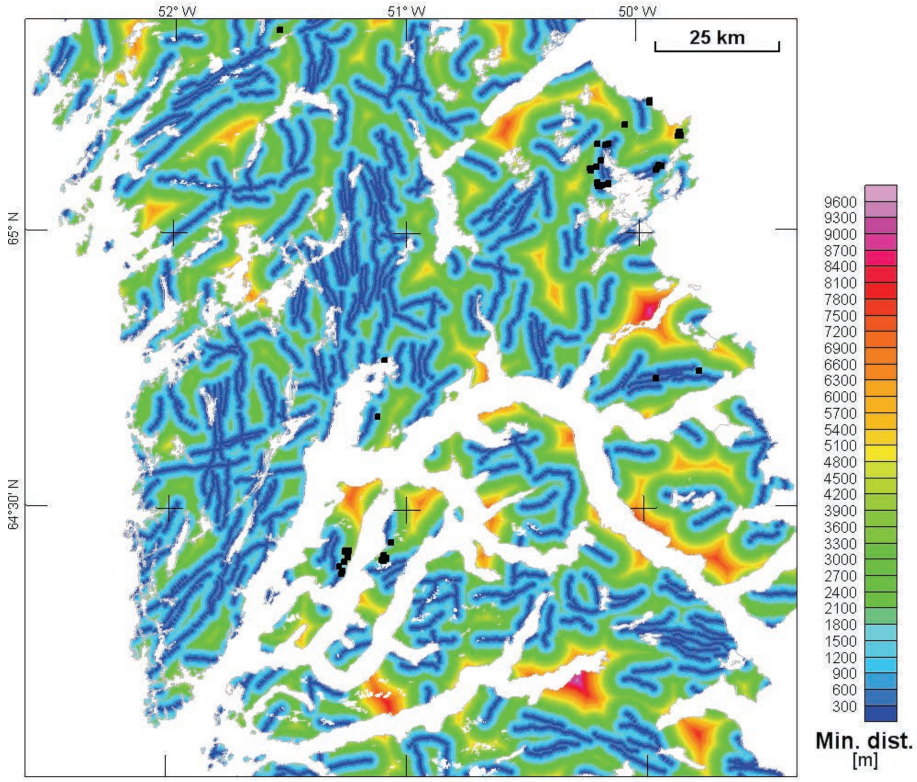

Figure 71. *Lineament statistics, mean direction, search radius 1000 m, for lineament lengths 6030–23600 m (90–100%).*

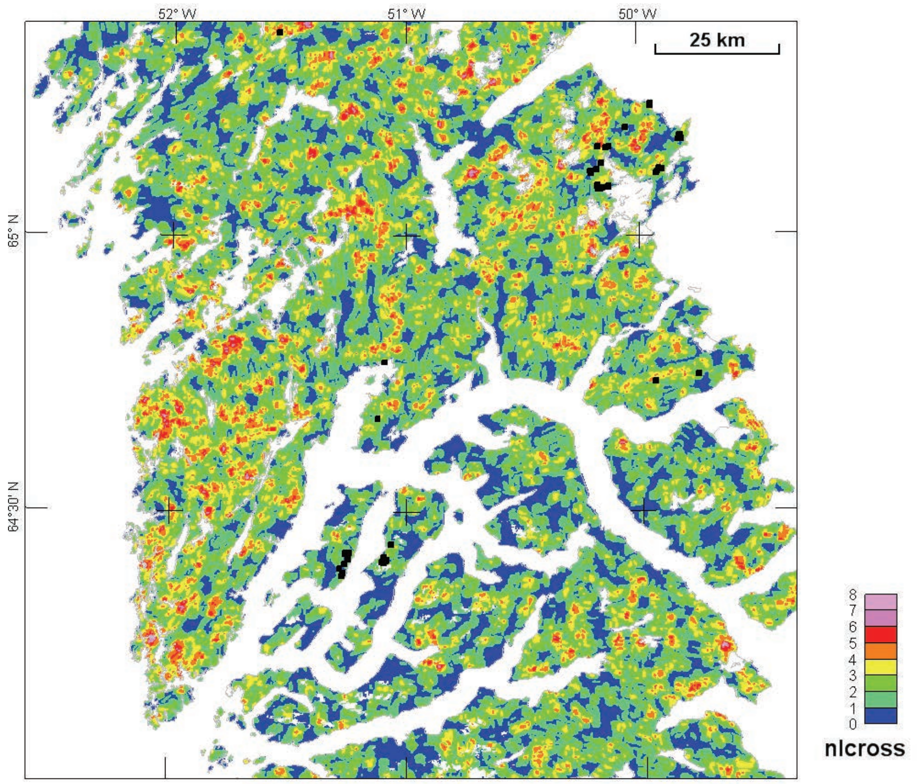

Figure 72. *Lineament statistics, number of crossing lineaments, search radius 1000 m, all lineament lengths.*

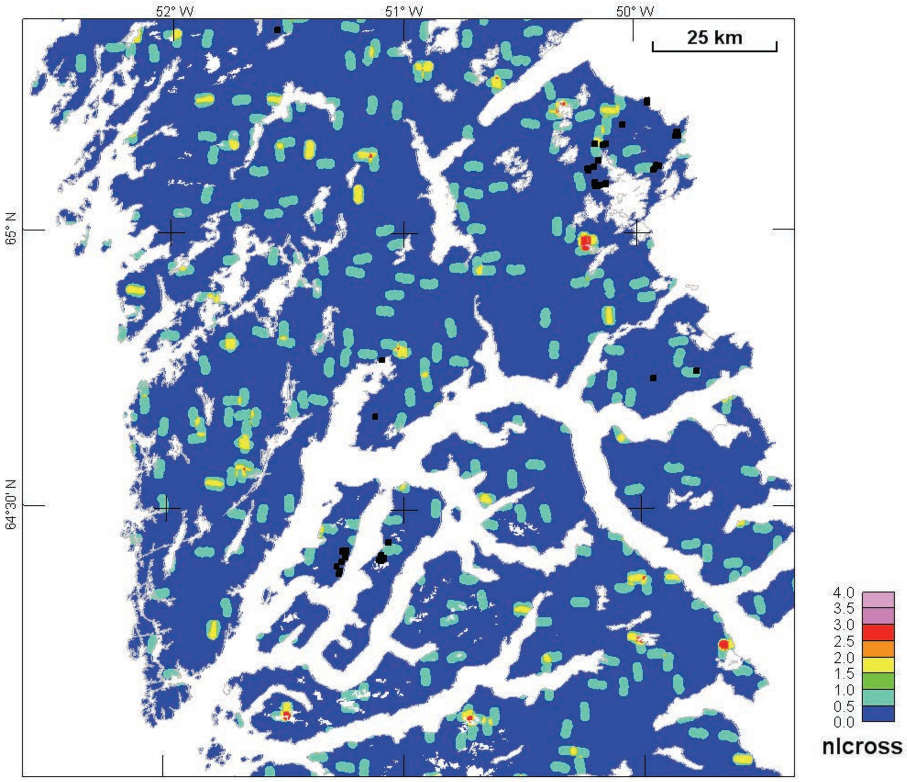

Figure 73. *Lineament statistics, number of crossing lineaments, search radius 1000 m, for lineaments lengths 2000–2100m (0–10%).*

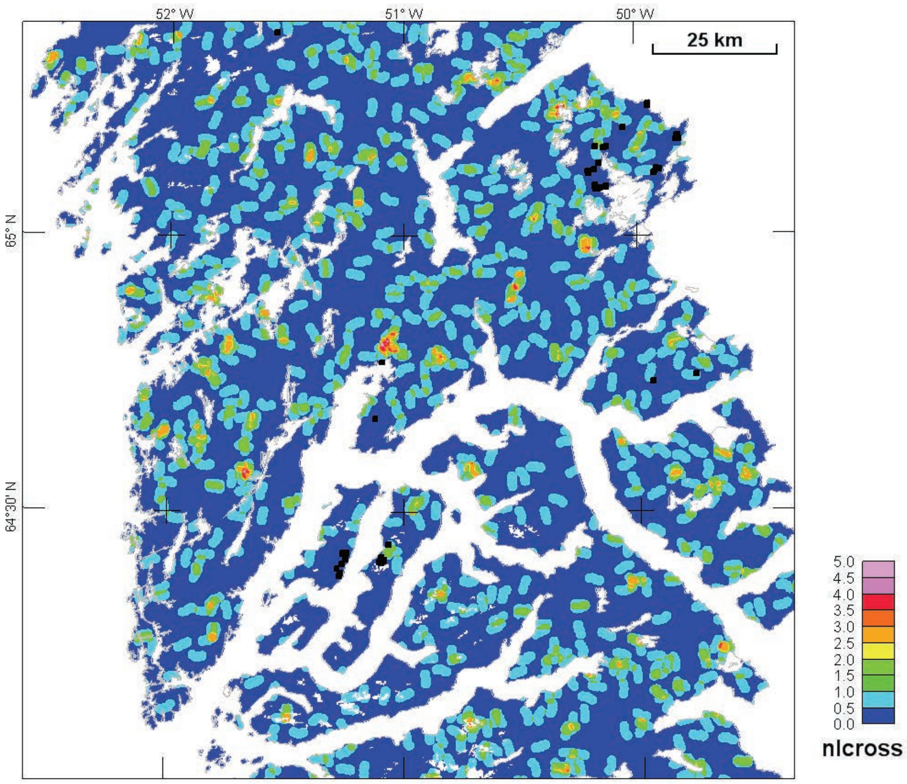

Figure 74. *Lineament statistics, number of crossing lineaments, search radius 1000 m, for lineaments lengths 2000–2450m (0–25%).*

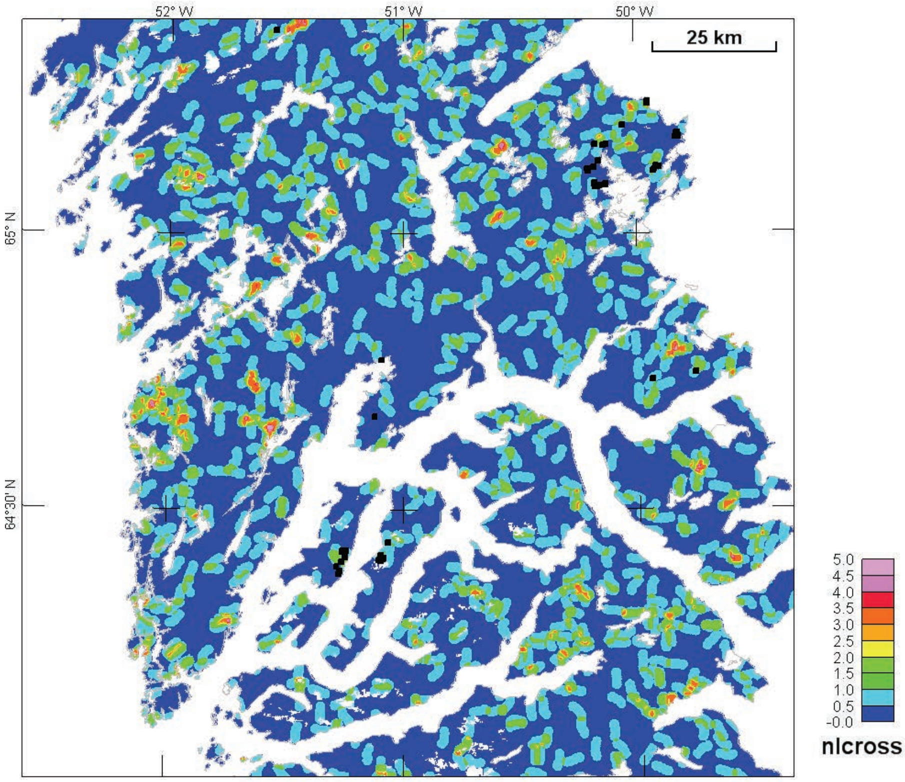

Figure 75. *Lineament statistics, number of crossing lineaments, search radius 1000 m, for lineaments lengths 2450–3100 m (25–50%).*

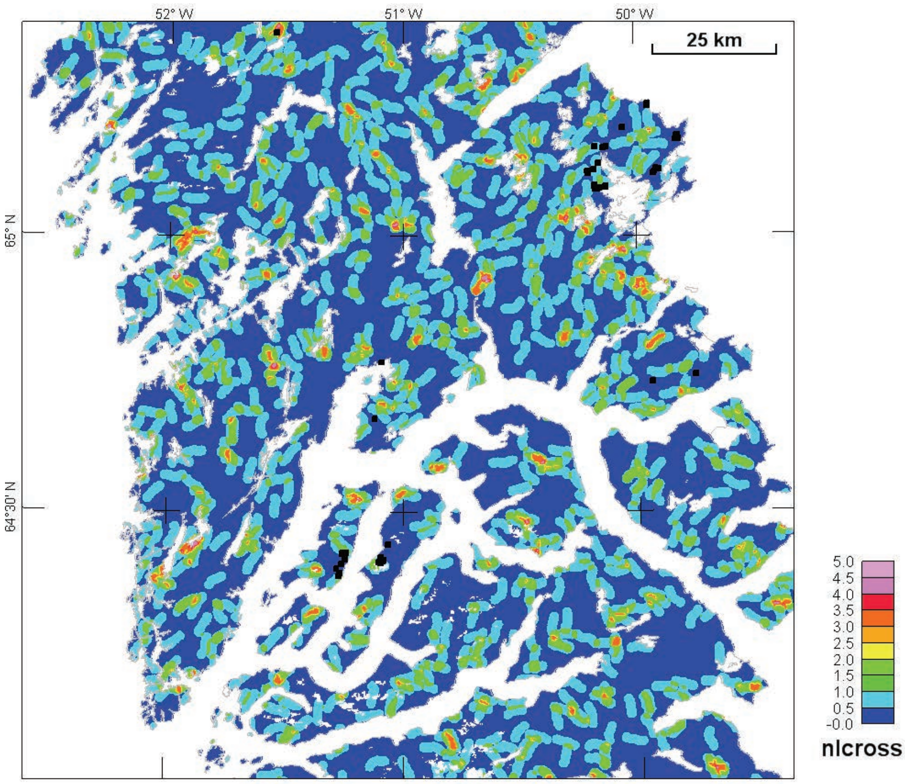

Figure 76. *Lineament statistics, number of crossing lineaments, search radius 1000 m, for lineament lengths 3100–4250 m (50–75%).*

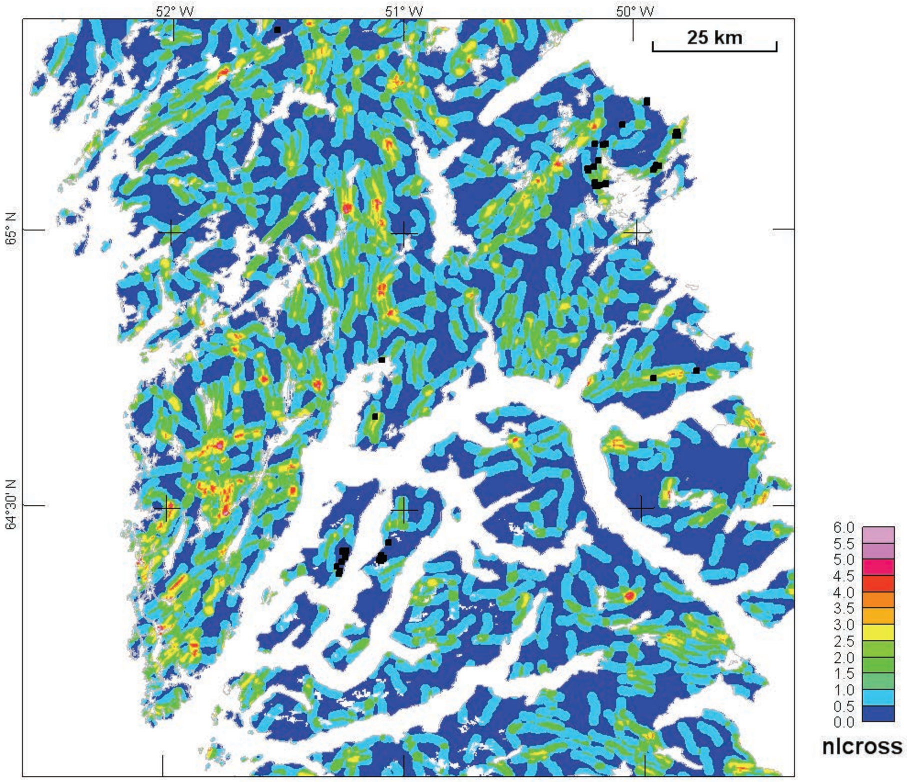

Figure 77. *Lineament statistics, number of crossing lineaments, search radius 1000 m, for lineament lengths 4250–23600 m (75–100%).*

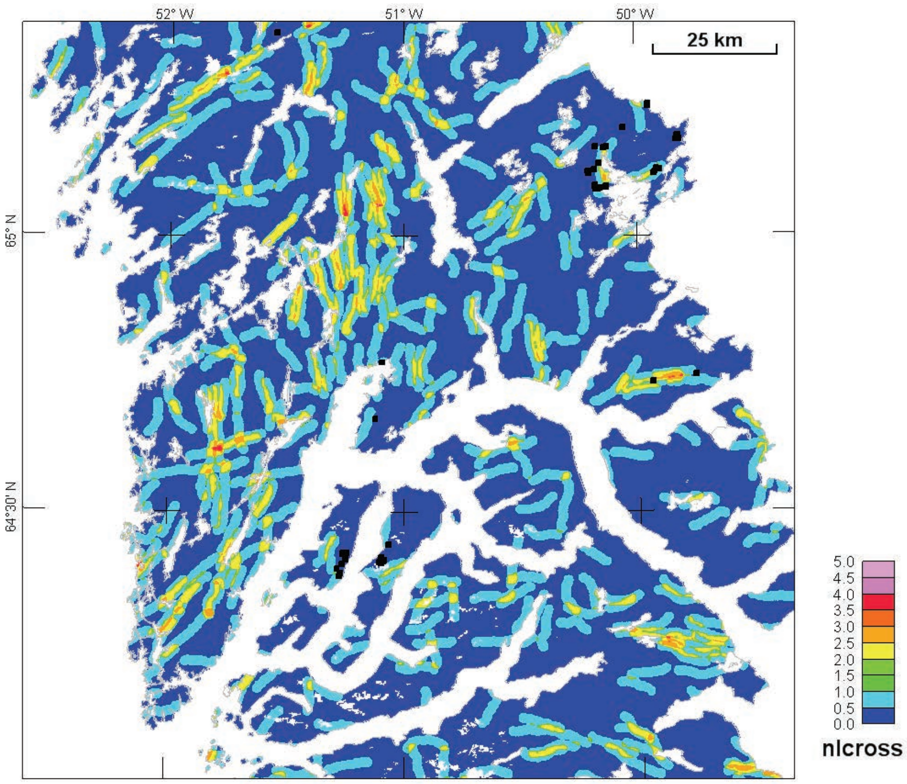

Figure 78. *Lineament statistics, number of crossing lineaments, search radius 1000 m, for lineament lengths 6030–23600 m (90–100%).*

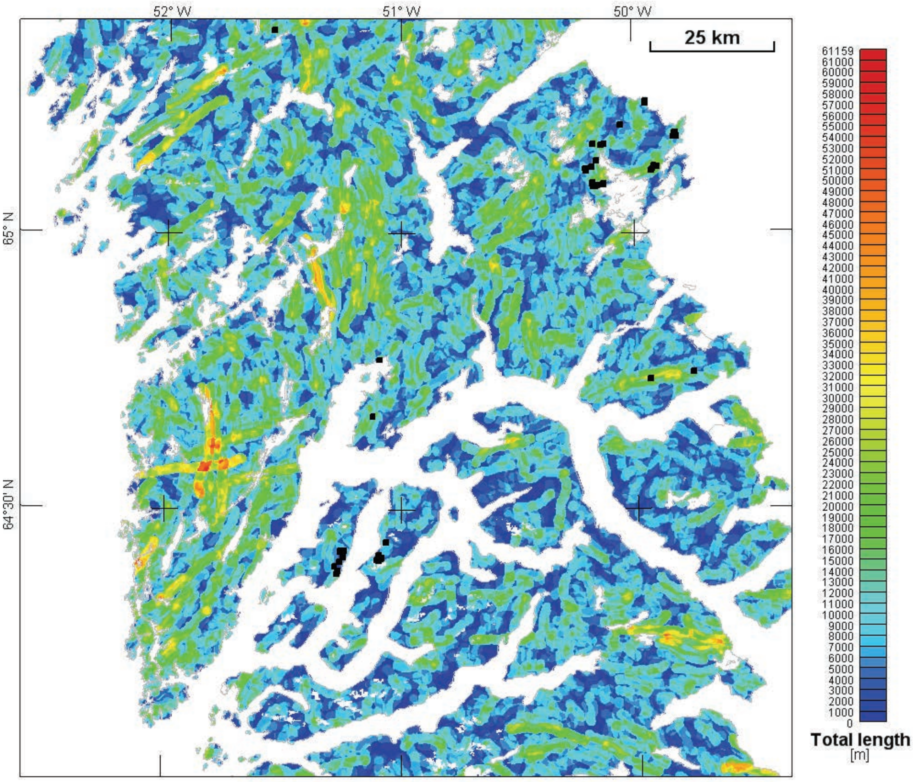

Figure 79. *Lineament statistics, total length of lineaments, search radius 1000 m, all lineament lengths.*

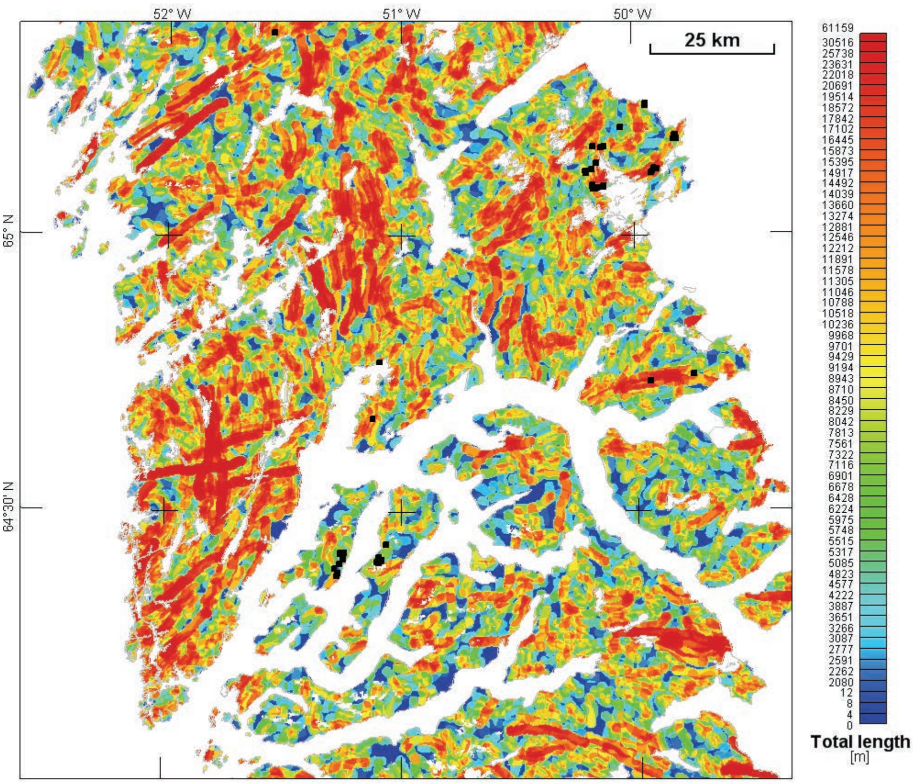

Figure 80. *Lineament statistics, total length of lineaments, search radius 1000 m, all lineament lengths. Histogram equalisation colour scale.*

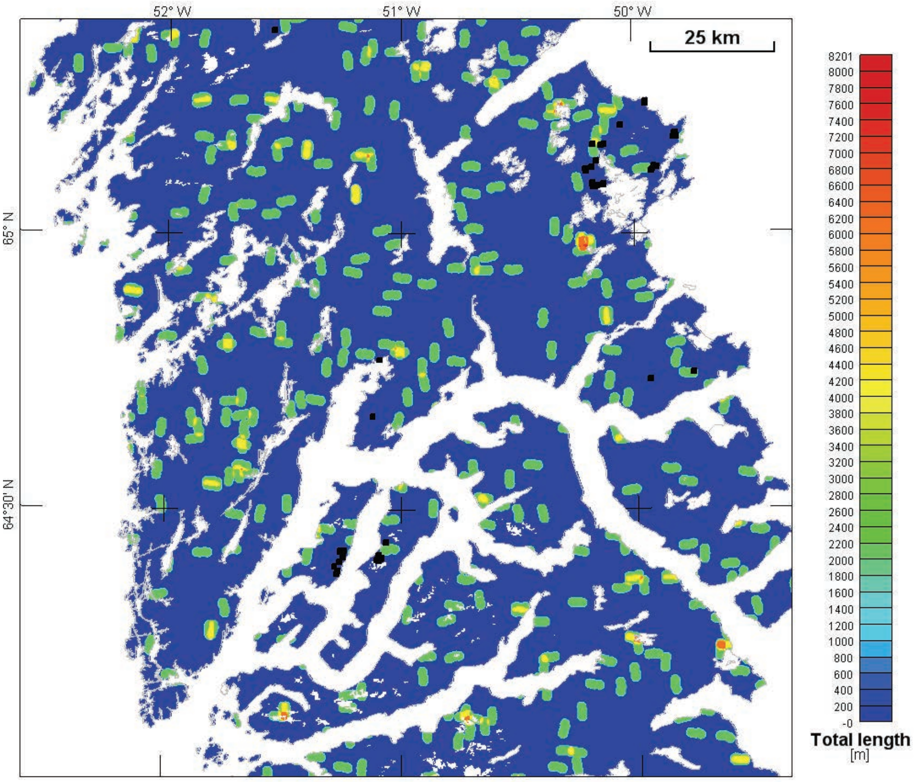

Figure 81. *Lineament statistics, total length of lineaments, search radius 1000 m, for lineaments lengths 2000–2100m (0–10%).*

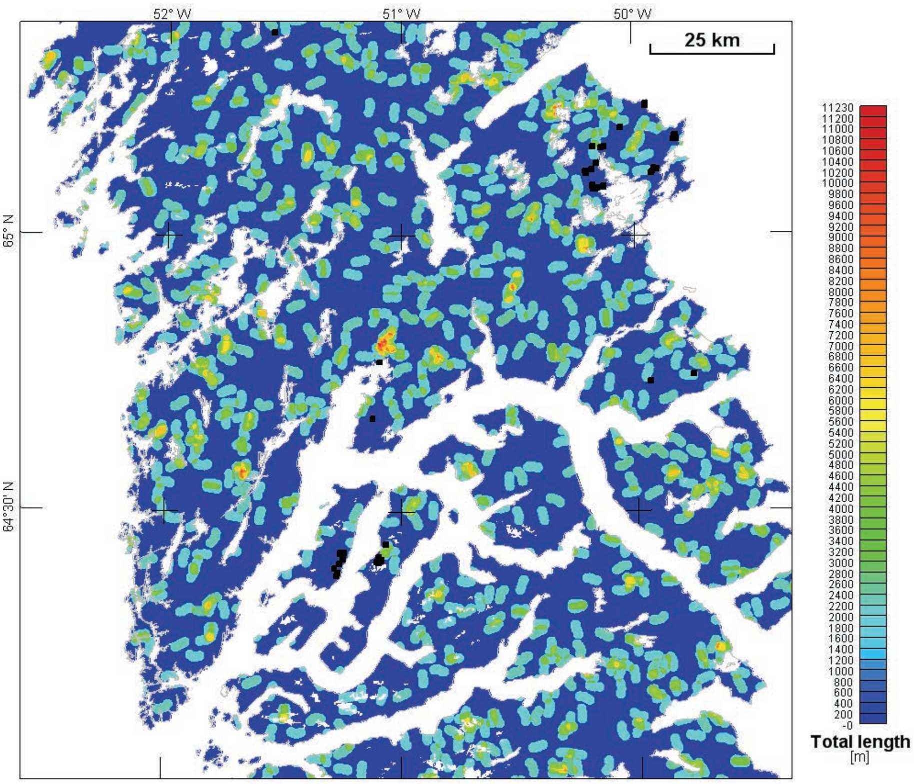

Figure 82. *Lineament statistics, total length of lineaments, search radius 1000 m, for lineaments lengths 2000–2450m (0–25%).*

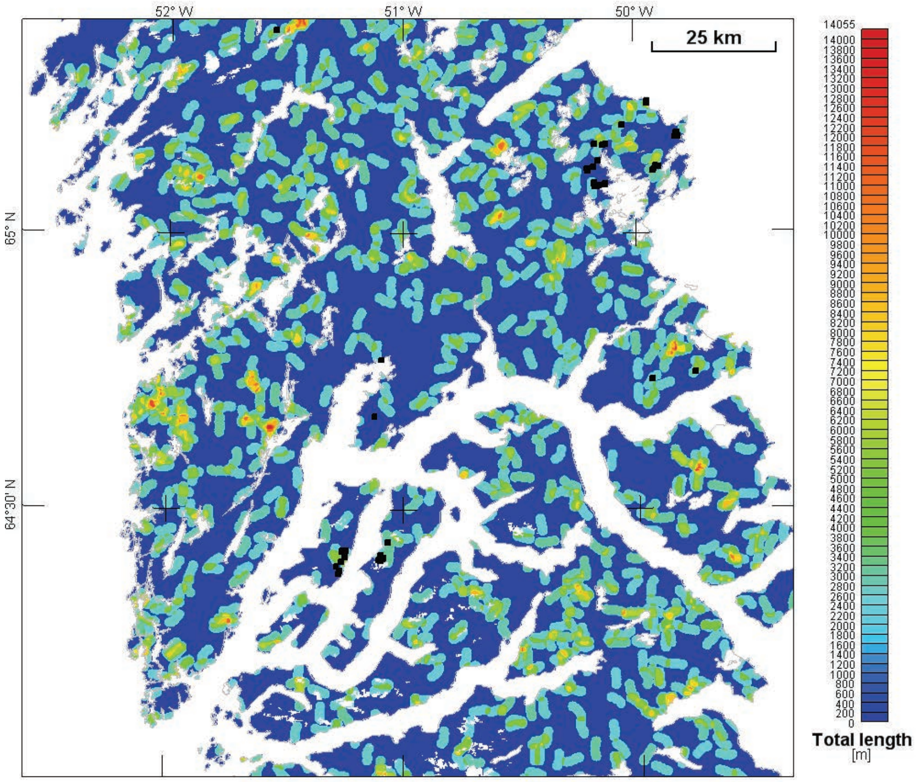

Figure 83. *Lineament statistics, total length of lineaments, search radius 1000 m, for lineaments lengths 2450–3100 m (25–50%).*

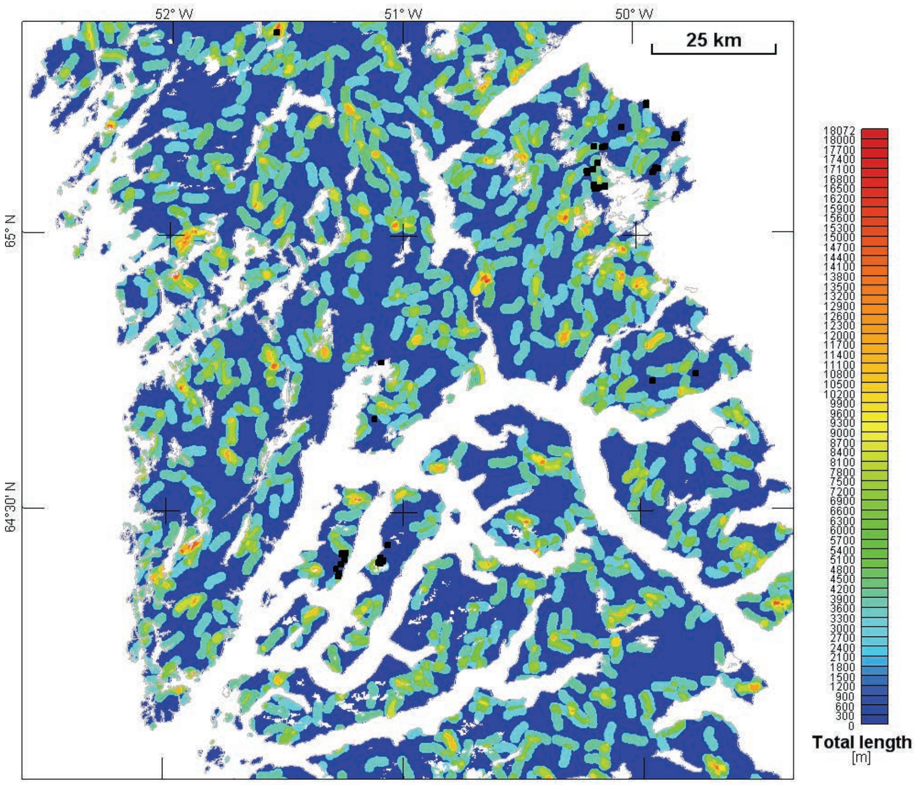

Figure 84. *Lineament statistics, total length of lineaments, search radius 1000 m, for lineament lengths 3100–4250 m (50–75%).*

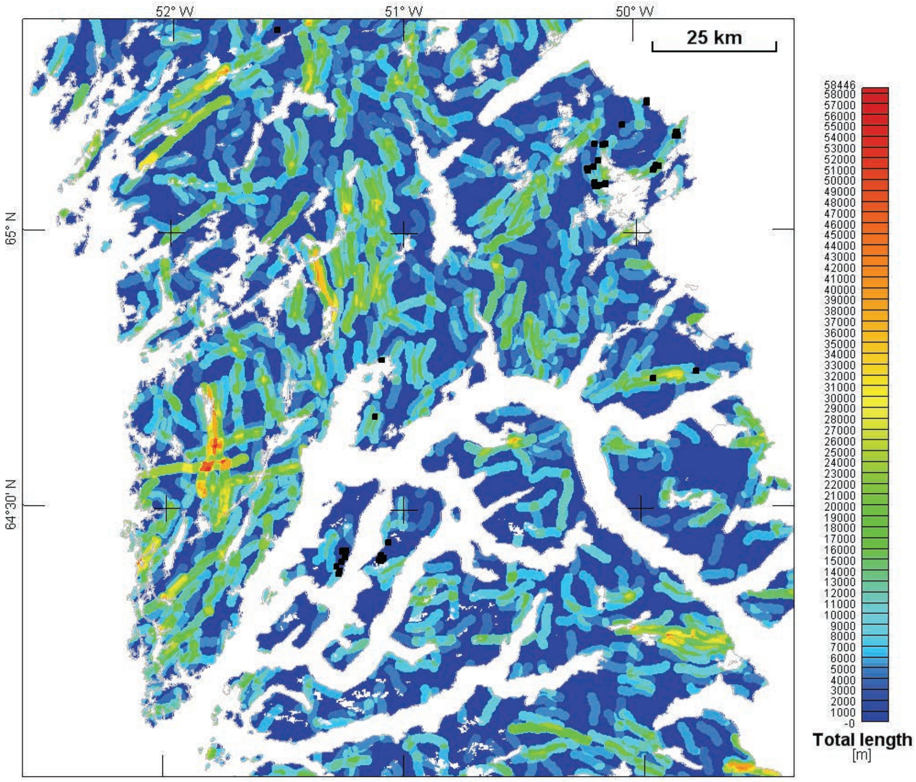

Figure 85. *Lineament statistics, total length of lineaments, search radius 1000 m, for lineament lengths 4250–23600 m (75–100%).*

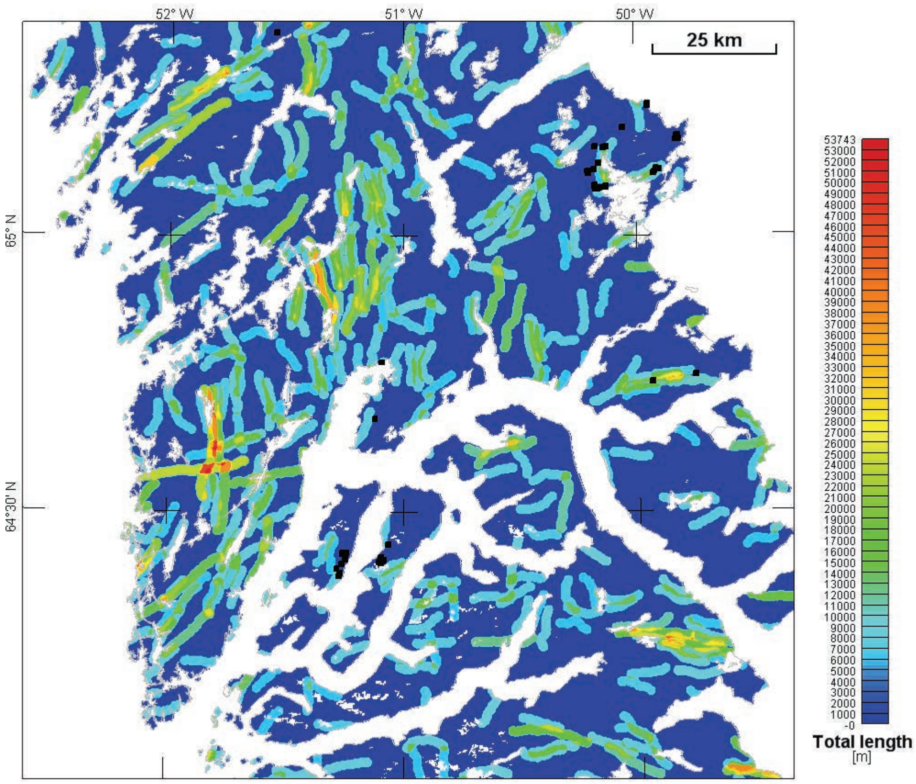

Figure 86. *Lineament statistics, total length of lineaments, search radius 1000 m, for lineament lengths 6030–23600 m (90–100%).*

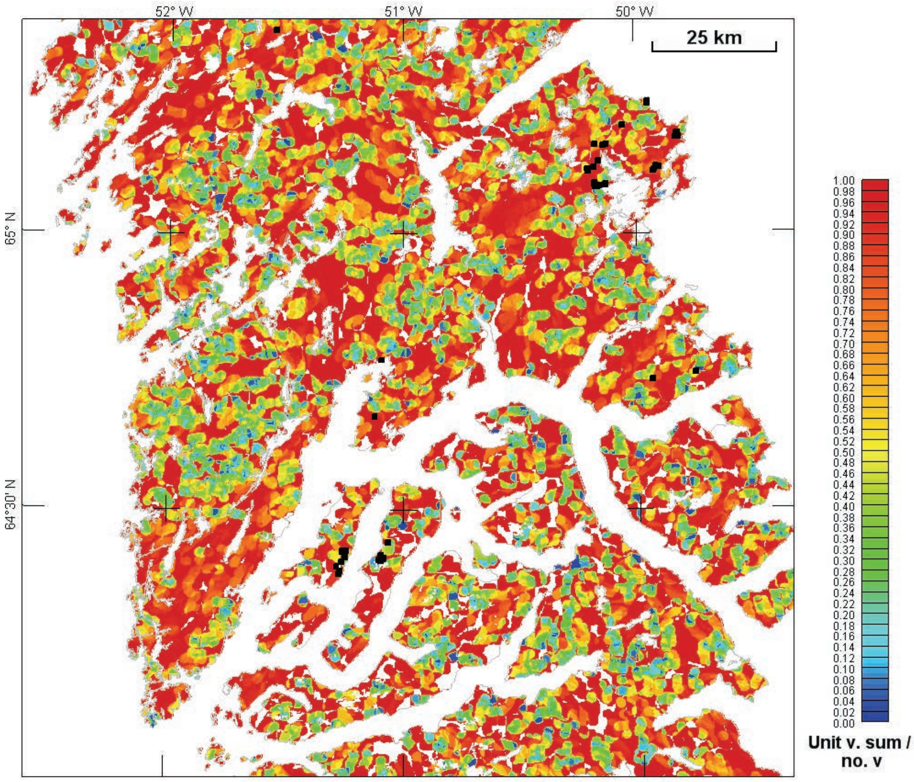

Figure 87. *Lineament statistics, sum of unit vectors divided by number of vectors (complexity), search radius 1000 m, all lineament lengths.*

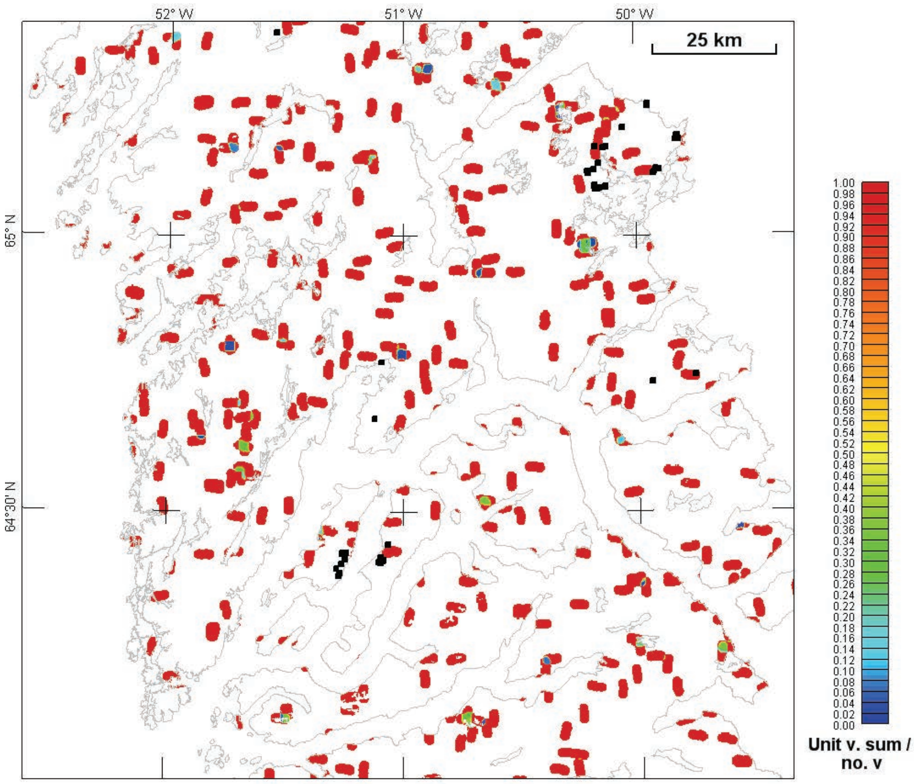

Figure 88. *Lineament statistics, sum of unit vectors divided by number of vectors (complexity), search radius 1000 m, for lineaments lengths 2000–2100m (0–10%).*

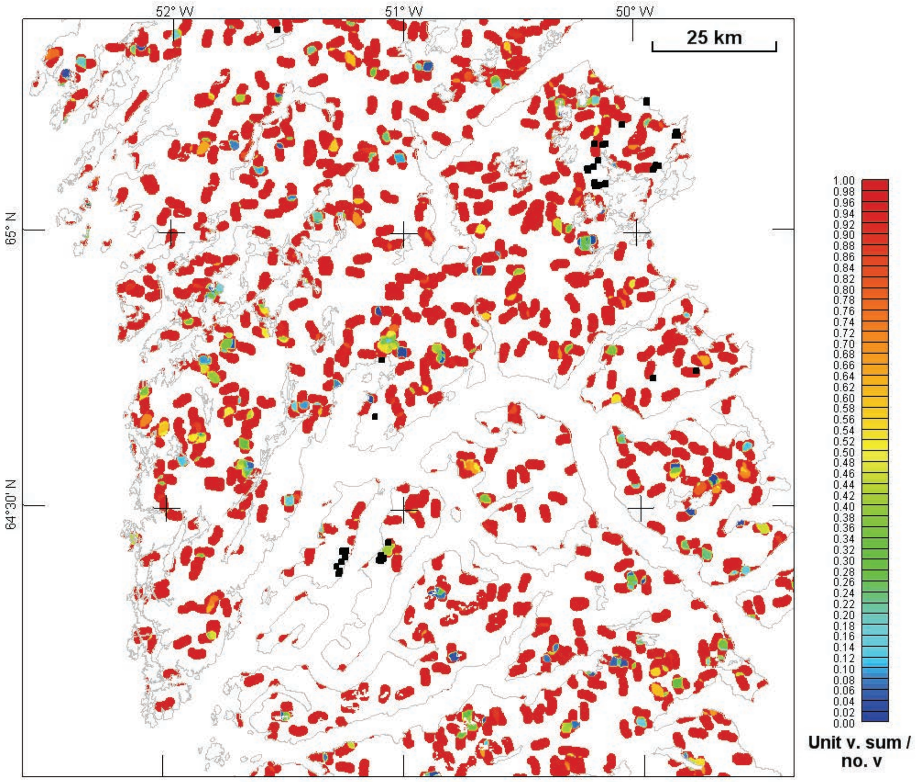

Figure 89. *Lineament statistics, sum of unit vectors divided by number of vectors (complexity), for lineaments lengths 2000–2450m (0–25%).*

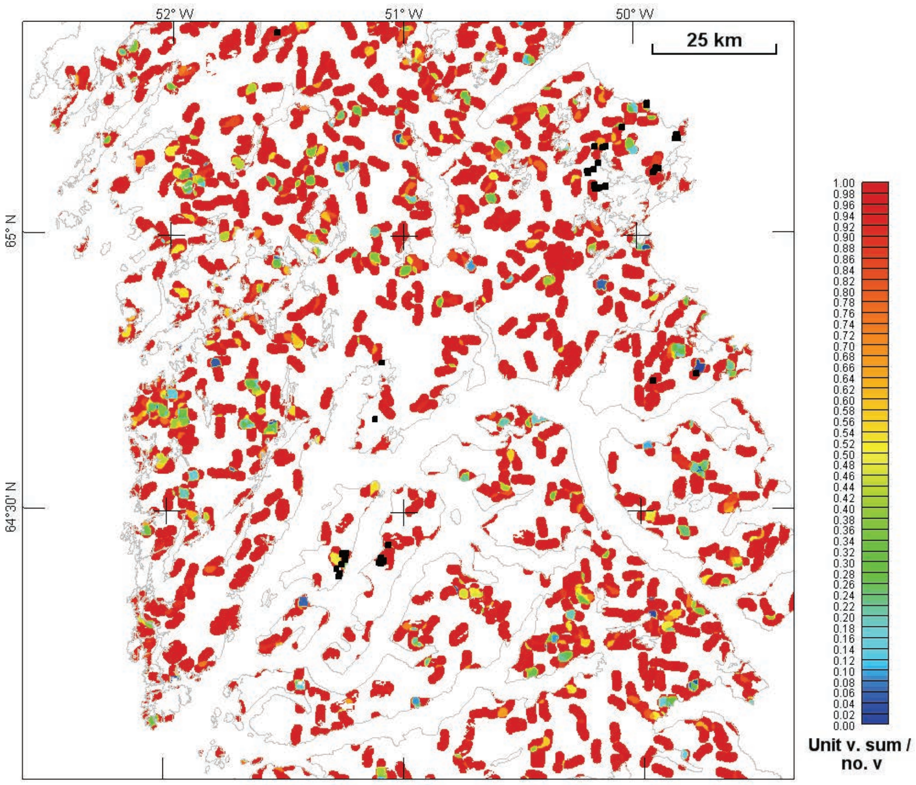

Figure 90. *Lineament statistics, sum of unit vectors divided by number of vectors (complexity), search radius 1000 m, for lineaments lengths 2450–3100 m (25–50%).*

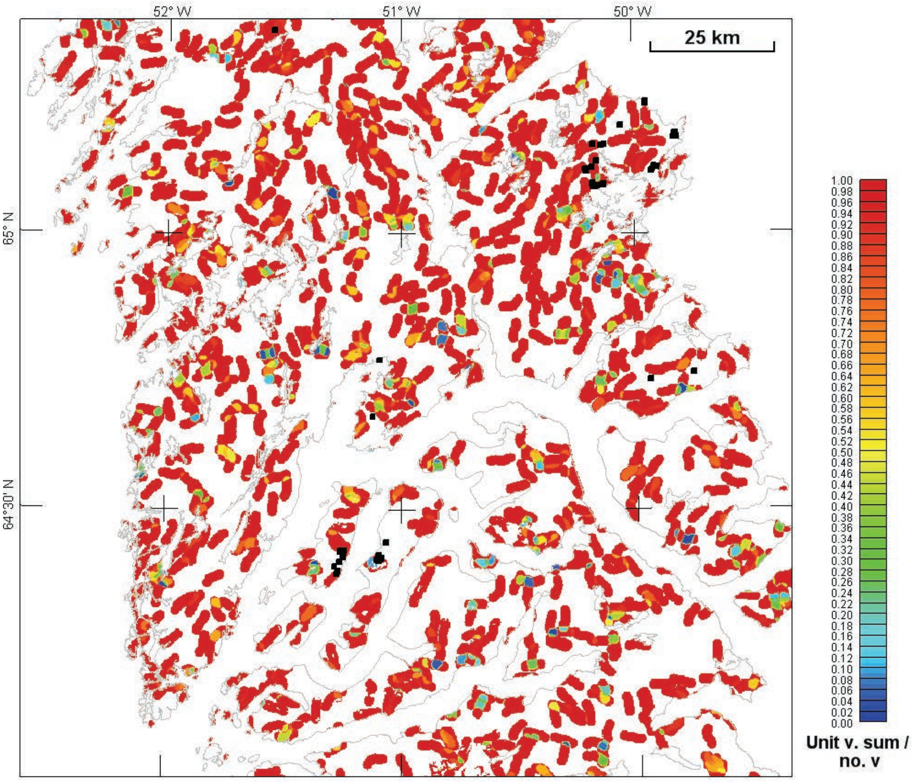

Figure 91. *Lineament statistics, sum of unit vectors divided by number of vectors (complexity), search radius 1000 m, for lineament lengths 3100–4250 m (50–75%).*

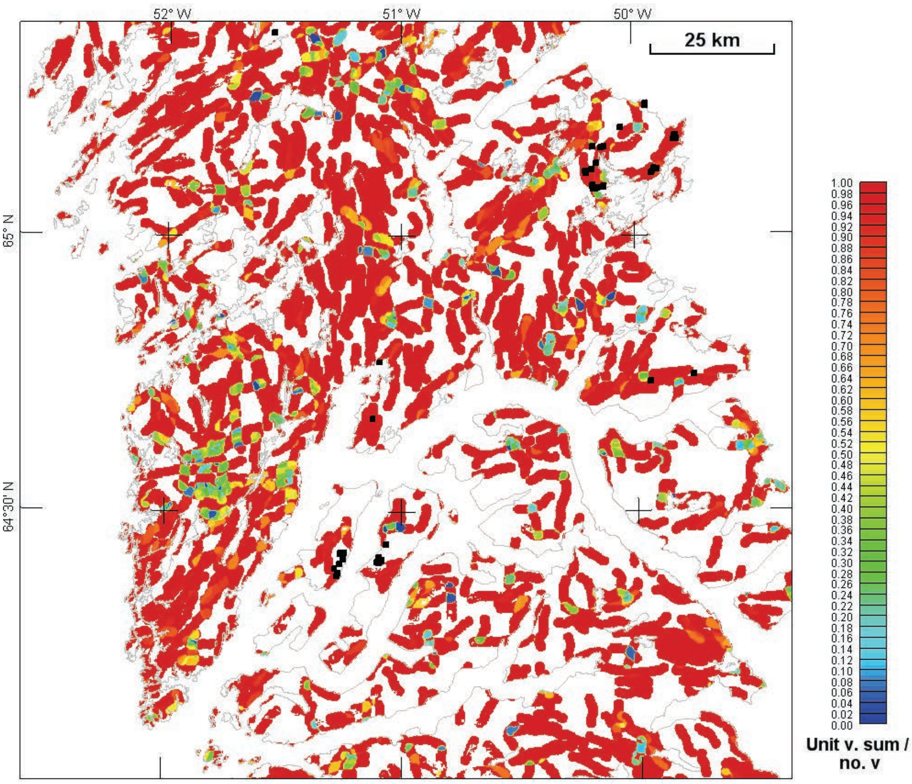

Figure 92. *Lineament statistics, sum of unit vectors divided by number of vectors (complexity), search radius 1000 m, for lineament lengths 4250–23600 m (75–100%).*

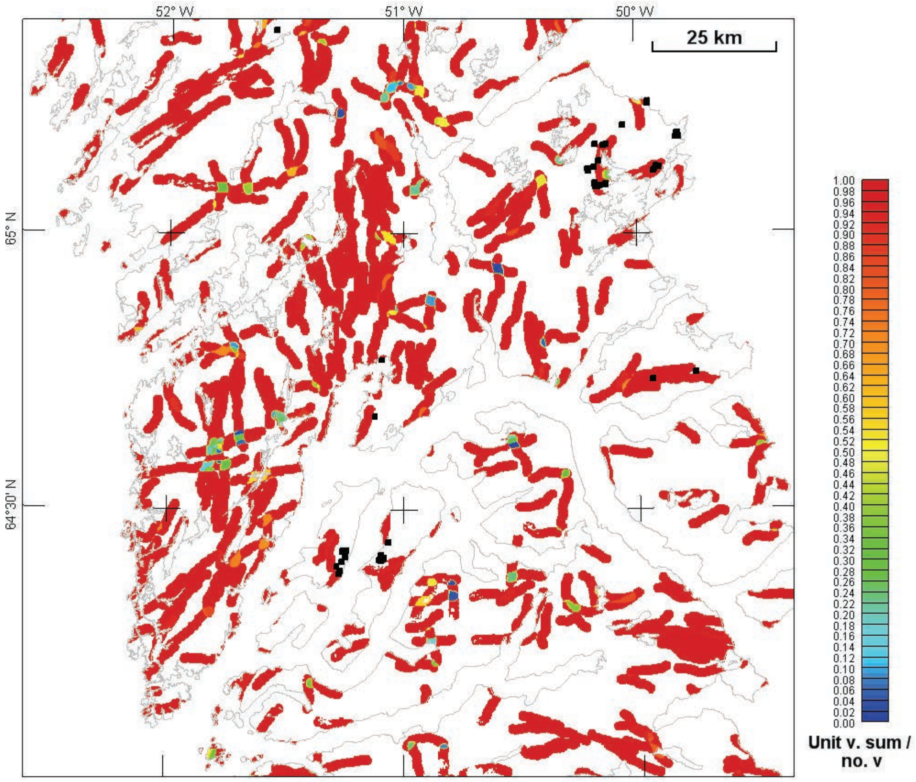

Figure 93. *Lineament statistics, sum of unit vectors divided by number of vectors (complexity), search radius 1000 m, for lineament lengths 6030–23600 m (90–100%).*

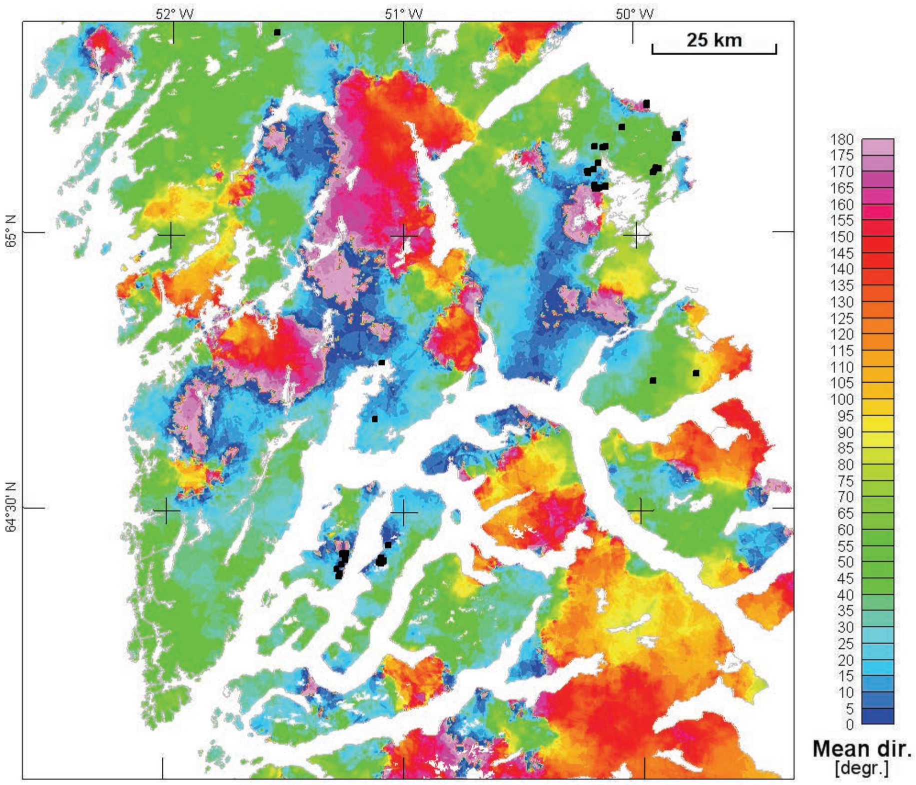

Figure 94. *Lineament statistics, mean direction, search radius 5000 m, all lineament lengths.*

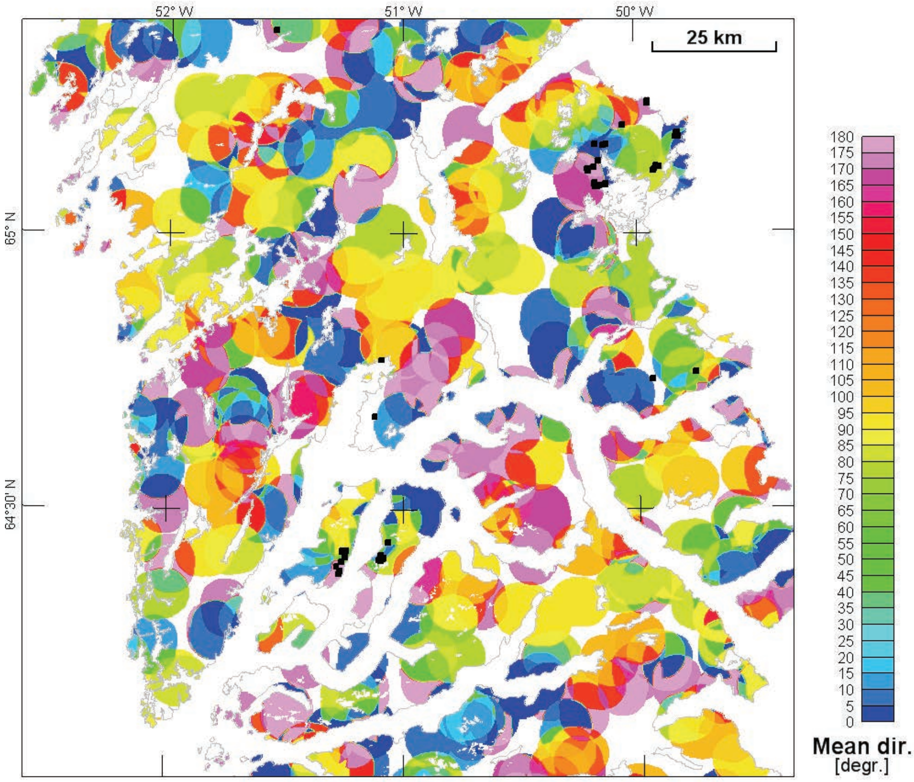

Figure 95. *Lineament statistics, mean direction, search radius 5000 m, for lineaments lengths 2000–2100m (0–10%).*

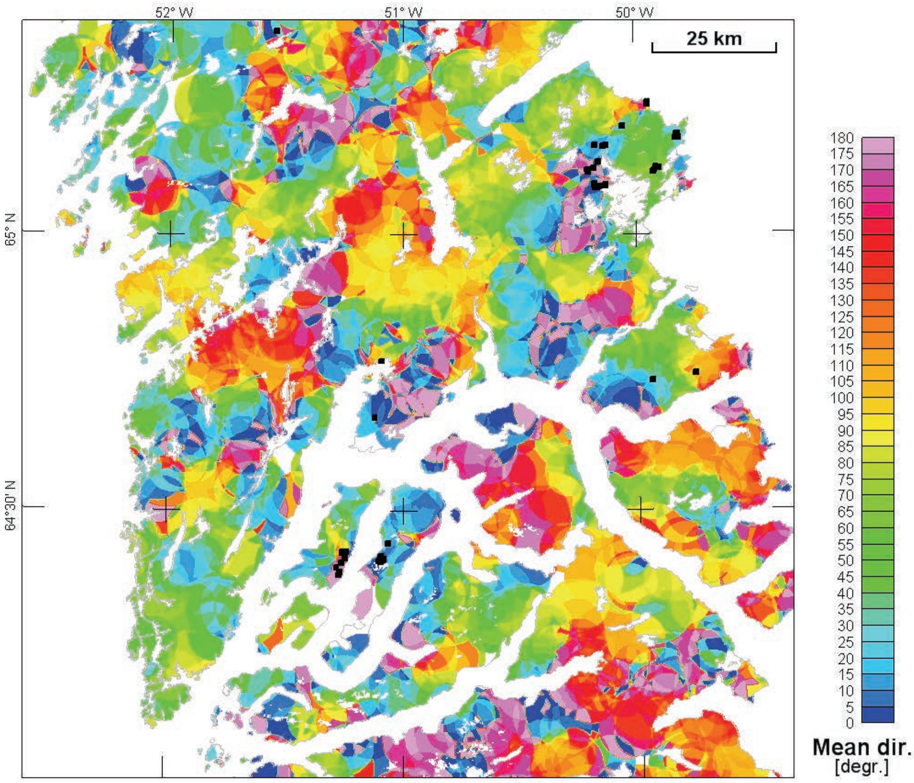

Figure 96. *Lineament statistics, mean direction, search radius 5000 m, for lineaments lengths 2000–2450m (0–25%).*

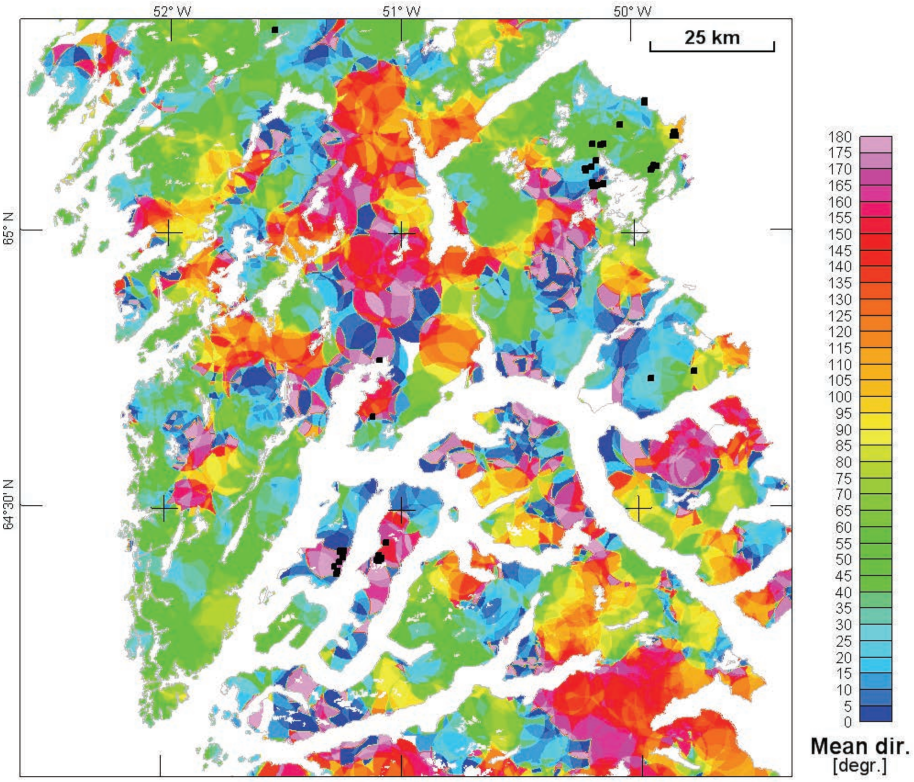

Figure 97. *Lineament statistics, mean direction, search radius 5000 m, for lineaments lengths 2450–3100 m (25–50%).*

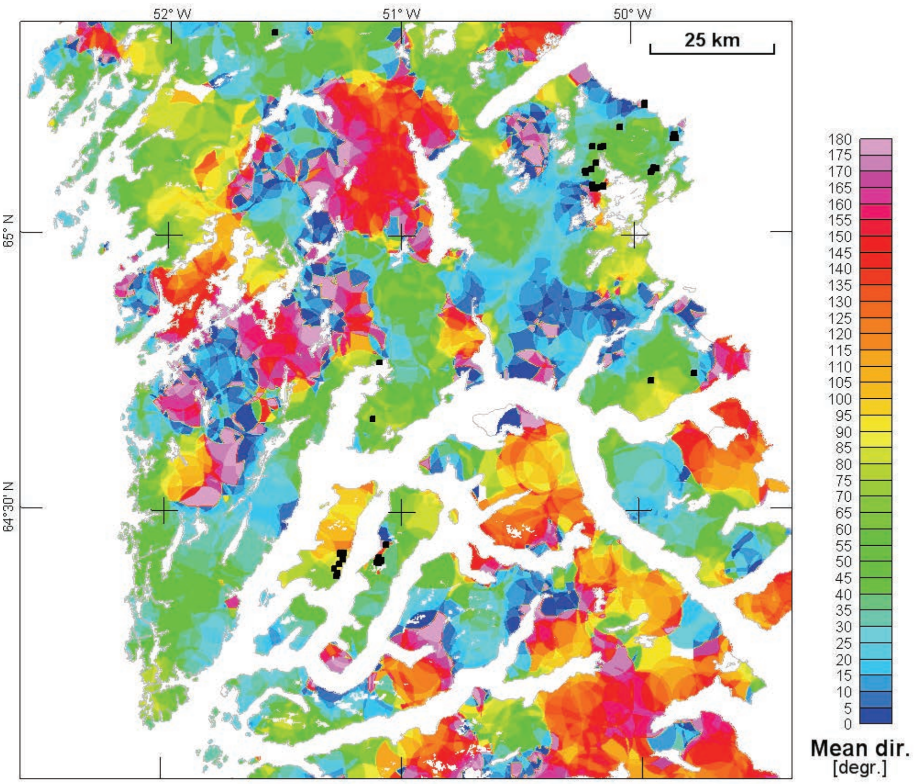

Figure 98. *Lineament statistics, mean direction, search radius 5000 m, for lineament lengths 3100–4250 m (50–75%).*

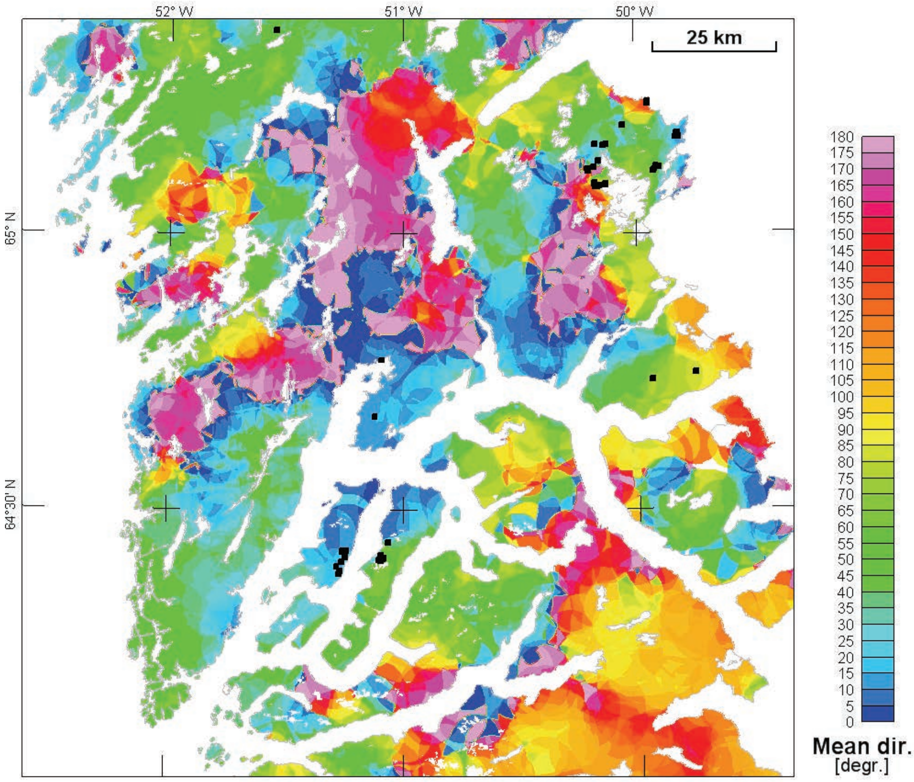

Figure 99. *Lineament statistics, mean direction, search radius 5000 m, for lineament lengths 4250–23600 m (75–100%).*

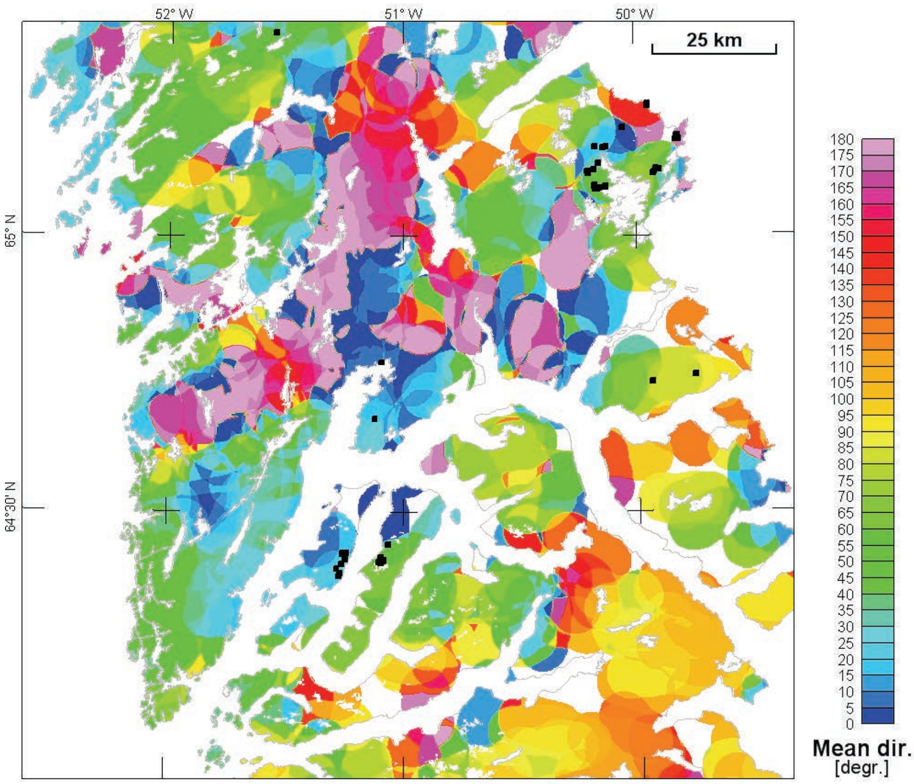

Figure 100. *Lineament statistics, mean direction, search radius 5000 m, for lineament lengths 6030–23600 m (90–100%).*

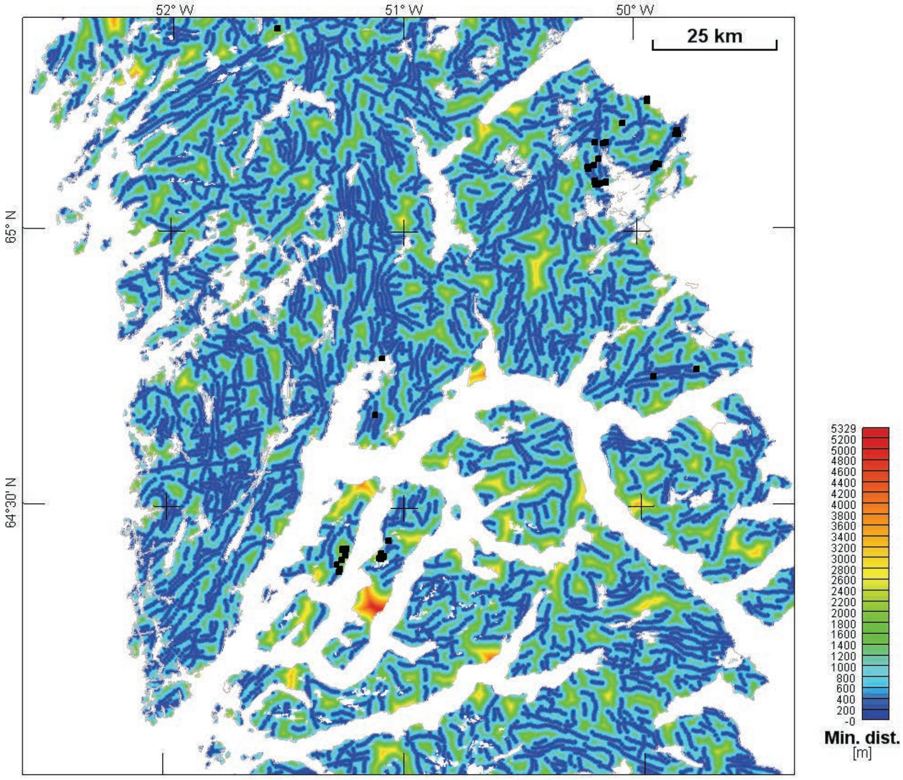

Figure 101. *Lineament statistics, minimum distance to nearest lineament, search radius 5000 m, all lineament lengths.*

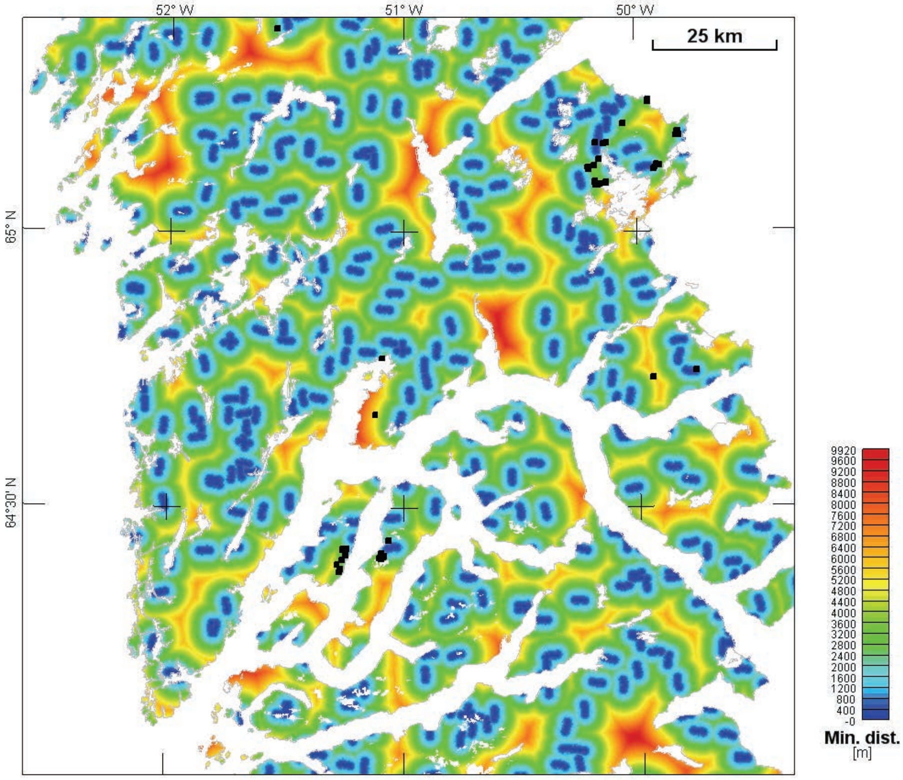

Figure 102. *Lineament statistics, minimum distance to nearest lineament, search radius 5000 m, for lineaments lengths 2000–2100m (0–10%).*

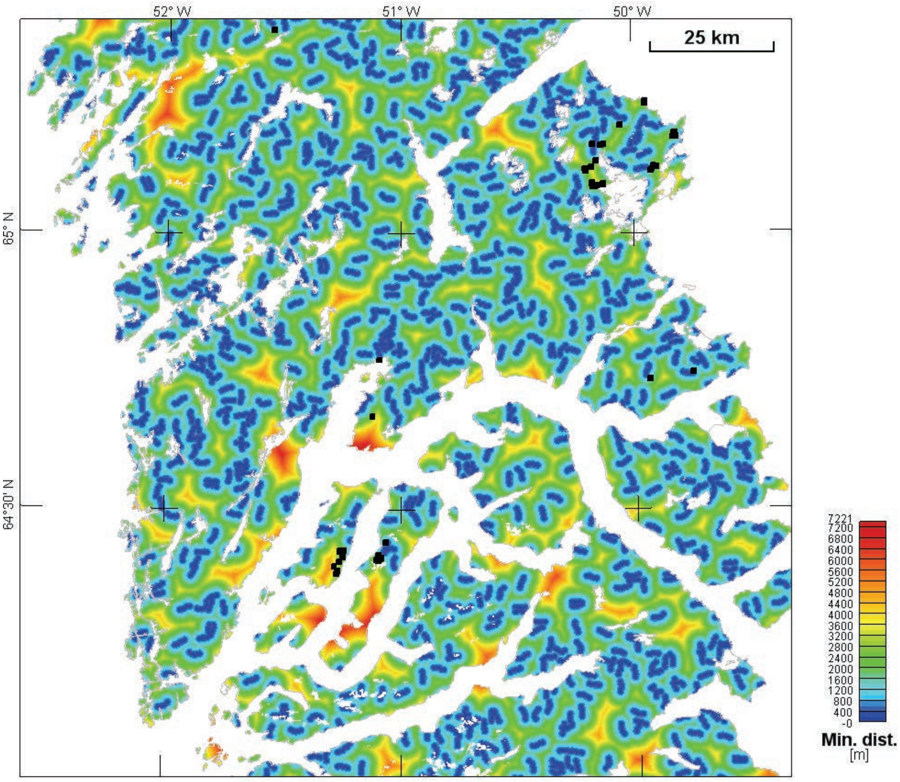

Figure 103. *Lineament statistics, minimum distance to nearest lineament, search radius 5000 m, for lineaments lengths 2000–2100m (0–25%).*

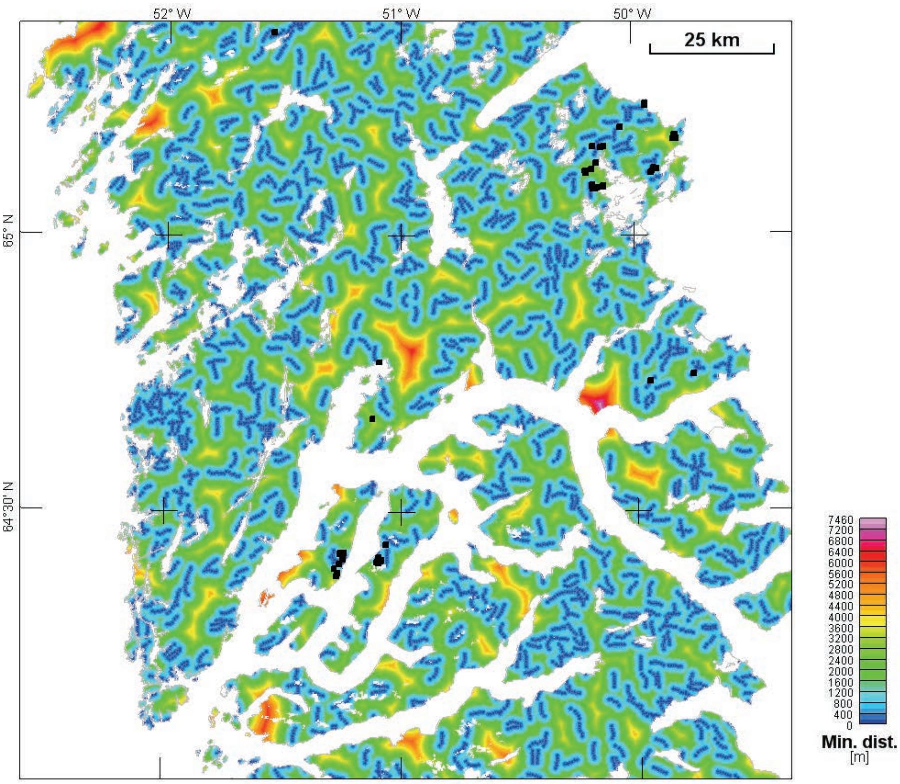

Figure 104. *Lineament statistics, minimum distance to nearest lineament, for lineaments lengths 2450–3100 m (25–50%).*

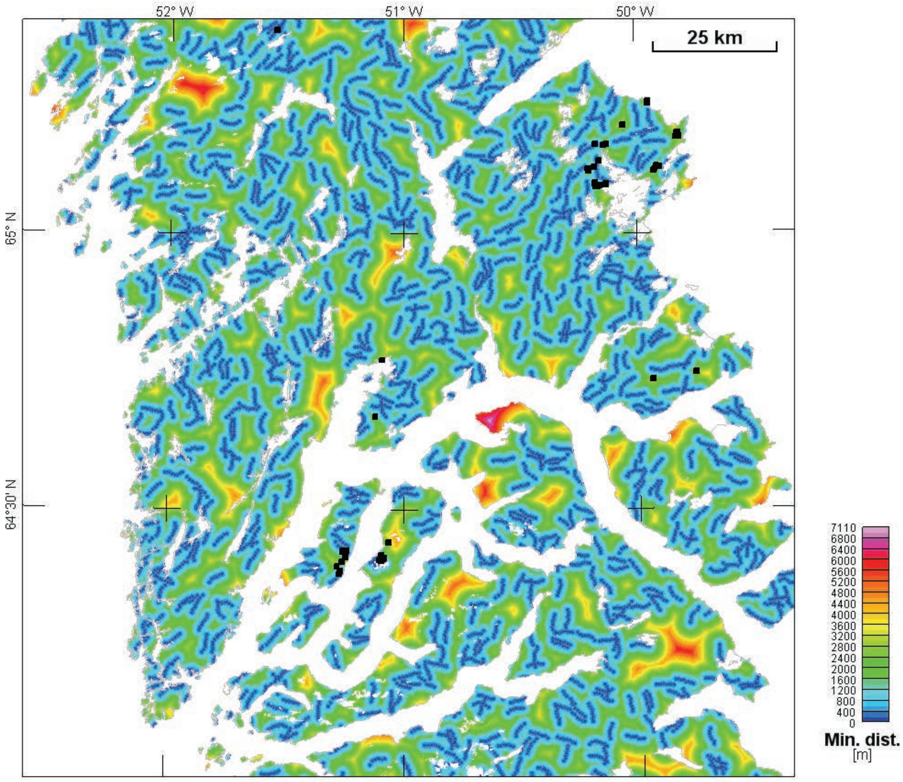

Figure 105. *Lineament statistics, minimum distance to nearest lineament, search radius 5000 m, for lineament lengths 3100–4250 m (50–75%).*

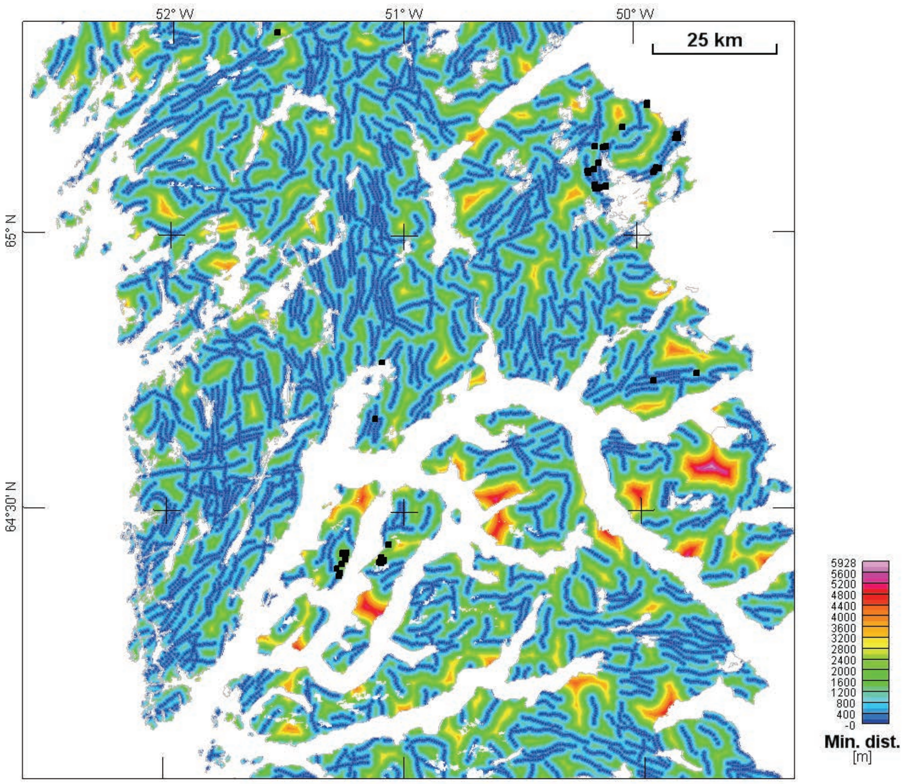

Figure 106. *Lineament statistics, minimum distance to nearest lineament, search radius 5000 m, for lineament lengths 4250–23600 m (75–100%).*

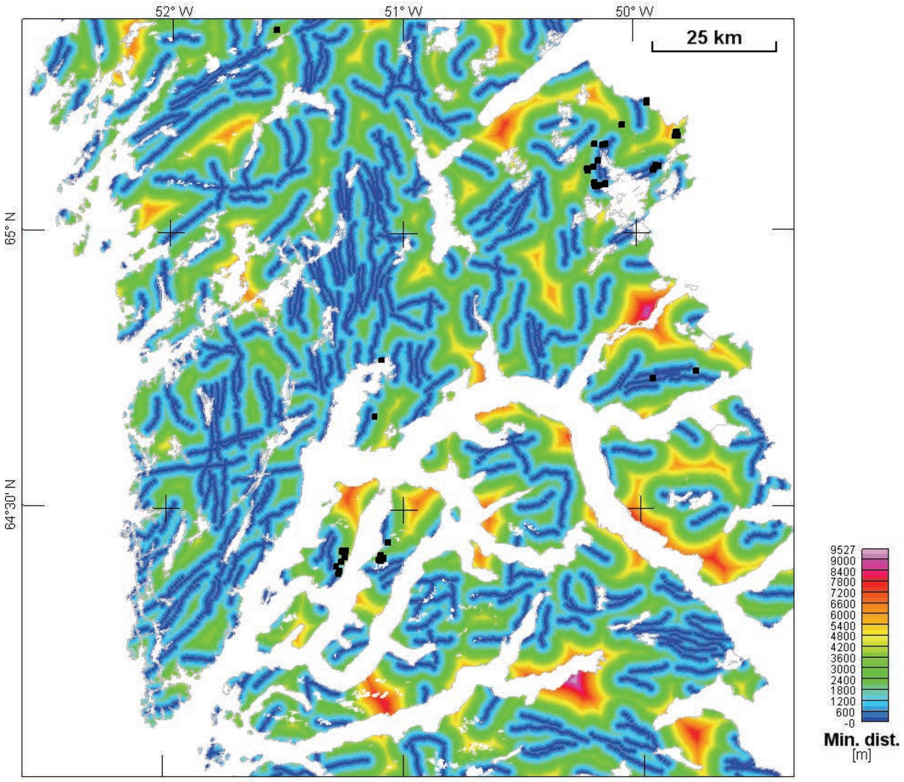

Figure 107. Lineament statistics, minimum distance to nearest lineament, search radius 5000 m, for lineament lengths 6030–23600 m (90–100%).

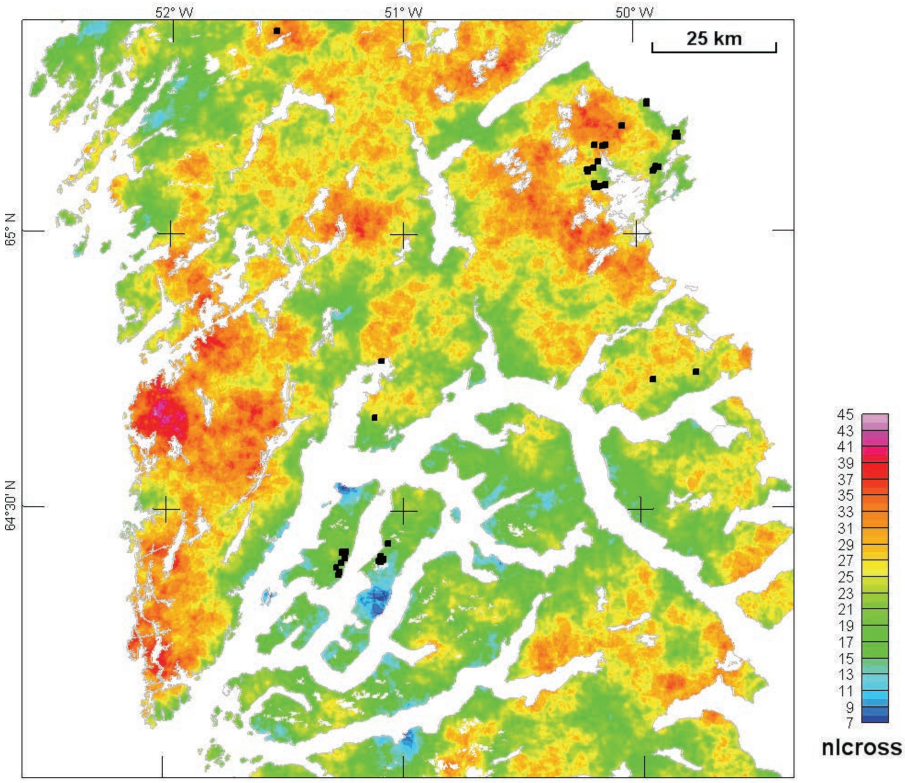

Figure 108. *Lineament statistics, number of crossing lineaments, search radius 5000 m, all lineament lengths.*

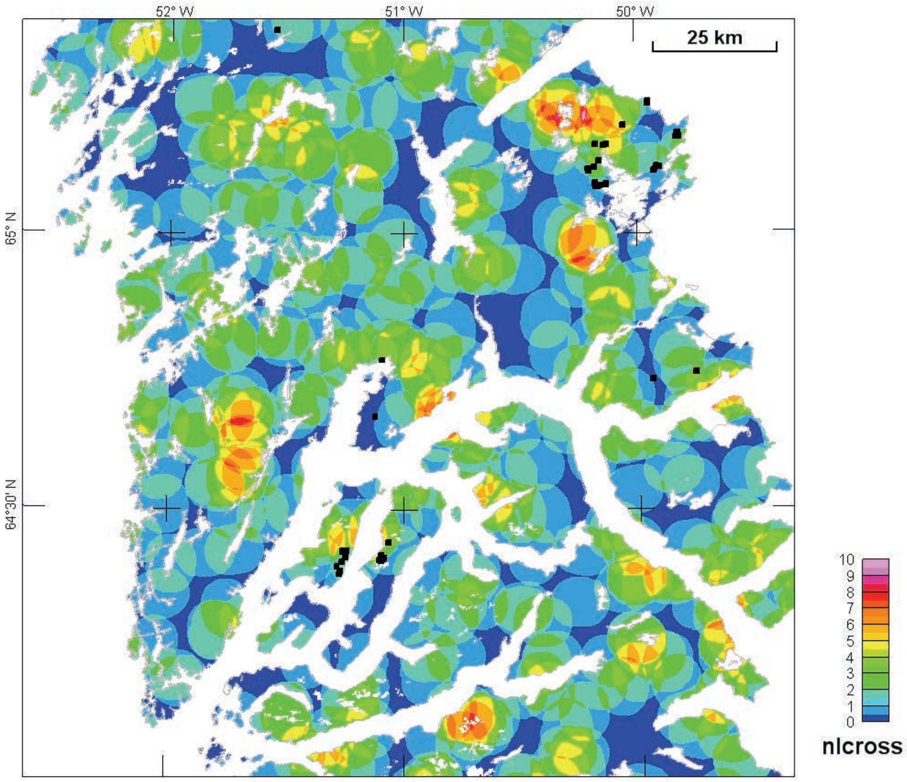

Figure 109. *Lineament statistics, number of crossing lineaments, search radius 5000 m, for lineaments lengths 2000–2100m (0–10%).*

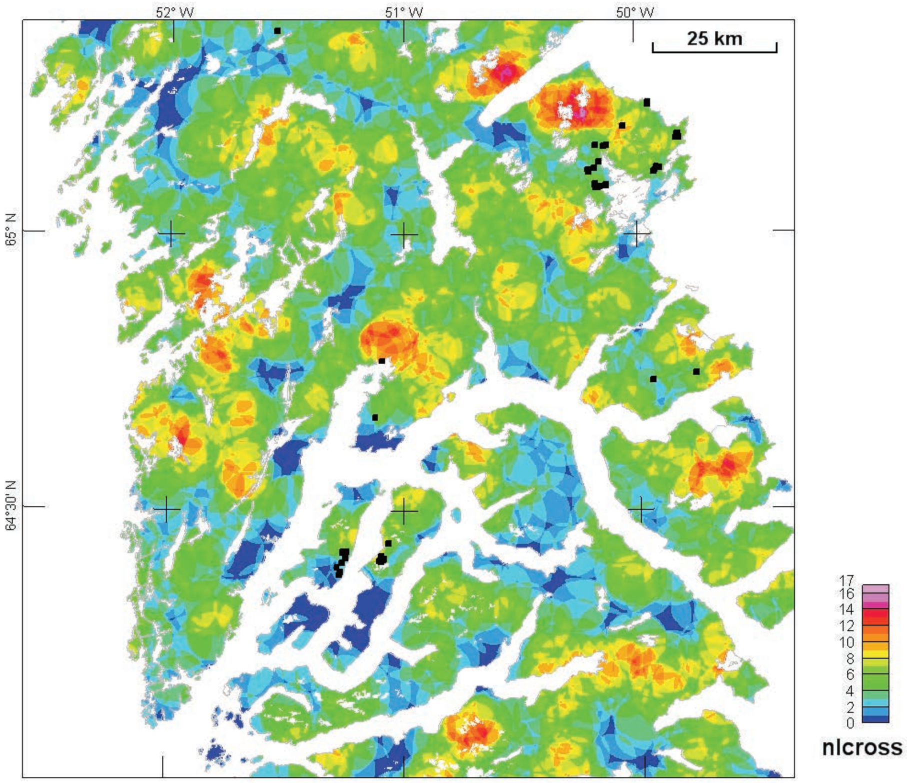

Figure 110. *Lineament statistics, number of crossing lineaments, search radius 5000 m, for lineaments lengths 2000–2100m (0–25%).*

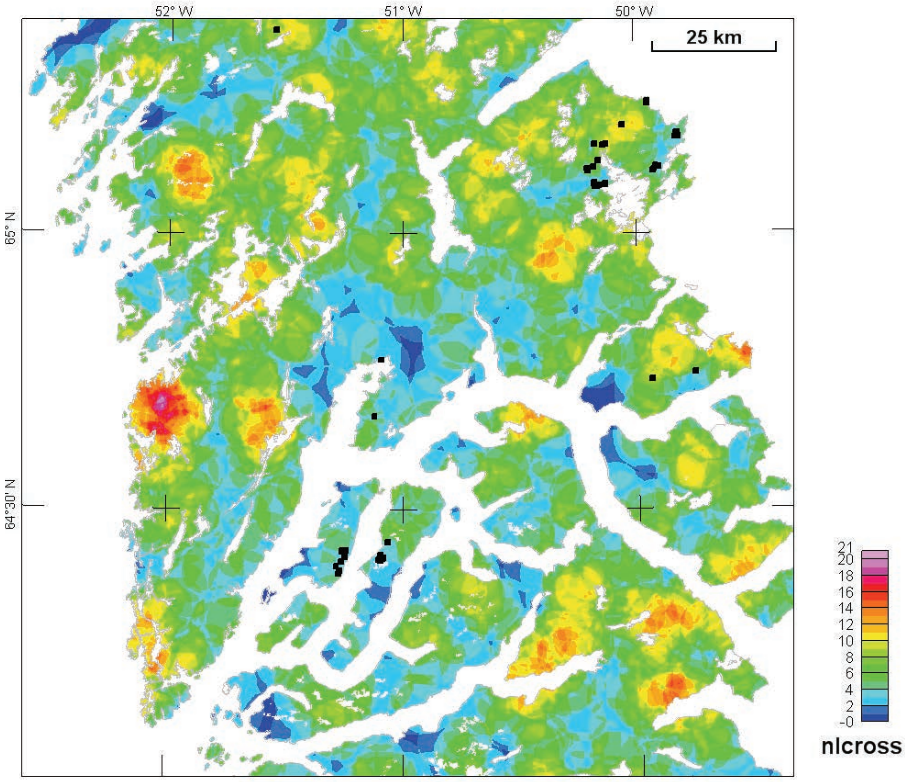

Figure 111. *Lineament statistics, number of crossing lineaments, for lineaments lengths 2450–3100 m (25–50%).*

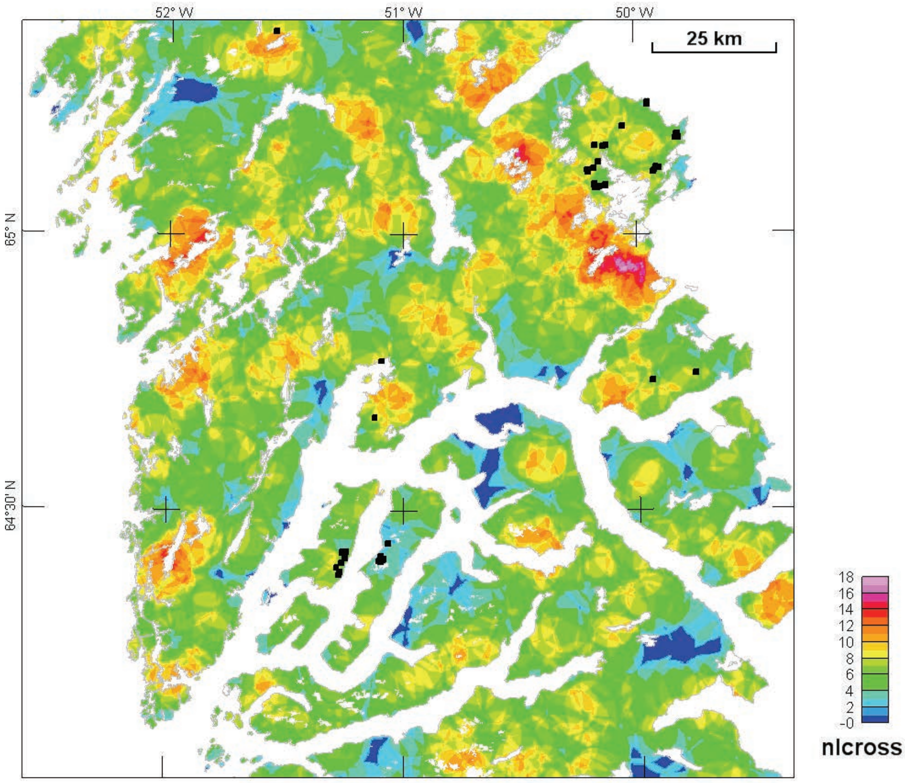

Figure 112. *Lineament statistics, number of crossing lineaments, search radius 5000 m, for lineament lengths 3100–4250 m (50–75%).*

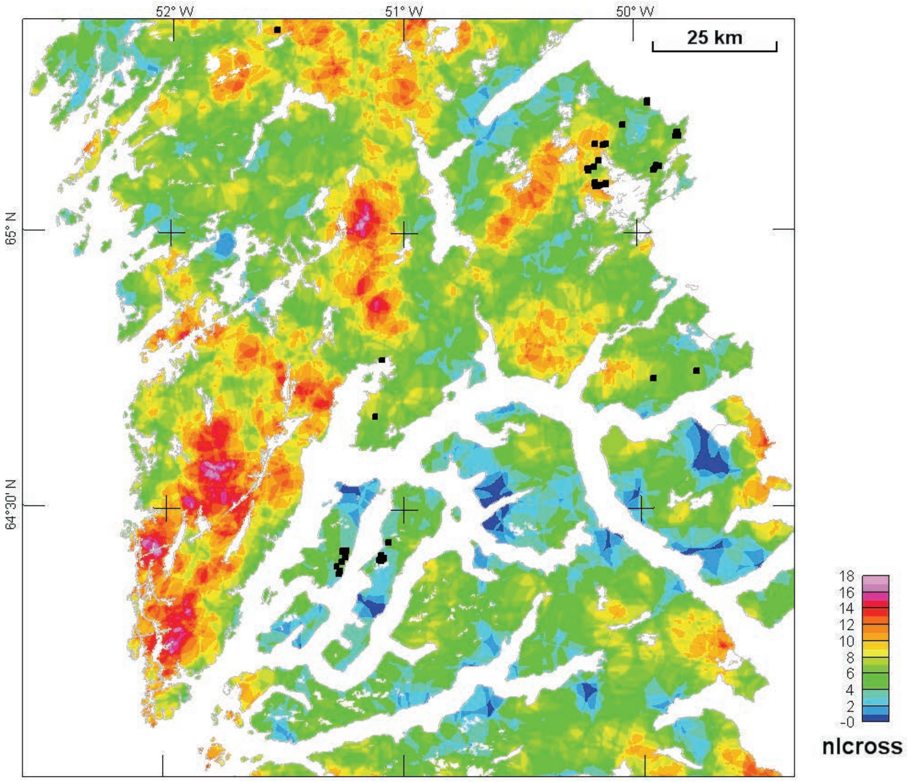

Figure 113. *Lineament statistics, number of crossing lineaments, search radius 5000 m, for lineament lengths 4250–23600 m (75–100%).*

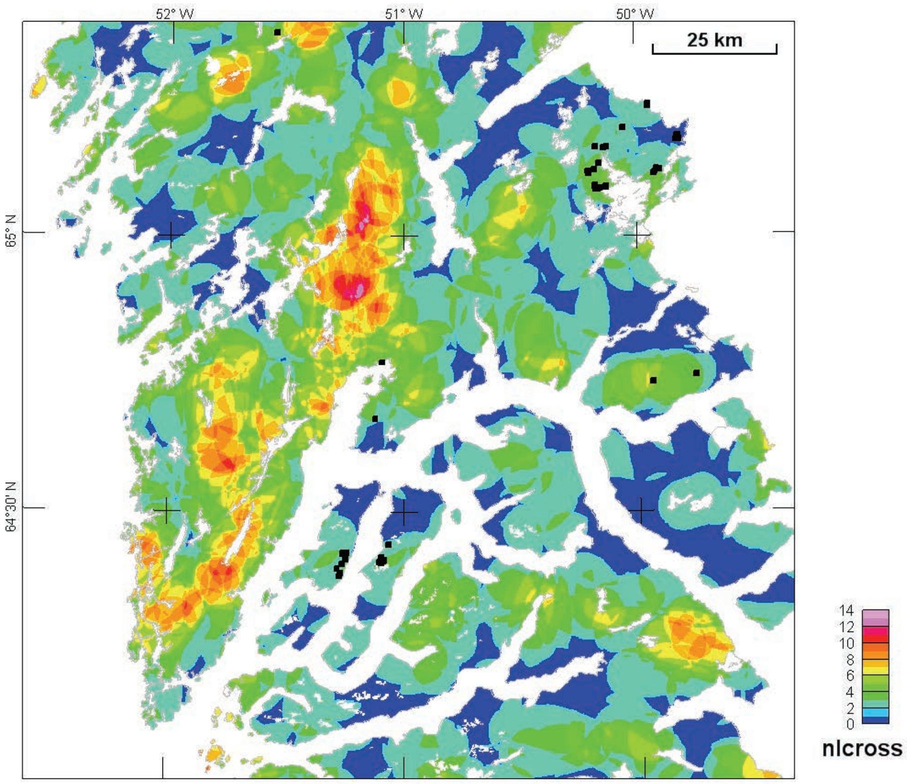

Figure 114. *Lineament statistics, number of crossing lineaments, search radius 5000 m, for lineament lengths 6030–23600 m (90–100%).*

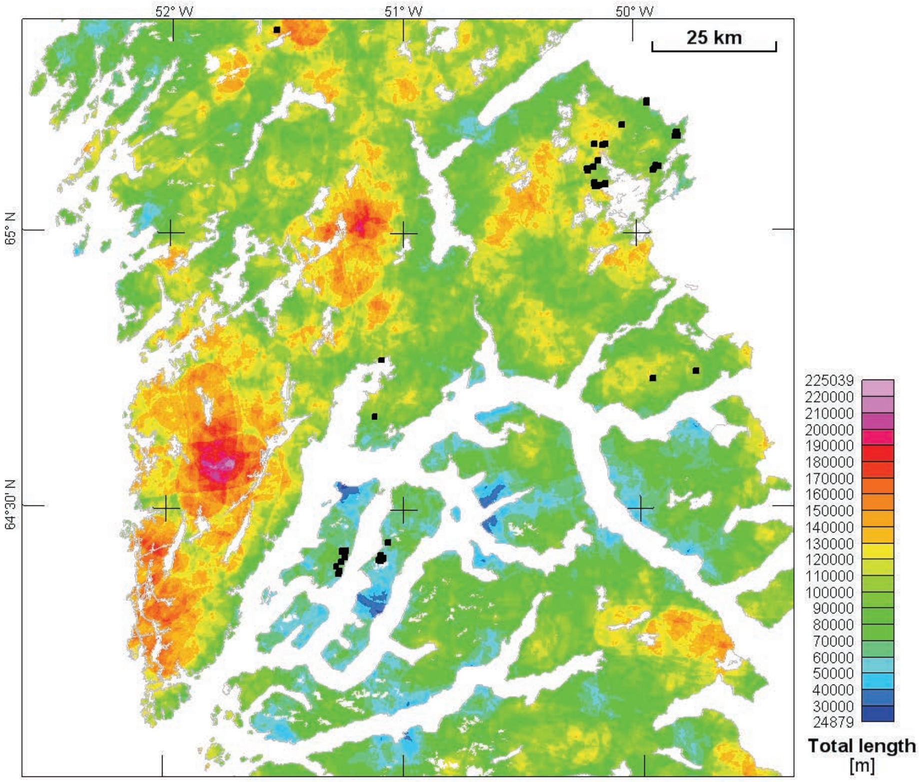

Figure 115. *Lineament statistics, total length of lineaments, search radius 5000 m, all lineament lengths.*

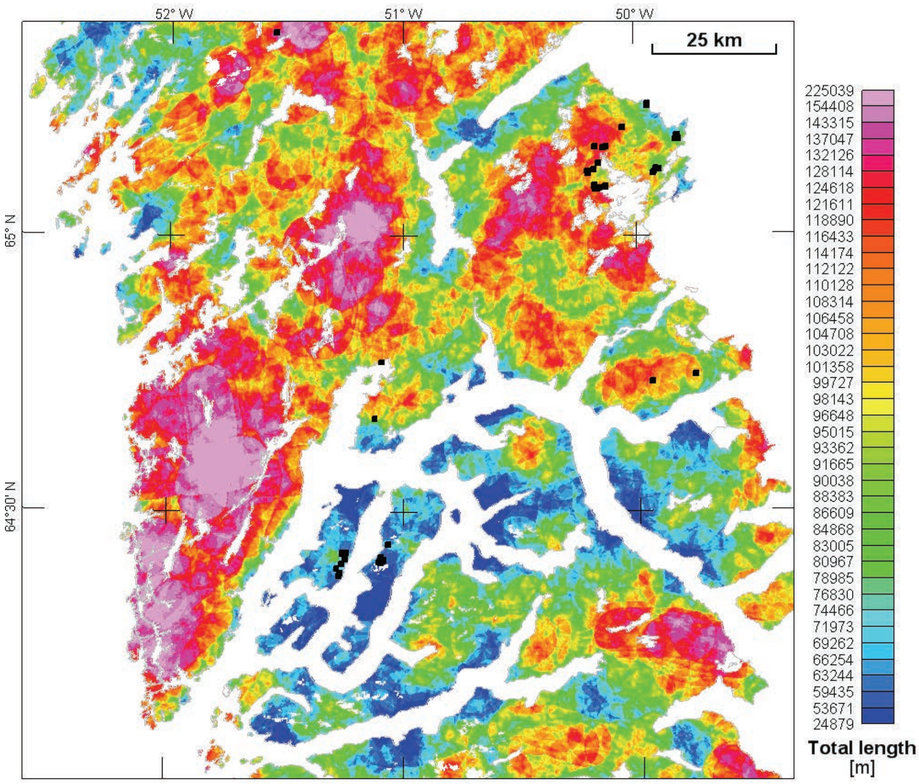

Figure 116. *Lineament statistics, total length of lineaments, search radius 5000 m, all lineament lengths. Histogram equalisation colour scale.*

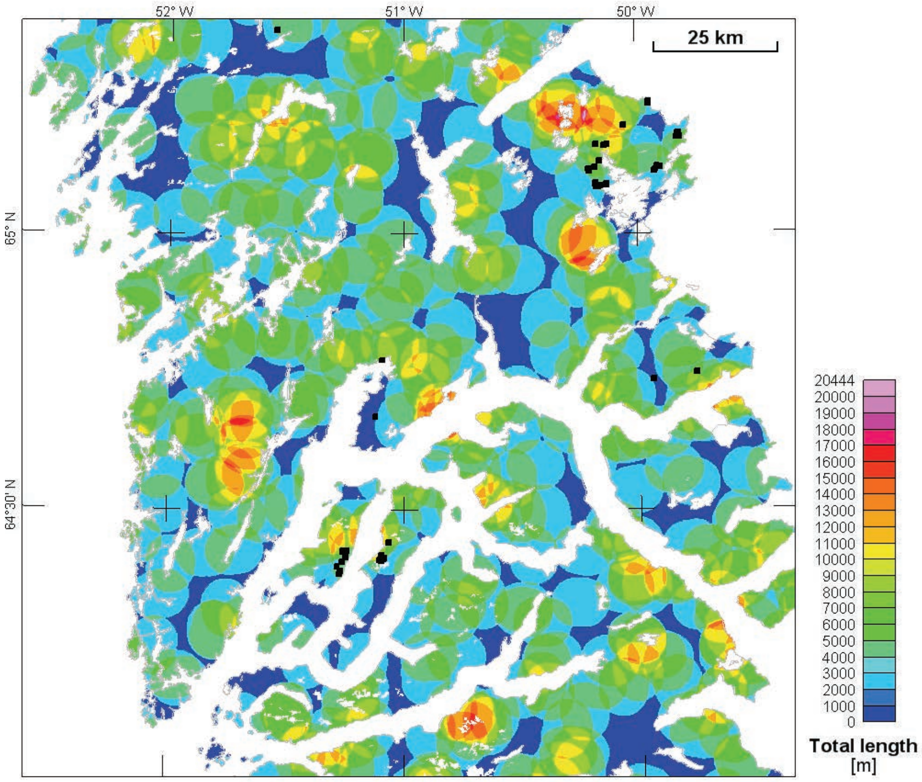

Figure 117. *Lineament statistics, total length of lineaments, search radius 5000 m, for lineaments lengths 2000–2100m (0–10%).*

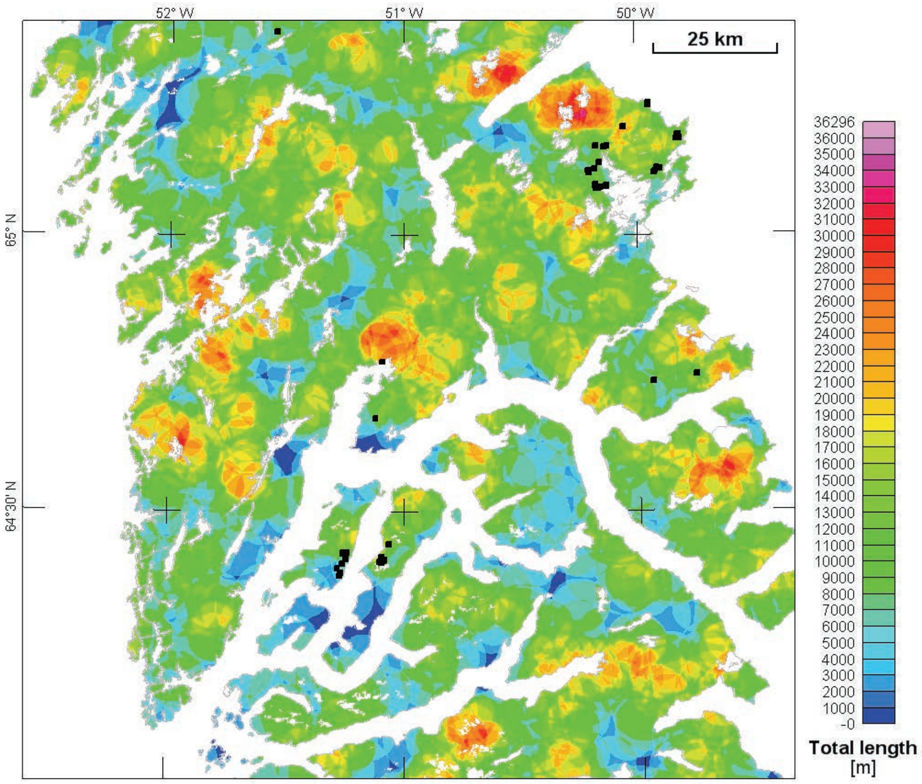

Figure 118. *Lineament statistics, total length of lineaments, search radius 5000 m, for lineaments lengths 2000–2100m (0–25%).*

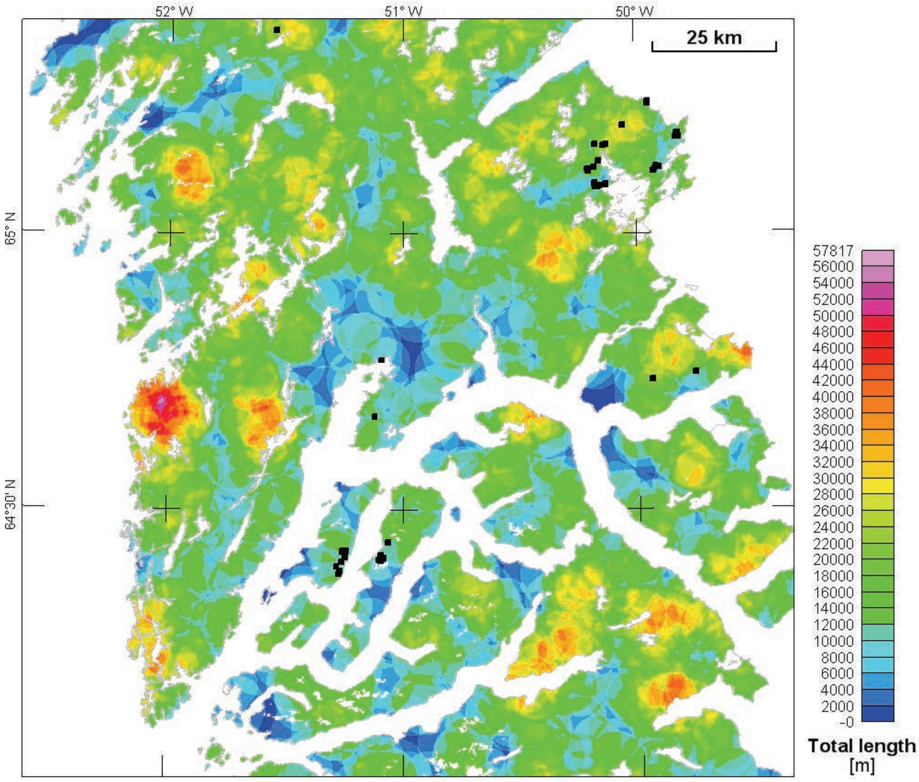

Figure 119. *Lineament statistics, total length of lineaments, for lineaments lengths 2450–3100 m (25–50%).*

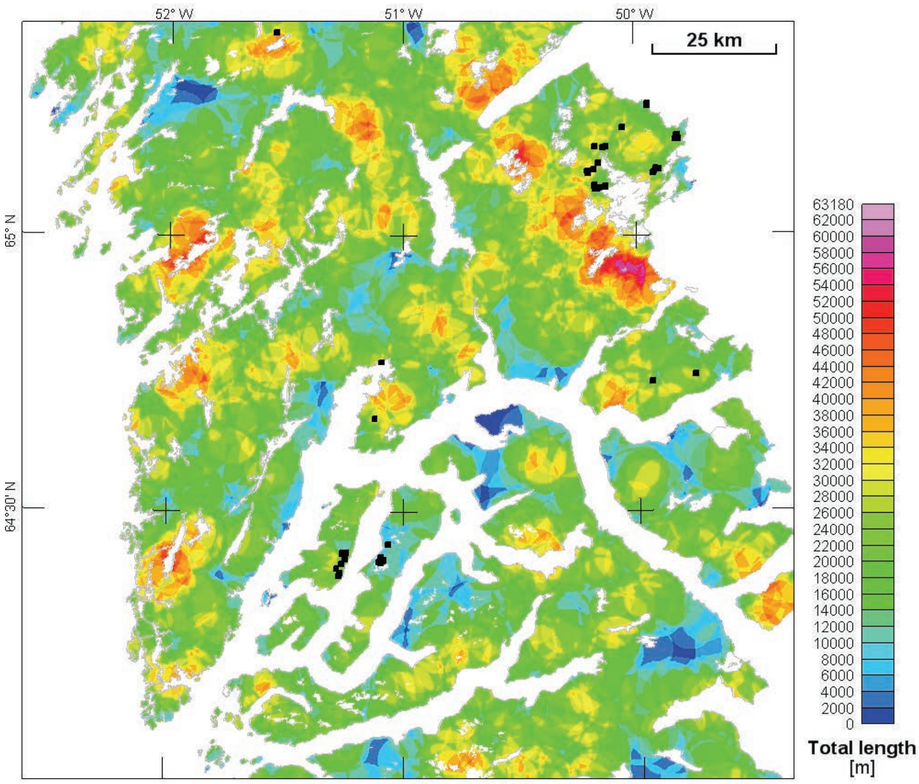

Figure 120. *Lineament statistics, total length of lineaments, search radius 5000 m, for lineament lengths 3100–4250 m (50–75%).*

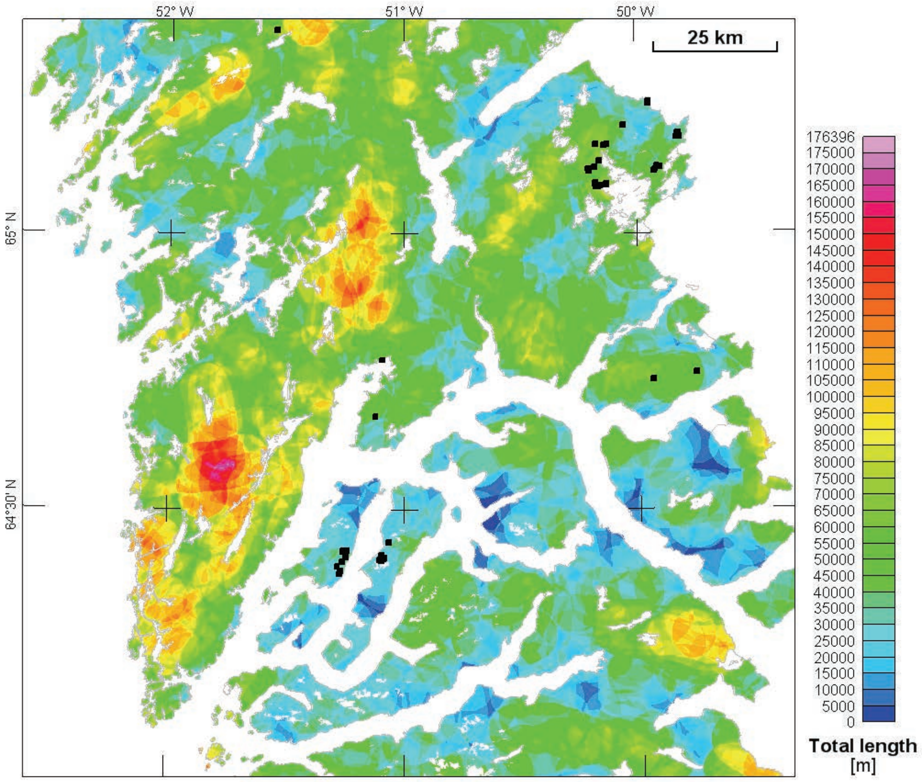

Figure 121. *Lineament statistics, total length of lineaments, search radius 5000 m, for lineament lengths 4250–23600 m (75–100%).*

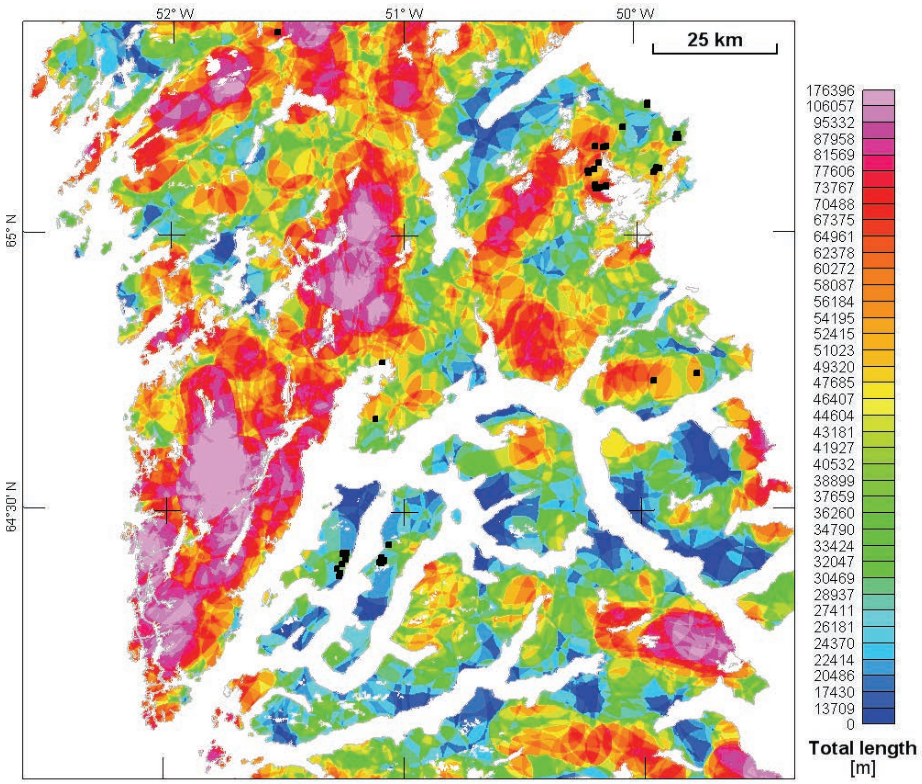

Figure 122. *Lineament statistics, total length of lineaments, search radius 5000 m, for lineament lengths 4250–23600 m (75–100%). Histogram equalisation colour scale.*

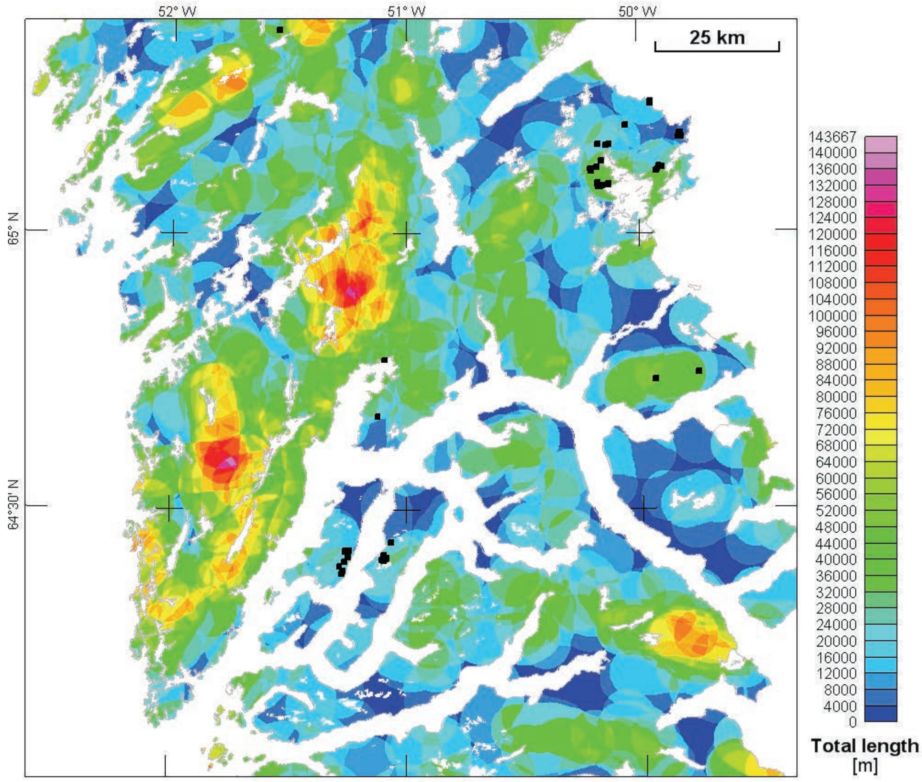

Figure 123. *Lineament statistics, total length of lineaments, search radius 5000 m, for lineament lengths 6030–23600 m (90–100%).*

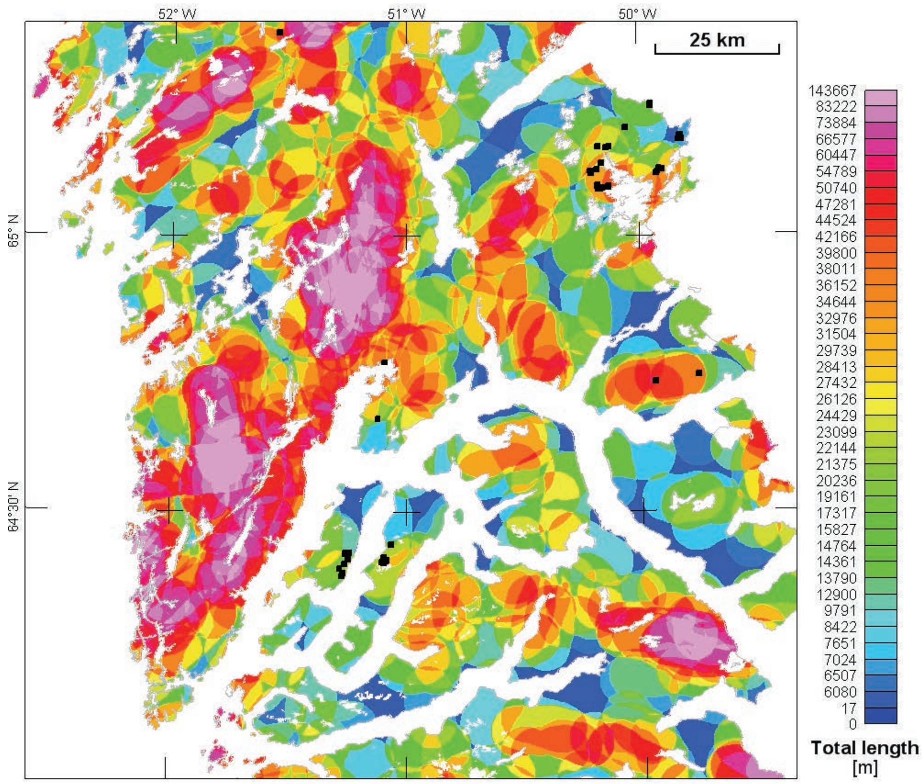

Figure 124. *Lineament statistics, total length of lineaments, search radius 5000 m, for lineament lengths 6030–23600 m (90–100%). Histogram equalisation colour scale.*

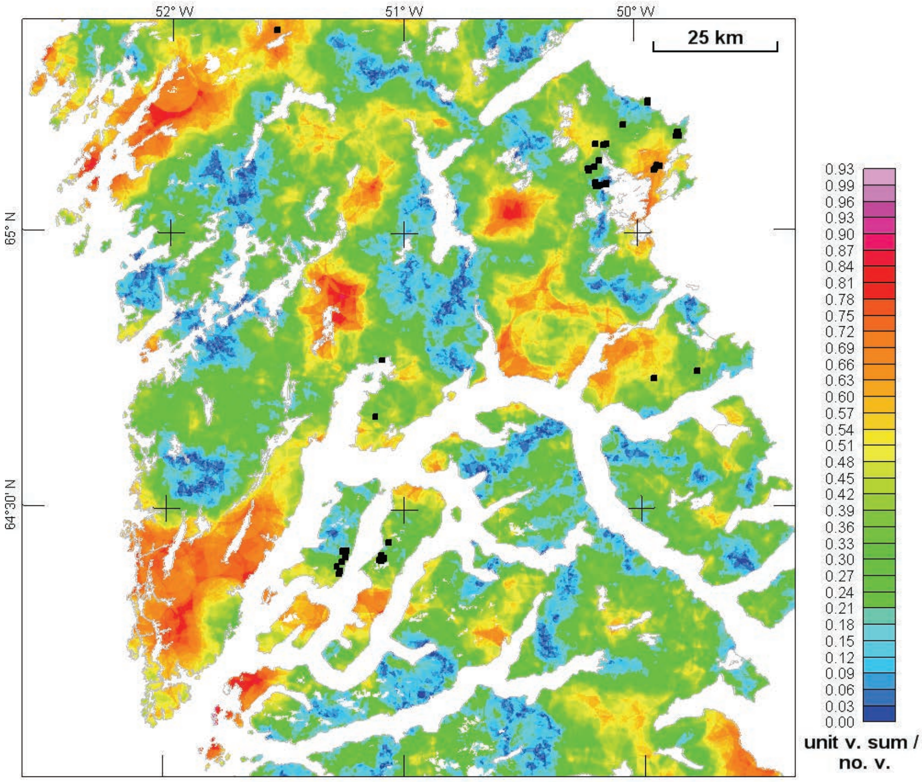

Figure 125. *Lineament statistics, sum of unit vectors divided by number of vectors (complexity), search radius 5000 m, all lineament lengths.*

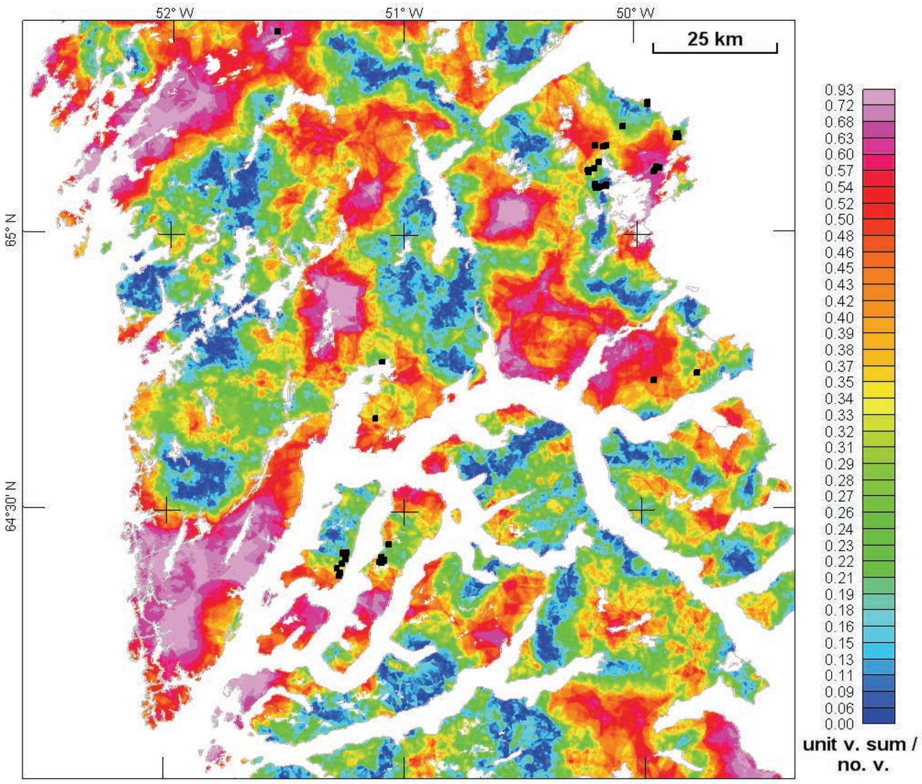

Figure 126. *Lineament statistics, sum of unit vectors divided by number of vectors (complexity), search radius 5000 m, all lineament lengths. Histogram equalisation colour scale.*

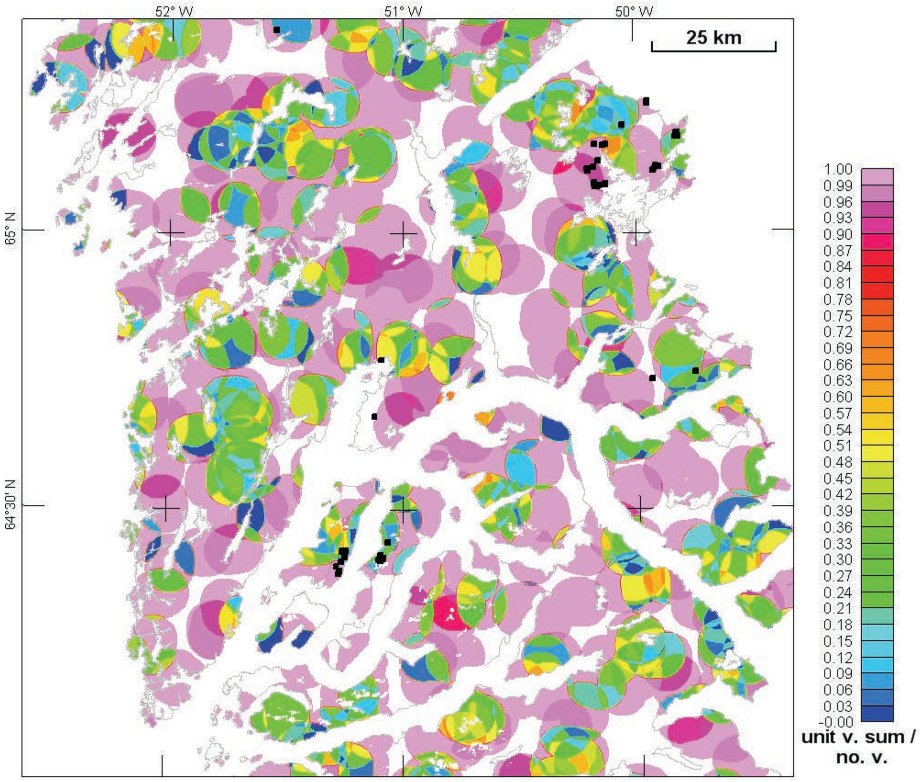

Figure 127. *Lineament statistics, sum of unit vectors divided by number of vectors (complexity), search radius 5000 m, for lineaments lengths 2000–2100m (0–10%).*

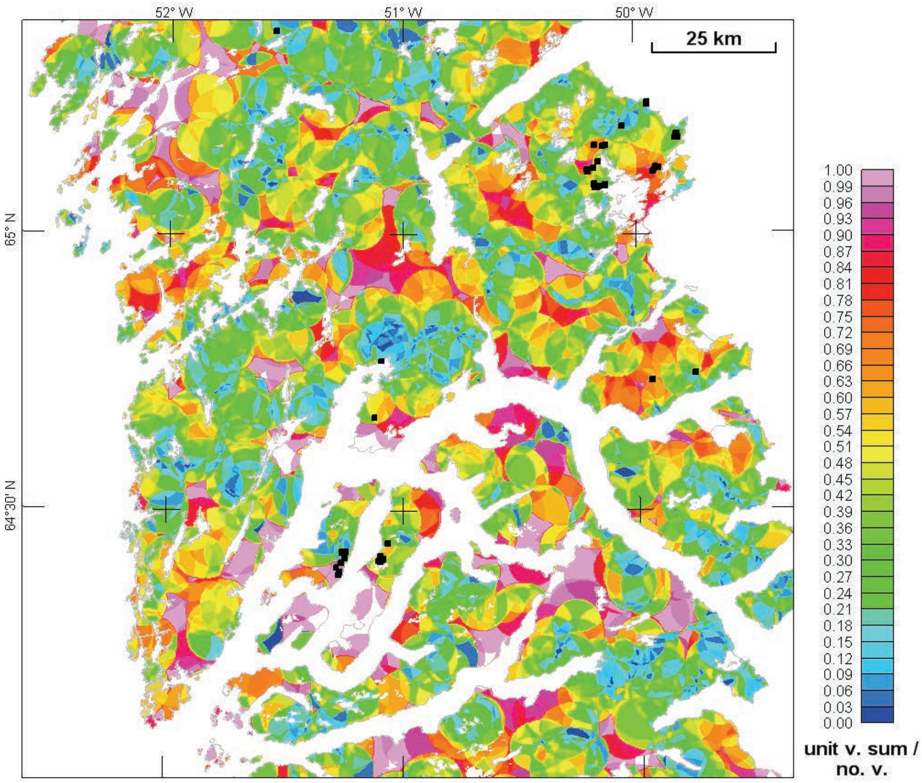

Figure 128. *Lineament statistics, sum of unit vectors divided by number of vectors (complexity), search radius 5000 m, for lineaments lengths 2000–2100m (0–25%).*

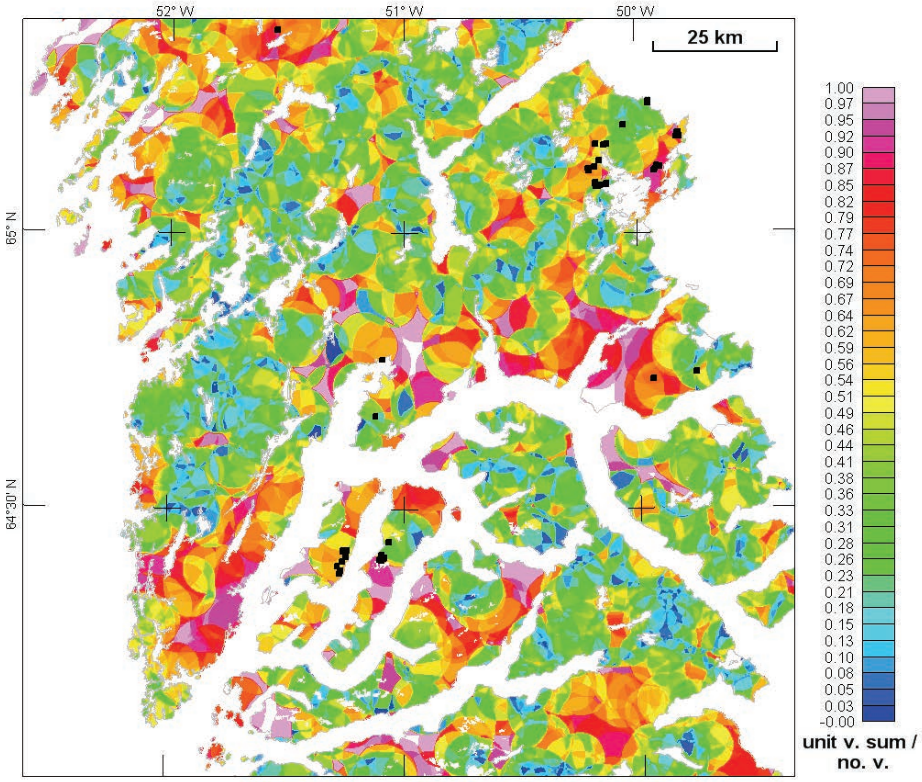

Figure 129. *Lineament statistics, sum of unit vectors divided by number of vectors (complexity), for lineaments lengths 2450–3100 m (25–50%).*

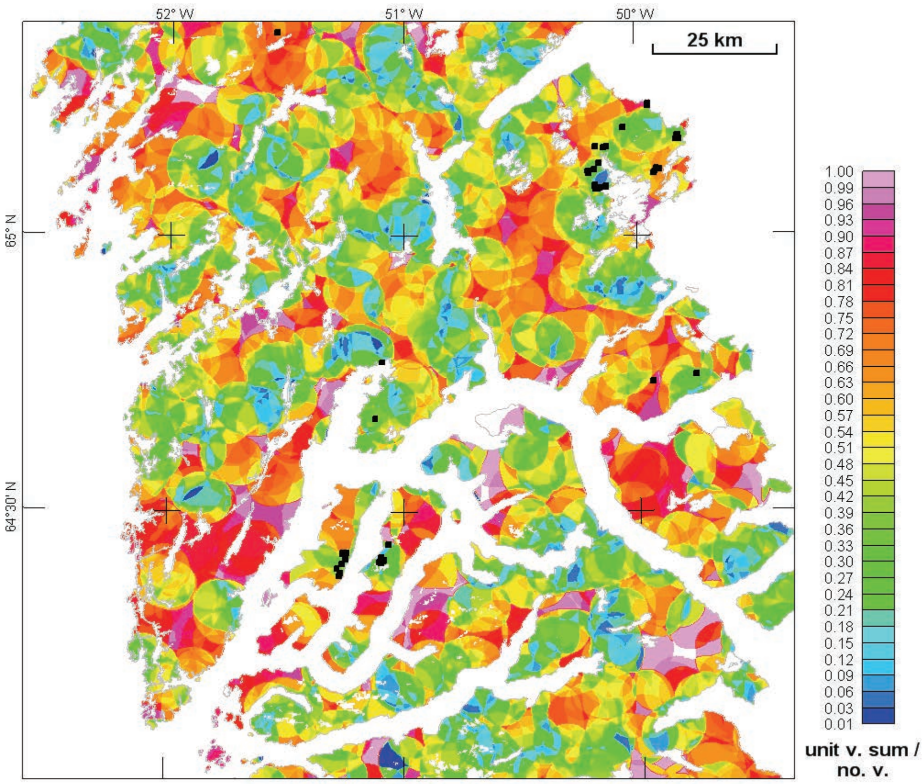

Figure 130. *Lineament statistics, sum of unit vectors divided by number of vectors (complexity), search radius 5000 m, for lineament lengths 3100–4250 m (50–75%).*

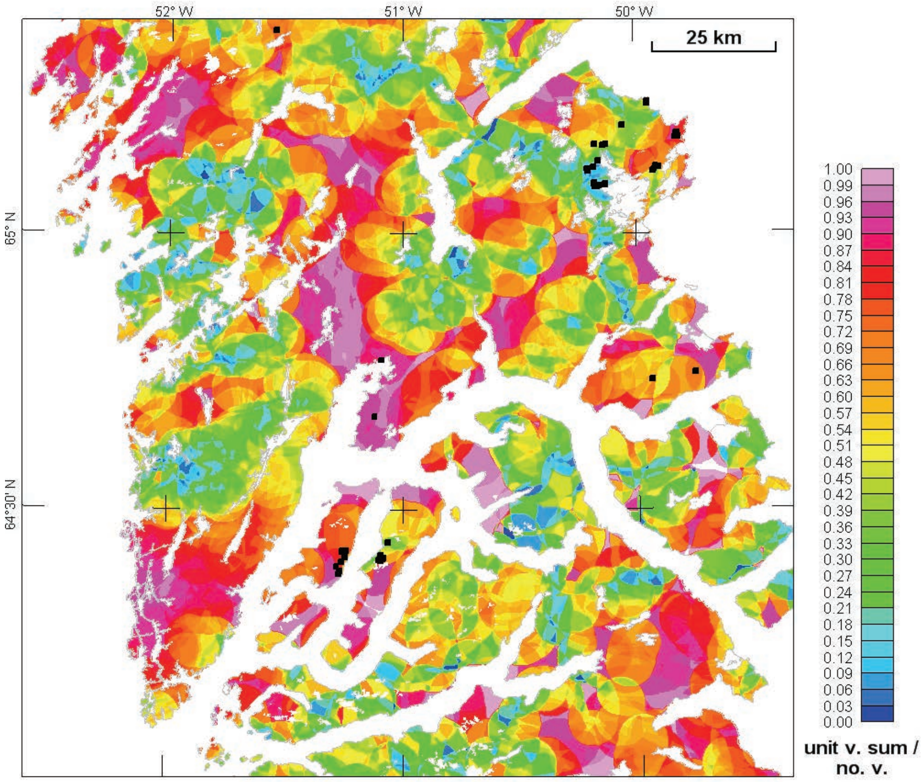

Figure 131. *Lineament statistics, sum of unit vectors divided by number of vectors (complexity), search radius 5000 m, for lineament lengths 4250–23600 m (75–100%).*

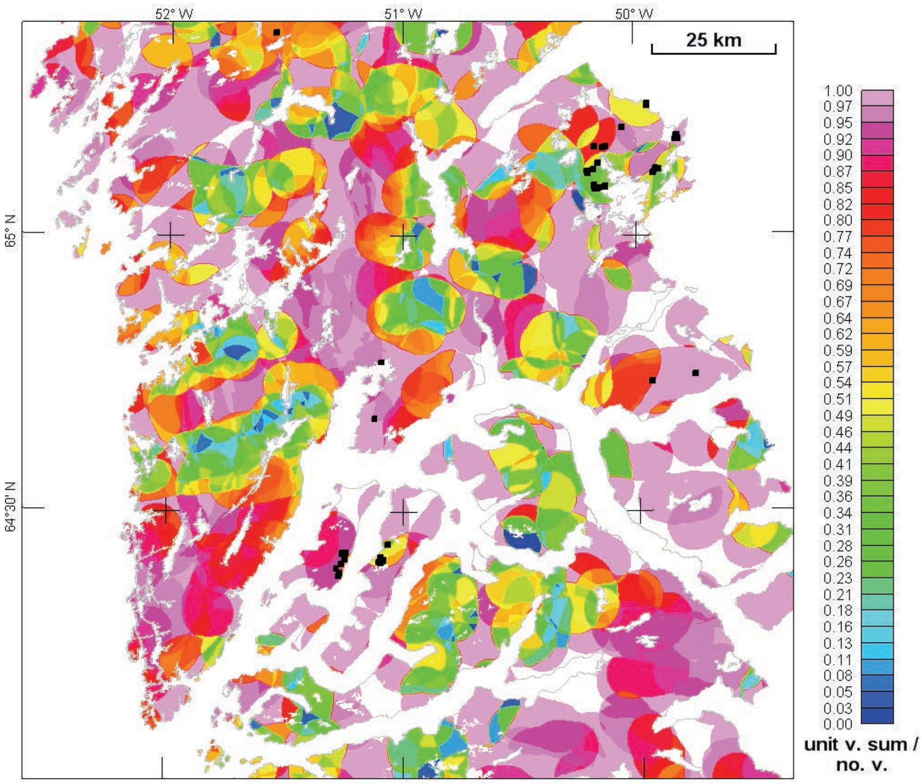

Figure 132. *Lineament statistics, sum of unit vectors divided by number of vectors (complexity), search radius 5000 m, for lineament lengths 6030–23600 m (90–100%).*

Appendix C – Signatures

Signatures in regional fine fraction stream sediment geochemistry

See Nielsen et al. (2004) for further description of the data and the used gridding technique.

Abbreviations in diagrams:

s.p. 4% refers to a spread parameter of 4 % used in the Kernel function for smoothing the empirical distribution function (Nielsen *et al.* 2004).

Al_2O_3, GEUS, minimum curvature, 200 m
spread parameter 4%

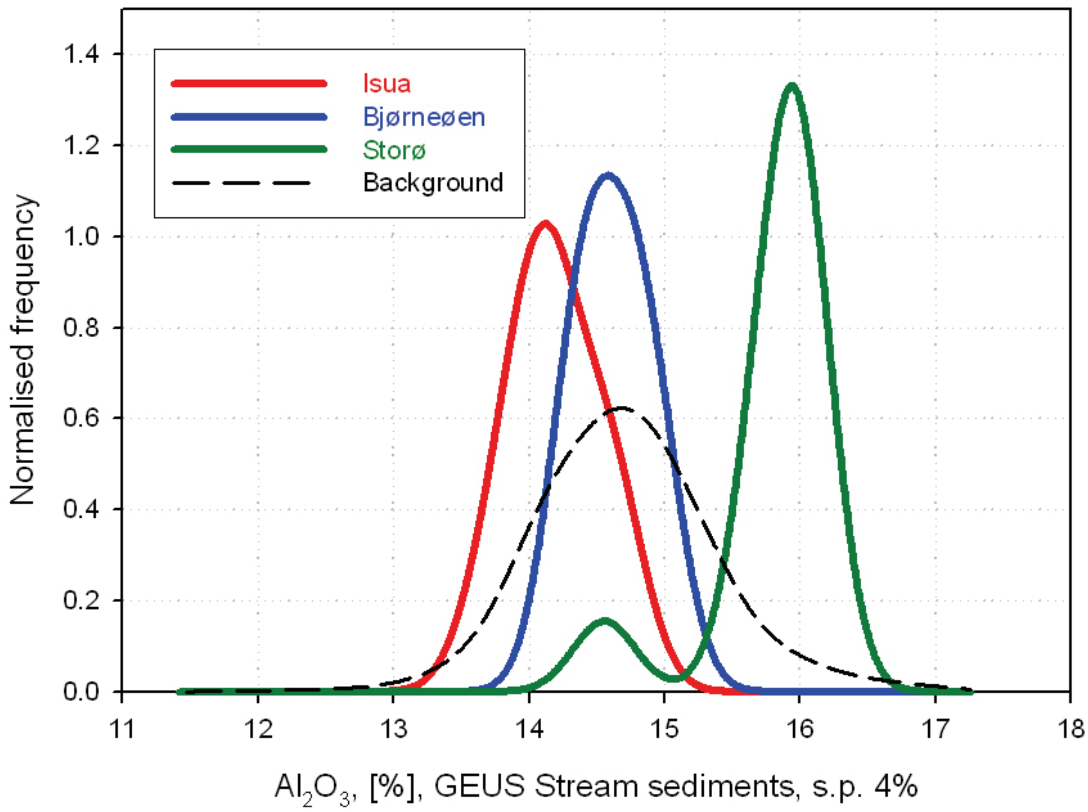

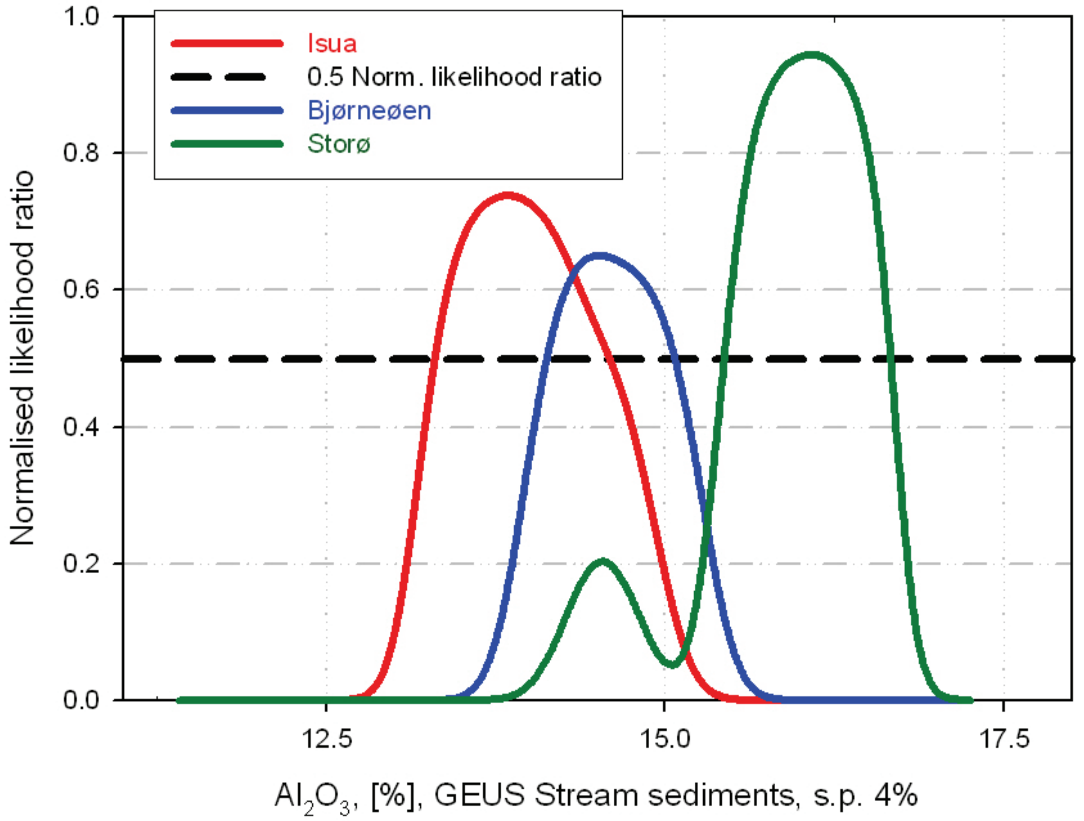

As, GEUS, minimum curvature, modified 200 m
spread parameter 4%

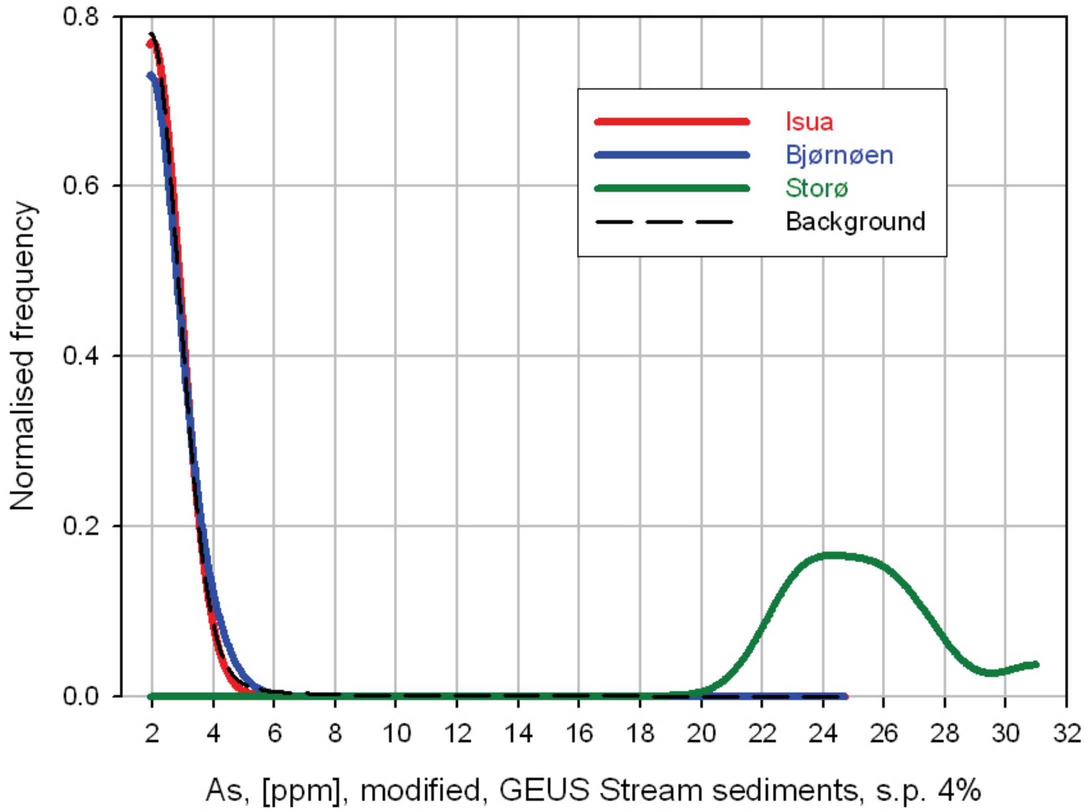

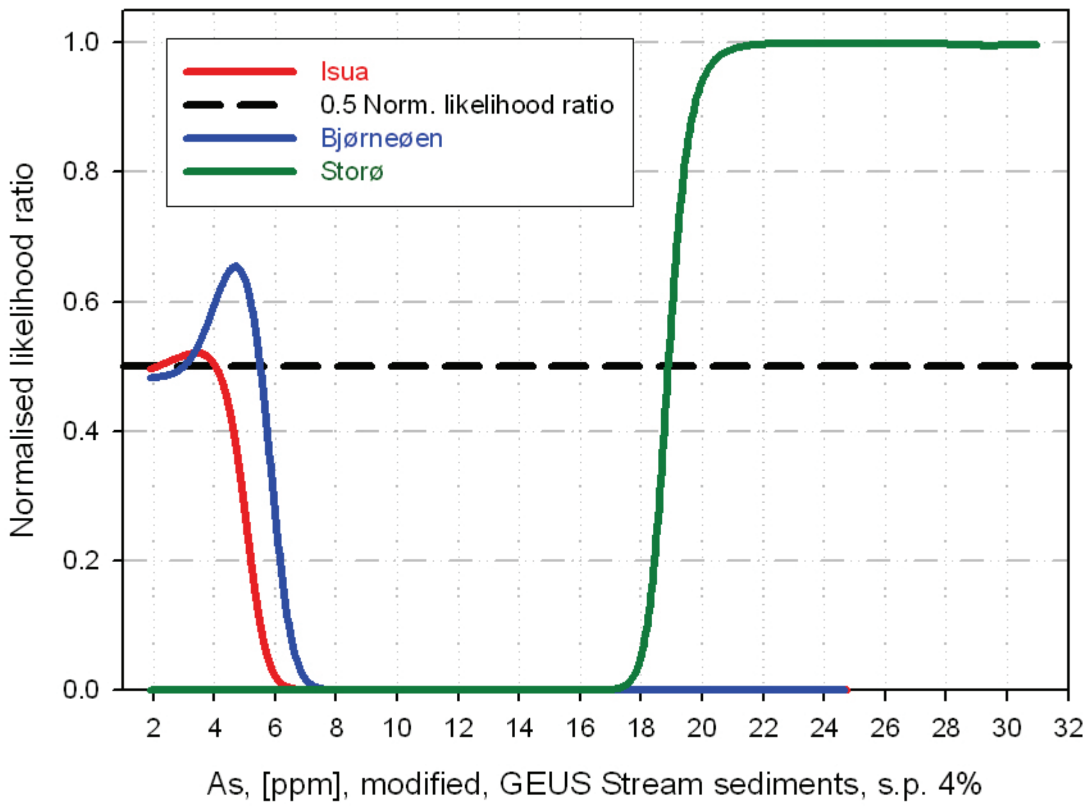

Au, GEUS, minimum curvature, modified 200 m
spread parameter 4%

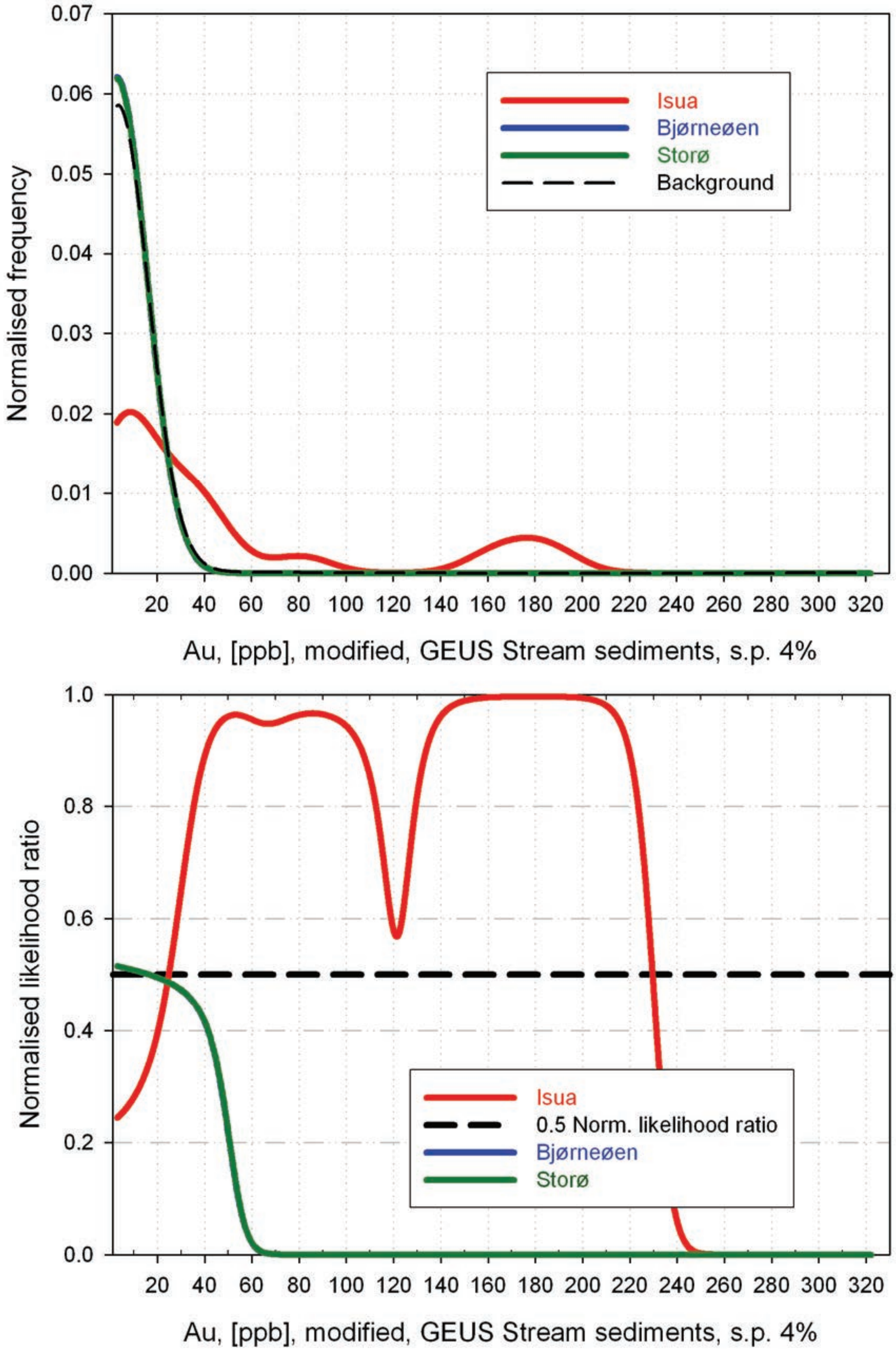

CaO, GEUS, minimum curvature, 200 m
spread parameter 4%

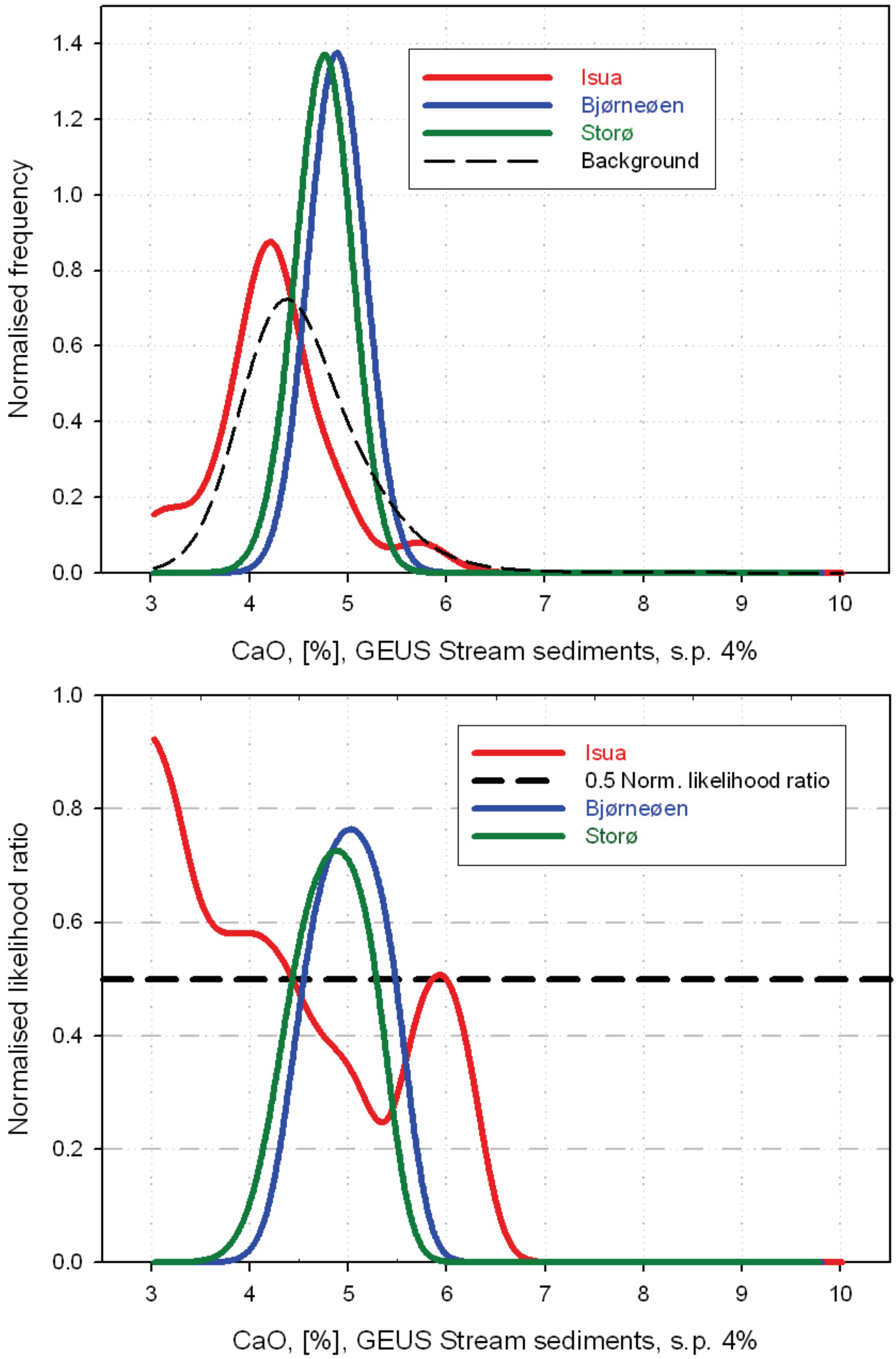

Cs, GEUS, minimum curvature, modified 200 m
spread parameter 4%

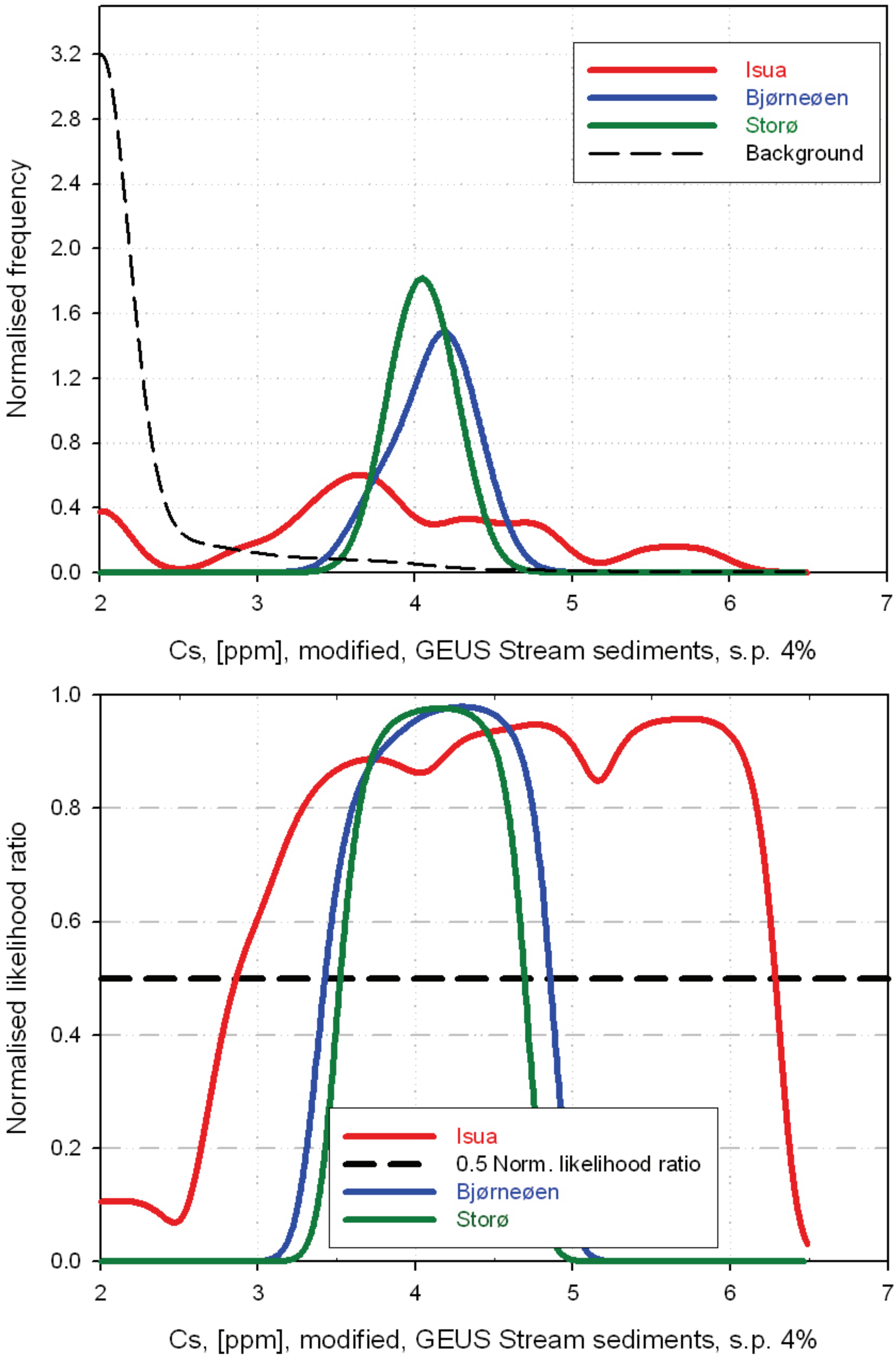

Fe_2O_3, GEUS, minimum curvature, 200 m
spread parameter 4%

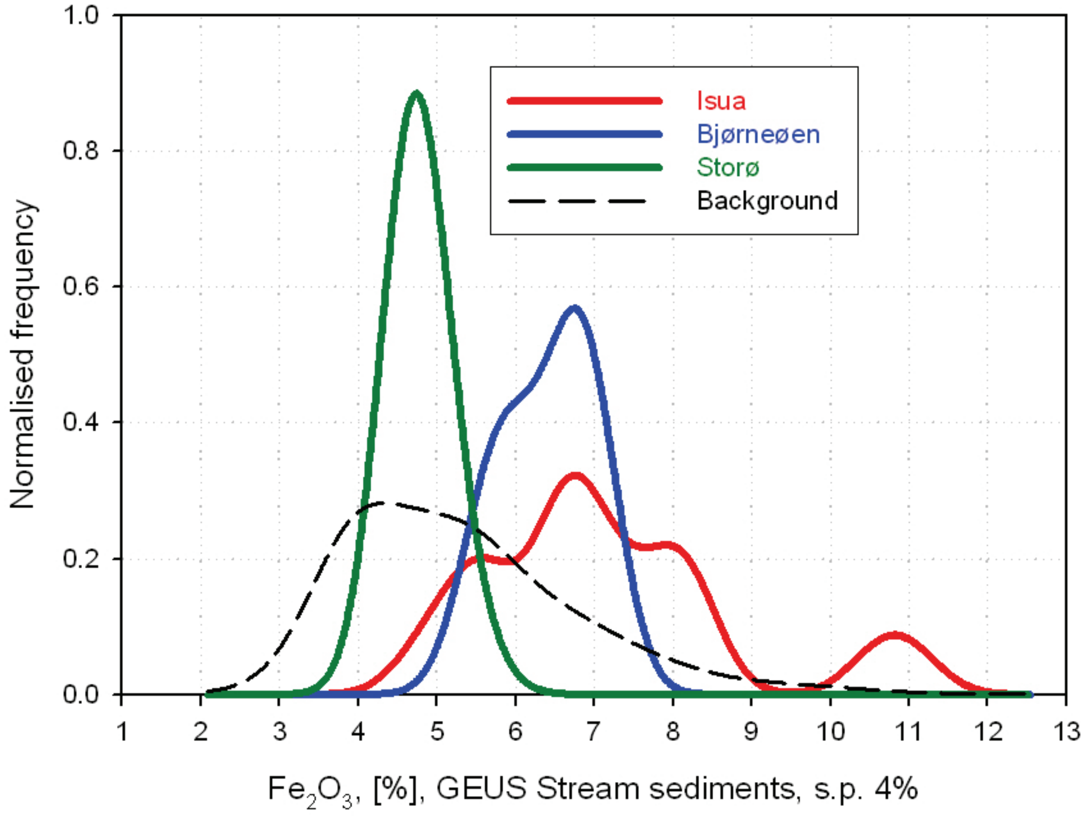

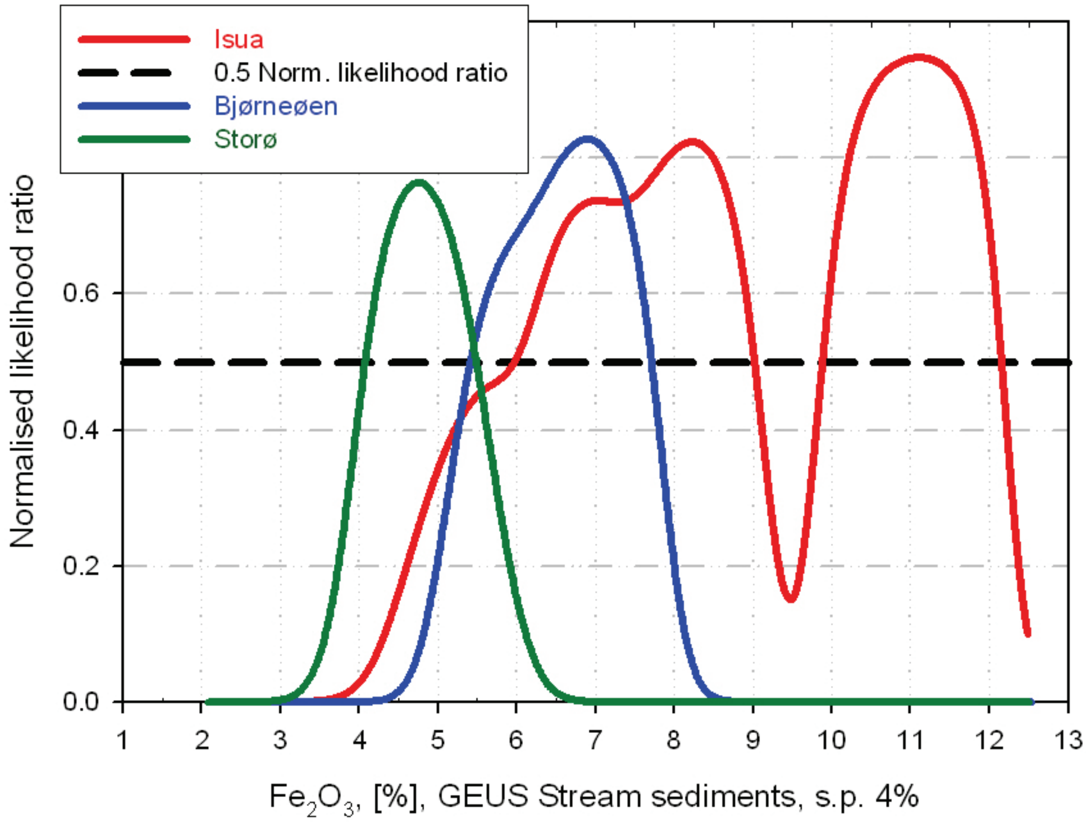

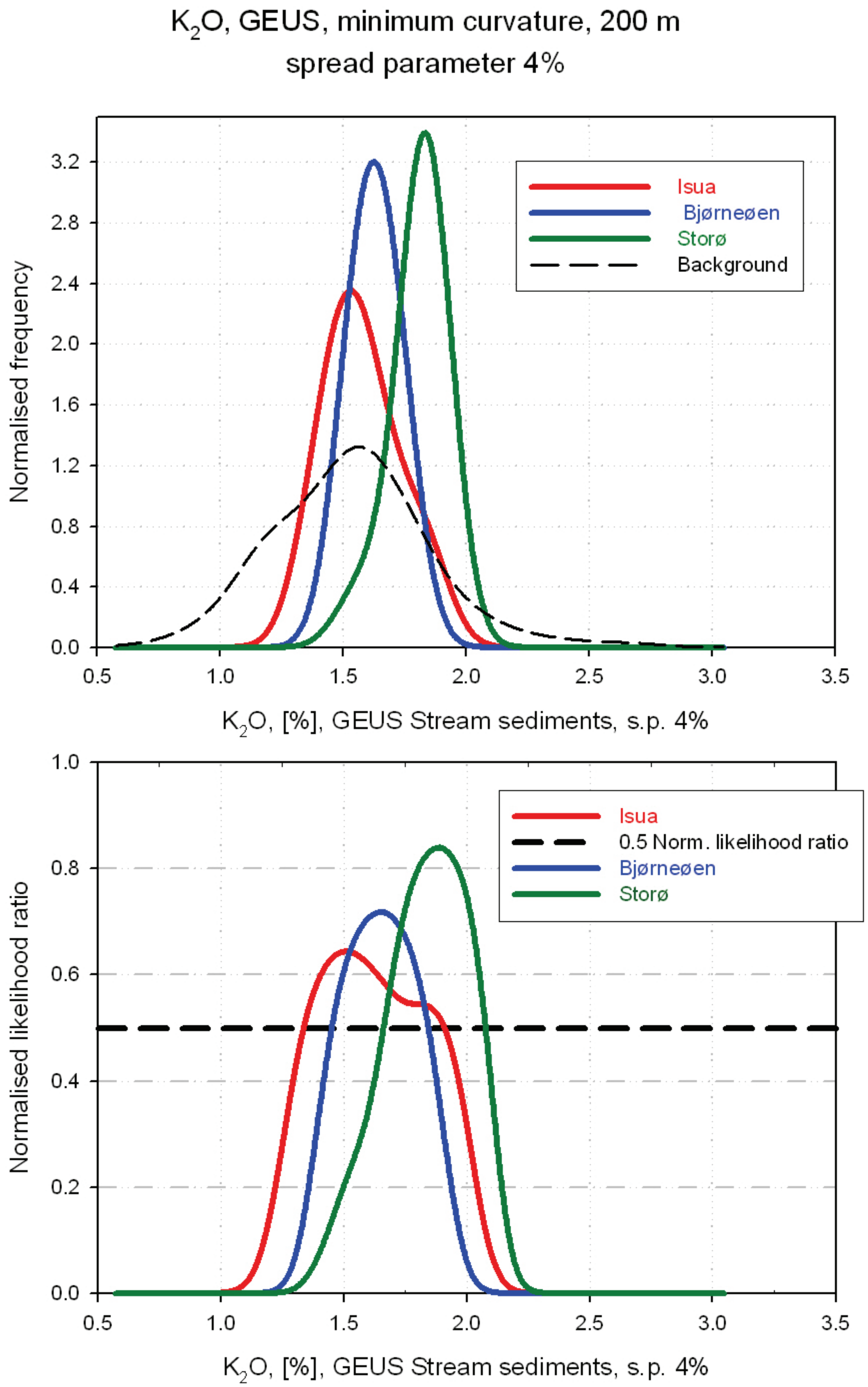

K2O, GEUS, minimum curvature, 200 m
spread parameter 4%
Normalised frequency
3.2
2.8
2.4
2.0
1.6
1.2
0.8
0.4
0.0
0.5
1.0
1.5
2.0
2.5
3.0
3.5
Isua
Bjørneøen
Storø
Background
K2O, [%], GEUS Stream sediments, s.p. 4%
Normalised likelihood ratio
1.0
0.8
0.6
0.4
0.2
0.0
Isua
0.5 Norm. likelihood ratio
Bjørneøen
Storø
K2O, [%], GEUS Stream sediments, s.p. 4%

MgO, GEUS, minimum curvature, 200 m
spread parameter 4%

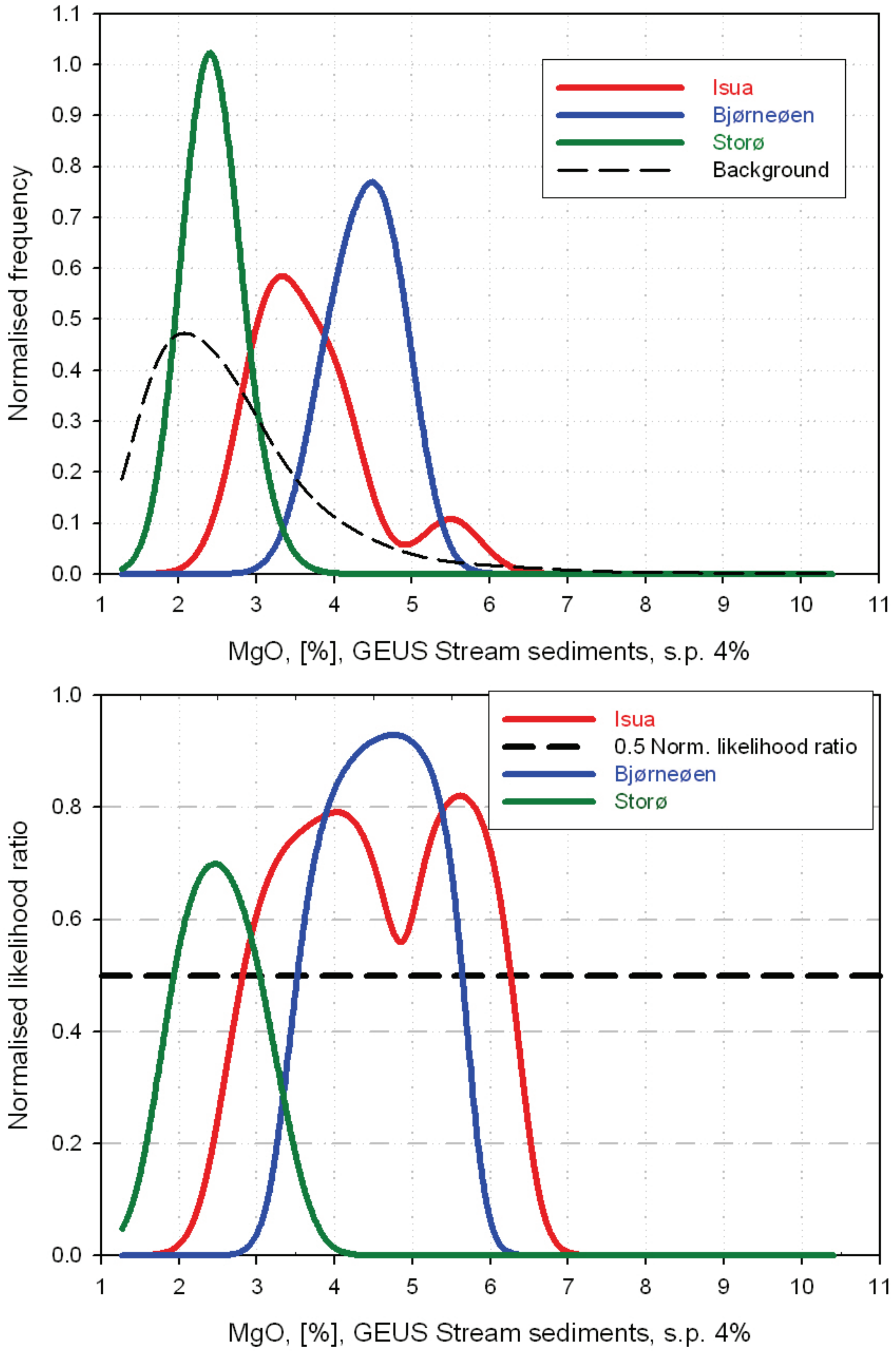

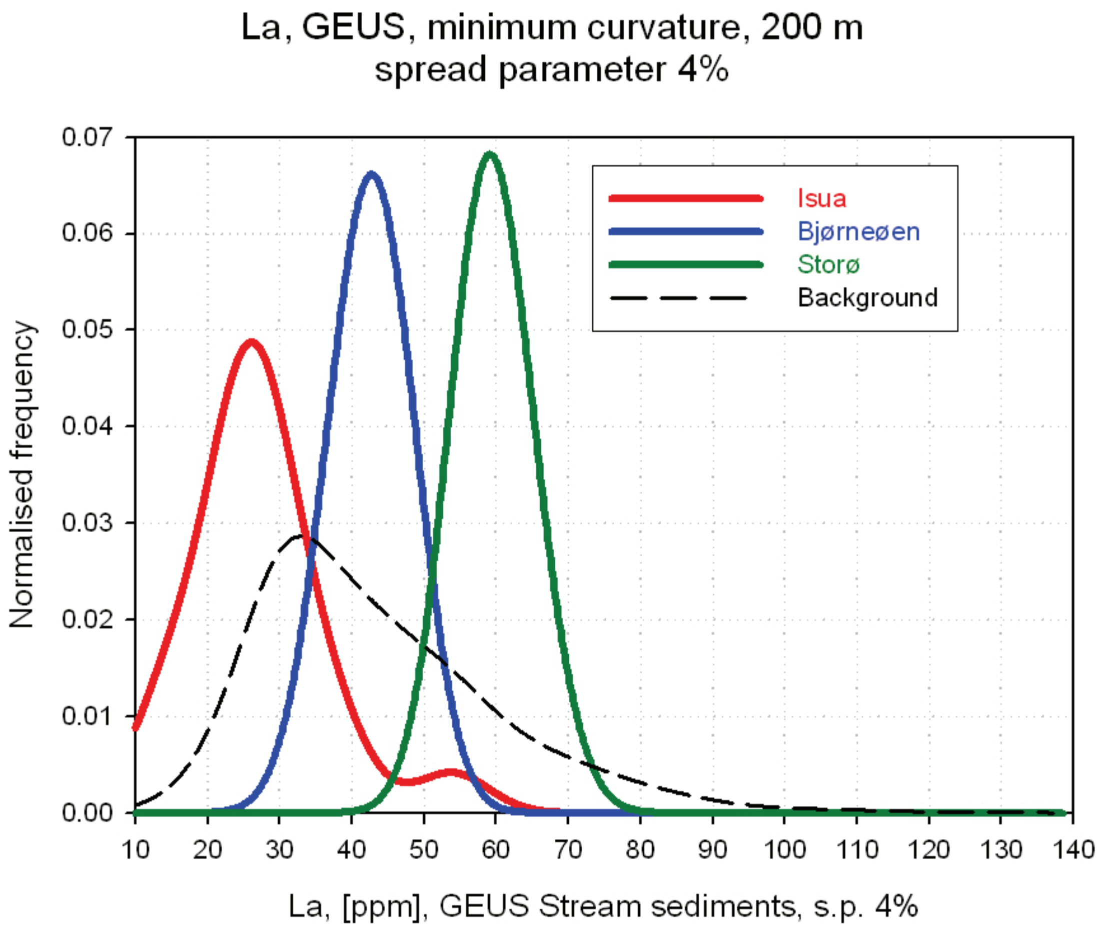
La, GEUS, minimum curvature, 200 m
spread parameter 4%
Normalised frequency
0.07
0.06
0.05
0.04
0.03
0.02
0.01
0.00
10
20
30
40
50
60
70
80
90
100
110
120
130
140
La, [ppm], GEUS Stream sediments, s.p. 4%
Isua
Bjørneøen
Storø
Background

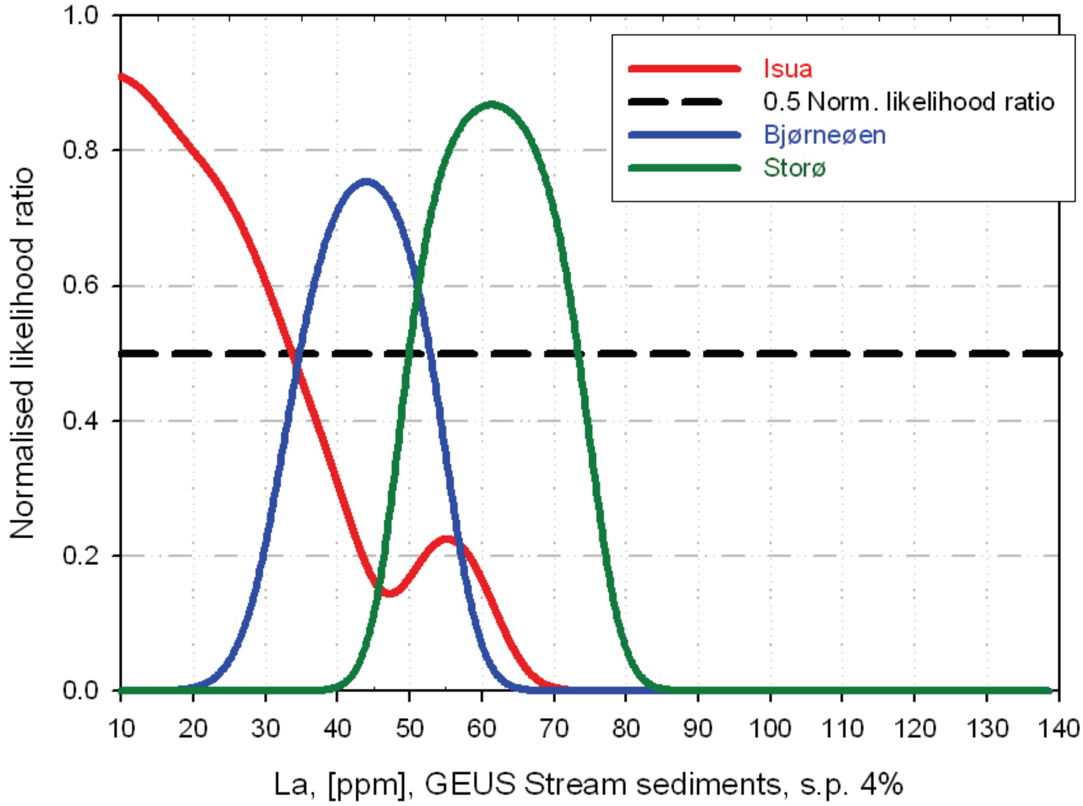
Normalised likelihood ratio
1.0
0.8
0.6
0.4
0.2
0.0
10
20
30
40
50
60
70
80
90
100
110
120
130
140
La, [ppm], GEUS Stream sediments, s.p. 4%
Isua
0.5 Norm. likelihood ratio
Bjørneøen
Storø

Ni + Cr, GEUS, minimum curvature, 200 m
spread parameter 4%

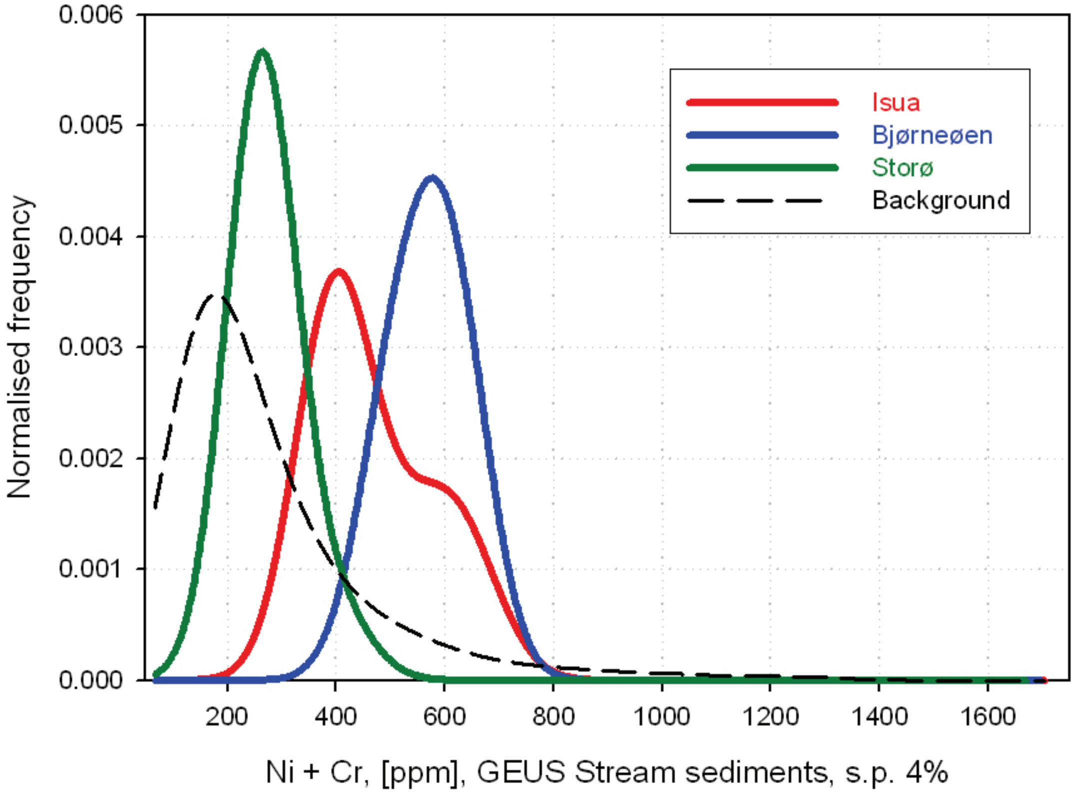

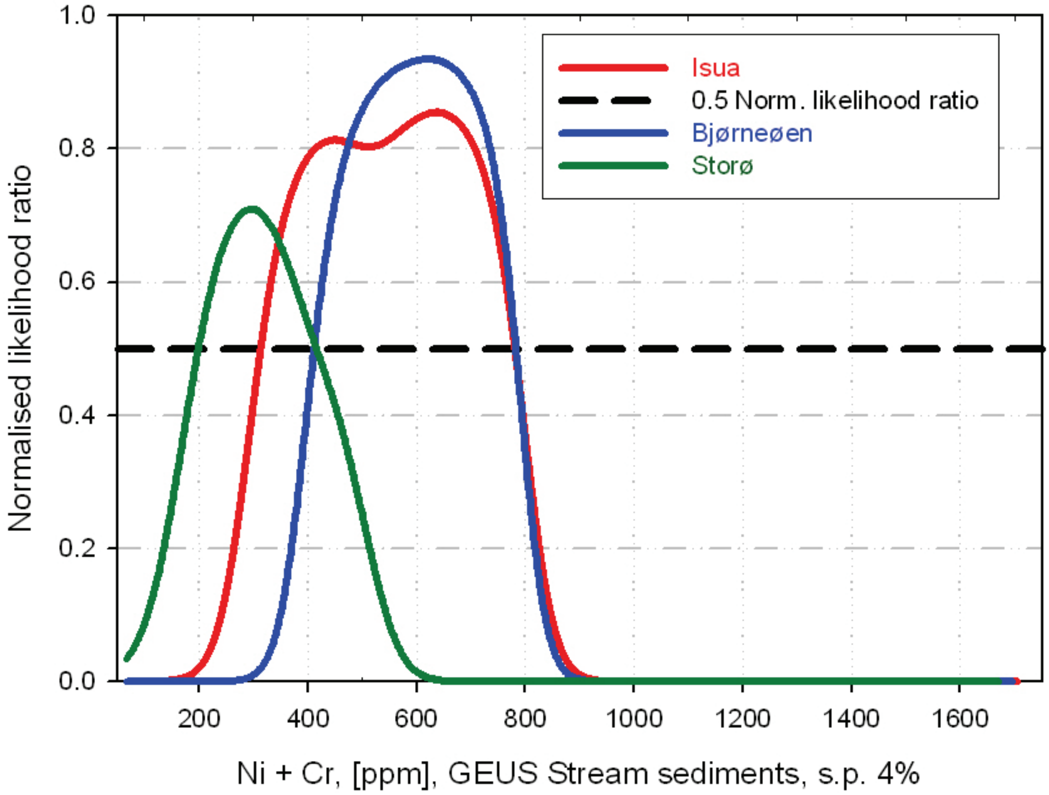

Na$_2$O, GEUS, minimum curvature, 200 m
spread parameter 4%

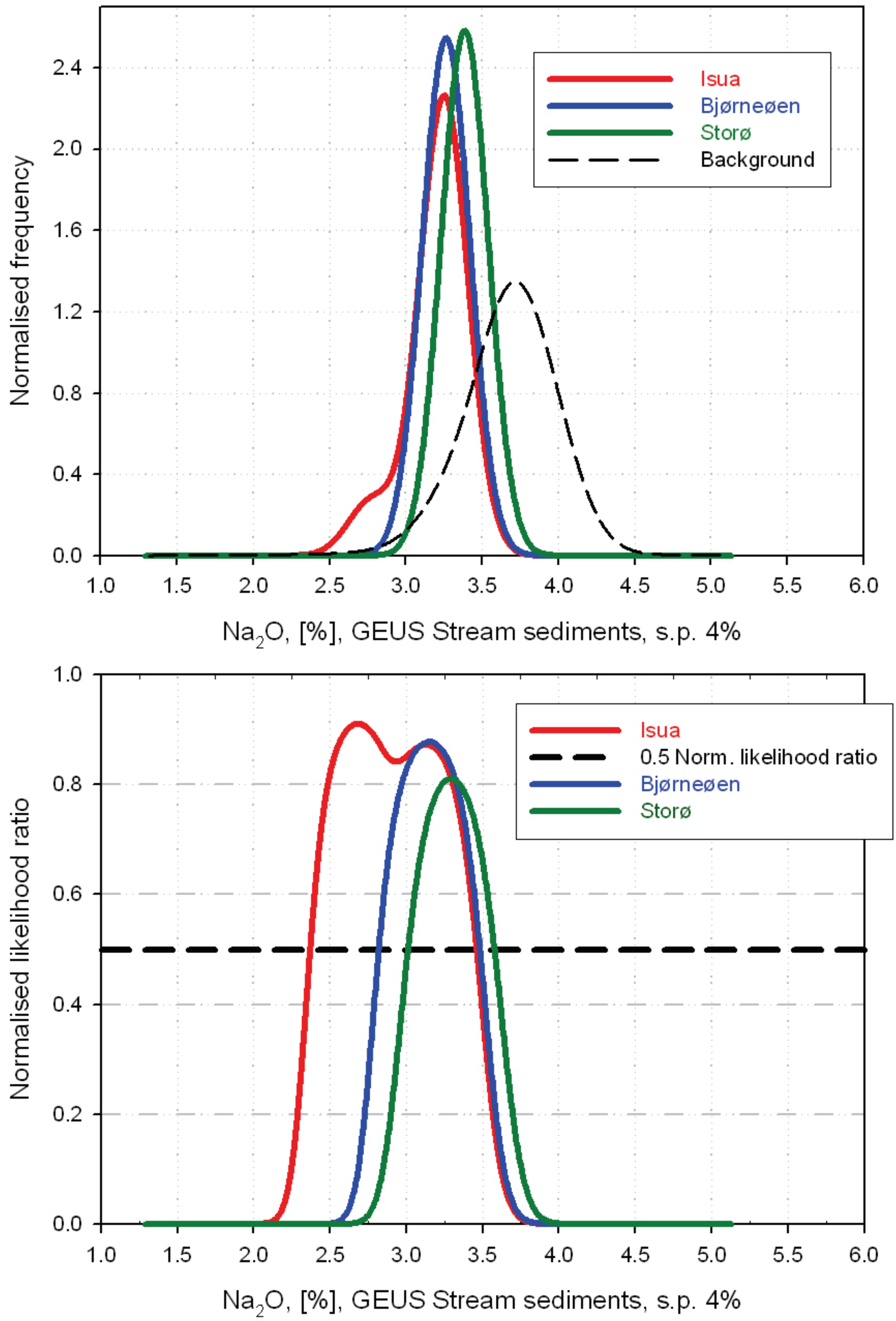

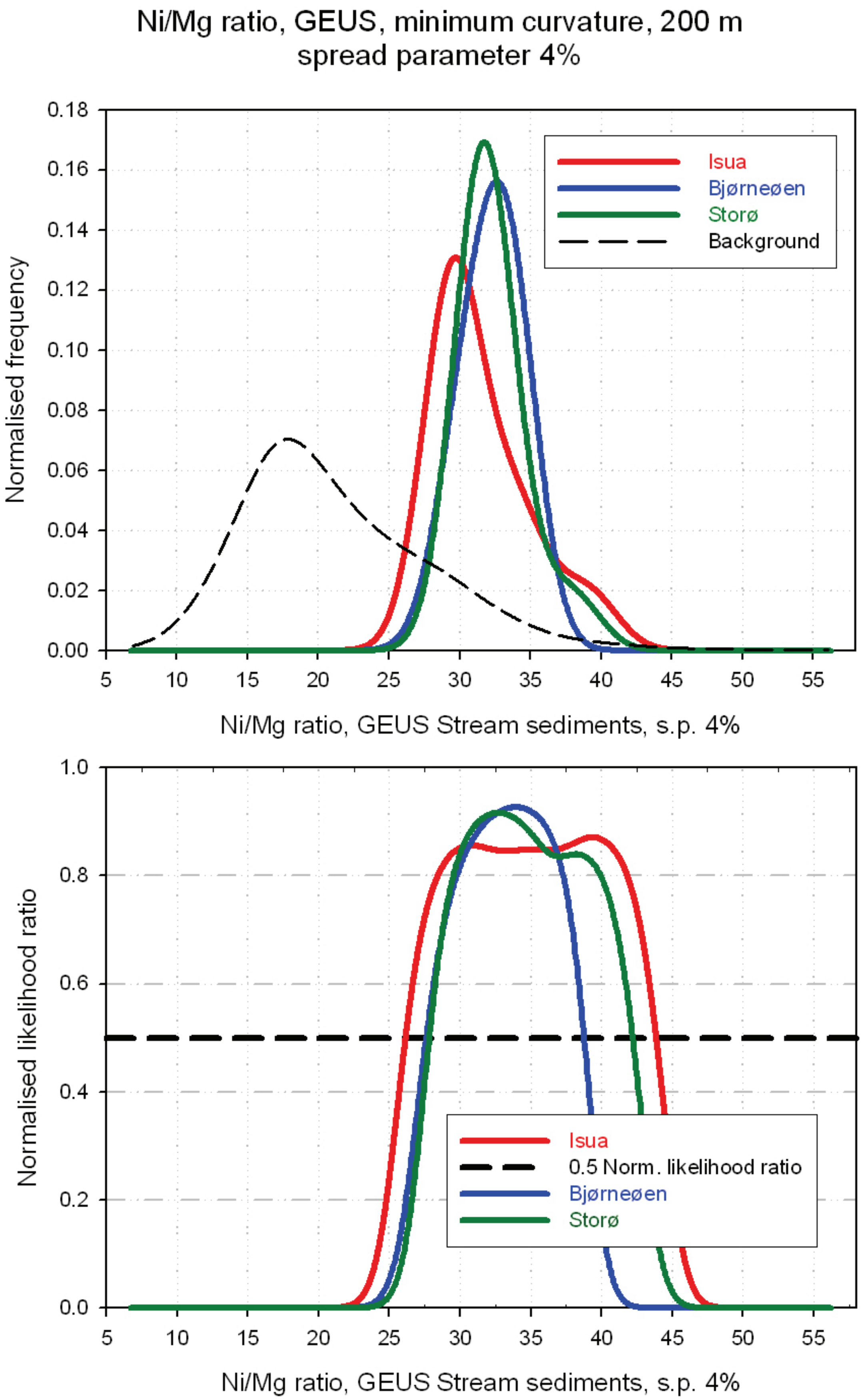
Ni/Mg ratio, GEUS, minimum curvature, 200 m
spread parameter 4%
Normalised frequency
Isua
Bjørneøen
Storø
Background
Ni/Mg ratio, GEUS Stream sediments, s.p. 4%
Normalised likelihood ratio
Isua
0.5 Norm. likelihood ratio
Bjørneøen
Storø
Ni/Mg ratio, GEUS Stream sediments, s.p. 4%

P_2O_5, GEUS, minimum curvature, 200 m
spread parameter 4%

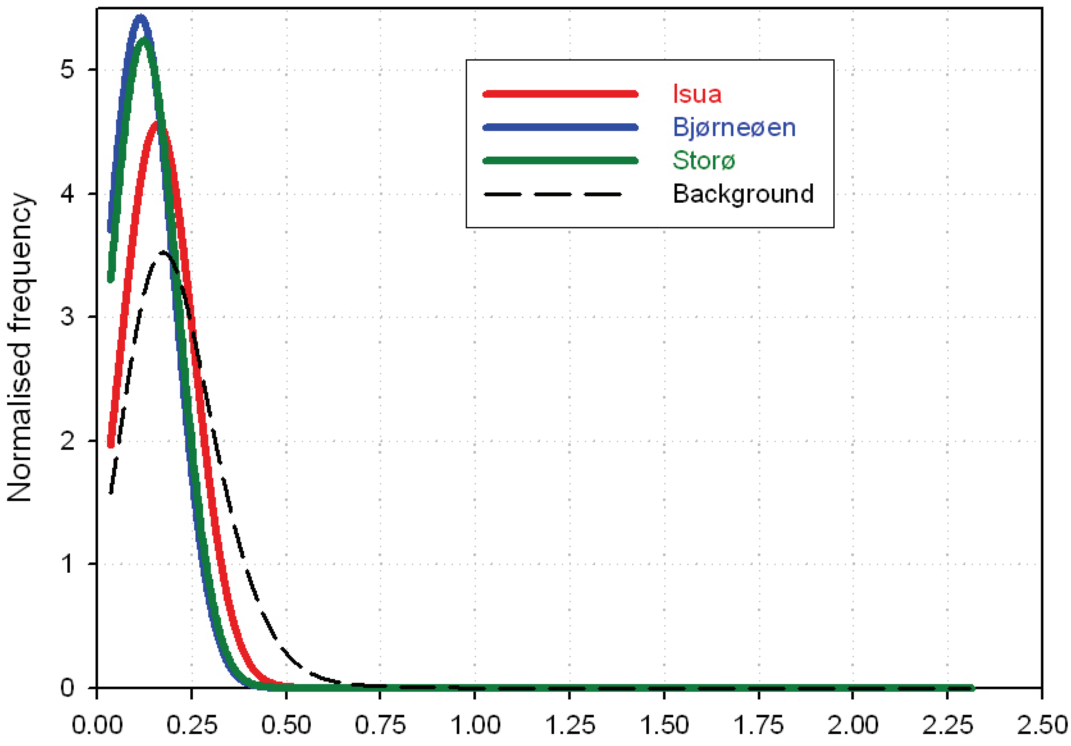

P_2O_5, [%], GEUS Stream sediments, s.p. 4%

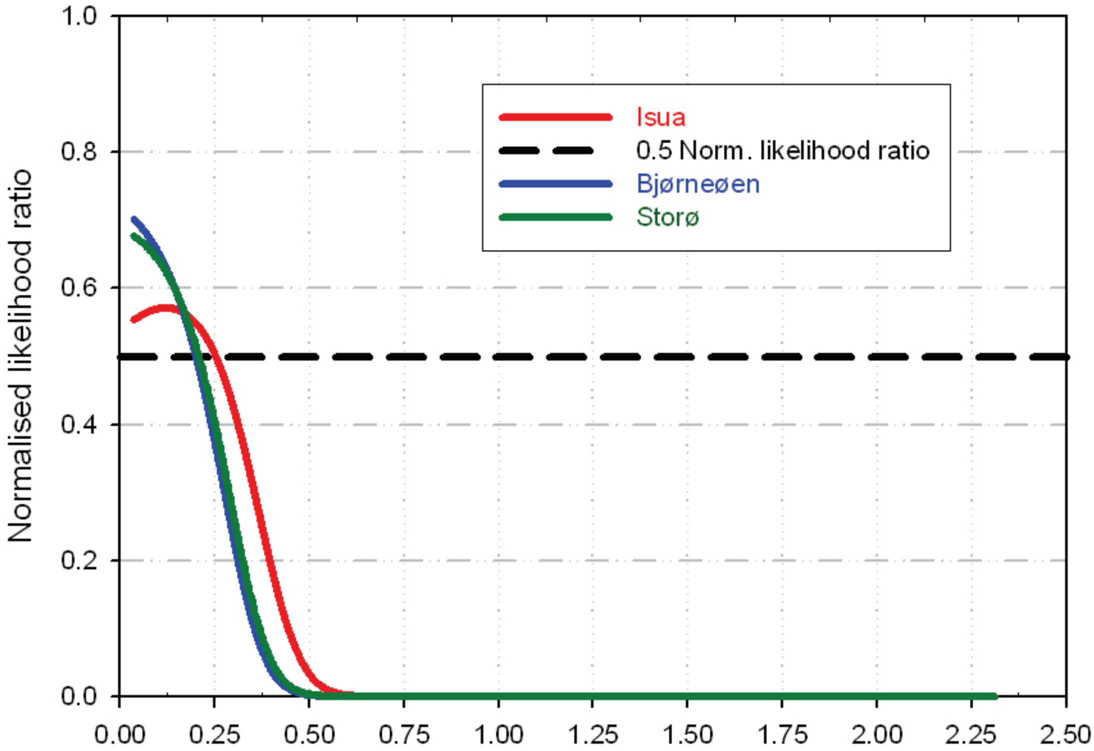

P_2O_5, [%], GEUS Stream sediments, s.p. 4%

Rb, GEUS, minimum curvature, 200 m
spread parameter 4%

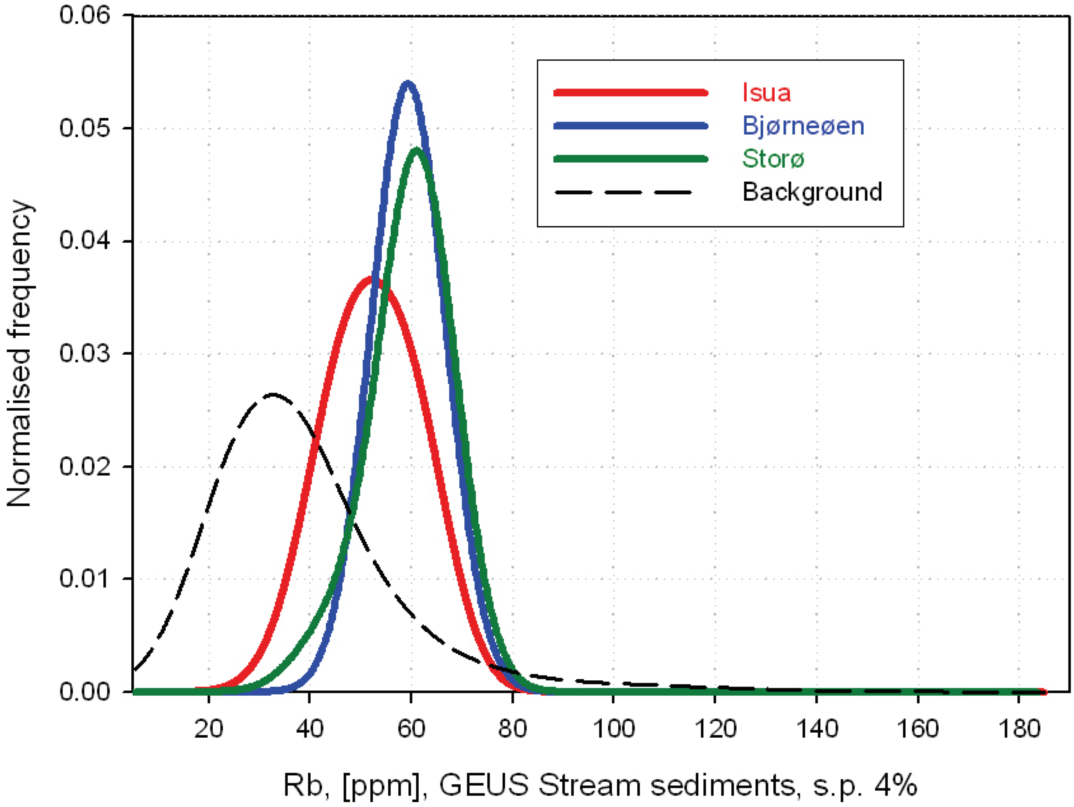

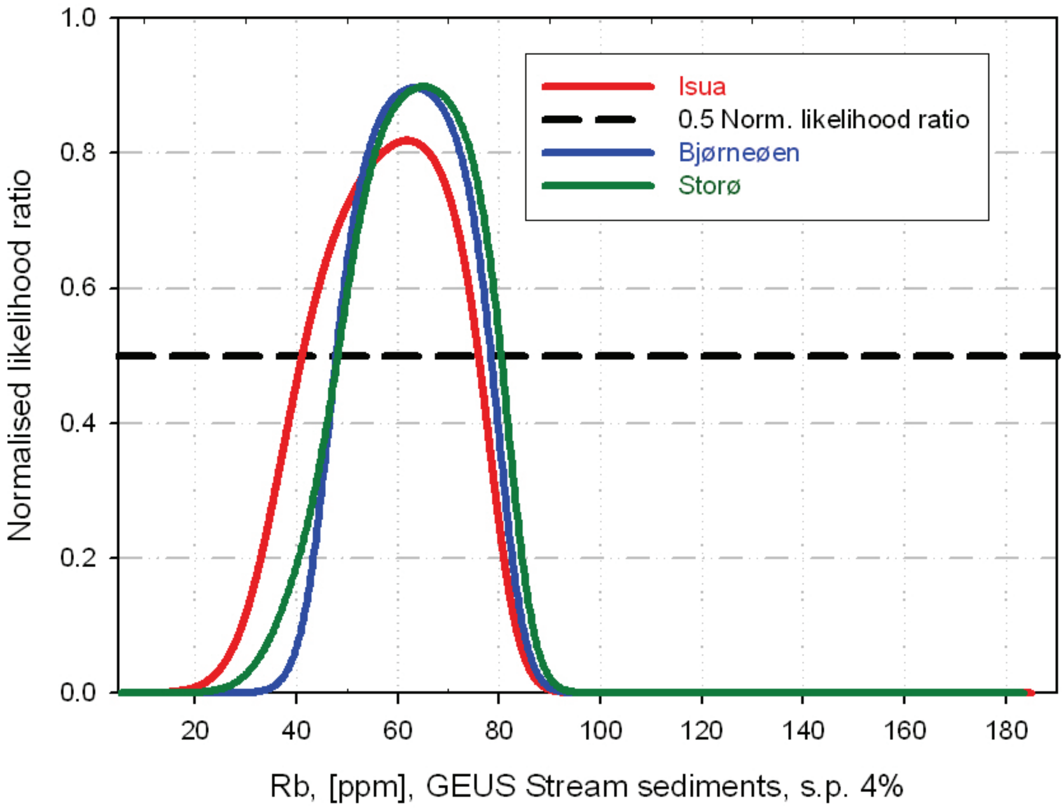

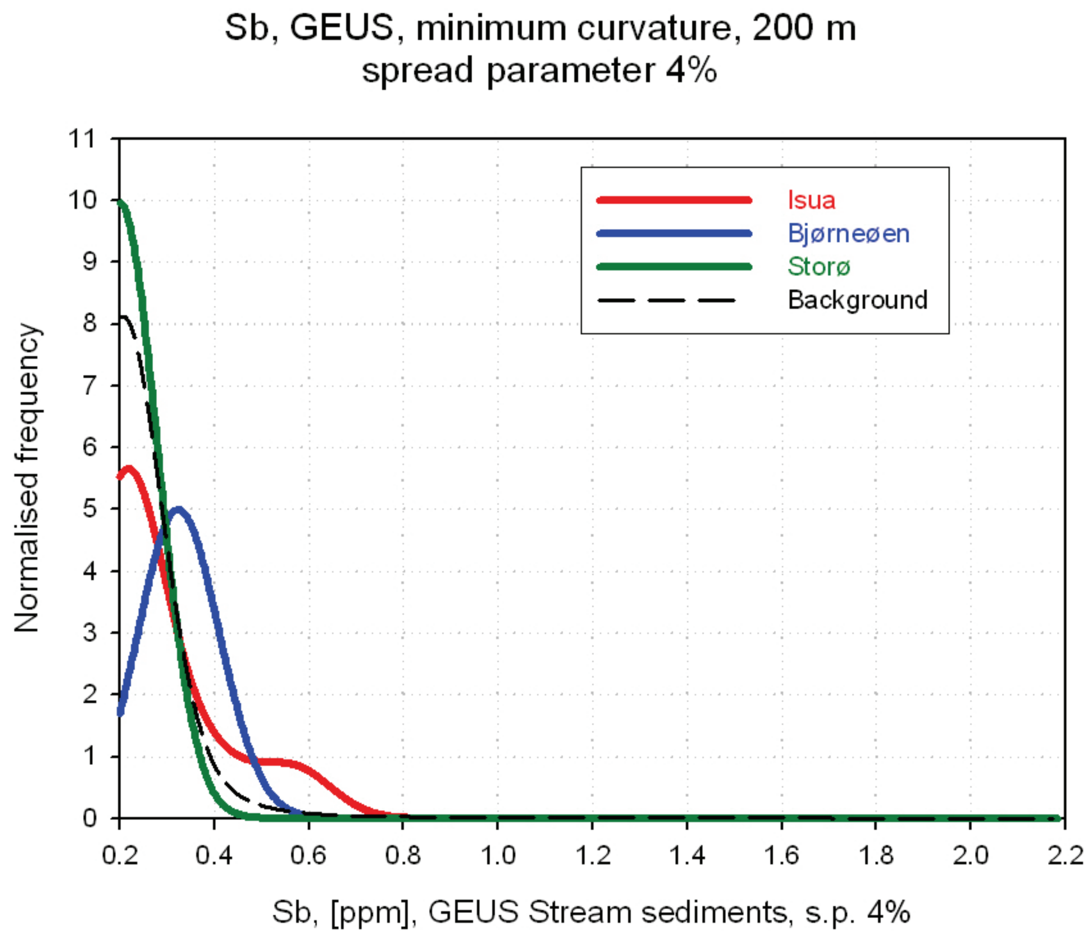
Sb, GEUS, minimum curvature, 200 m
spread parameter 4%
Normalised frequency
Isua
Bjørneøen
Storø
Background
0.2
0.4
0.6
0.8
1.0
1.2
1.4
1.6
1.8
2.0
2.2
Sb, [ppm], GEUS Stream sediments, s.p. 4%

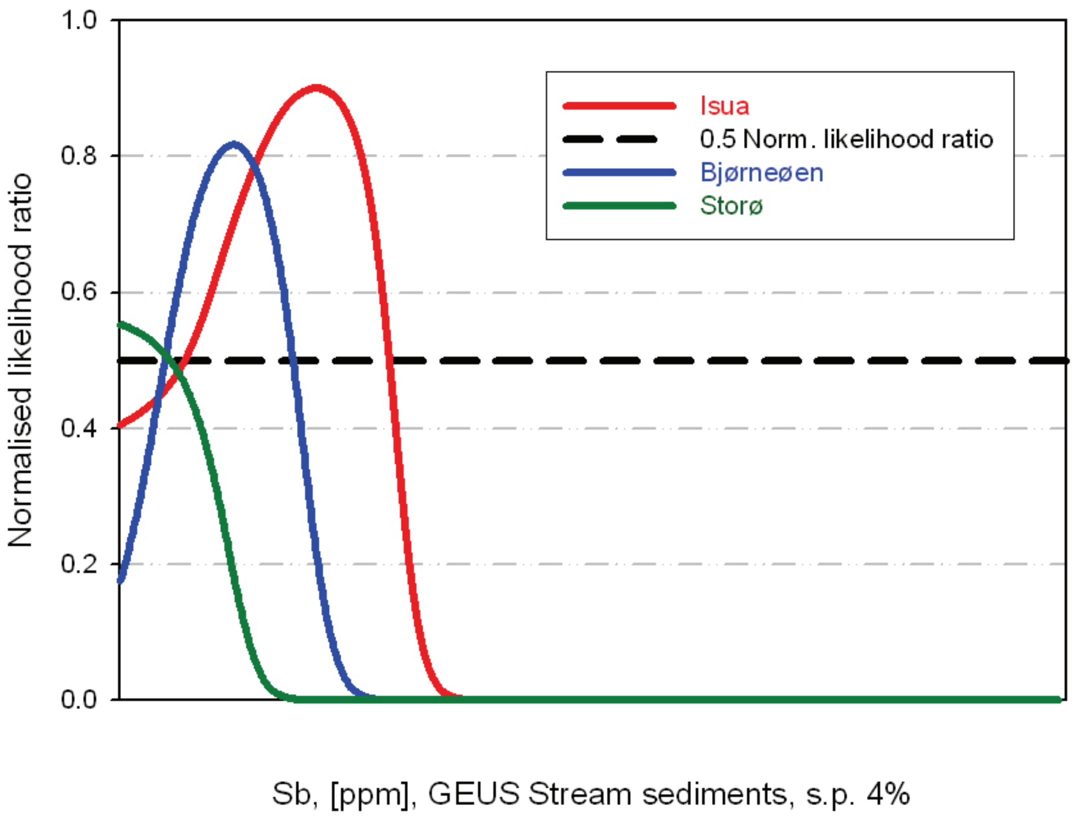
Normalised likelihood ratio
Isua
0.5 Norm. likelihood ratio
Bjørneøen
Storø
Sb, [ppm], GEUS Stream sediments, s.p. 4%

SiO_2, GEUS, minimum curvature, 200 m
spread parameter 4%

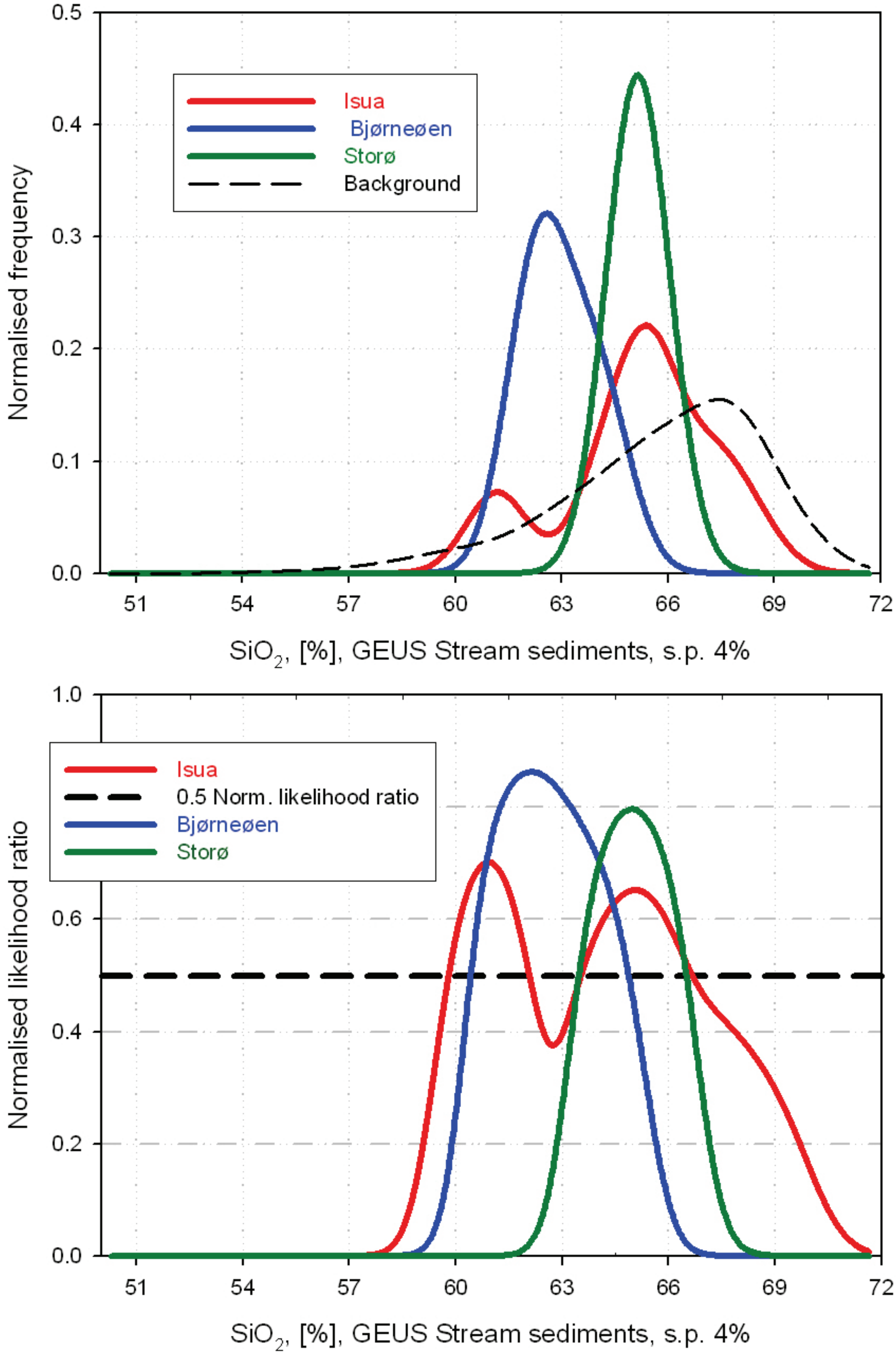

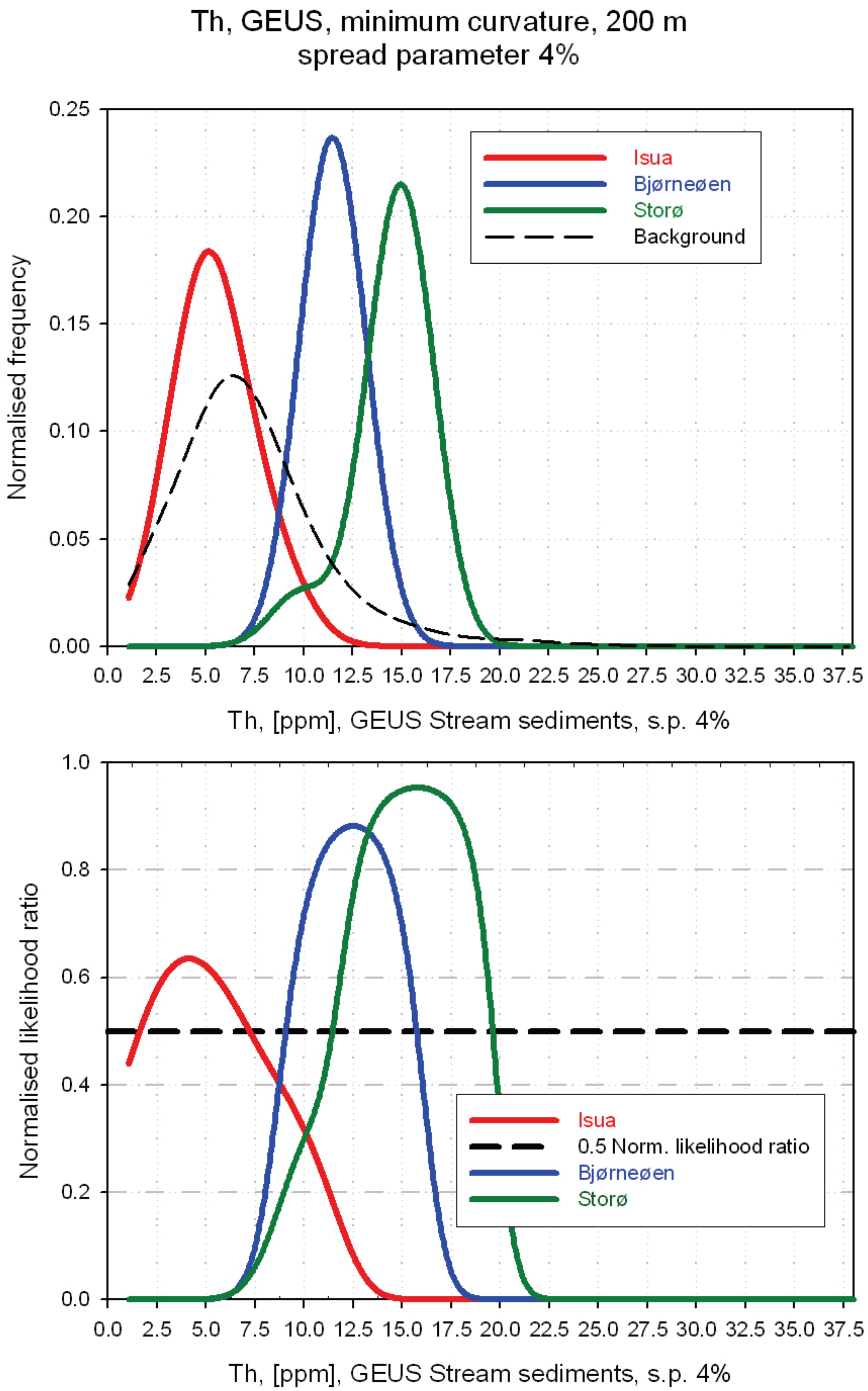
Th, GEUS, minimum curvature, 200 m
spread parameter 4%
Normalised frequency
0.25
0.20
0.15
0.10
0.05
0.00
0.0 2.5 5.0 7.5 10.0 12.5 15.0 17.5 20.0 22.5 25.0 27.5 30.0 32.5 35.0 37.5
Th, [ppm], GEUS Stream sediments, s.p. 4%
Isua
Bjørneøen
Storø
Background
Normalised likelihood ratio
1.0
0.8
0.6
0.4
0.2
0.0
0.0 2.5 5.0 7.5 10.0 12.5 15.0 17.5 20.0 22.5 25.0 27.5 30.0 32.5 35.0 37.5
Th, [ppm], GEUS Stream sediments, s.p. 4%
Isua
0.5 Norm. likelihood ratio
Bjørneøen
Storø

TiO_2, GEUS, minimum curvature, 200 m
spread parameter 4%

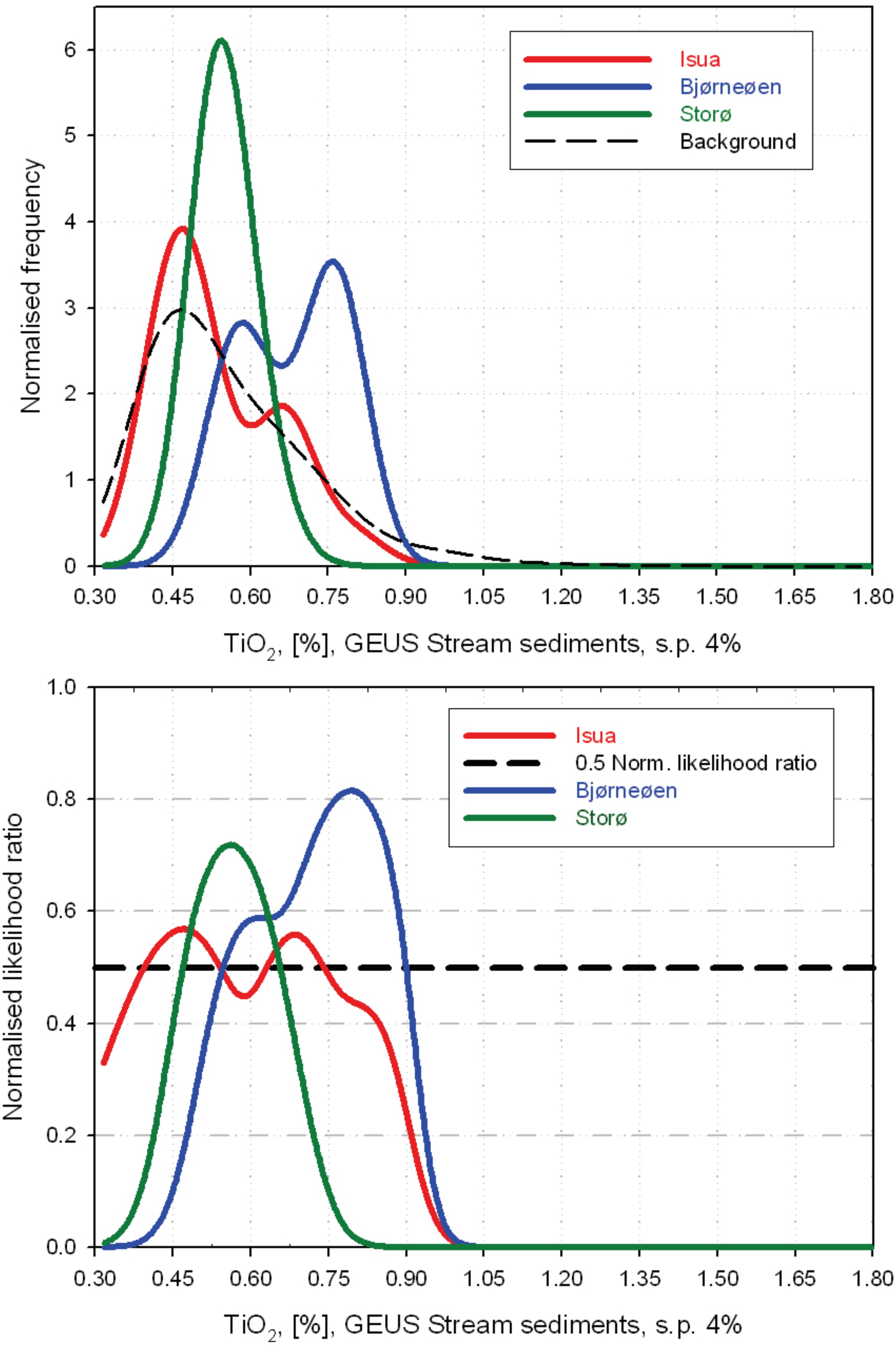

U, GEUS, minimum curvature, modified 200 m
spread parameter 4%

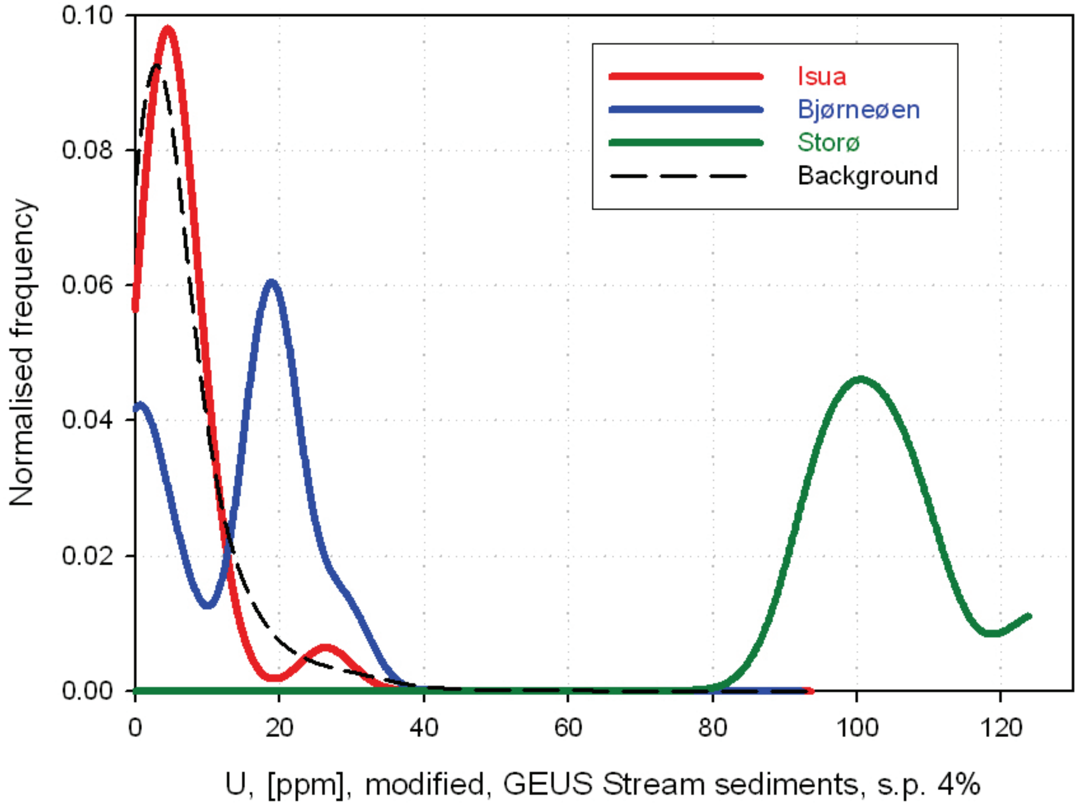

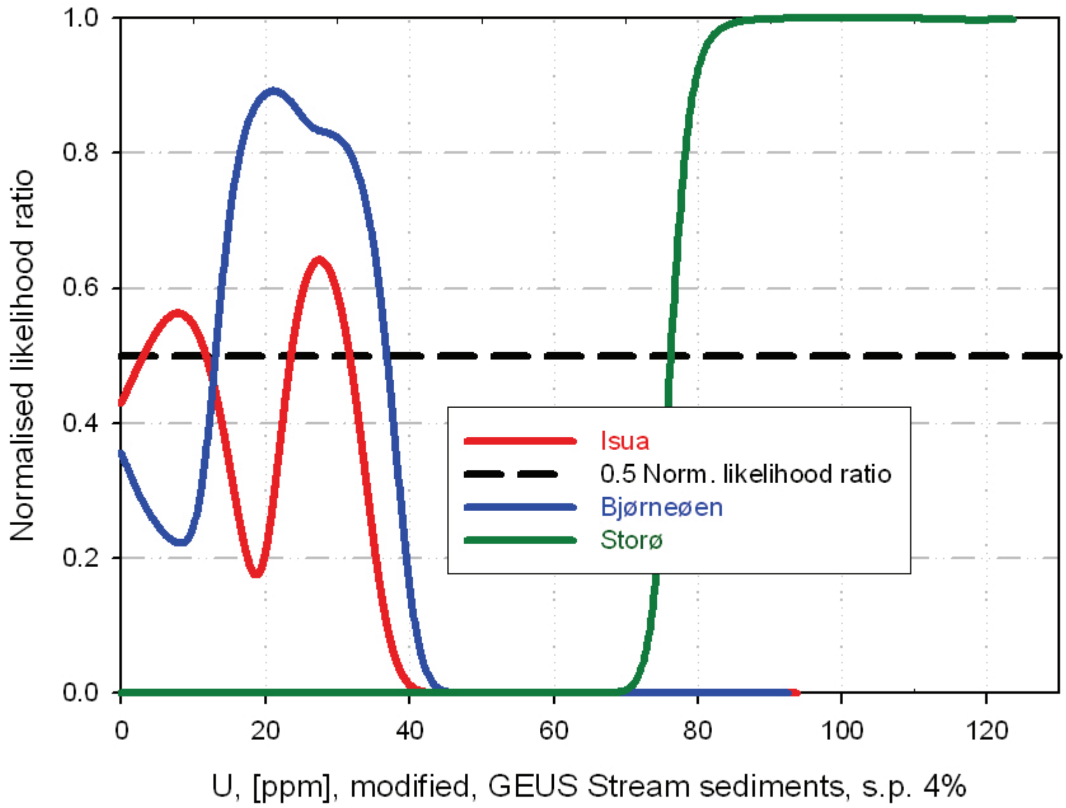

V, GEUS, minimum curvature, 200 m
spread parameter 4%

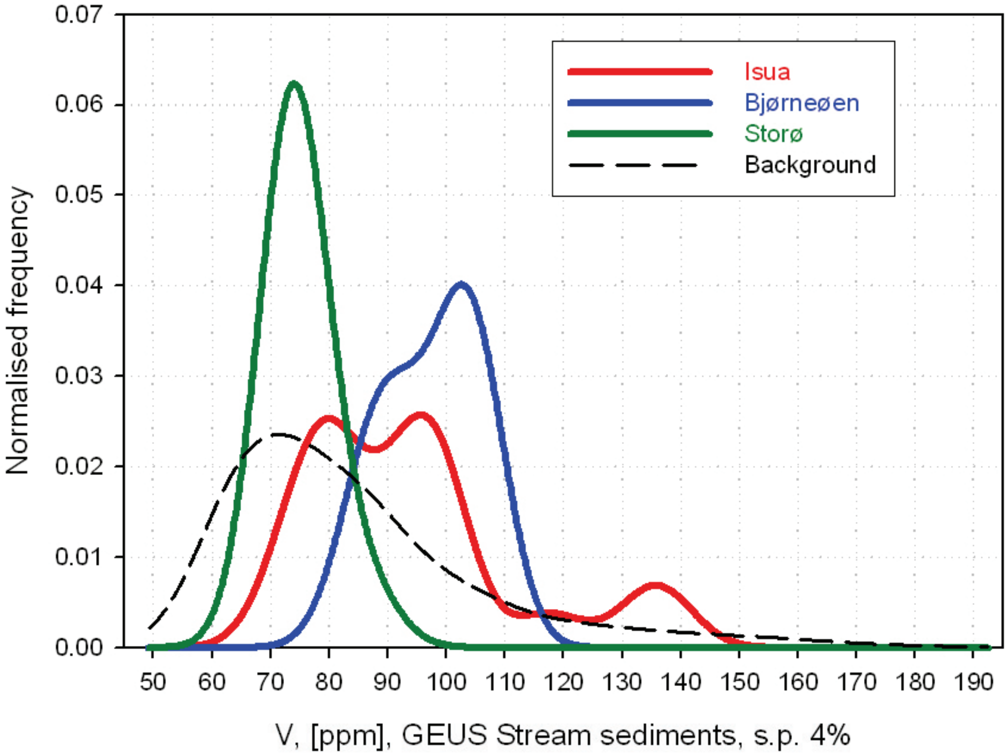

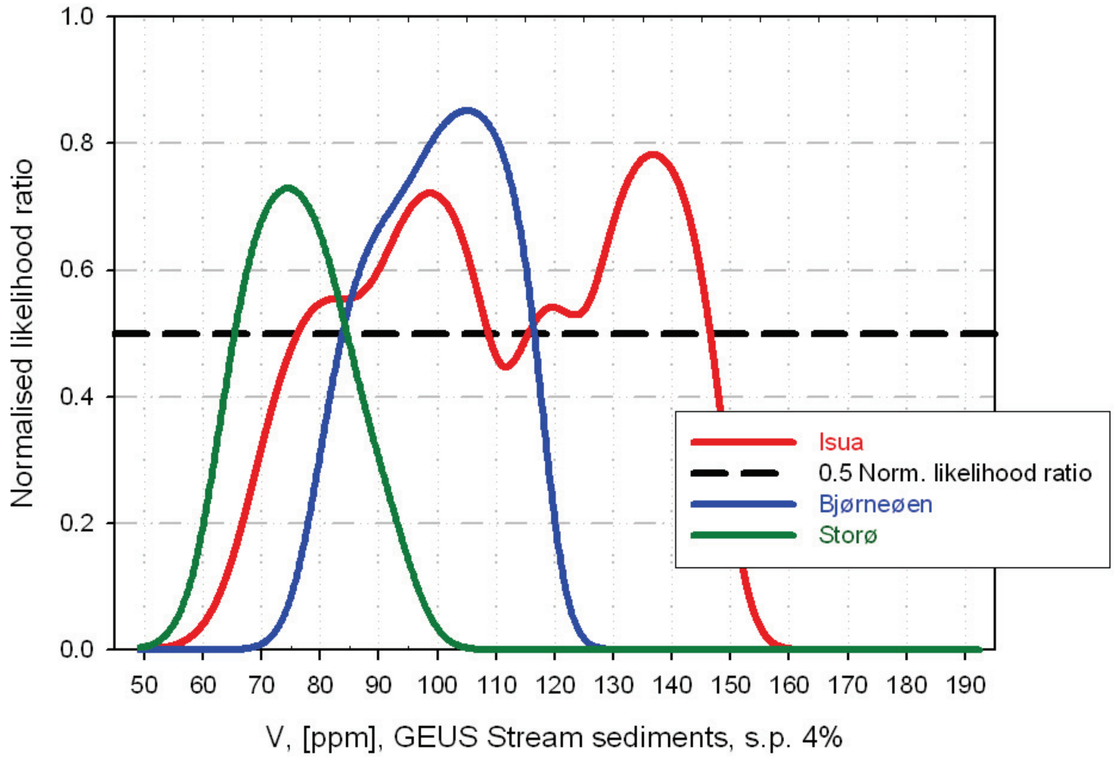

Zn, GEUS, minimum curvature, 200 m
spread parameter 4%

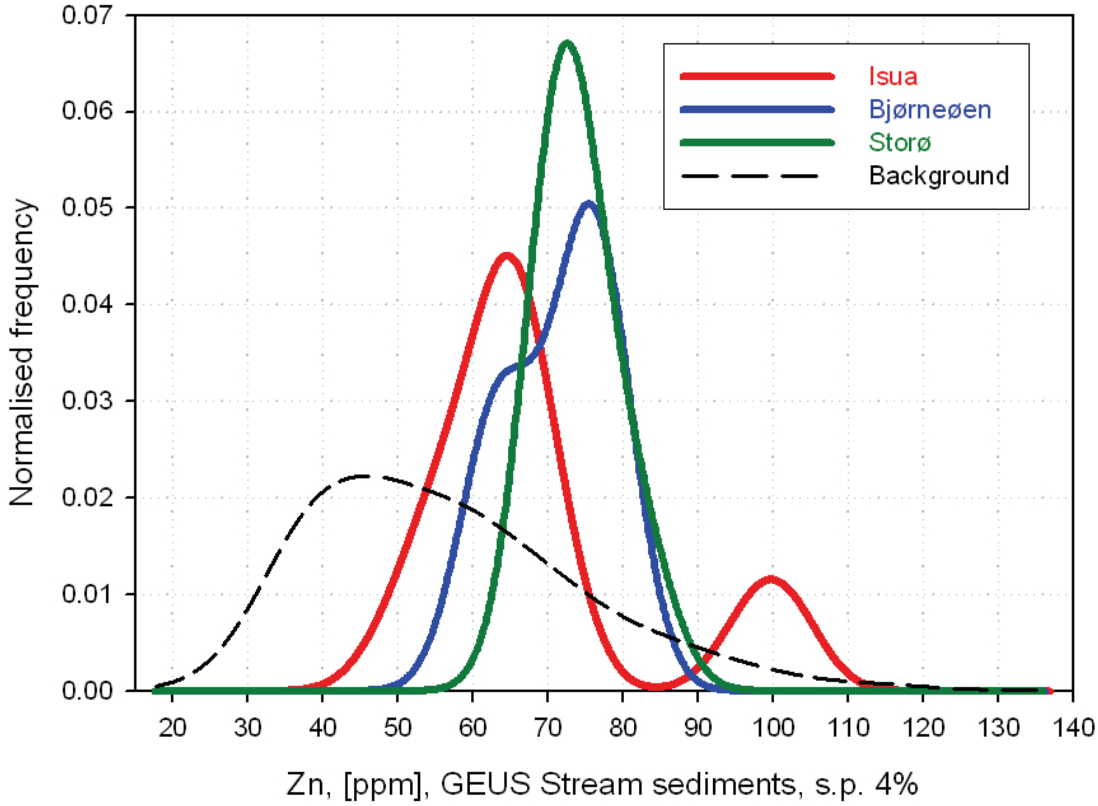

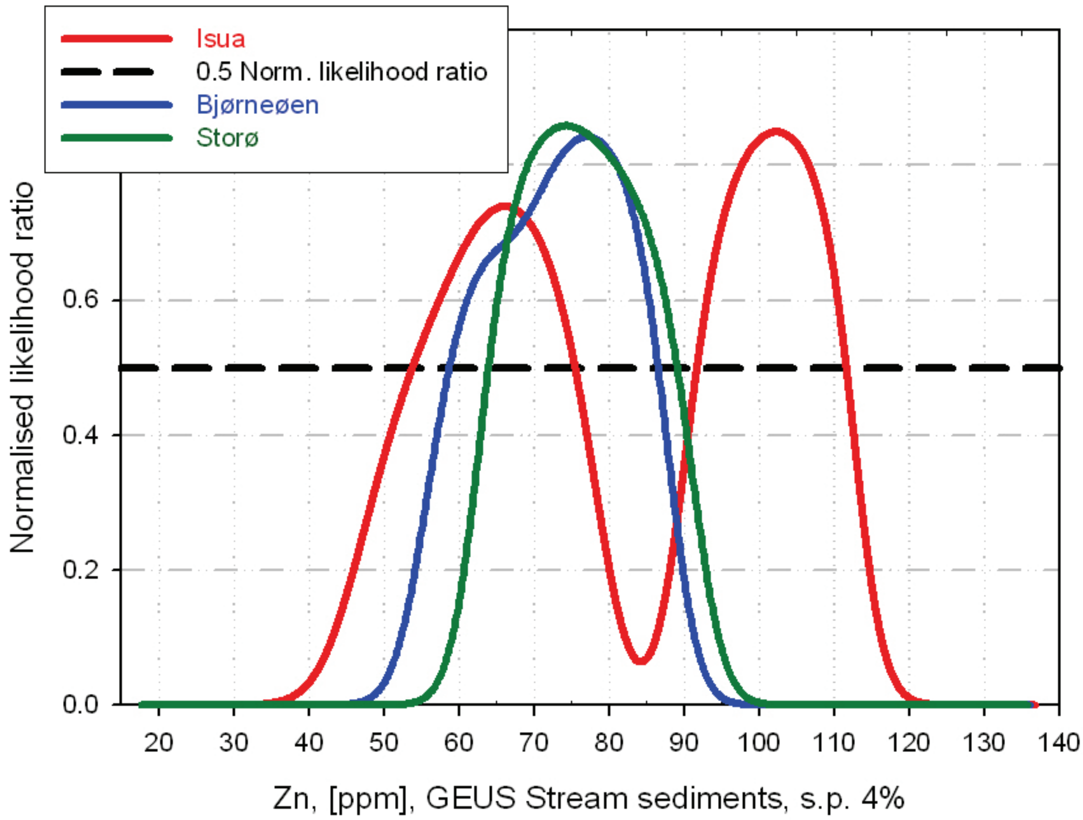

Zr, GEUS, minimum curvature, 200 m
spread parameter 4%

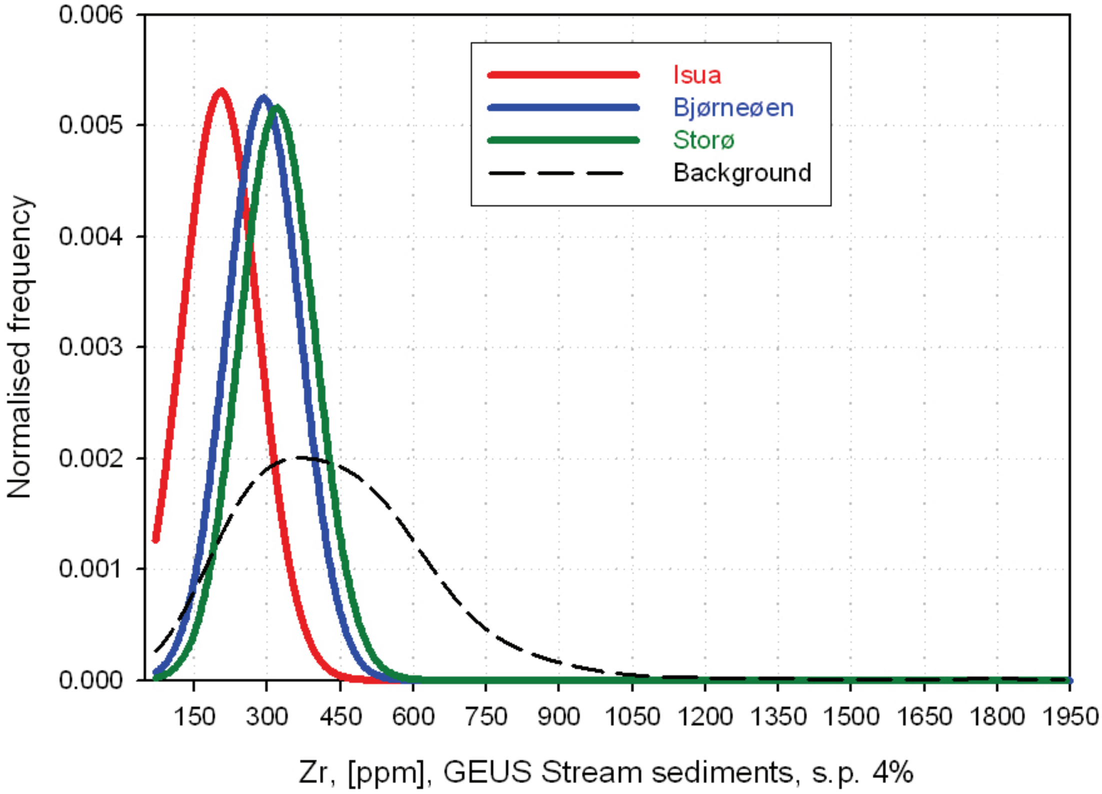

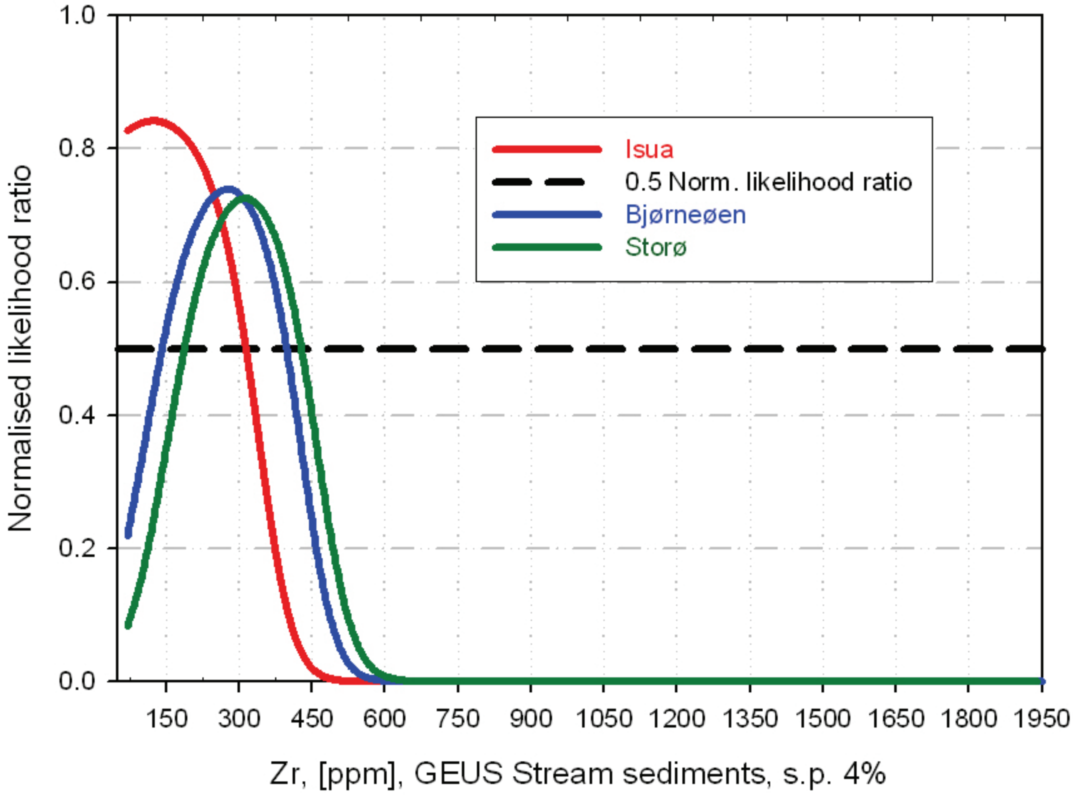

Signatures in regional aeromagnetic data

See Nielsen et al. (2004) for further description of the data and the used gridding technique.

Abbreviations in diagrams:

s.p. 4% refers to a spread parameter of 4 % used in the Kernel function for smoothing the empirical distribution function (Nielsen *et al.* 2004).

Amplitude of the horizontal gradients of TMI, gridcells 200 m spread parameter 4%

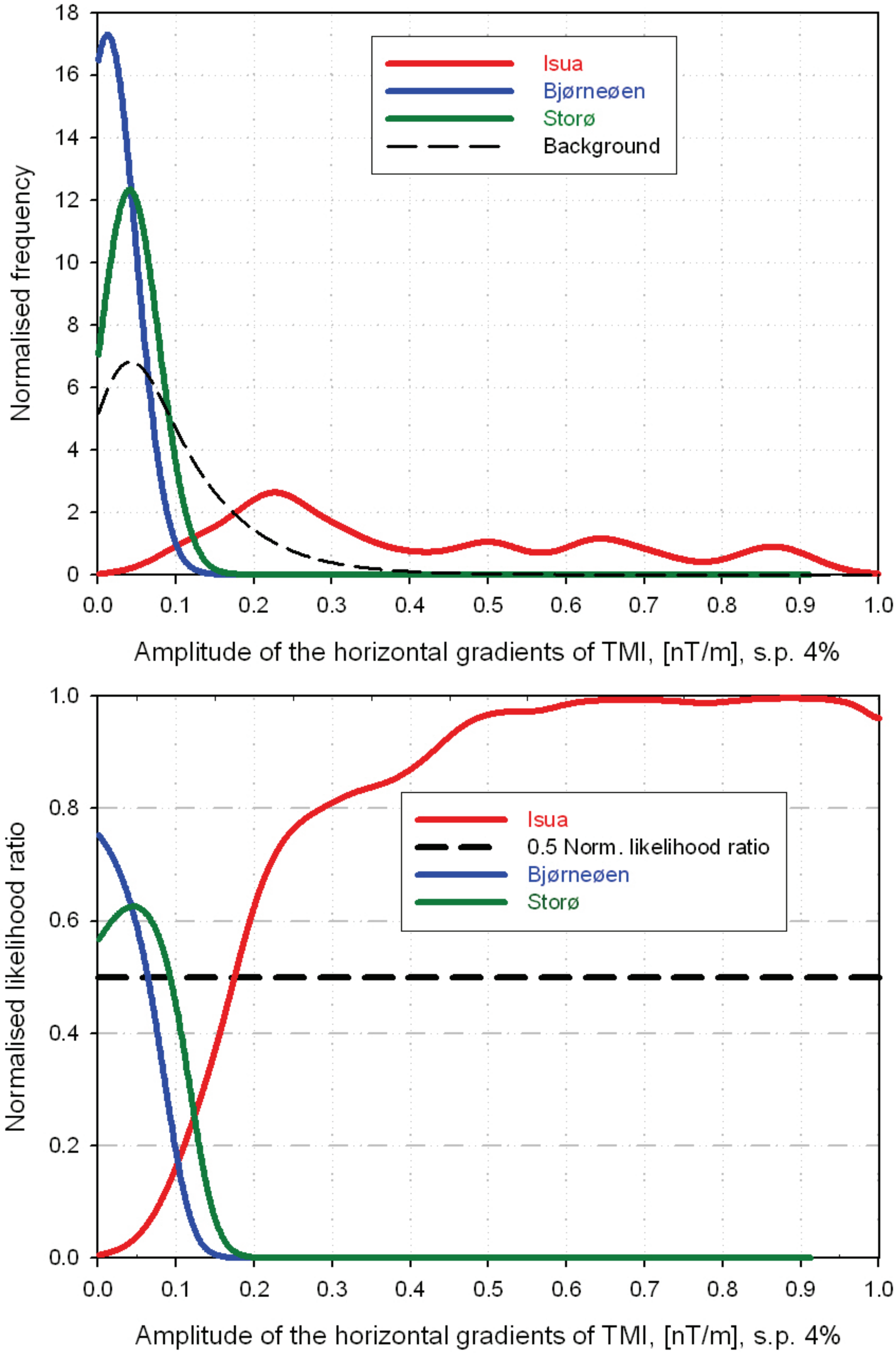

Total magnetic field intensity, gridcells 200 m
spread parameter 4%

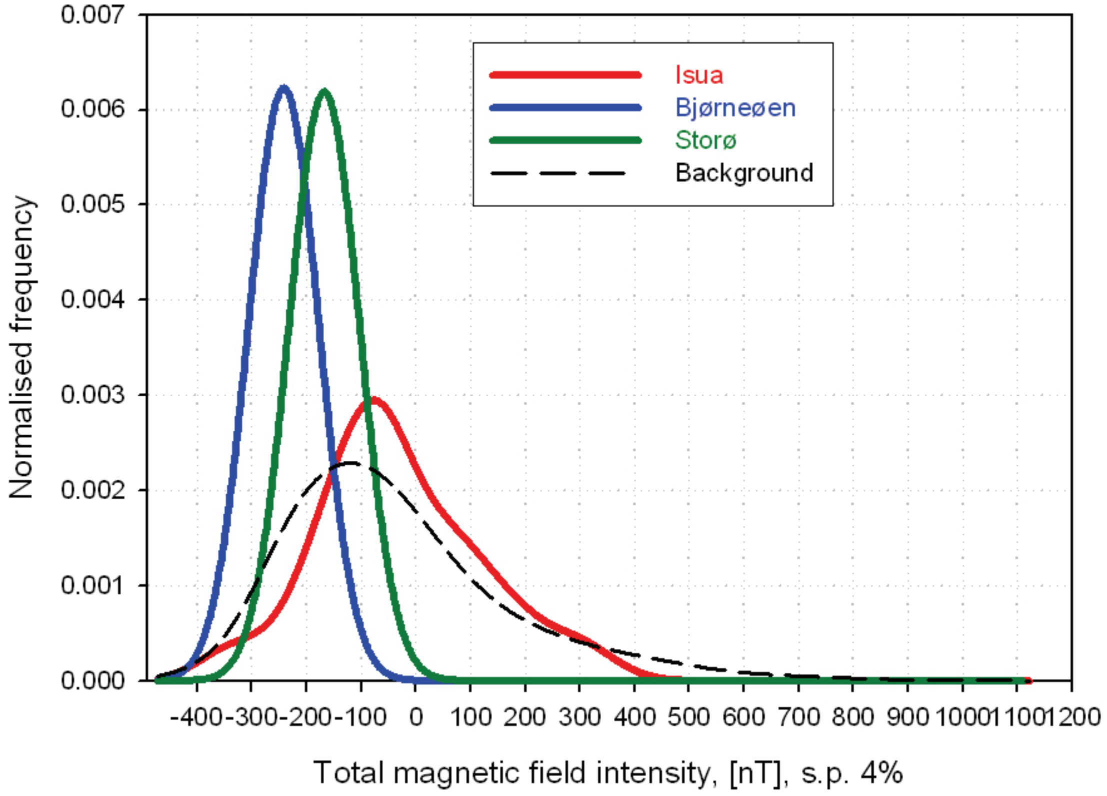

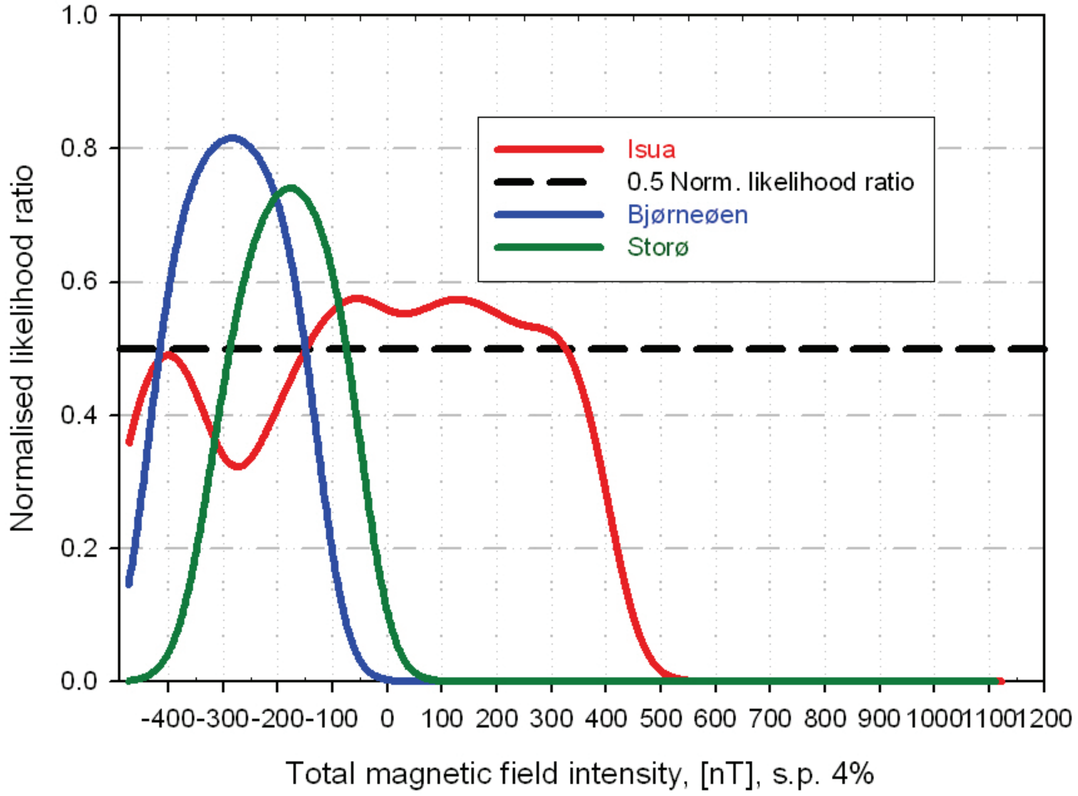

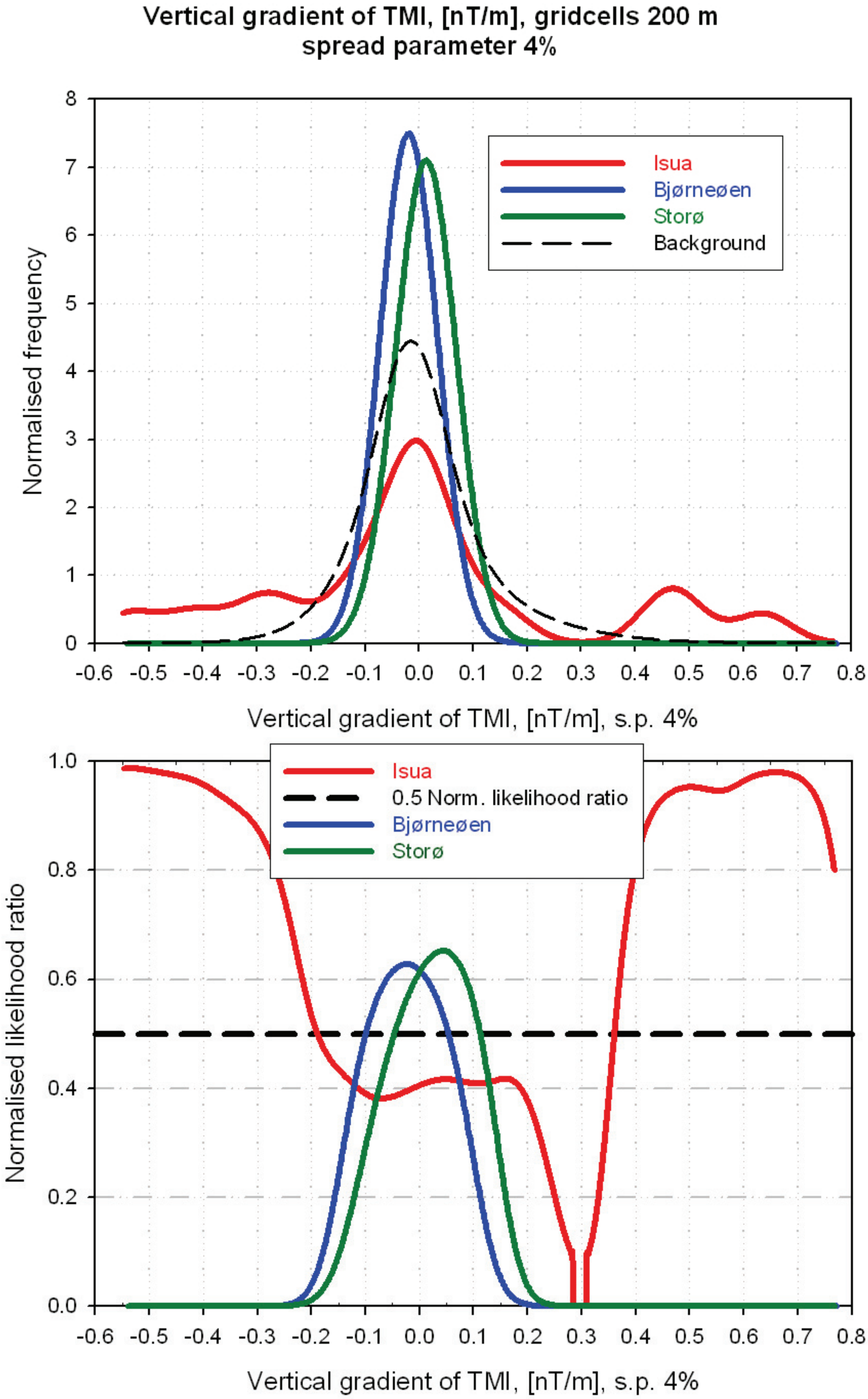
Vertical gradient of TMI, [nT/m], gridcells 200 m
spread parameter 4%
Normalised frequency
Isua
Bjørneøen
Storø
Background
Vertical gradient of TMI, [nT/m], s.p. 4%
Normalised likelihood ratio
Isua
0.5 Norm. likelihood ratio
Bjørneøen
Storø
Vertical gradient of TMI, [nT/m], s.p. 4%

Signatures in regional aeroradiometric data

See earlier sections for a description of the regional aeroradiometric data.

Abbreviations in diagrams:

s.p. 4% refers to a spread parameter of 4 % used in the Kernel function for smoothing the empirical distribution function (Nielsen *et al.* 2004).

Aeroradiometric K, GEUS, minimum curvature, modified spread parameter 4%

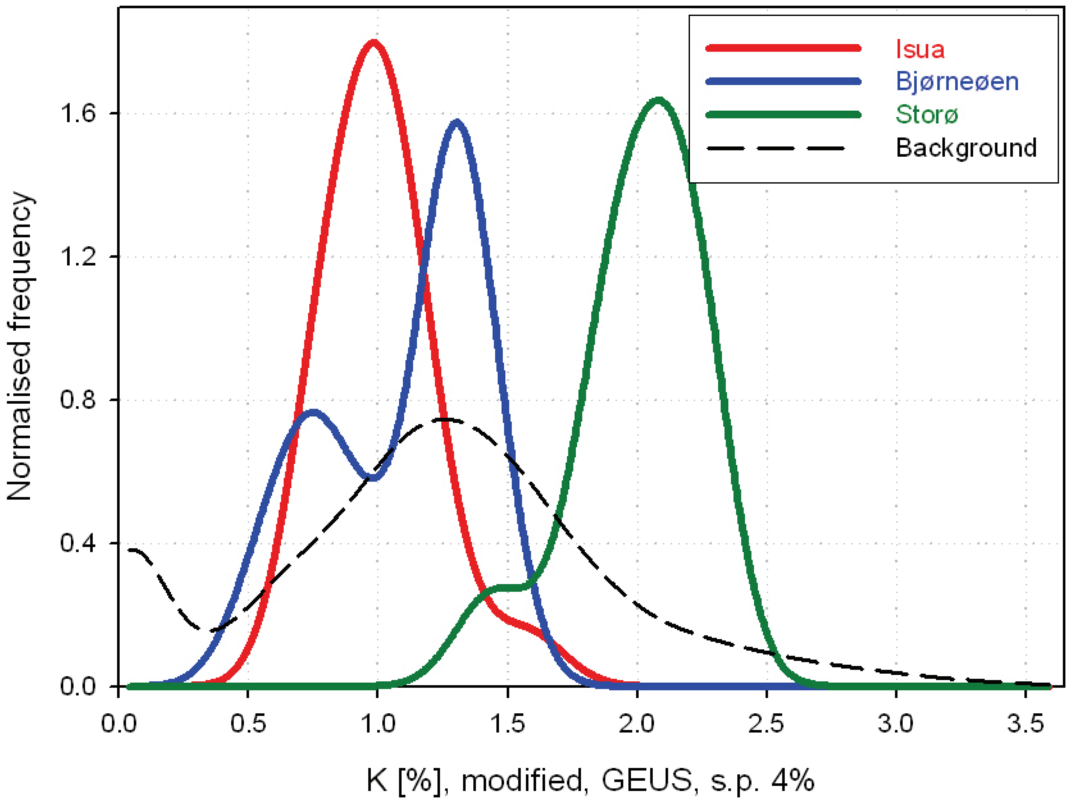

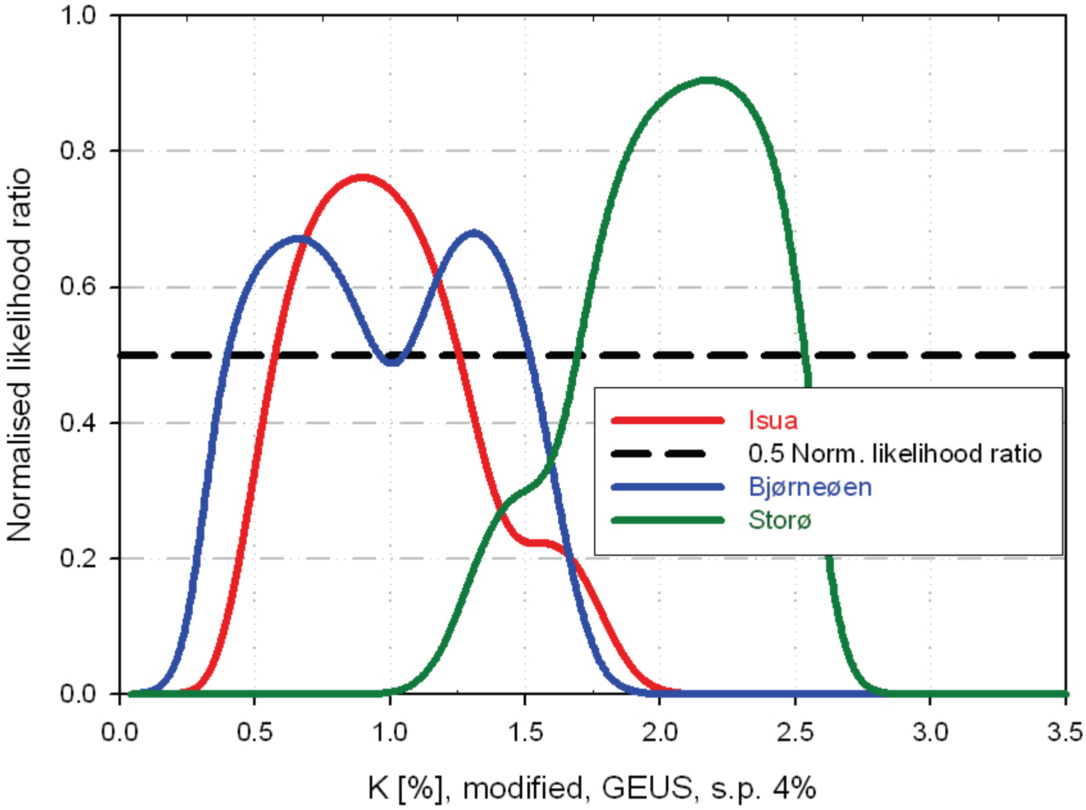

Aeroradiometric Th, GEUS, minimum curvature, modified spread parameter 4%

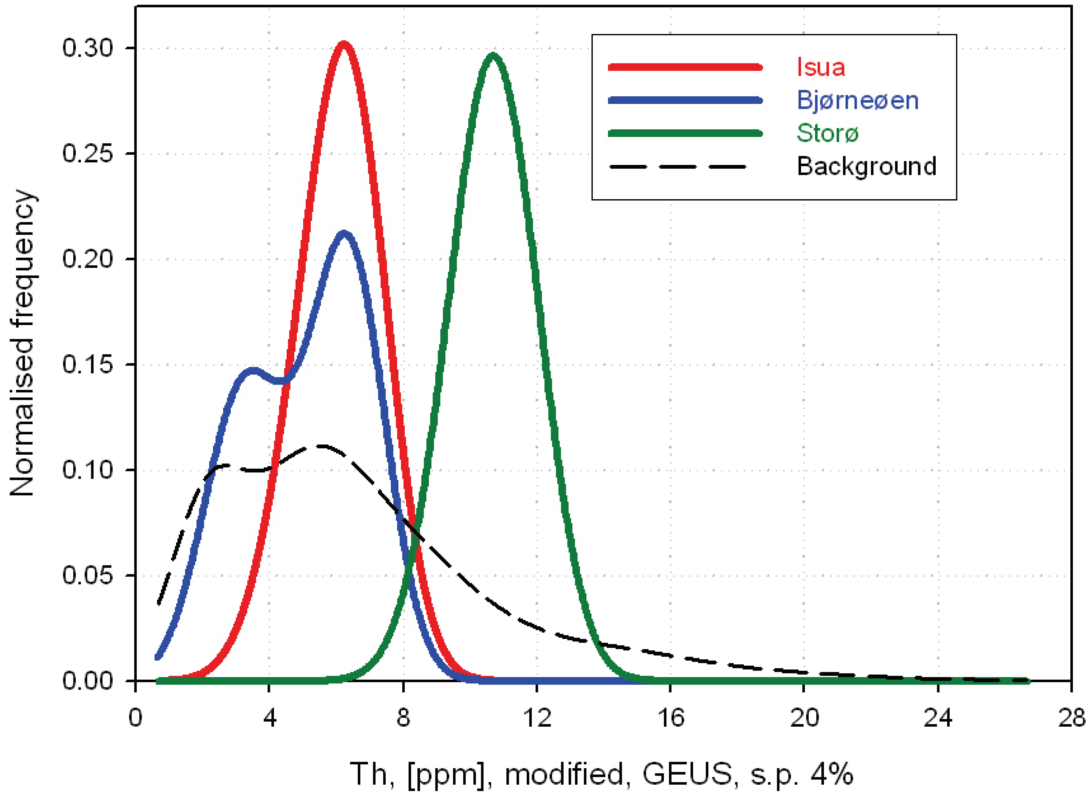

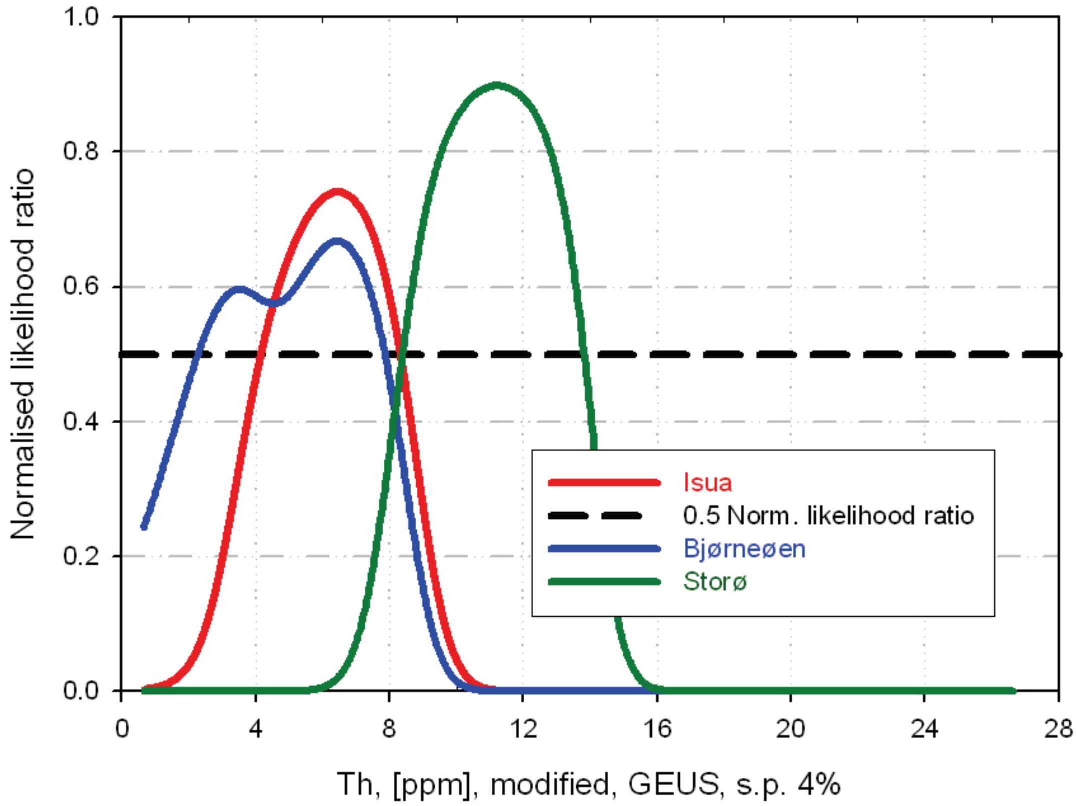

Aeroradiometric Total Gamma, GEUS, minimum curvature, modified spread parameter 4%

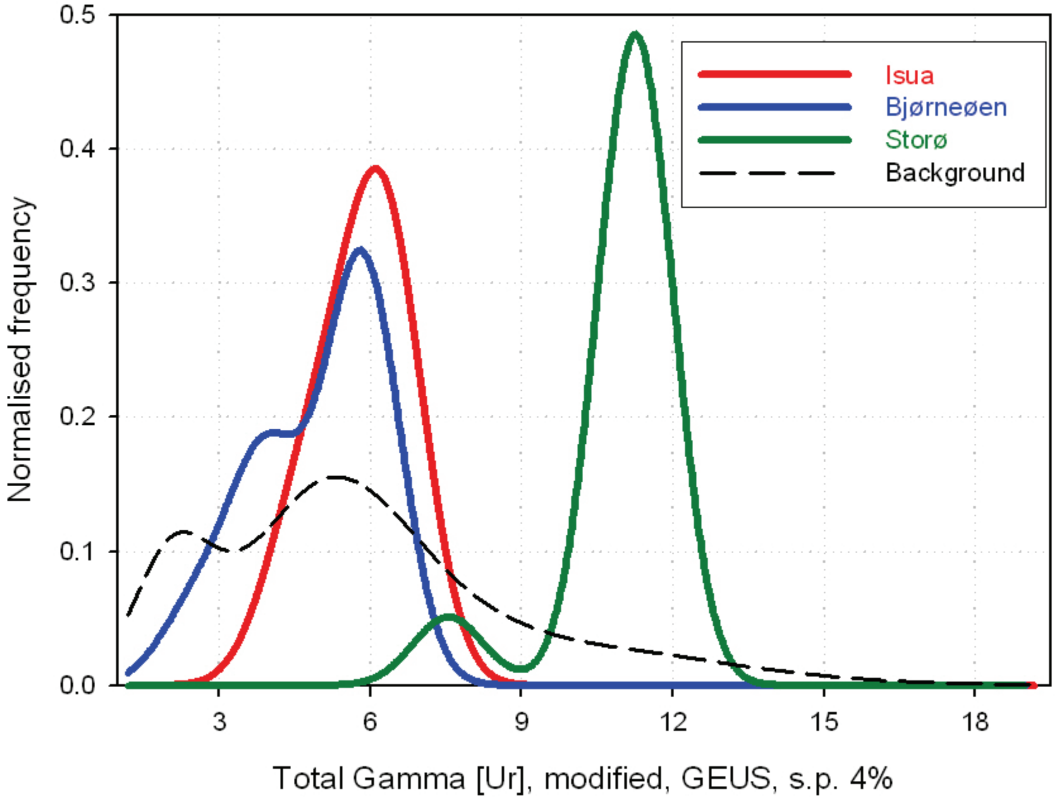

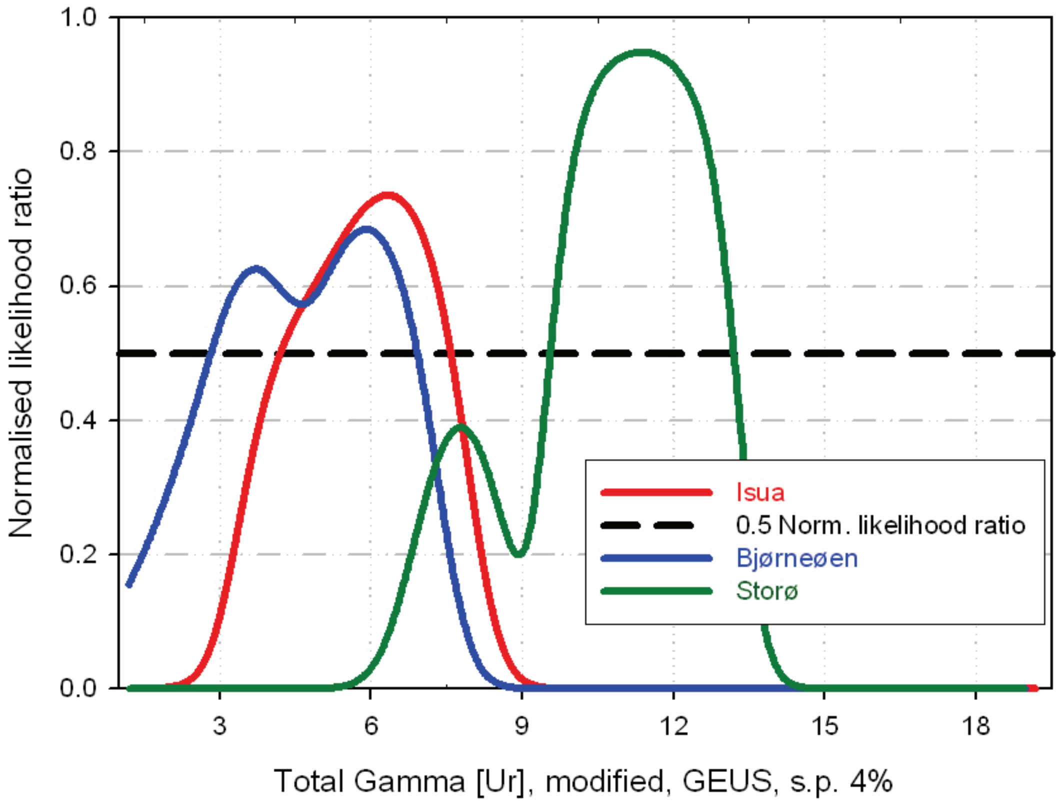

Aeroradiometric U, GEUS, minimum curvature, modified spread parameter 4%

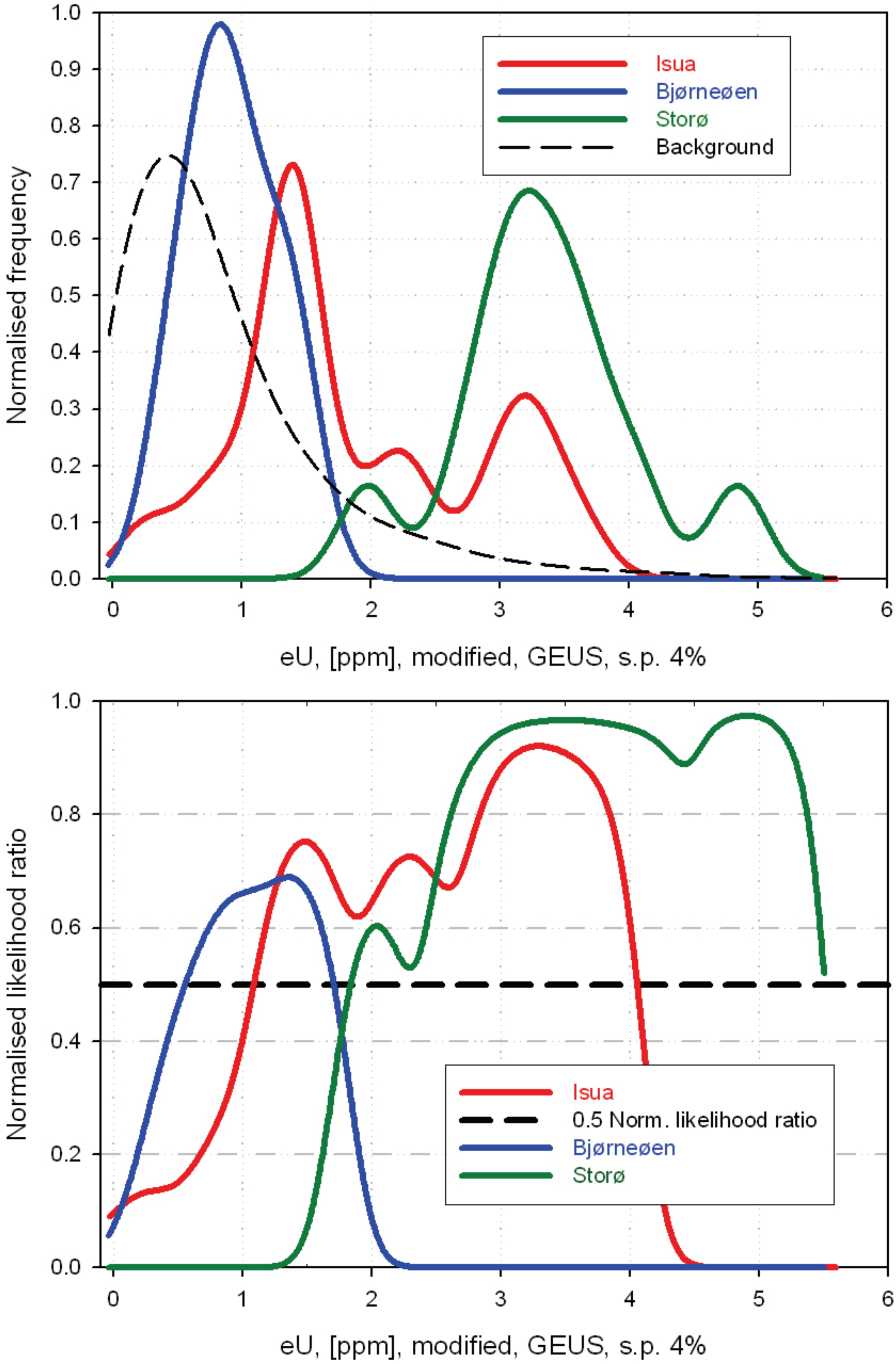

Aeroradiometric U/Th ratio, GEUS, minimum curvature, modified spread parameter 4%

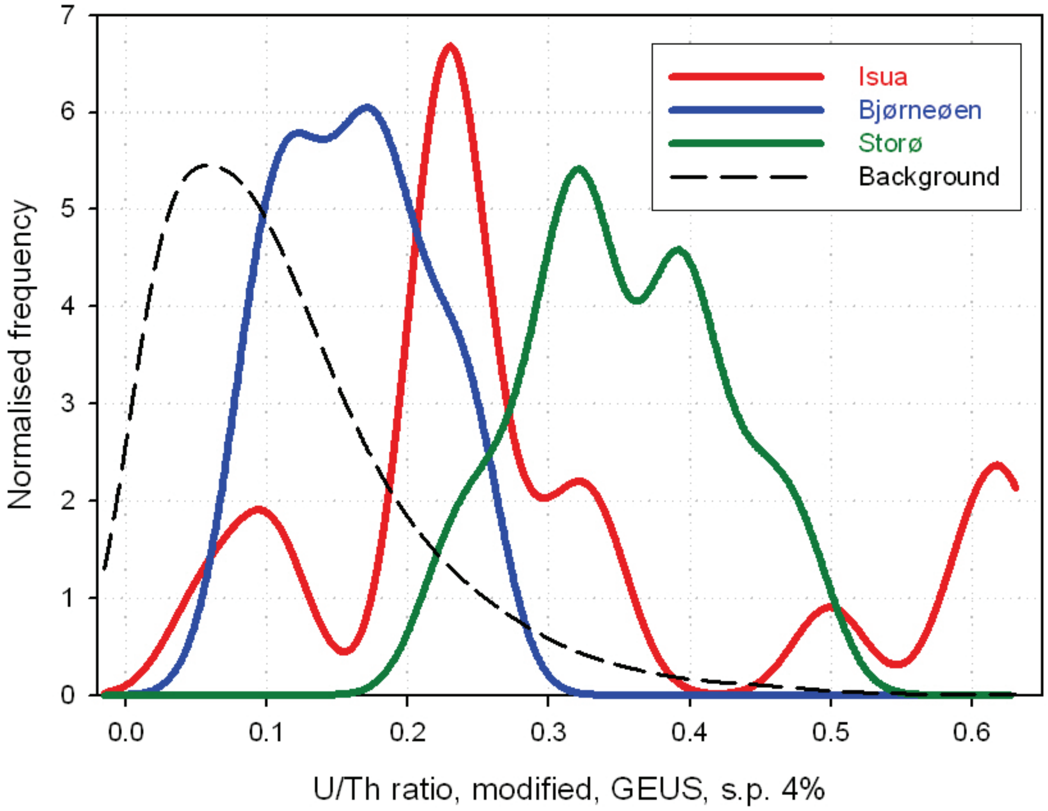

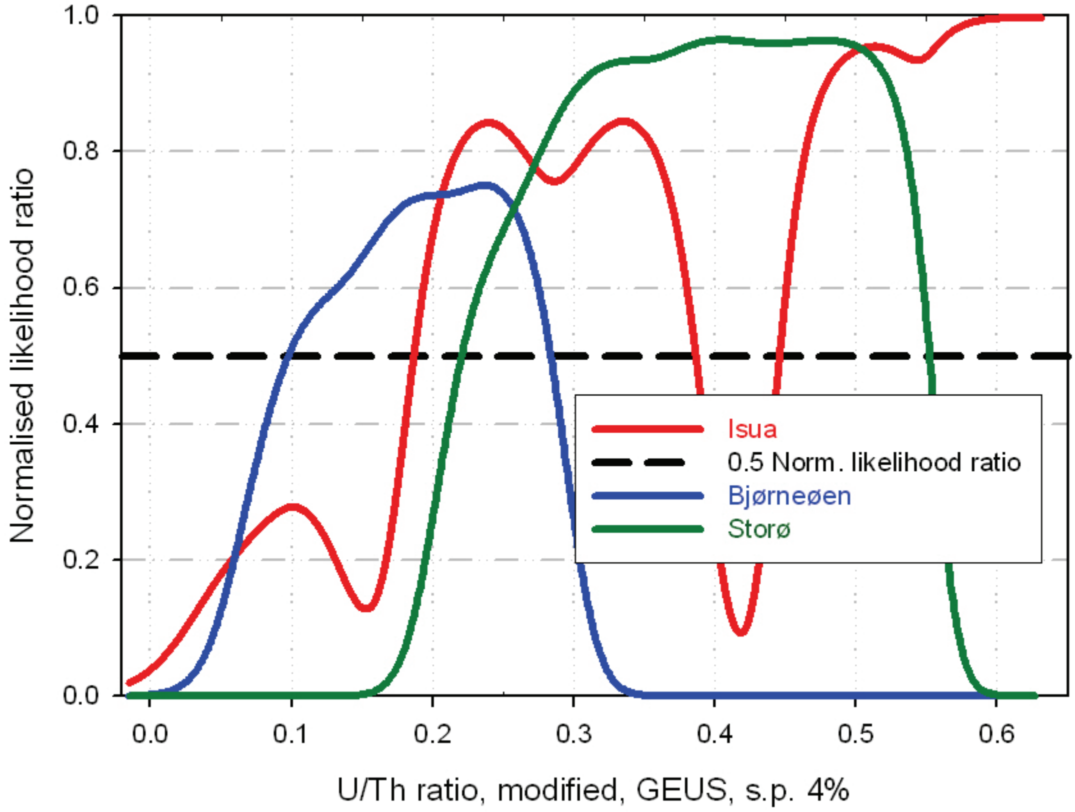

Signatures in statistically defined lineaments from aeromagnetic data

See earlier sections for a description of the statistical treatment of the extracted lineament information from the aeromagnetic data.

Abbreviations in diagrams:

r1000	Refers a search radius of 1000 m.

all lines	All lineaments, without considering their length, have been analysed.
0–10%	Only lineaments with a length which are 0–10% (2000–2100 m) of the maximum length of all lineaments have been analysed.
0–25%	Only lineaments with a length which are 0–25% (2000–2450 m) of the maximum length of all lineaments have been analysed.
25–50%	Only lineaments with a length which are 25–50% (2450–3100 m) of the maximum length of all lineaments have been analysed.
50–75%	Only lineaments with a length which are 50–75% (3100–4250 m) of the maximum length of all lineaments have been analysed.
75–100%	Only lineaments with a length which are 75–100% (4250–23600 m) of the maximum length of all lineaments have been analysed.
90–100%	Only lineaments with a length which are 90–100% (6030–23600 m) of the maximum length of all lineaments have been analysed.

mean direction	Mean direction of lineaments within the search radius (from 0 to 180°).
minimum distance	Minimum distance to nearest lineament within the search radius (in meters).
nlcross	Number of lineaments crossing the search radius (a number).
total length	The total length of the lineaments crossing the search radius (in meters).
unit vector sum	Uniformity – a complexity factor – length of vector sum of unit vectors divided by number of vectors within the search radius (from 0 to 1).

s.p. 4% refers to a spread parameter of 4 % used in the Kernel function for smoothing the empirical distribution function (Nielsen *et al.* 2004).

Aeromagnetic lineaments, mean direction, all lines, r1000m,
spread parameter 4%

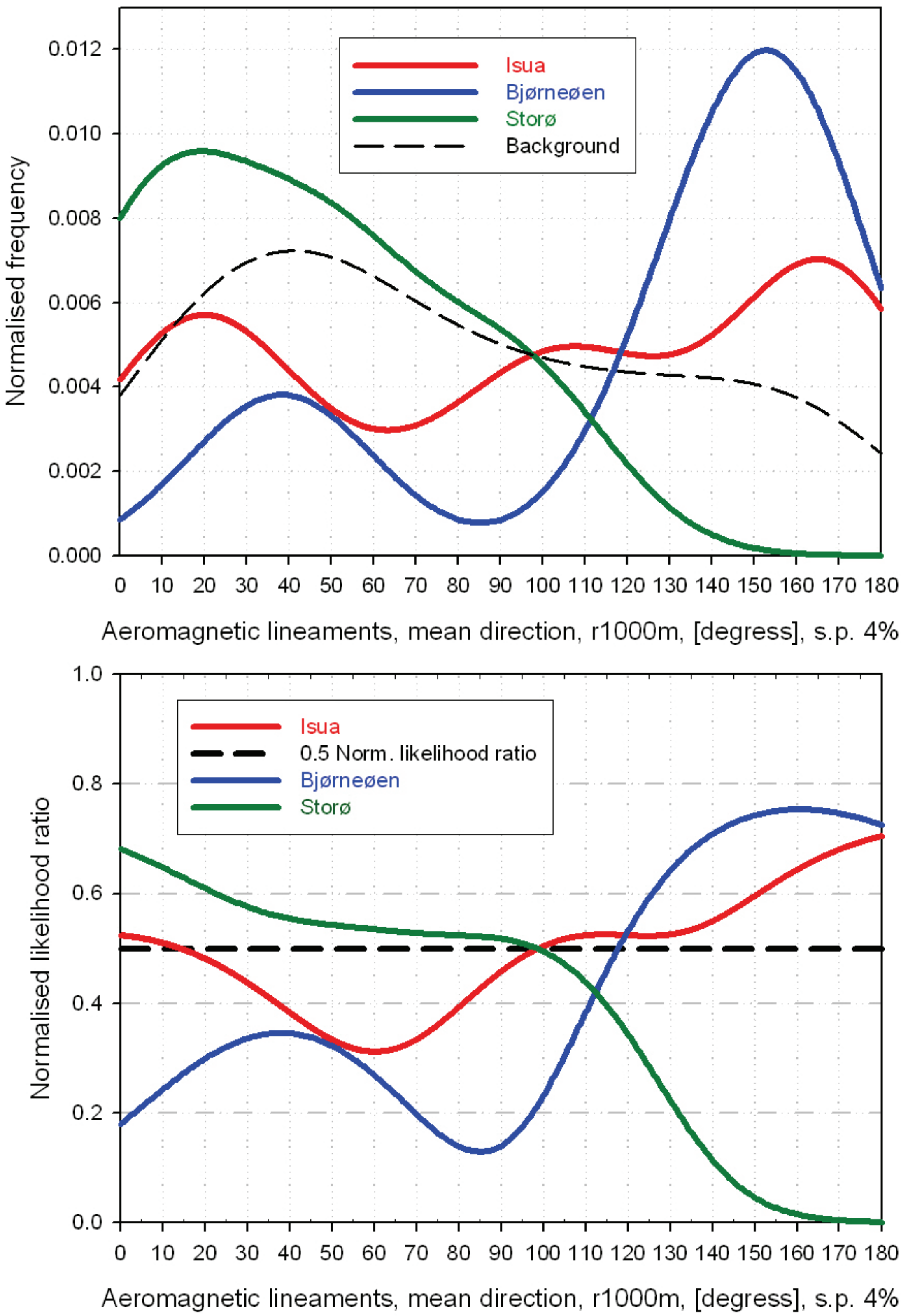

Aeromagnetic lineaments, mean direction, 0-10%, r1000m,
spread parameter 4%

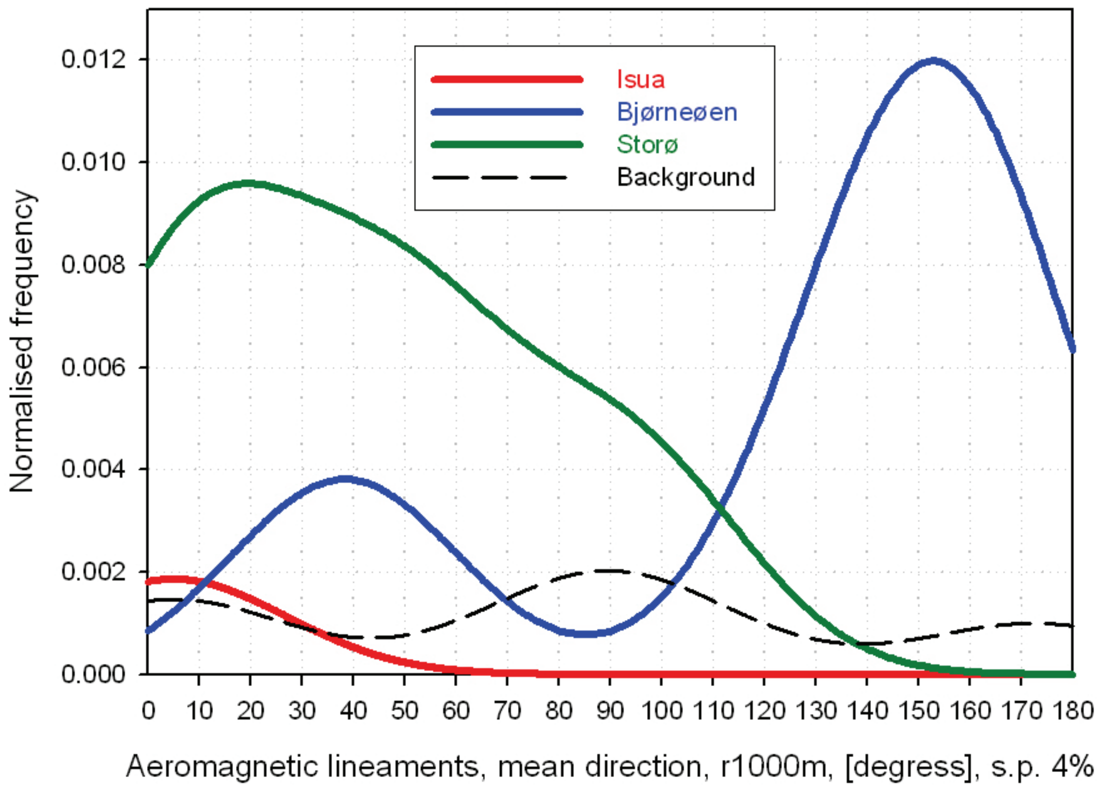

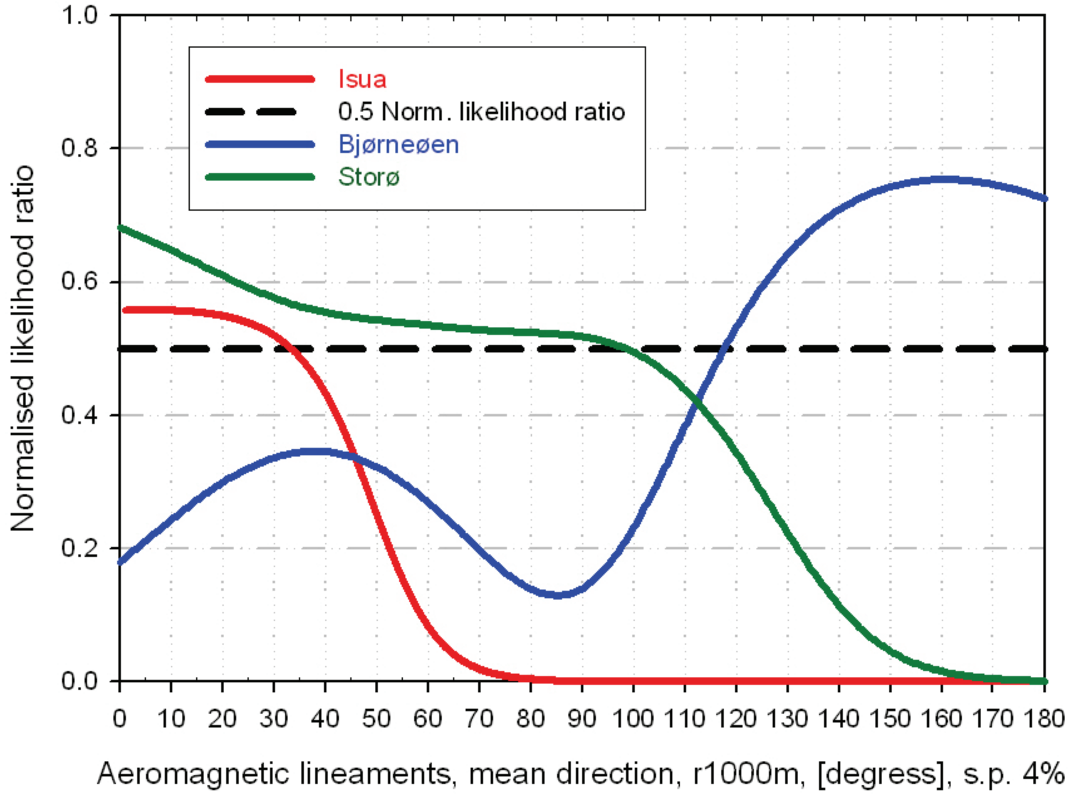

Aeromagnetic lineaments, mean direction, 0-25%, r1000m,
spread parameter 4%

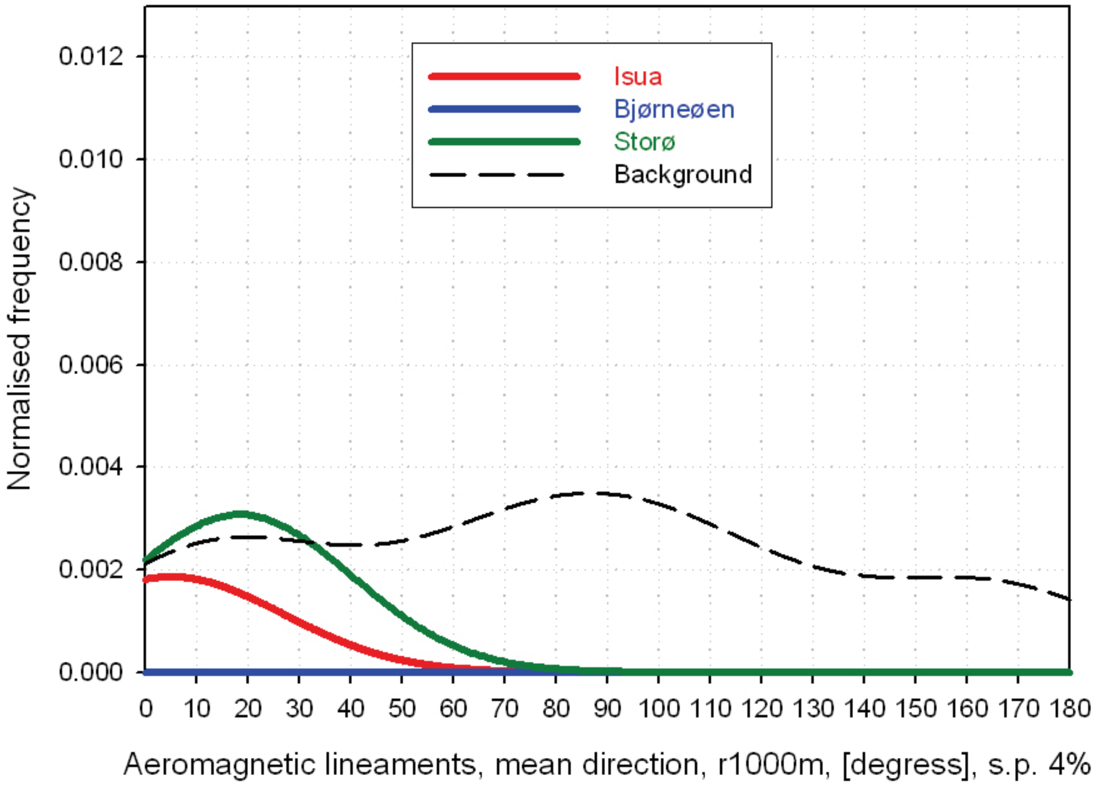

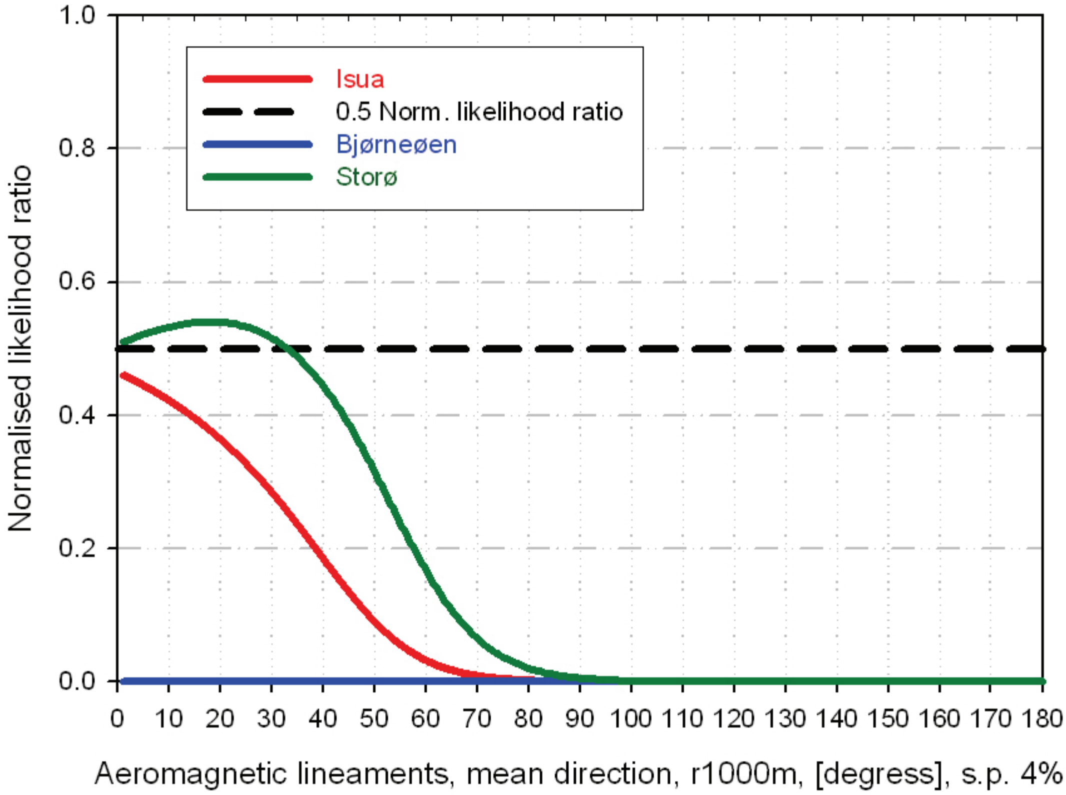

Aeromagnetic lineaments, mean direction, 25-50%, r1000m,
spread parameter 4%

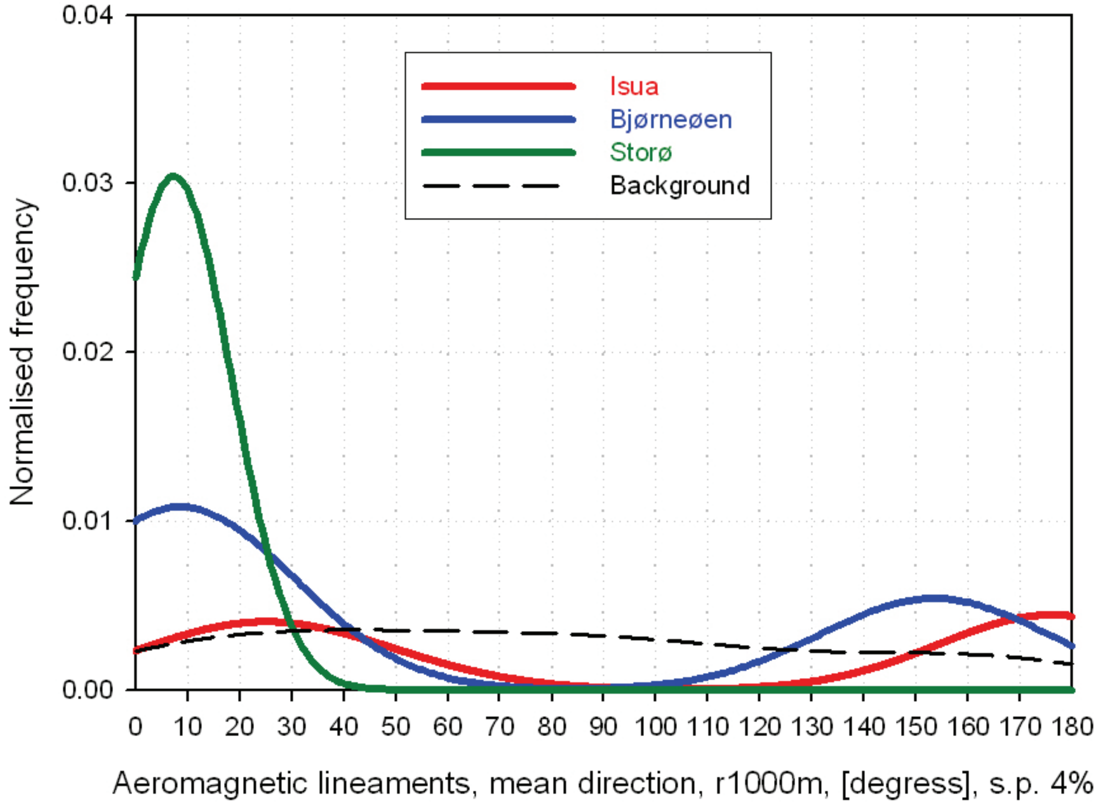

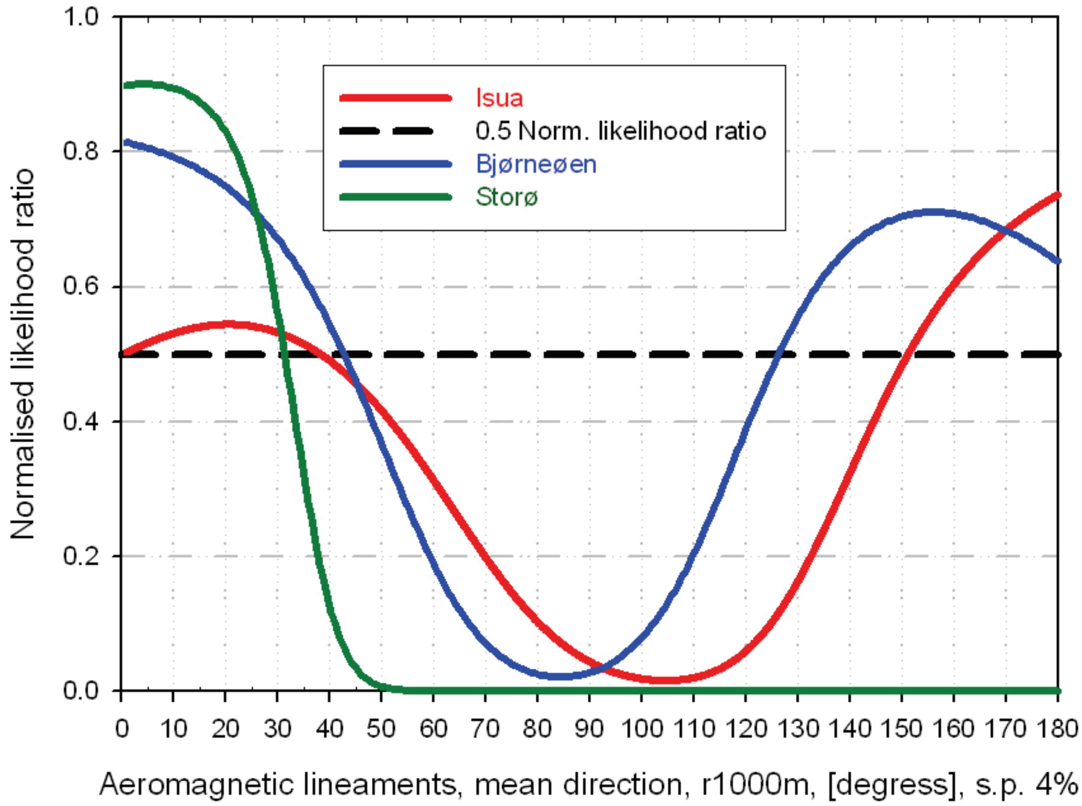

Aeromagnetic lineaments, mean direction, 50-75%, r1000m,
spread parameter 4%

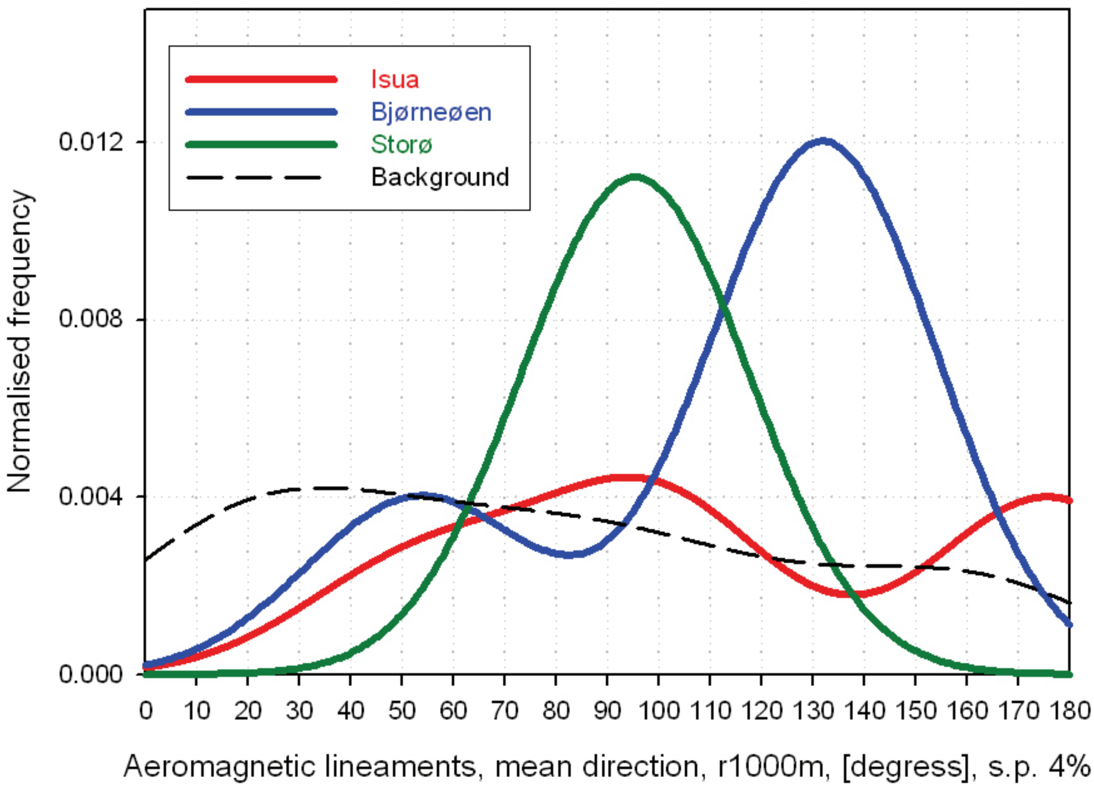

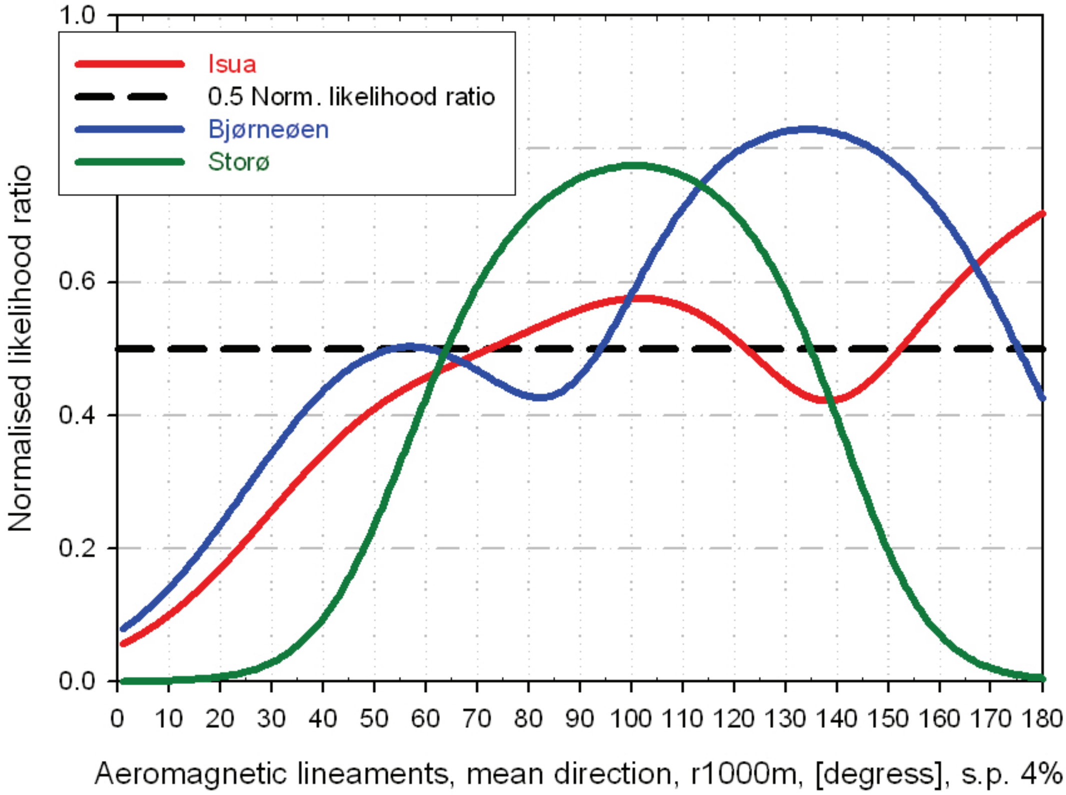

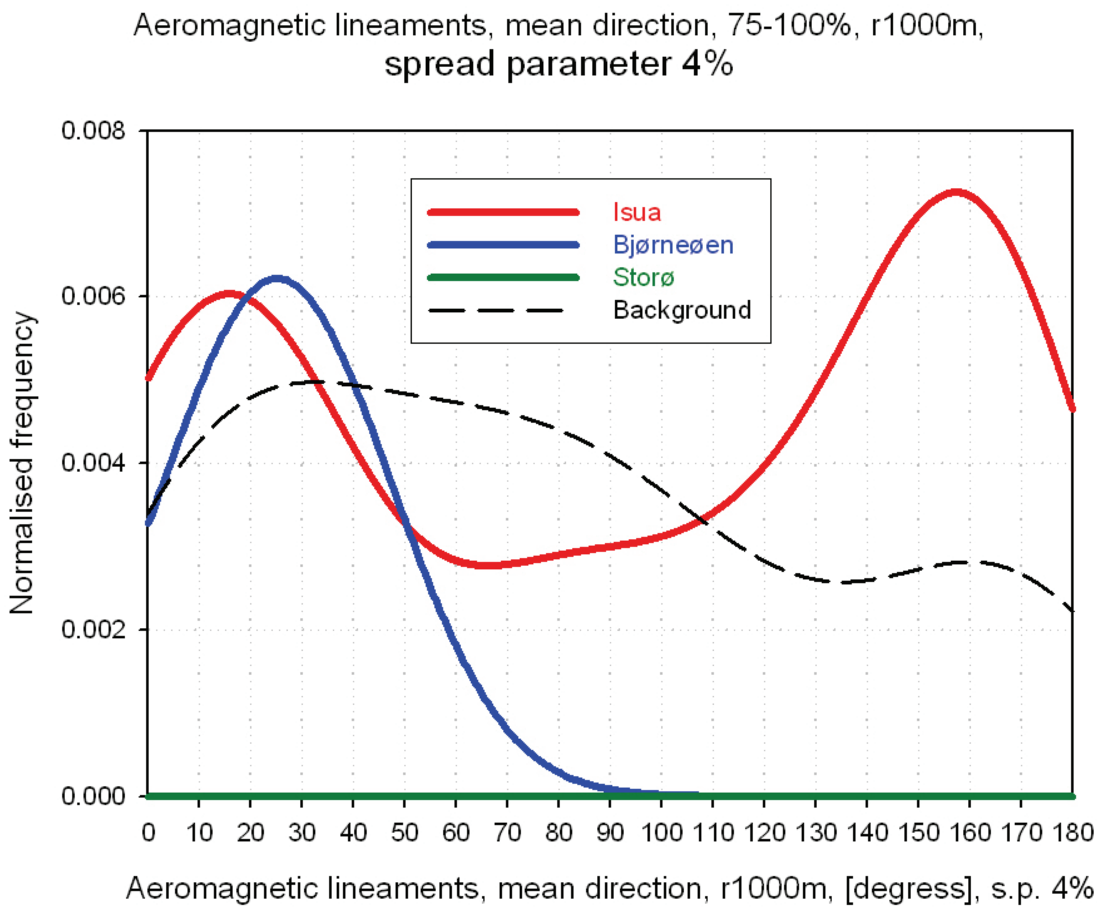
Aeromagnetic lineaments, mean direction, 75-100%, r1000m,
spread parameter 4%
Isua
Bjørneøen
Storø
Background
Normalised frequency
0.008
0.006
0.004
0.002
0.000
0 10 20 30 40 50 60 70 80 90 100 110 120 130 140 150 160 170 180
Aeromagnetic lineaments, mean direction, r1000m, [degress], s.p. 4%

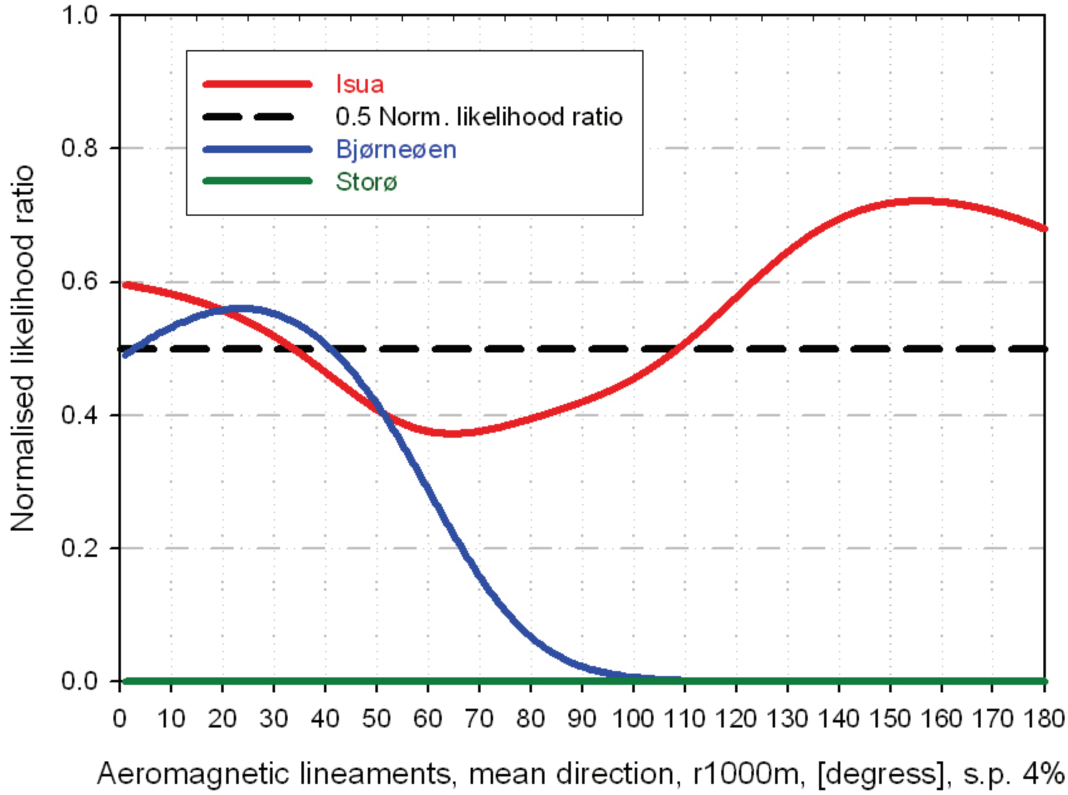
Isua
0.5 Norm. likelihood ratio
Bjørneøen
Storø
Normalised likelihood ratio
1.0
0.8
0.6
0.4
0.2
0.0
0 10 20 30 40 50 60 70 80 90 100 110 120 130 140 150 160 170 180
Aeromagnetic lineaments, mean direction, r1000m, [degress], s.p. 4%

Aeromagnetic lineaments, mean direction, 90-100%, r1000m,
spread parameter 4%

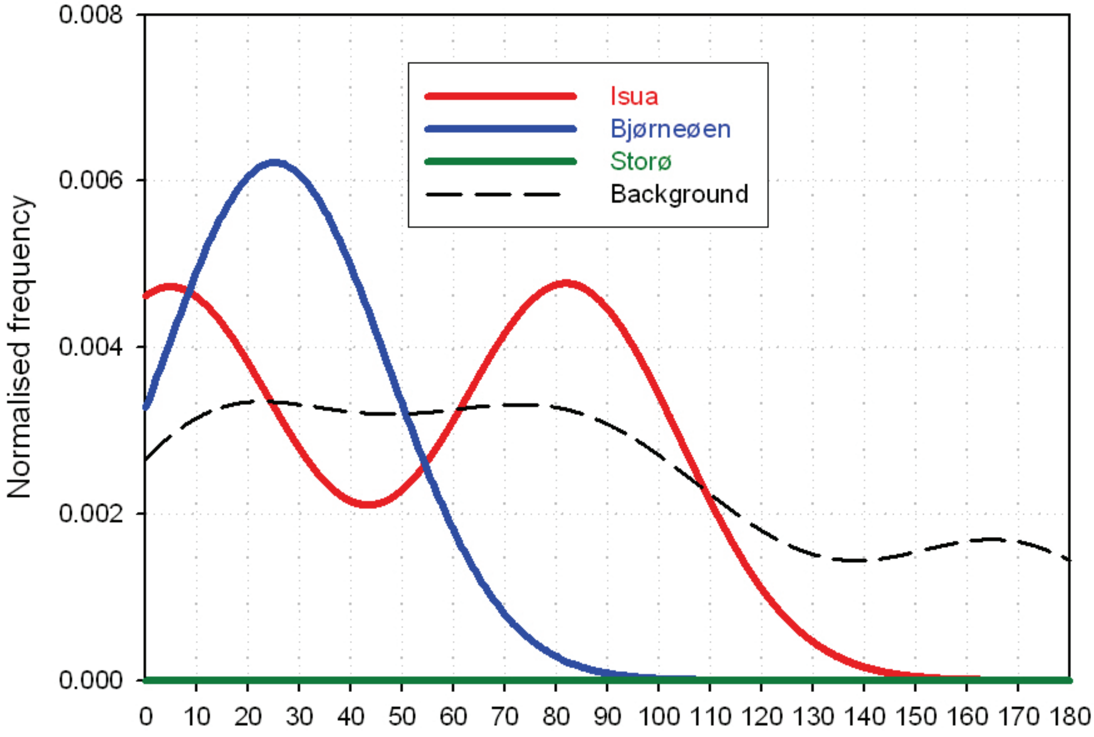

Aeromagnetic lineaments, mean direction, r1000m, [degress], s.p. 4%

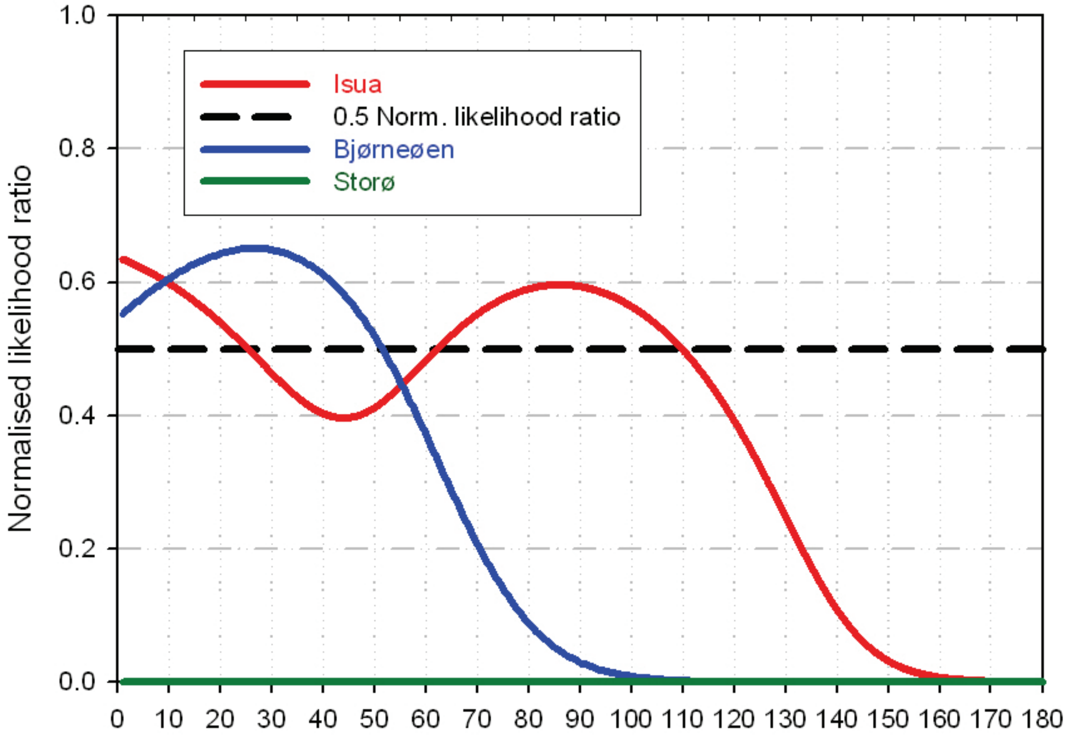

Aeromagnetic lineaments, mean direction, r1000m, [degress], s.p. 4%

Aeromagnetic lineaments, minimum distance, all lines, r1000m,
spread parameter 4%

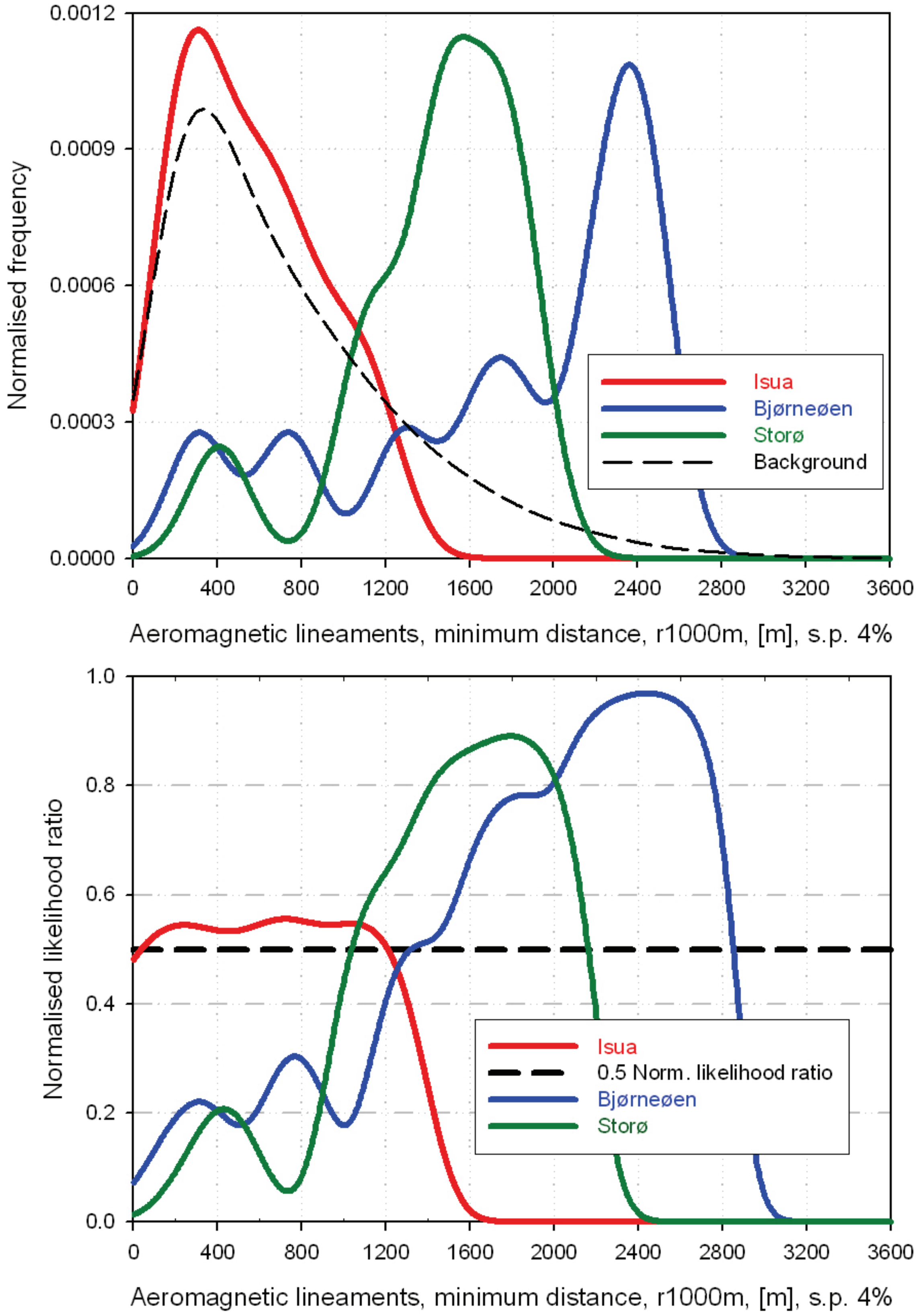

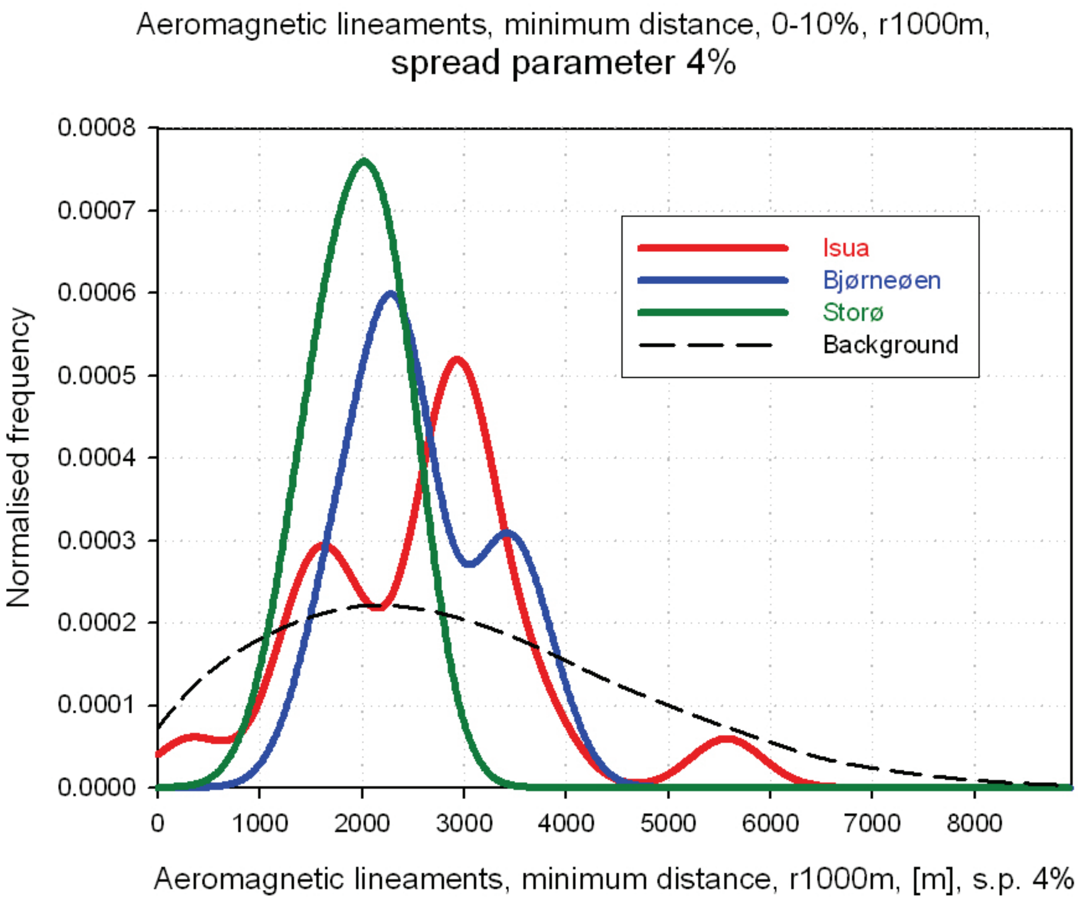
Aeromagnetic lineaments, minimum distance, 0-10%, r1000m,
spread parameter 4%
Normalised frequency
0.0008
0.0007
0.0006
0.0005
0.0004
0.0003
0.0002
0.0001
0.0000
0
1000
2000
3000
4000
5000
6000
7000
8000
Isua
Bjørneøen
Storø
Background
Aeromagnetic lineaments, minimum distance, r1000m, [m], s.p. 4%

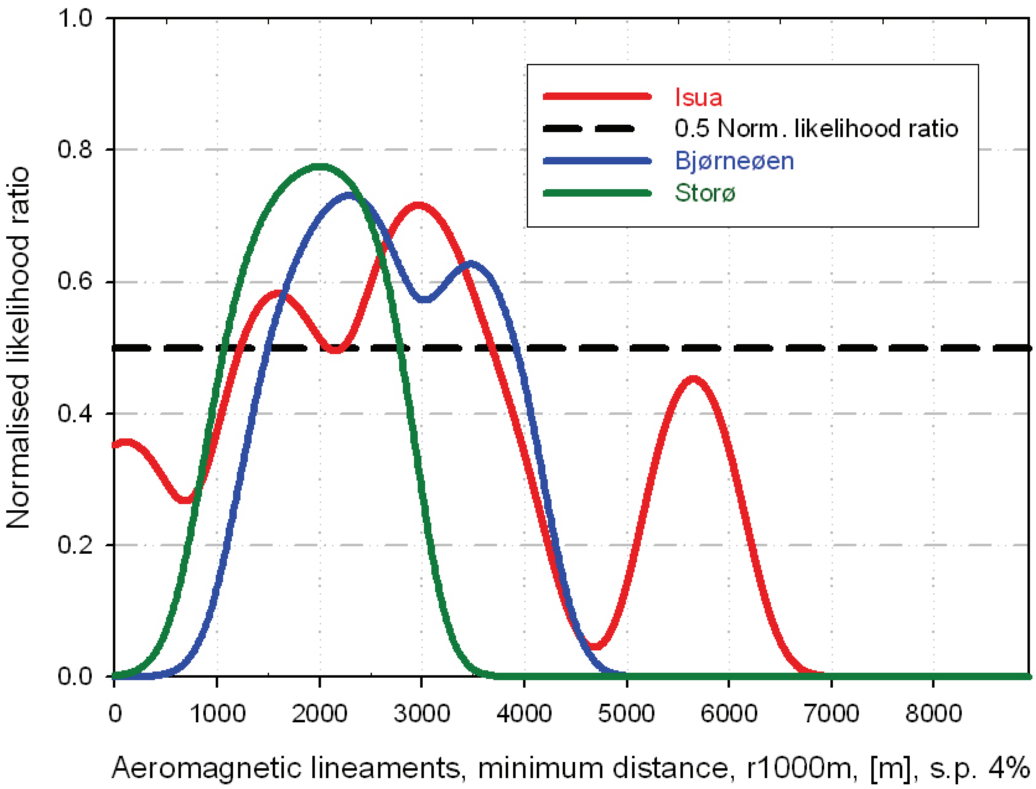
Normalised likelihood ratio
1.0
0.8
0.6
0.4
0.2
0.0
0
1000
2000
3000
4000
5000
6000
7000
8000
Isua
0.5 Norm. likelihood ratio
Bjørneøen
Storø
Aeromagnetic lineaments, minimum distance, r1000m, [m], s.p. 4%

Aeromagnetic lineaments, minimum distance, 0-25%, r1000m,
spread parameter 4%

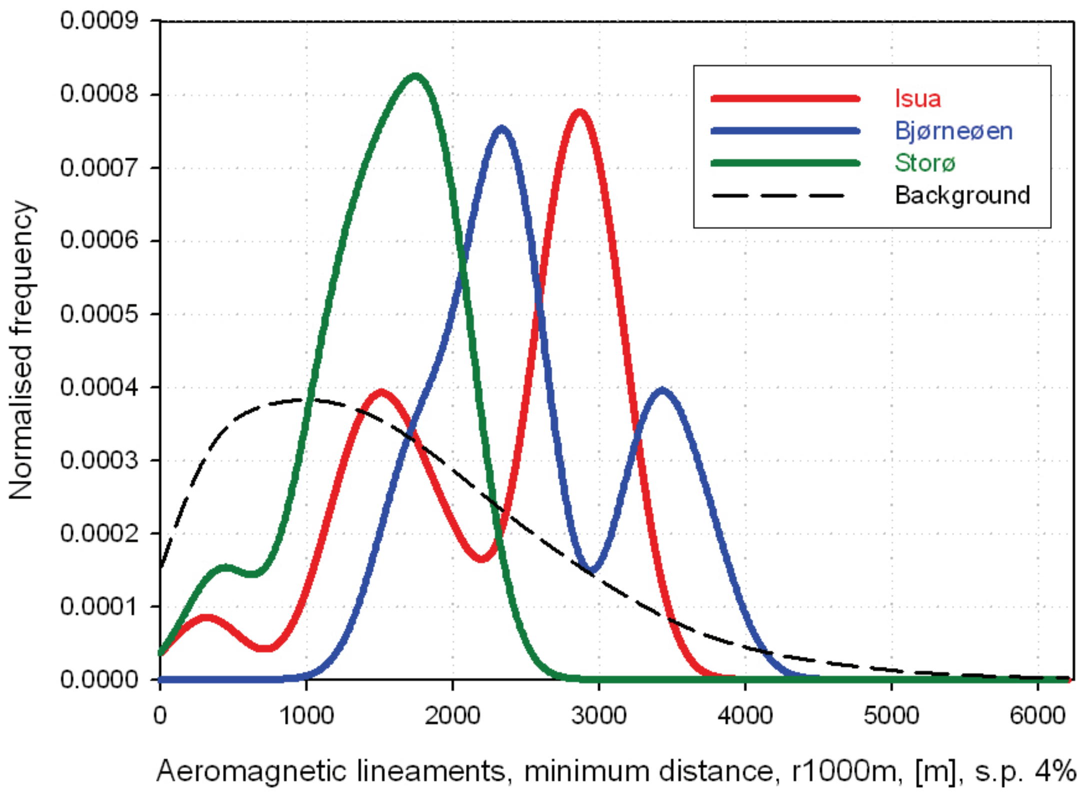

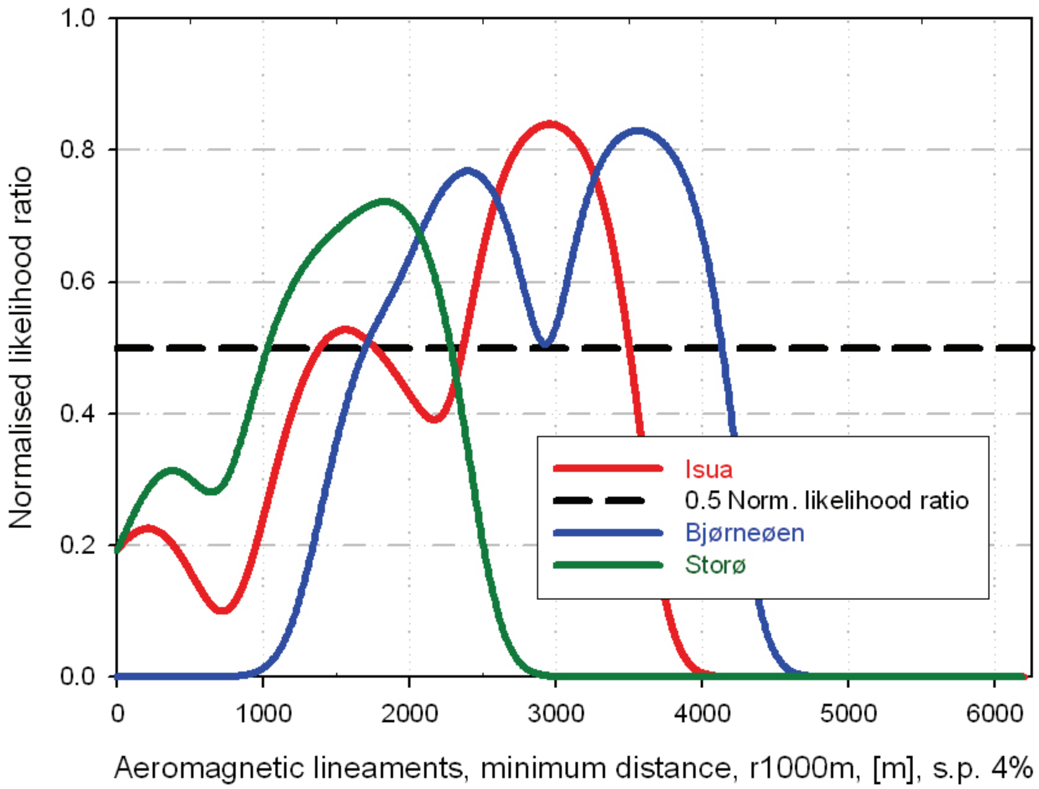

Aeromagnetic lineaments, minimum distance, 25-50%, r1000m,
spread parameter 4%

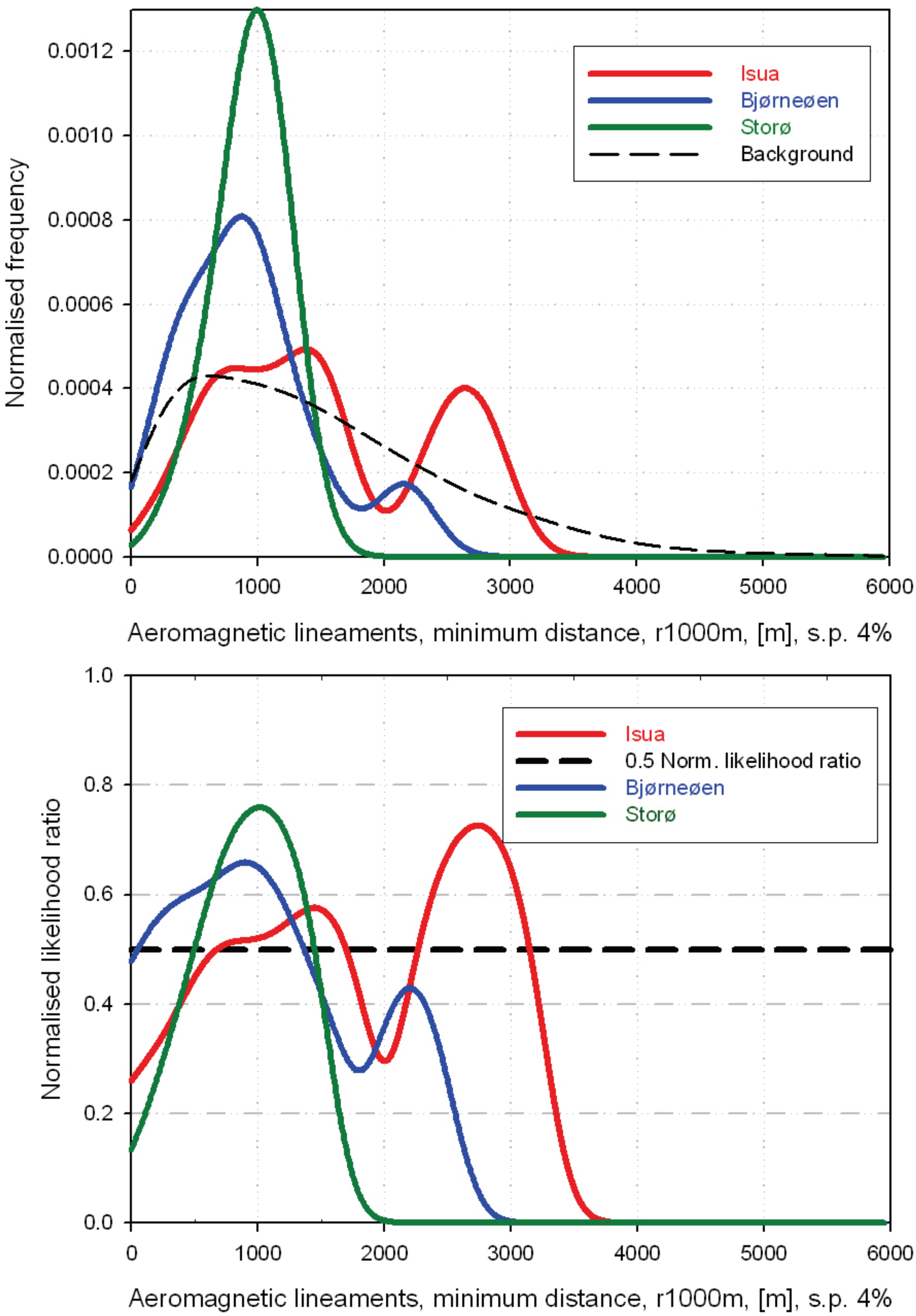

Aeromagnetic lineaments, minimum distance, 50-75%, r1000m,
spread parameter 4%

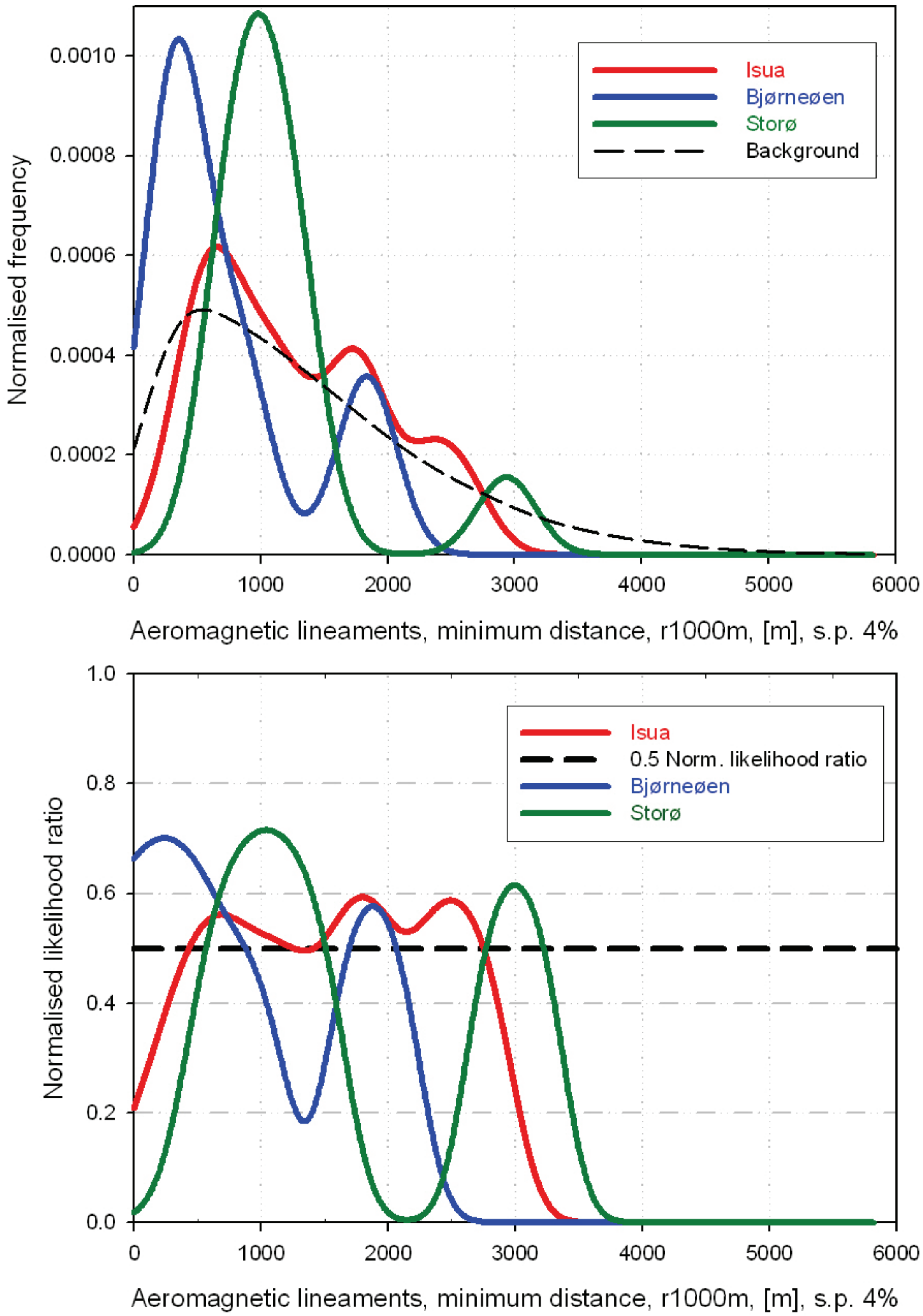

Aeromagnetic lineaments, minimum distance, 75-100%, r1000m,
spread parameter 4%

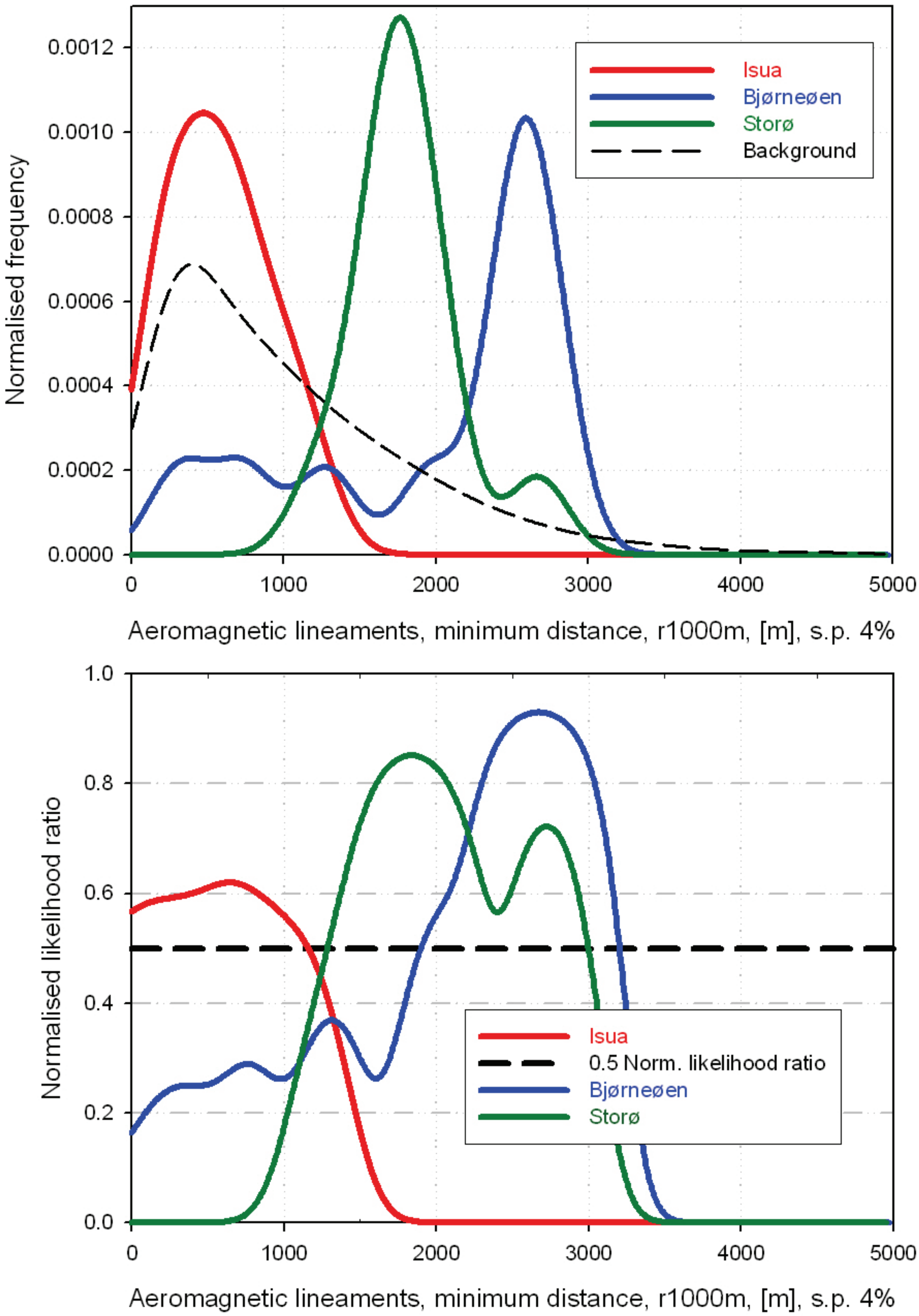

Aeromagnetic lineaments, minimum distance, 90-100%, r1000m,
spread parameter 4%

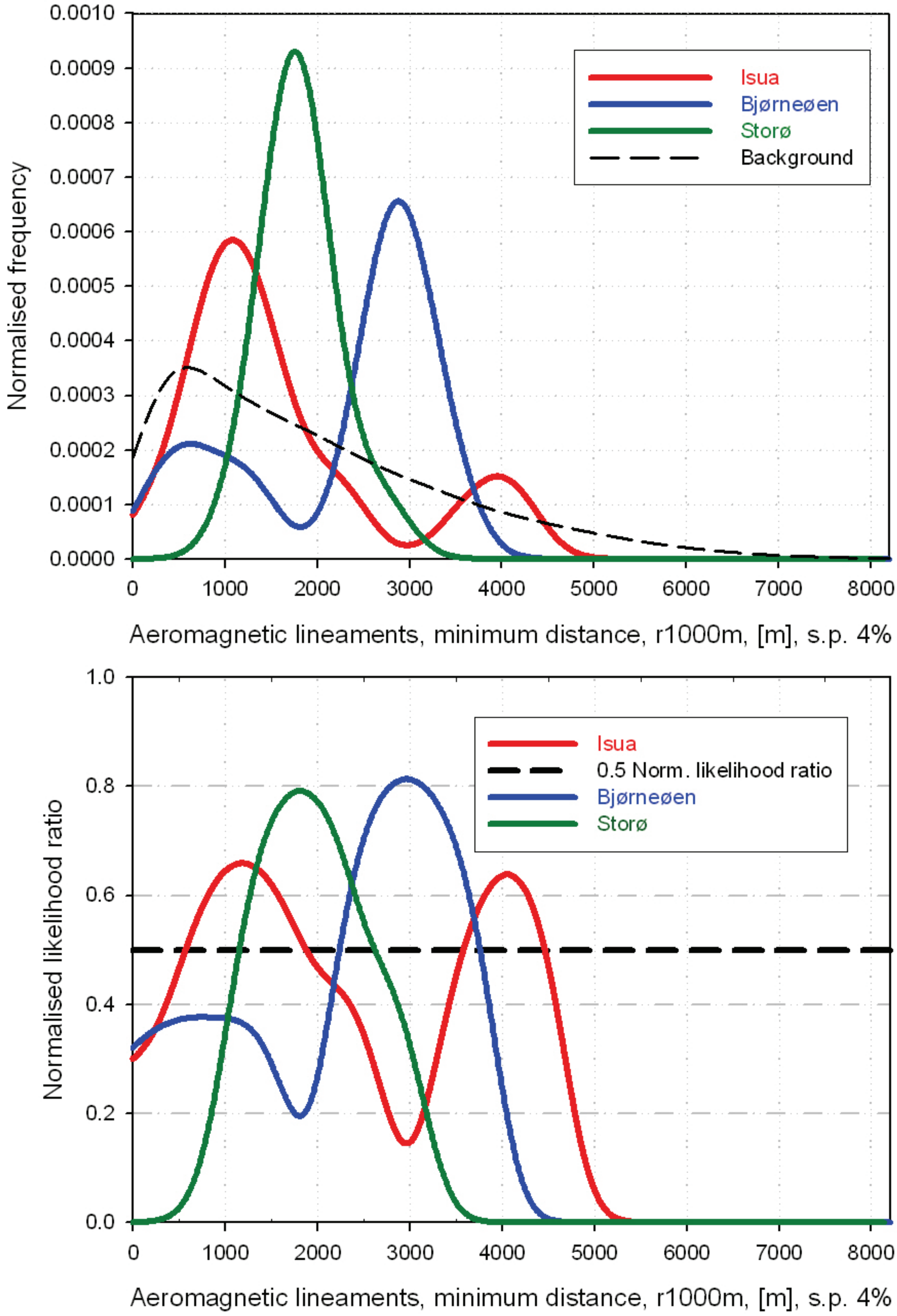

Aeromagnetic lineaments, nlcross, all lines, r1000m,
spread parameter 4%

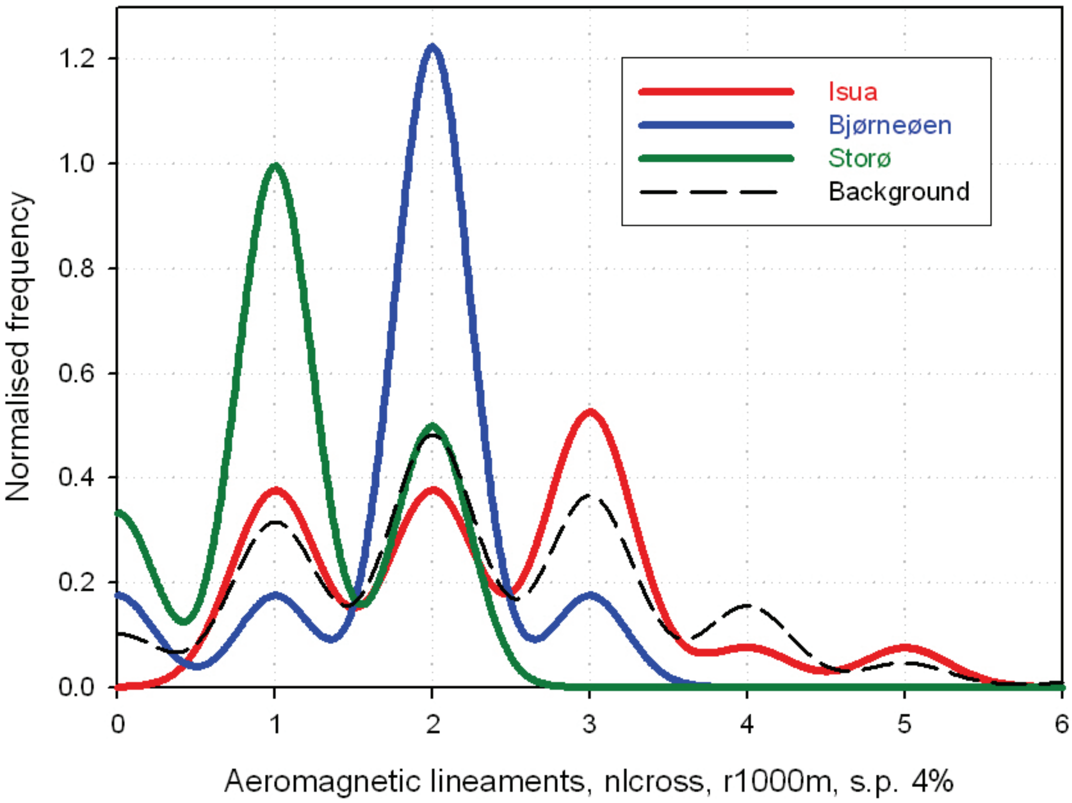

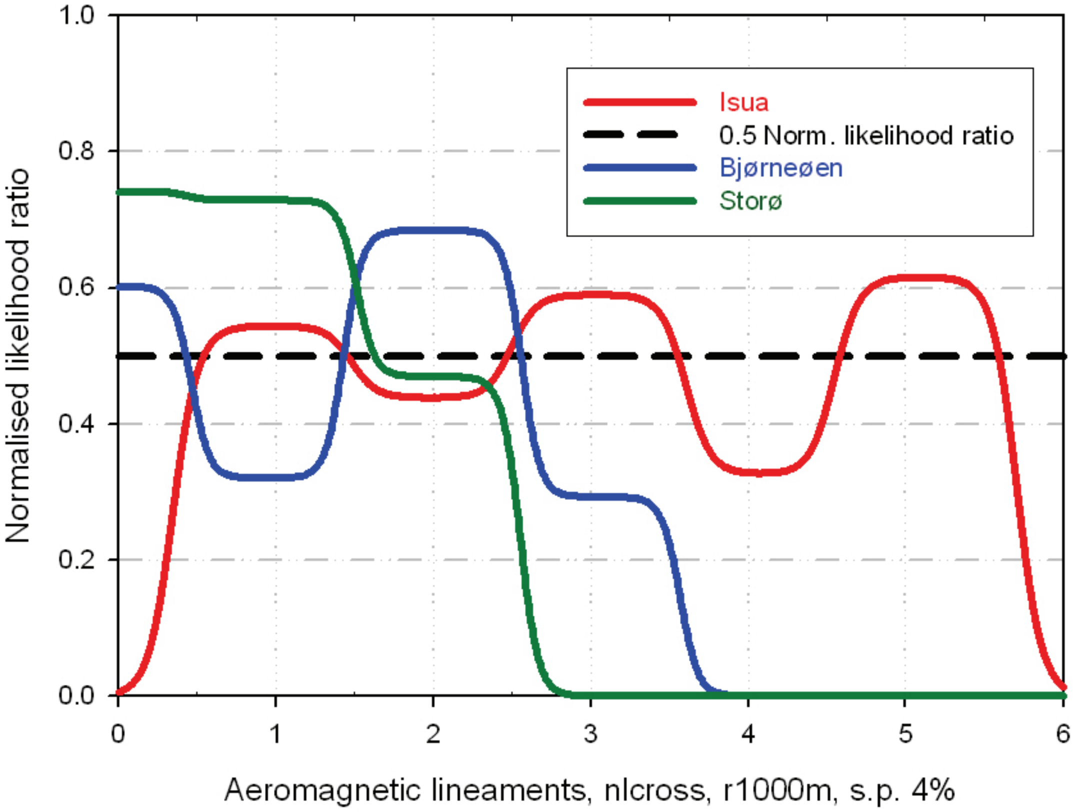

Aeromagnetic lineaments, nlcross, 0-10%, r1000m,
spread parameter 4%

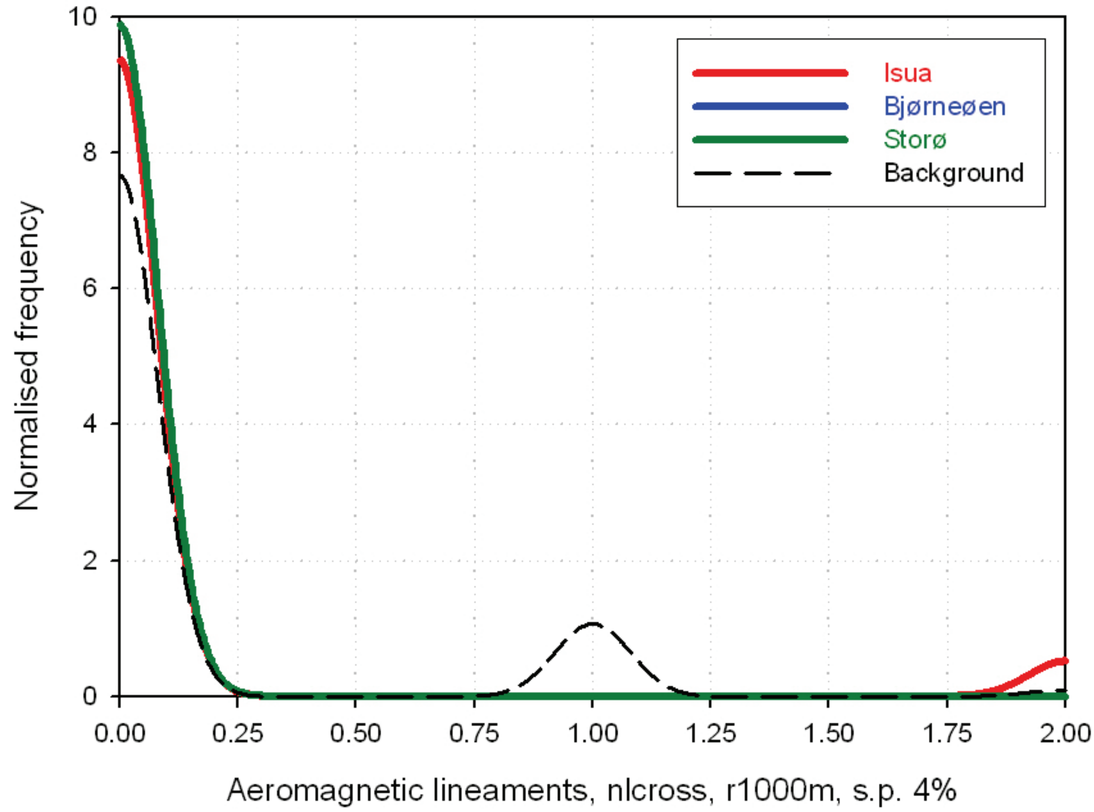

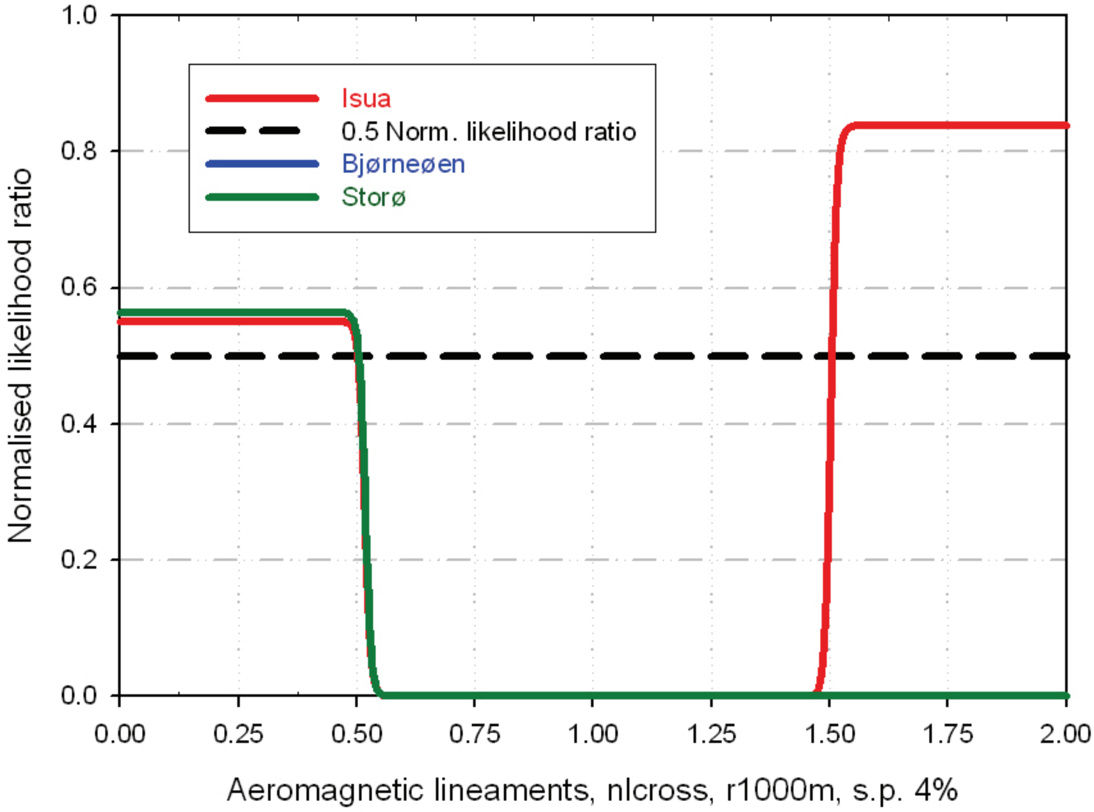

Aeromagnetic lineaments, nlcross, 0-25%, r1000m,
spread parameter 4%

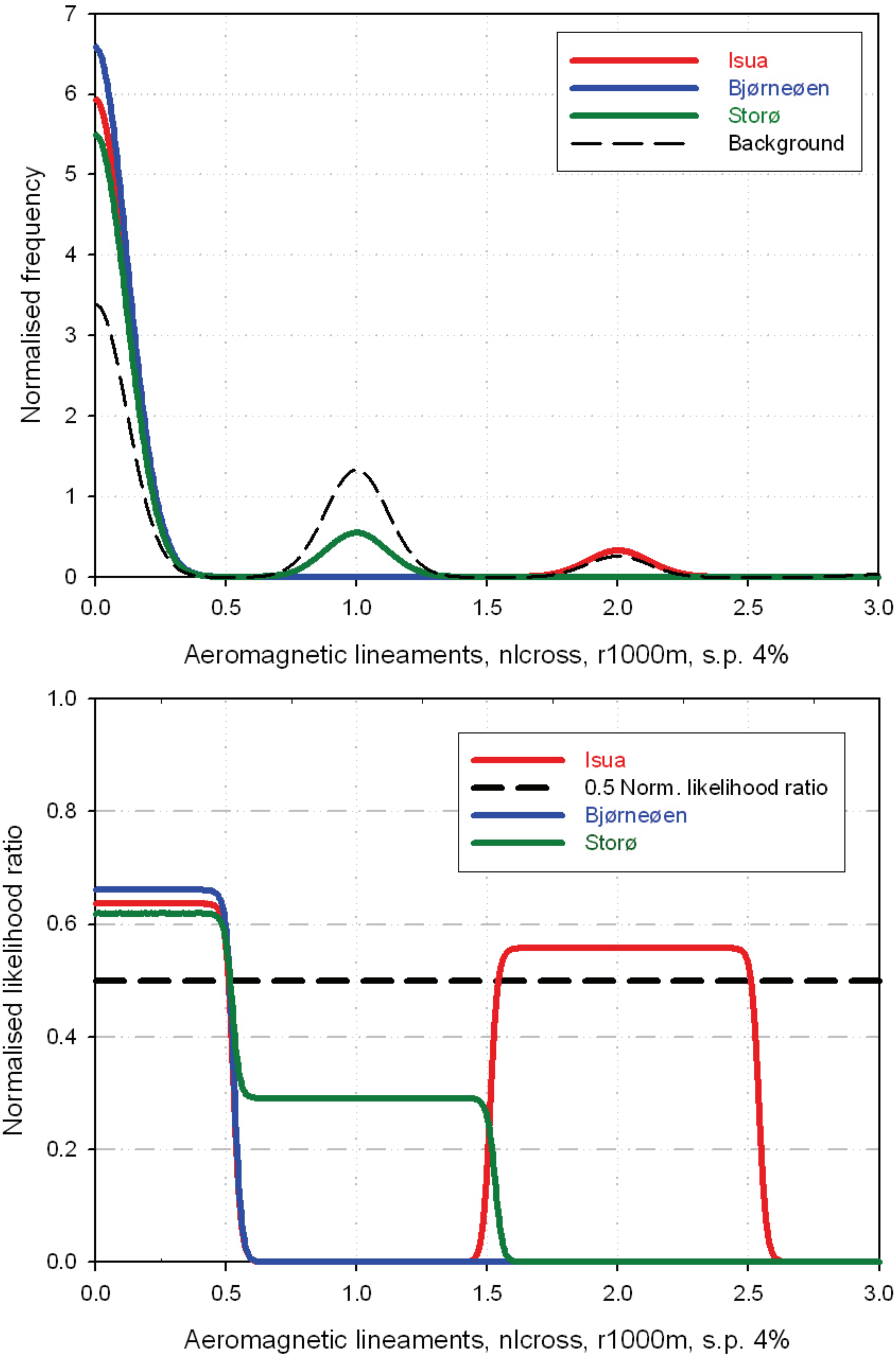

Aeromagnetic lineaments, nlcross, 25-50%, r1000m,
spread parameter 4%

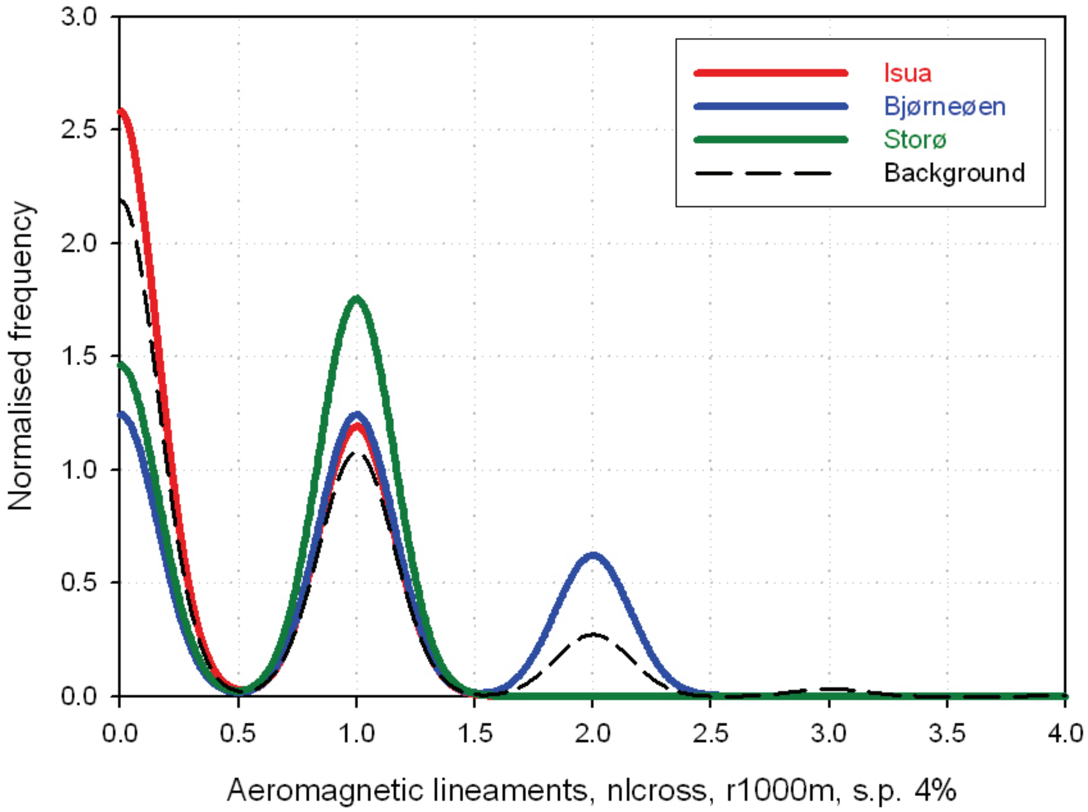

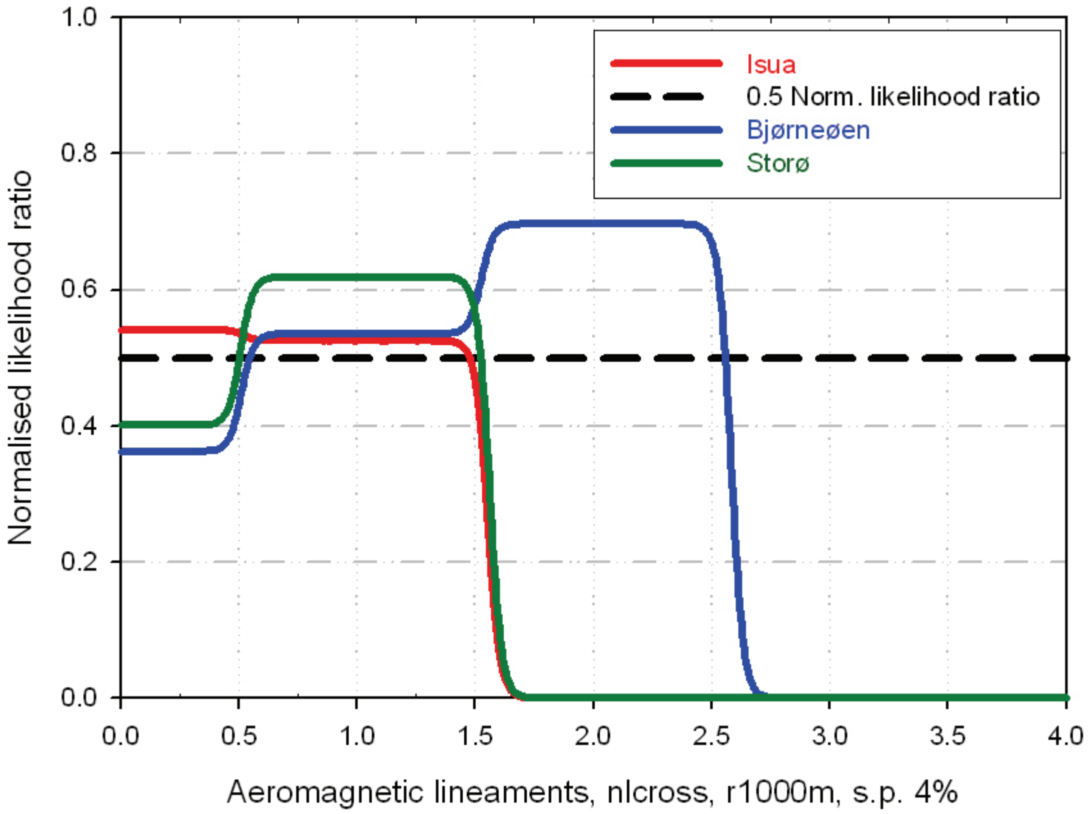

Aeromagnetic lineaments, nlcross, 50-75%, r1000m,
spread parameter 4%

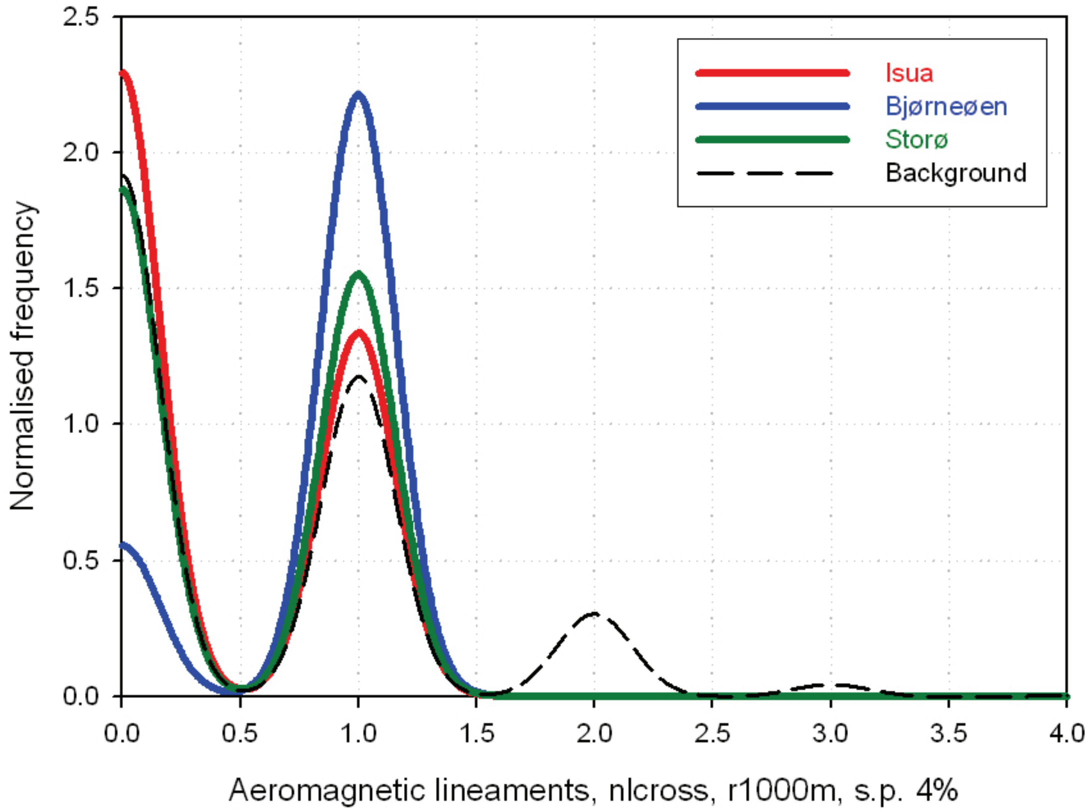

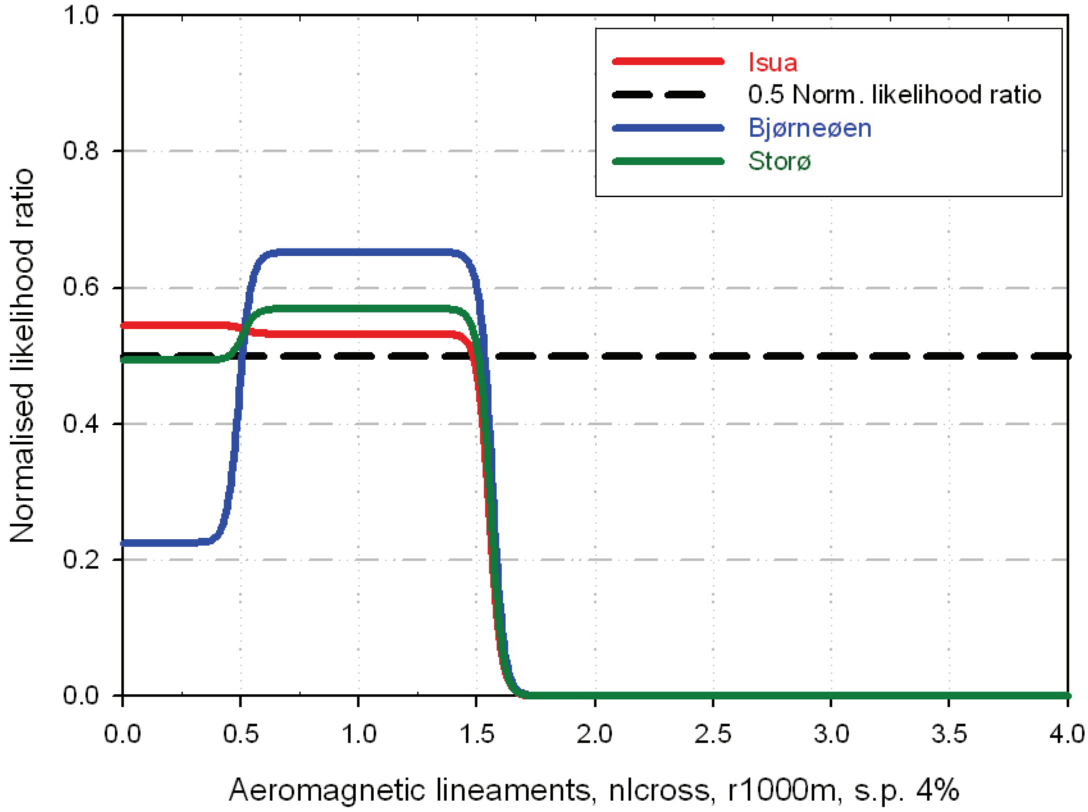

Aeromagnetic lineaments, nlcross, 75-100%, r1000m,
spread parameter 4%

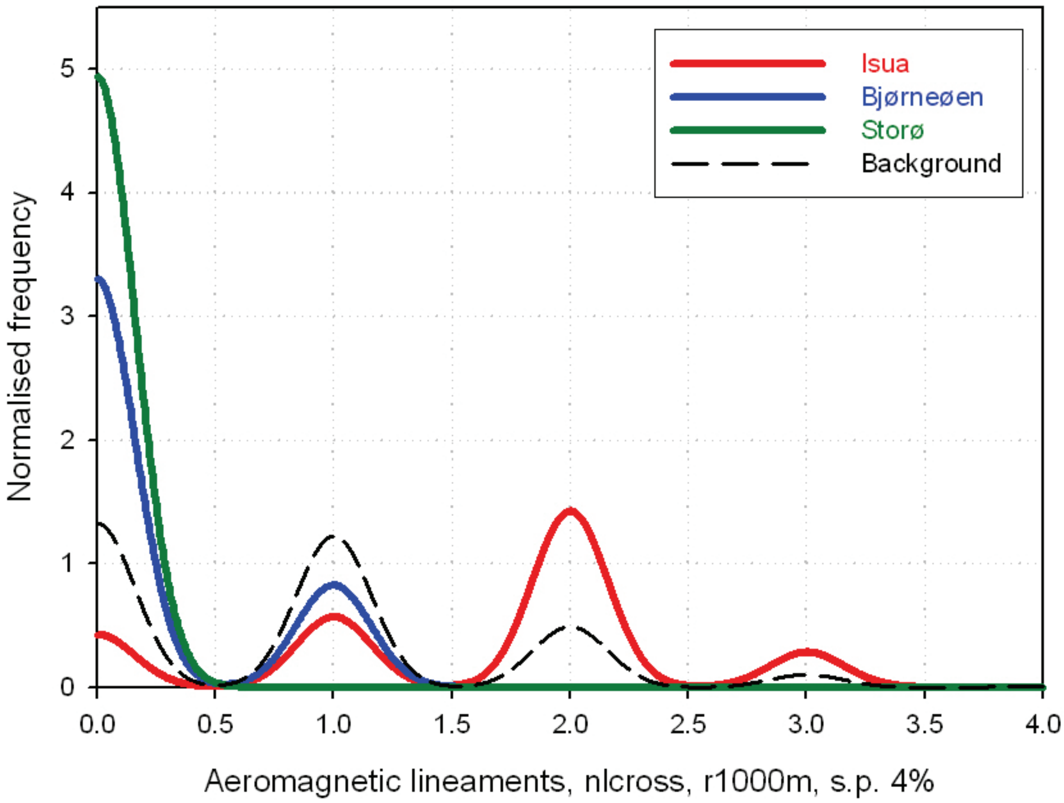

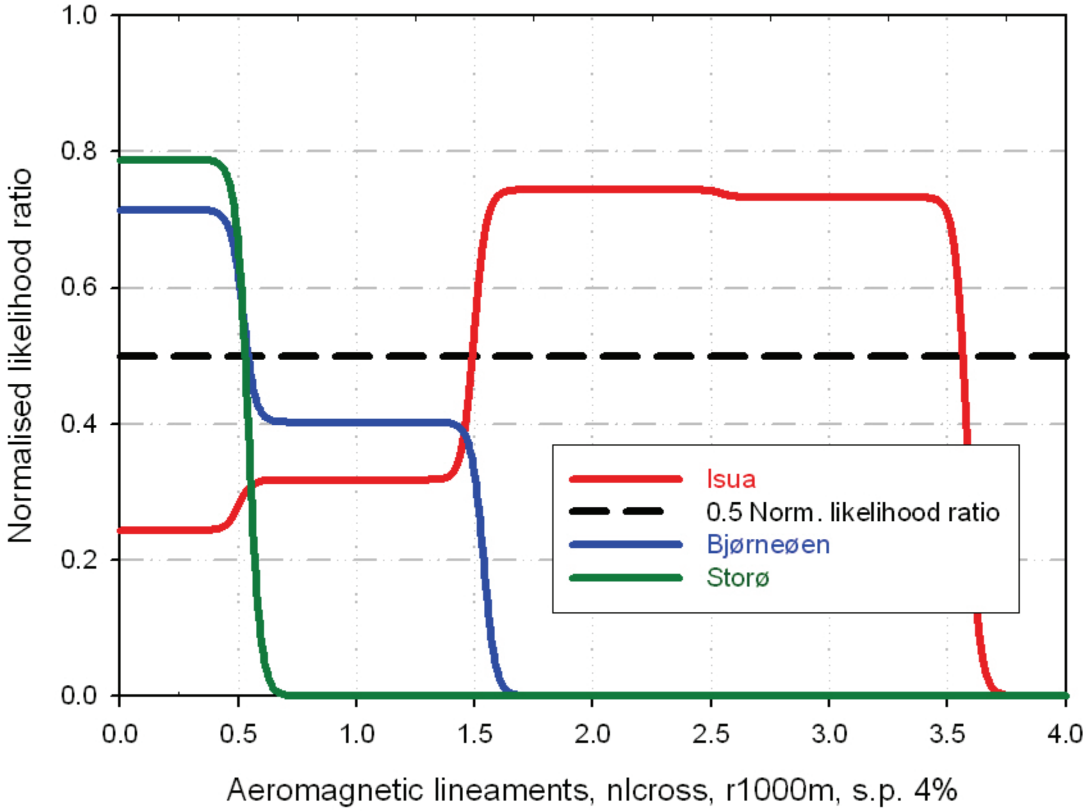

Aeromagnetic lineaments, nlcross, 90-100%, r1000m,
spread parameter 4%

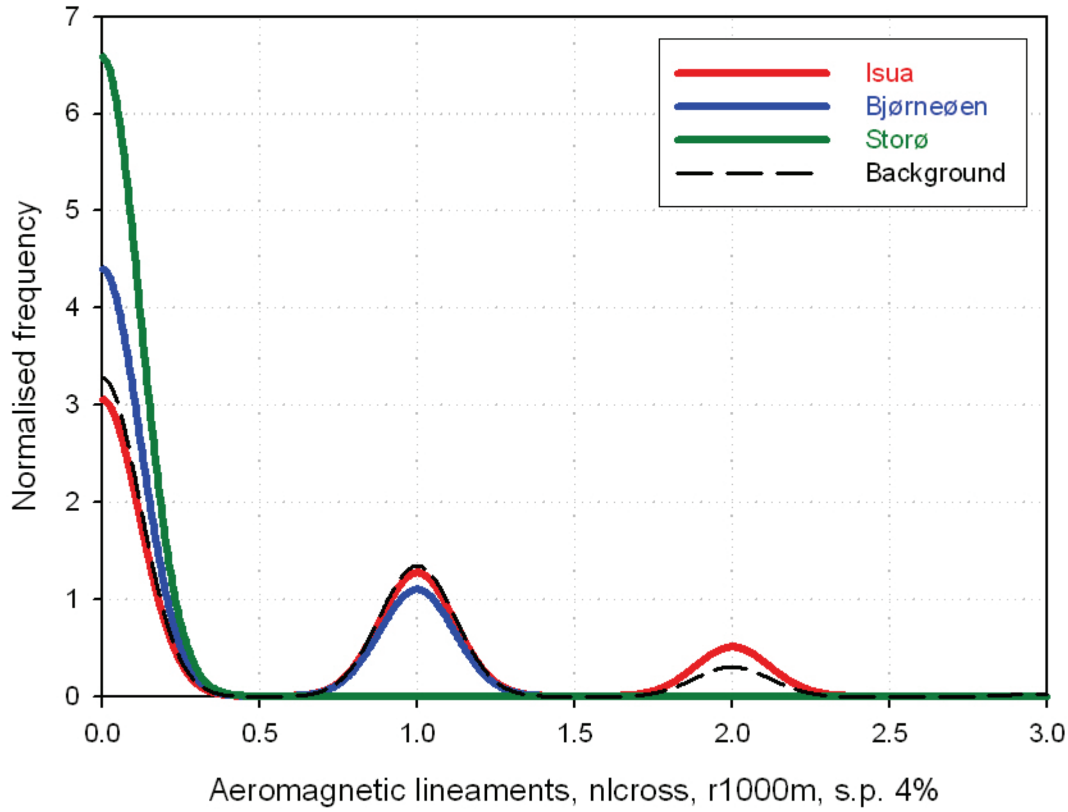

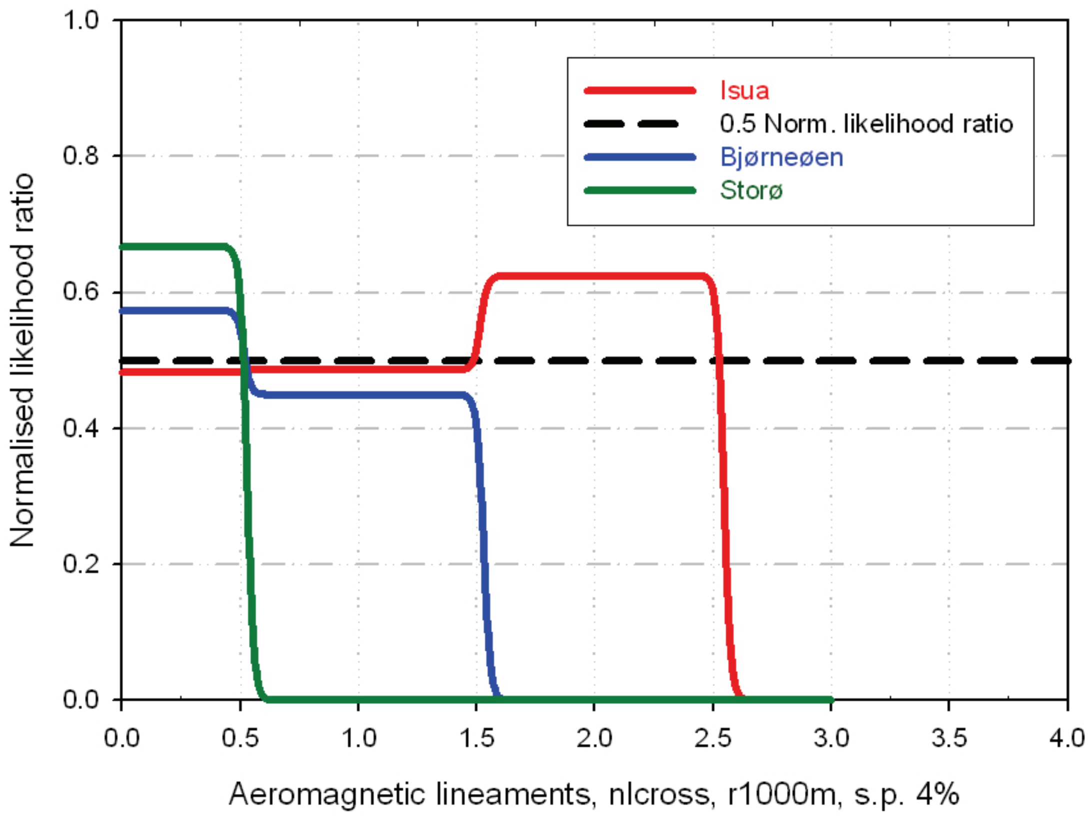

Aeromagnetic lineaments, total length, all lines, r1000m,
spread parameter 4%

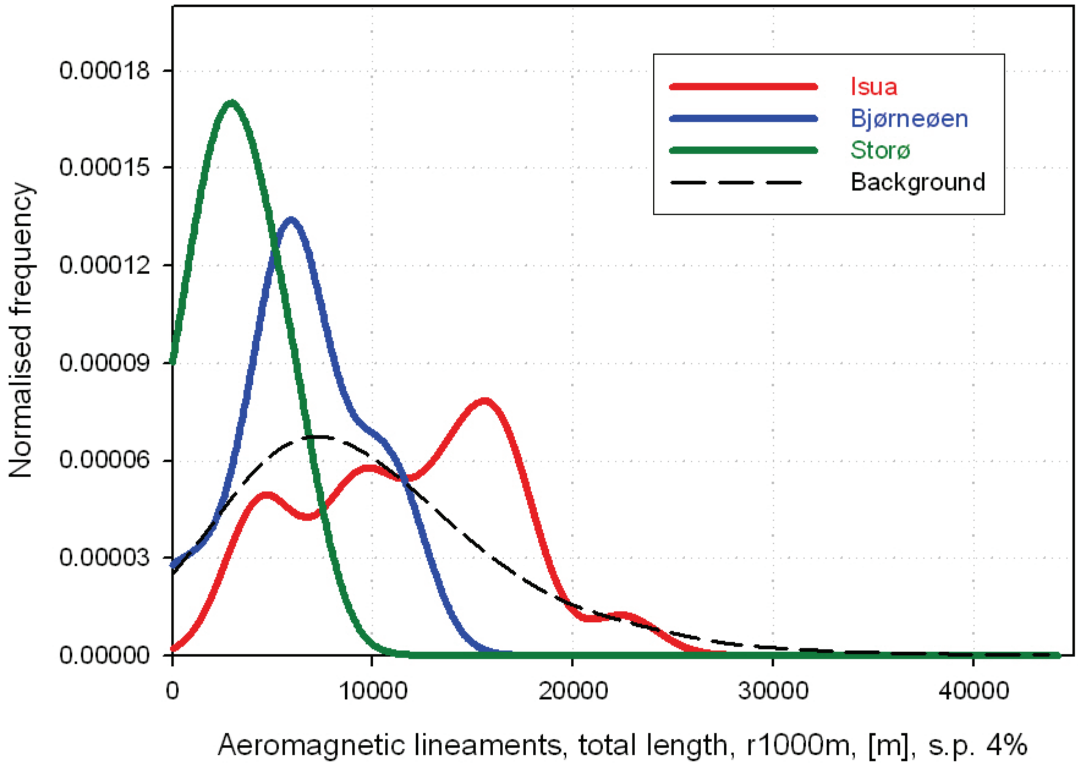

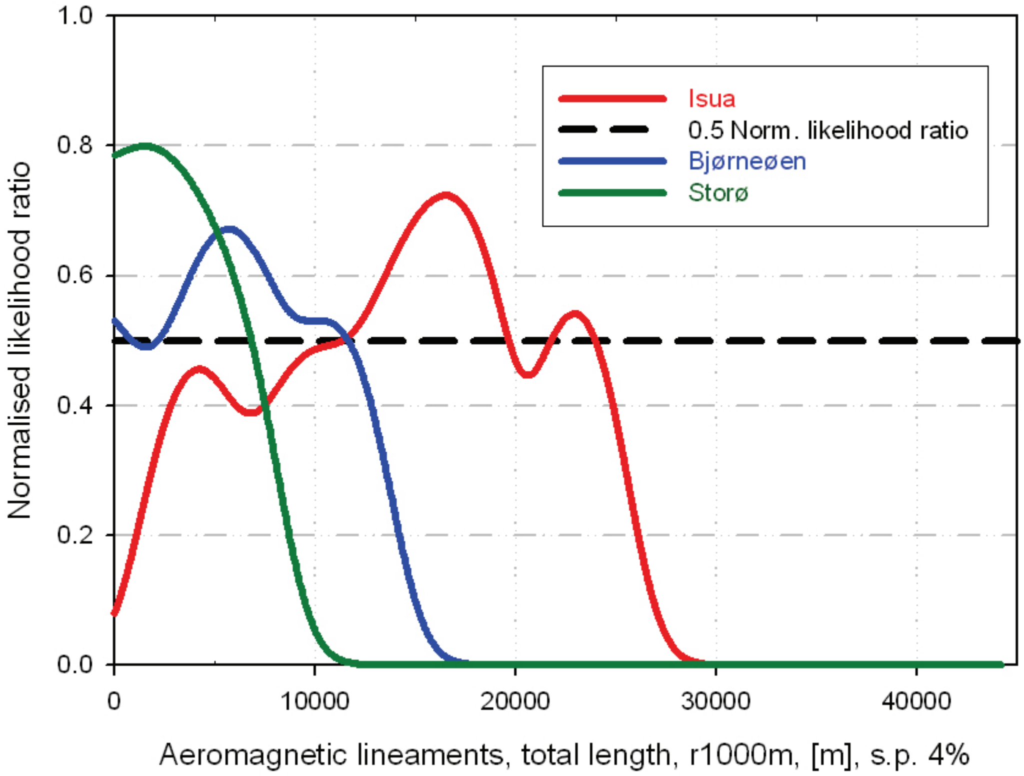

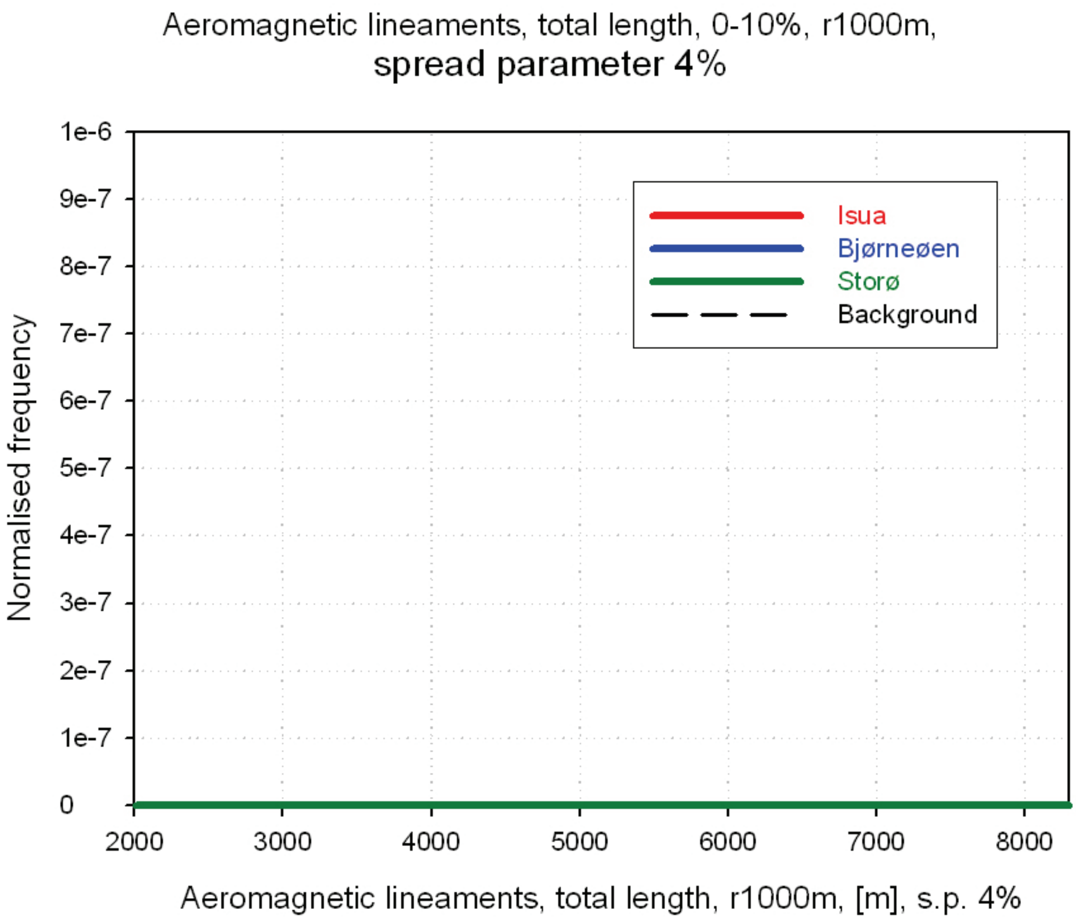
Aeromagnetic lineaments, total length, 0-10%, r1000m,
spread parameter 4%
Normalised frequency
1e-6
9e-7
8e-7
7e-7
6e-7
5e-7
4e-7
3e-7
2e-7
1e-7
0
2000
3000
4000
5000
6000
7000
8000
Isua
Bjørneøen
Storø
Background
Aeromagnetic lineaments, total length, r1000m, [m], s.p. 4%

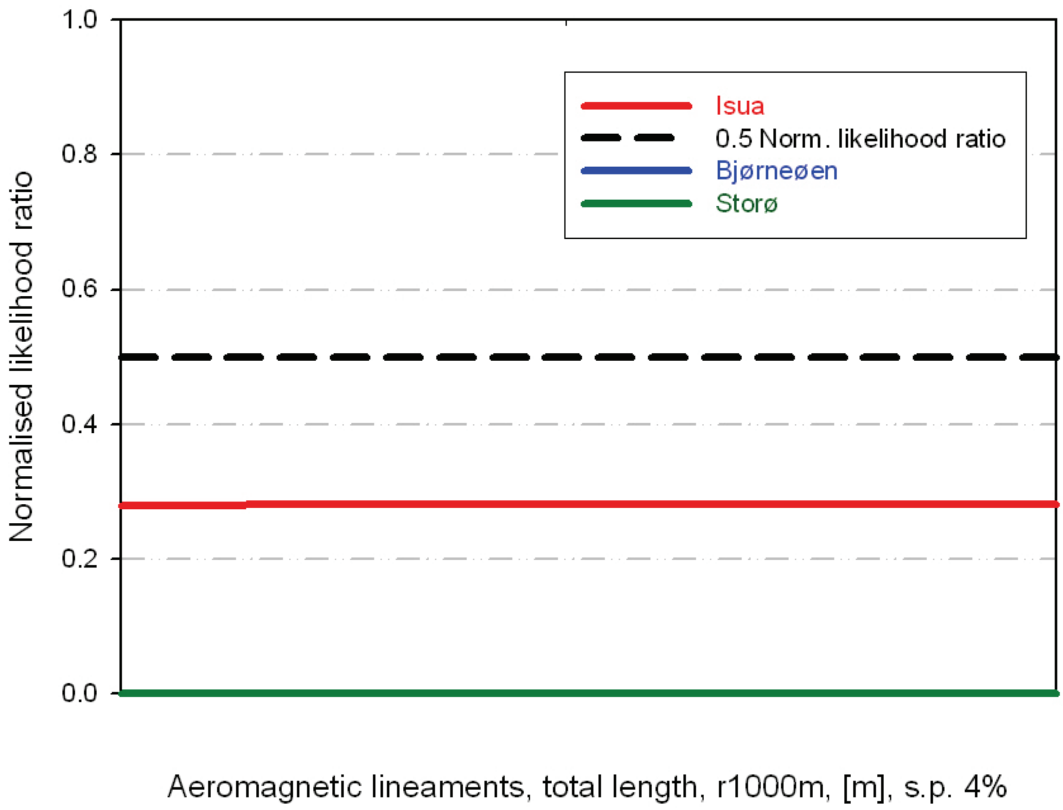
Normalised likelihood ratio
1.0
0.8
0.6
0.4
0.2
0.0
Isua
0.5 Norm. likelihood ratio
Bjørneøen
Storø
Aeromagnetic lineaments, total length, r1000m, [m], s.p. 4%

Aeromagnetic lineaments, total length, 0-25%, r1000m,
spread parameter 4%

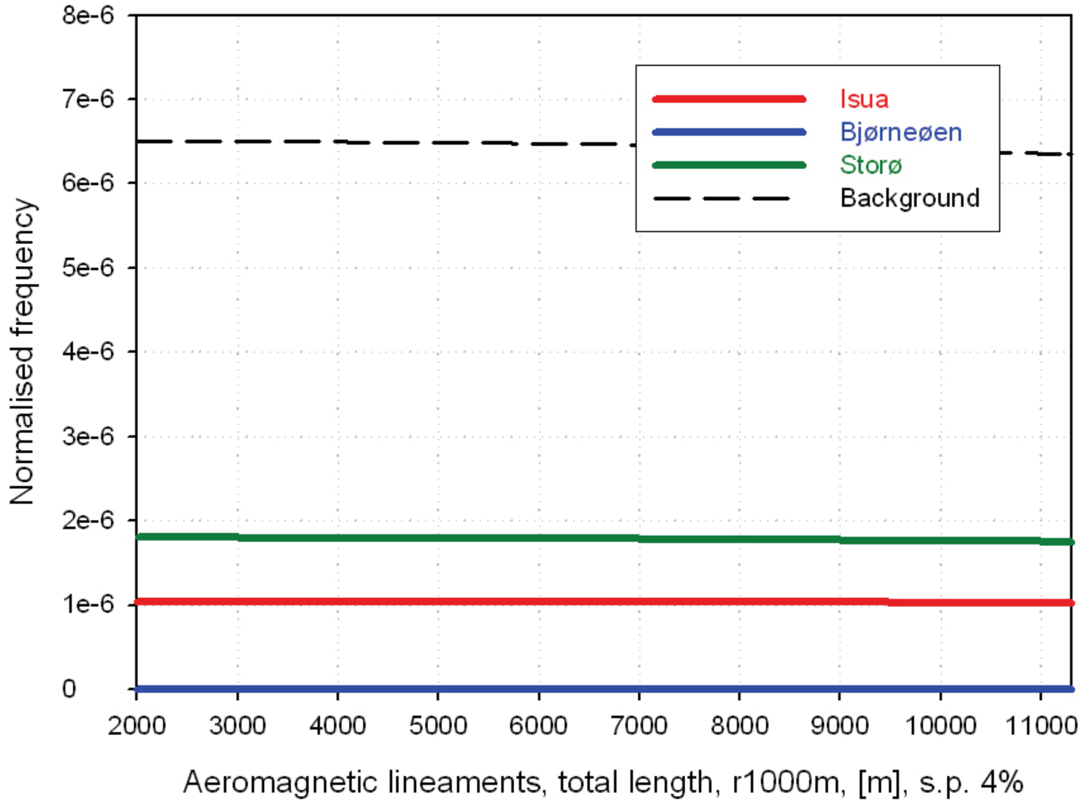

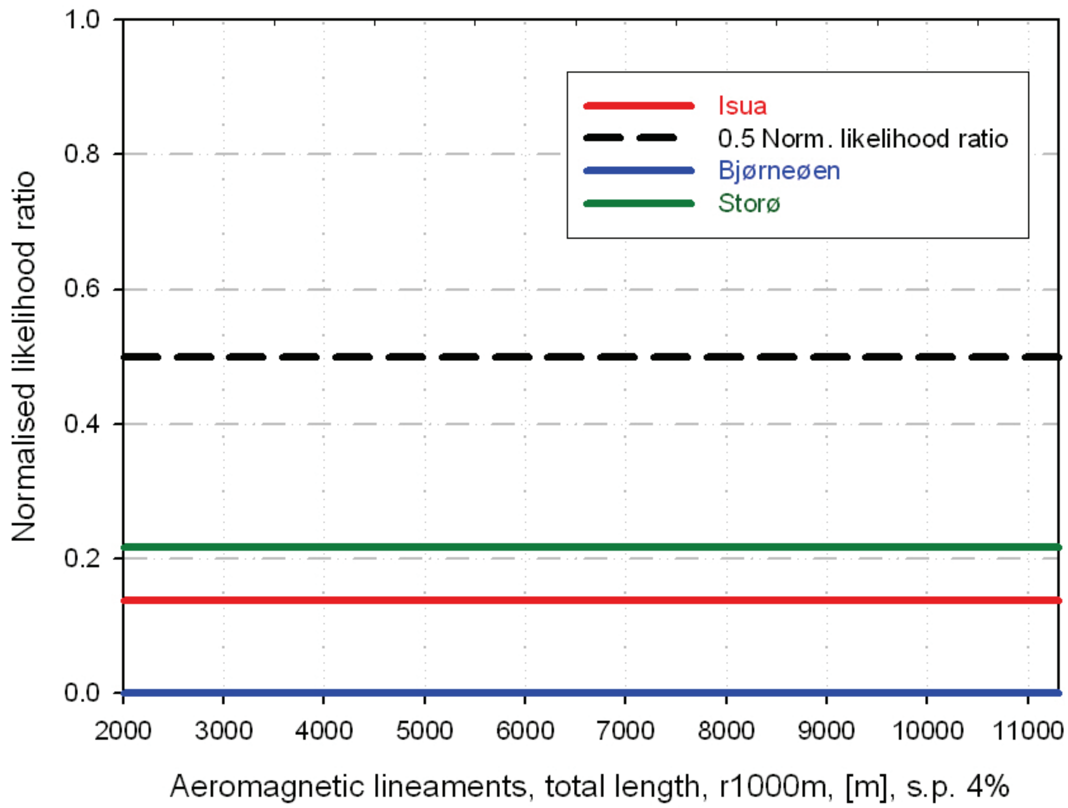

Aeromagnetic lineaments, total length, 25-50%, r1000m,
spread parameter 4%

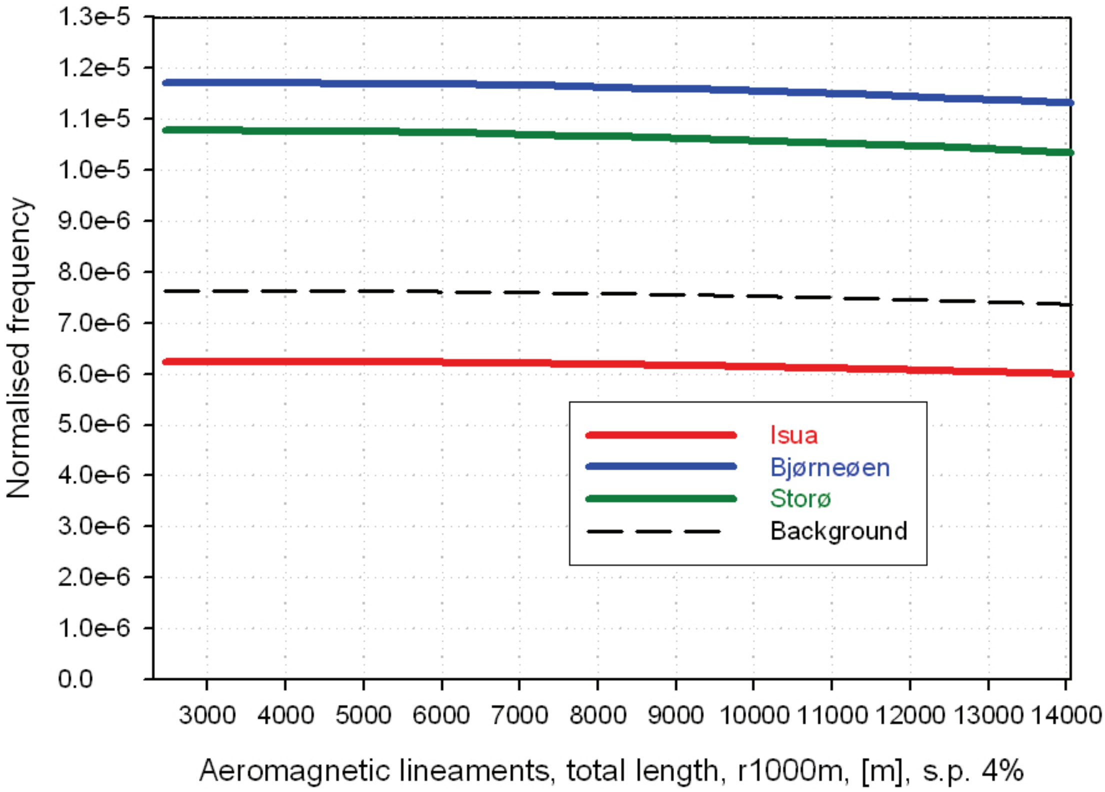

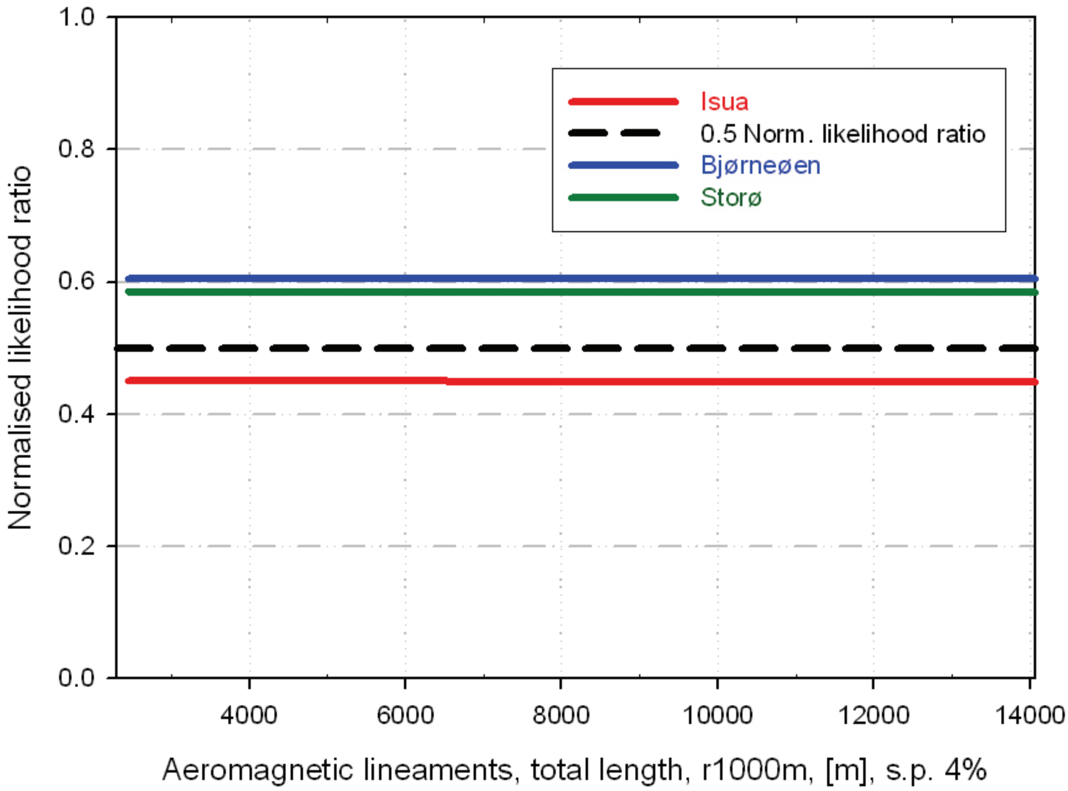

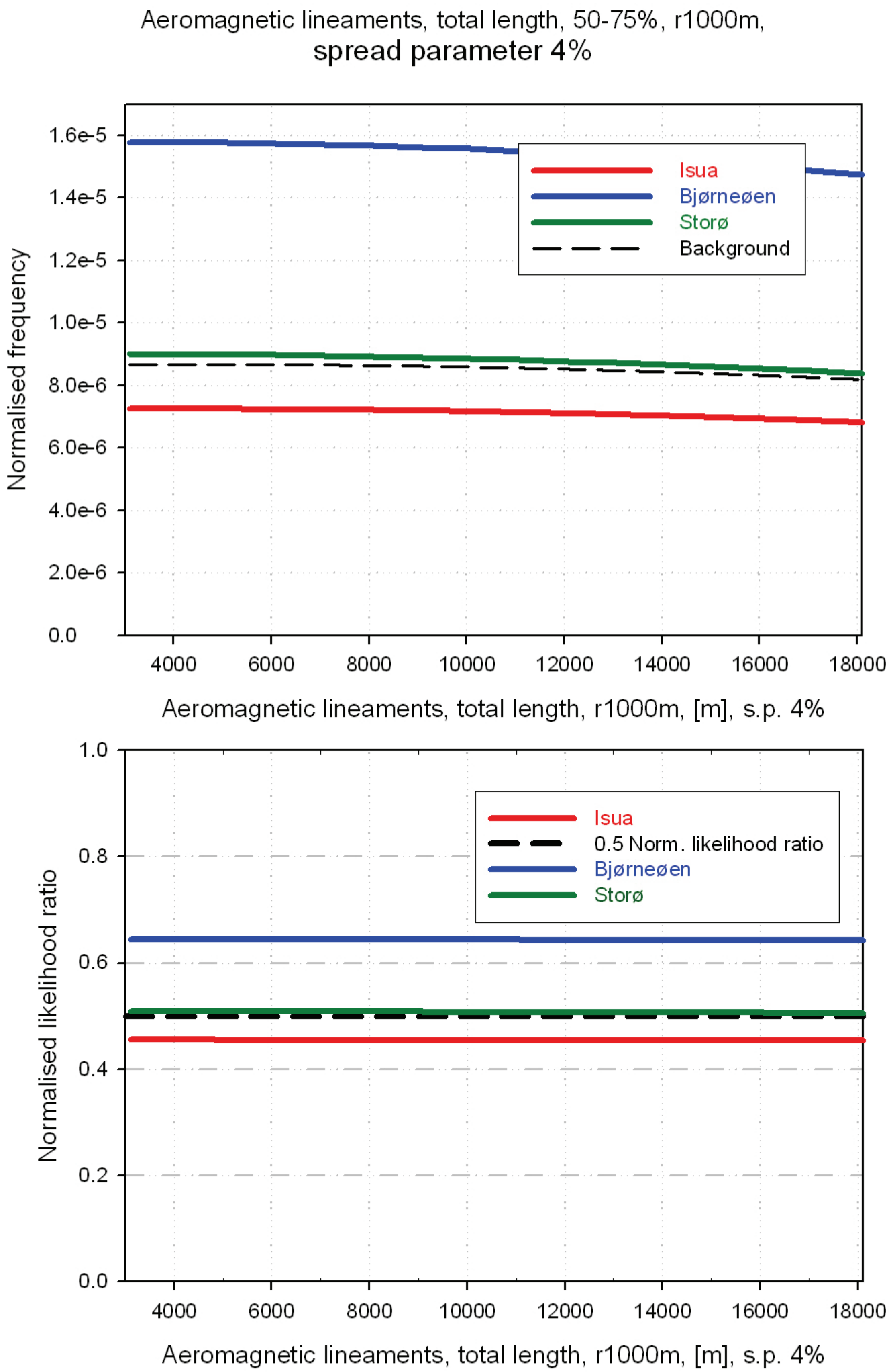
Aeromagnetic lineaments, total length, 50-75%, r1000m,
spread parameter 4%
Isua
Bjørneøen
Storø
Background
Normalised frequency
1.6e-5
1.4e-5
1.2e-5
1.0e-5
8.0e-6
6.0e-6
4.0e-6
2.0e-6
0.0
4000
6000
8000
10000
12000
14000
16000
18000
Aeromagnetic lineaments, total length, r1000m, [m], s.p. 4%
Isua
0.5 Norm. likelihood ratio
Bjørneøen
Storø
Normalised likelihood ratio
1.0
0.8
0.6
0.4
0.2
0.0
4000
6000
8000
10000
12000
14000
16000
18000
Aeromagnetic lineaments, total length, r1000m, [m], s.p. 4%

Aeromagnetic lineaments, total length, 75-100%, r1000m,
spread parameter 4%

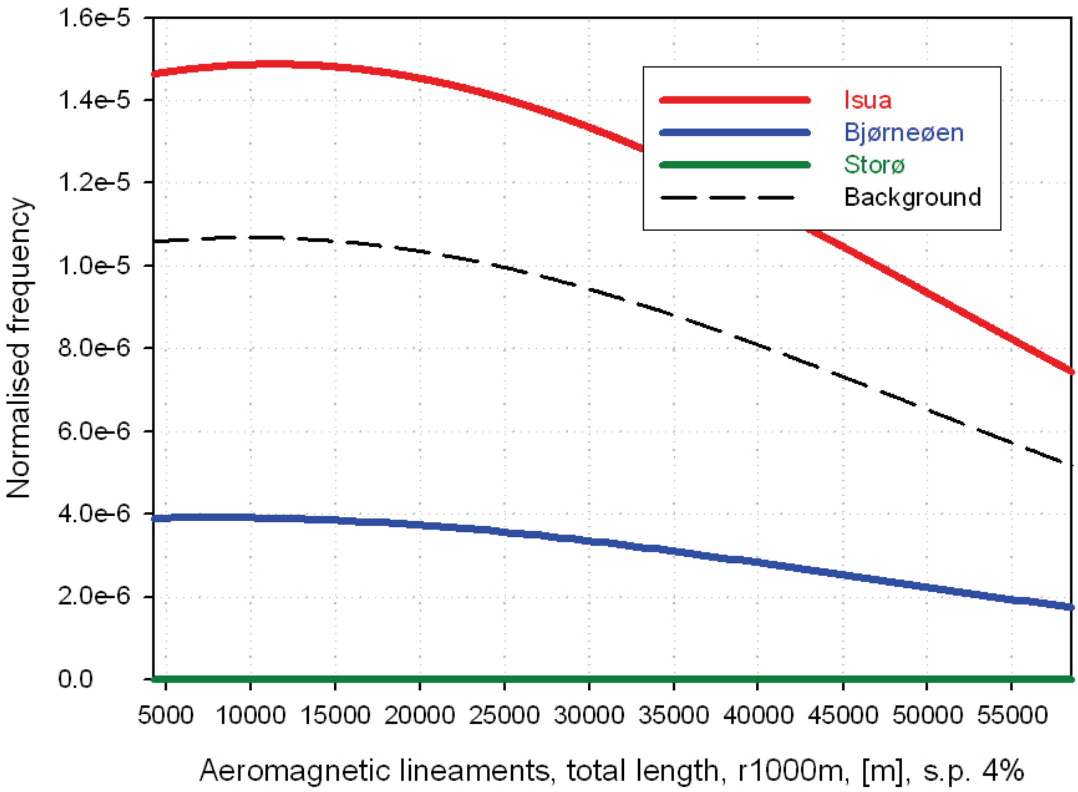

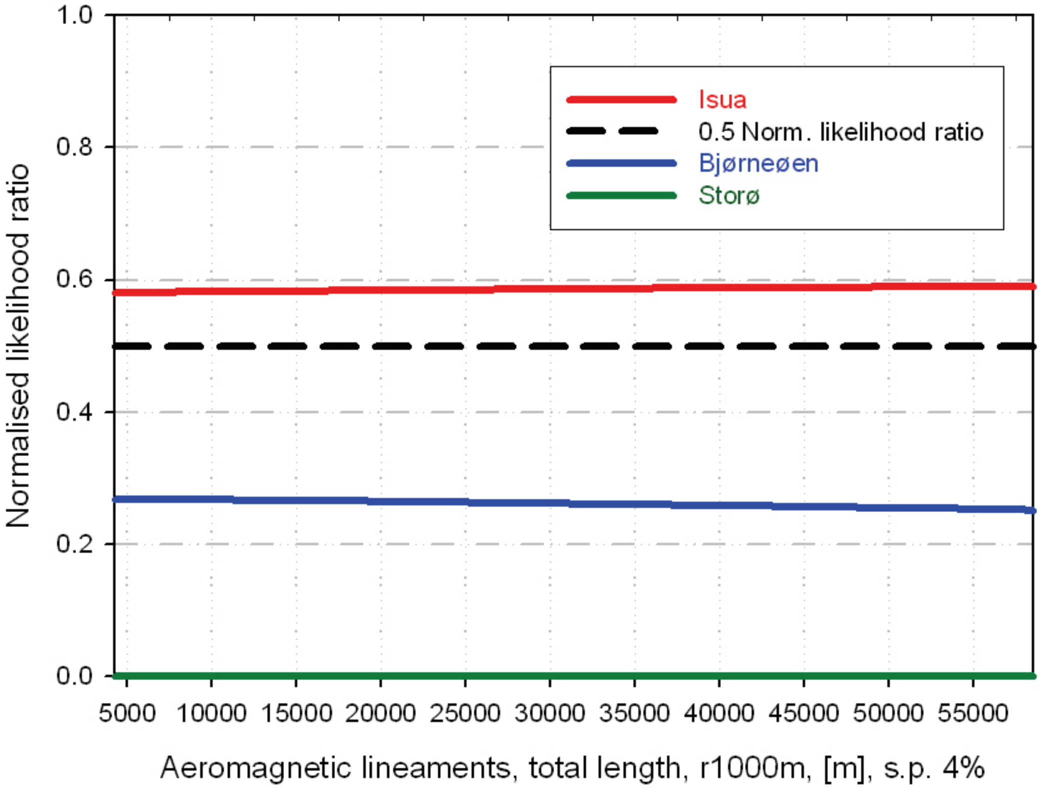

Aeromagnetic lineaments, total length, 90-100%, r1000m,
spread parameter 4%

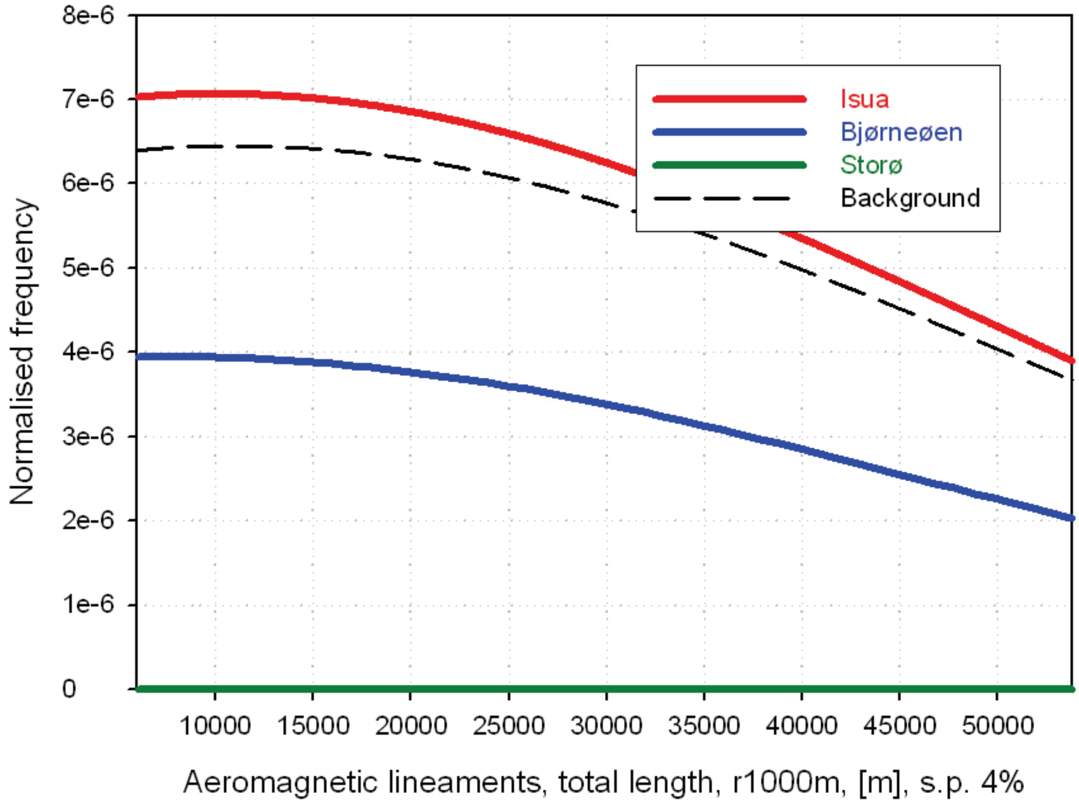

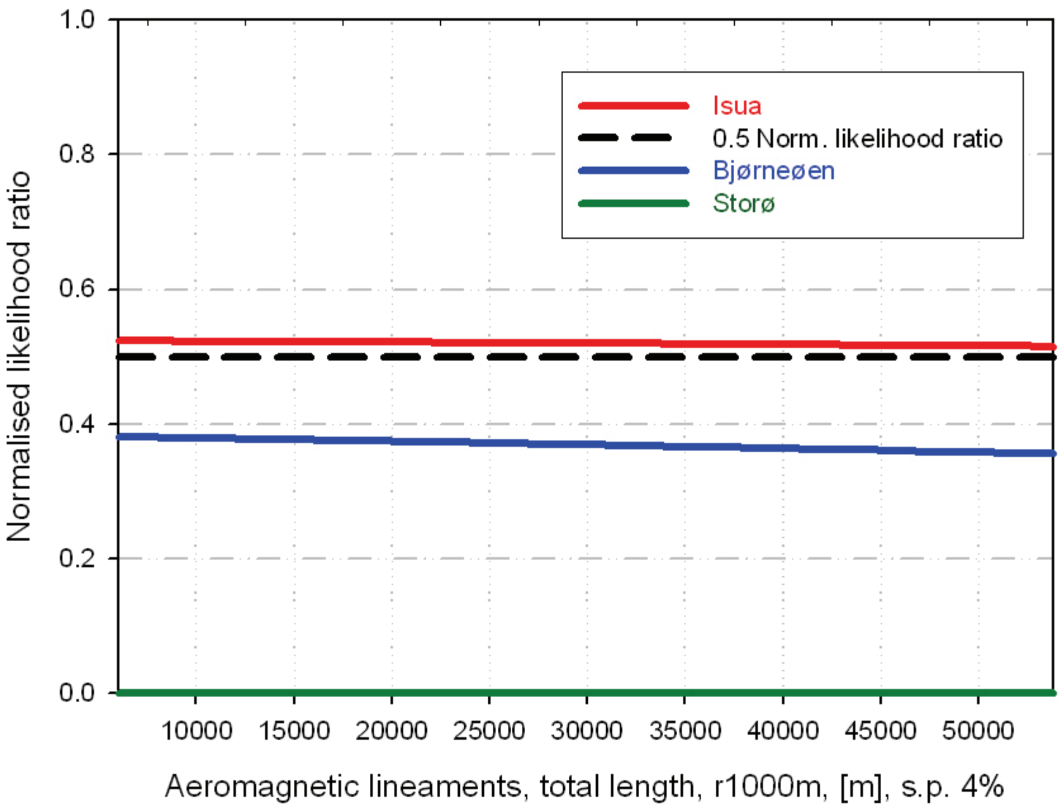

Aeromagnetic lineaments, unit vector sum (complexity), all lines, r1000m,
spread parameter 4%

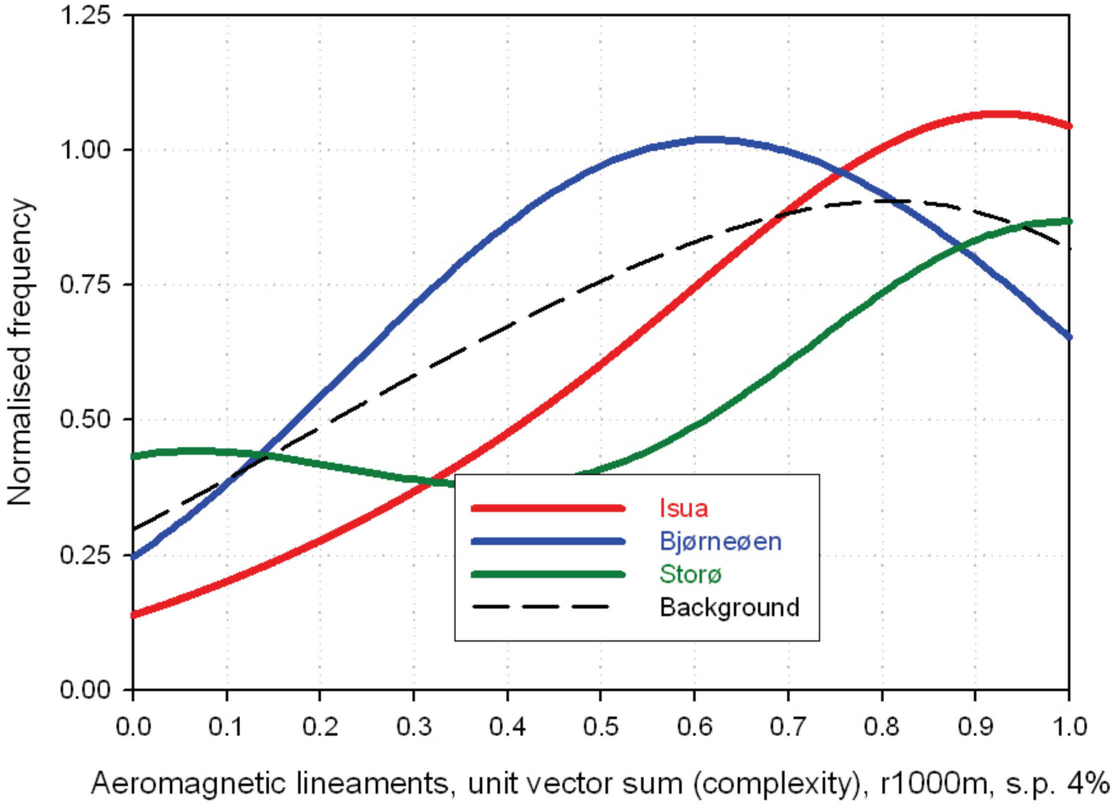

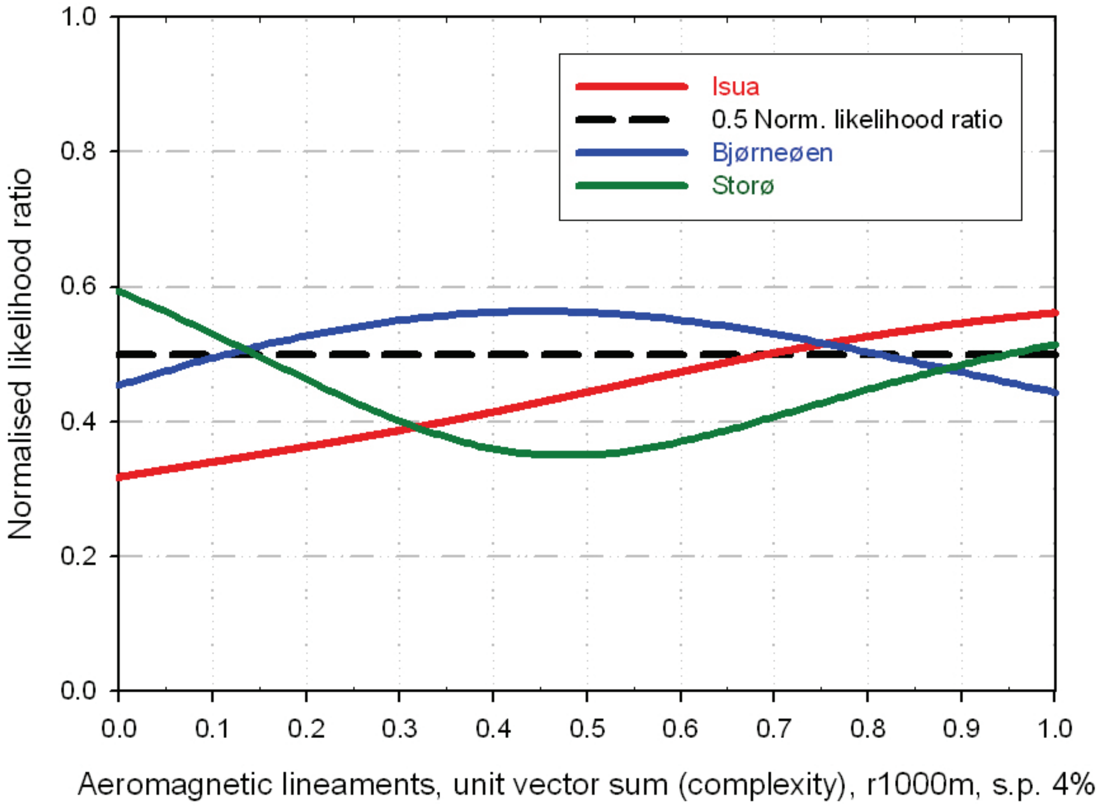

Aeromagnetic lineaments, unit vector sum (complexity), 0-10%, r1000m,
spread parameter 4%

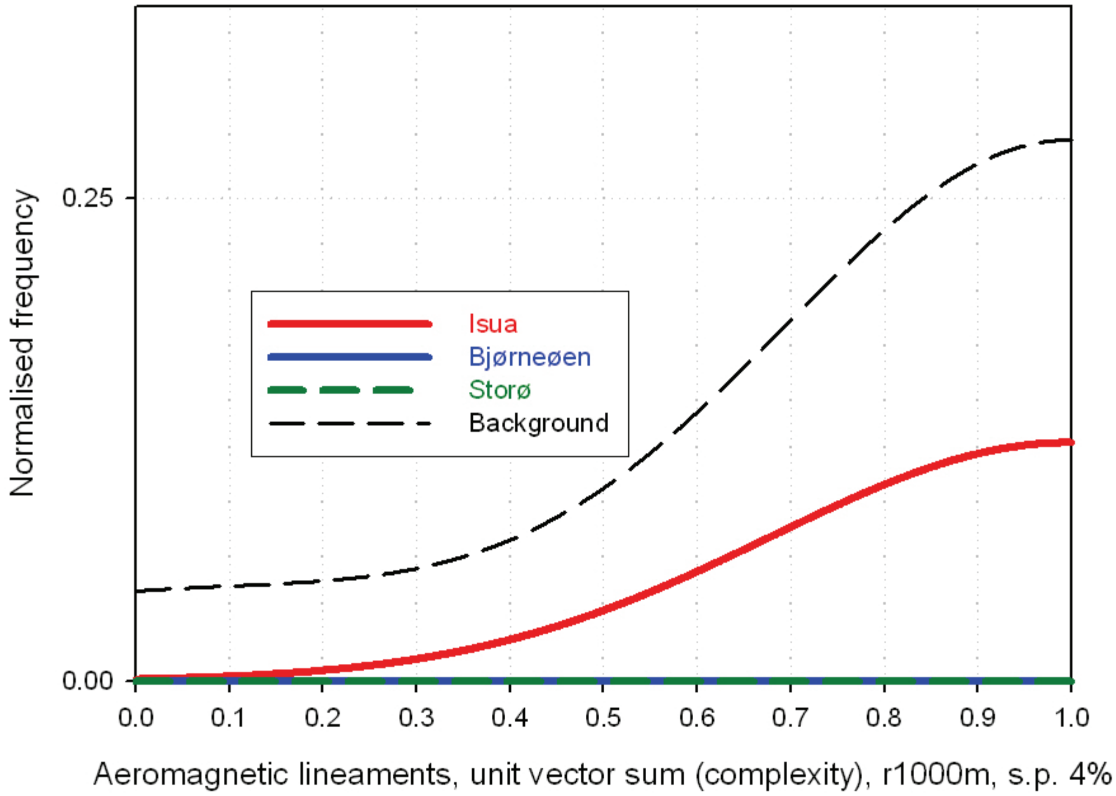

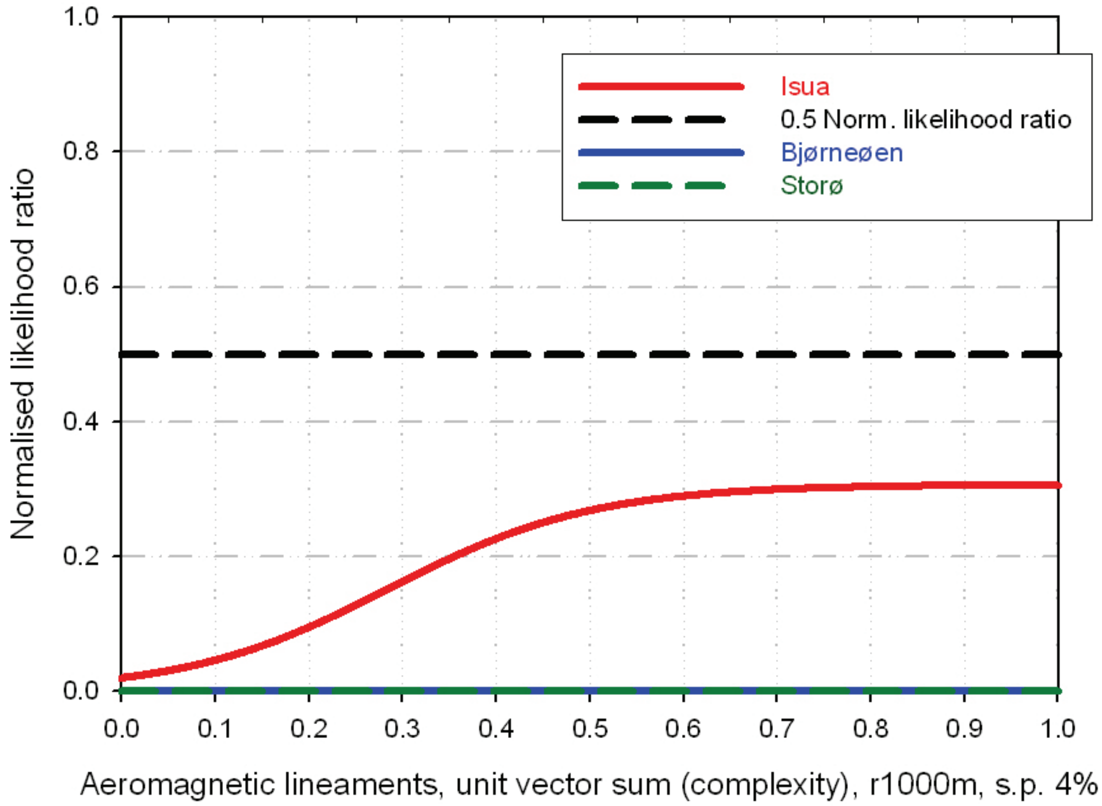

Aeromagnetic lineaments, unit vector sum (complexity), 50-75%, r1000m,
spread parameter 4%

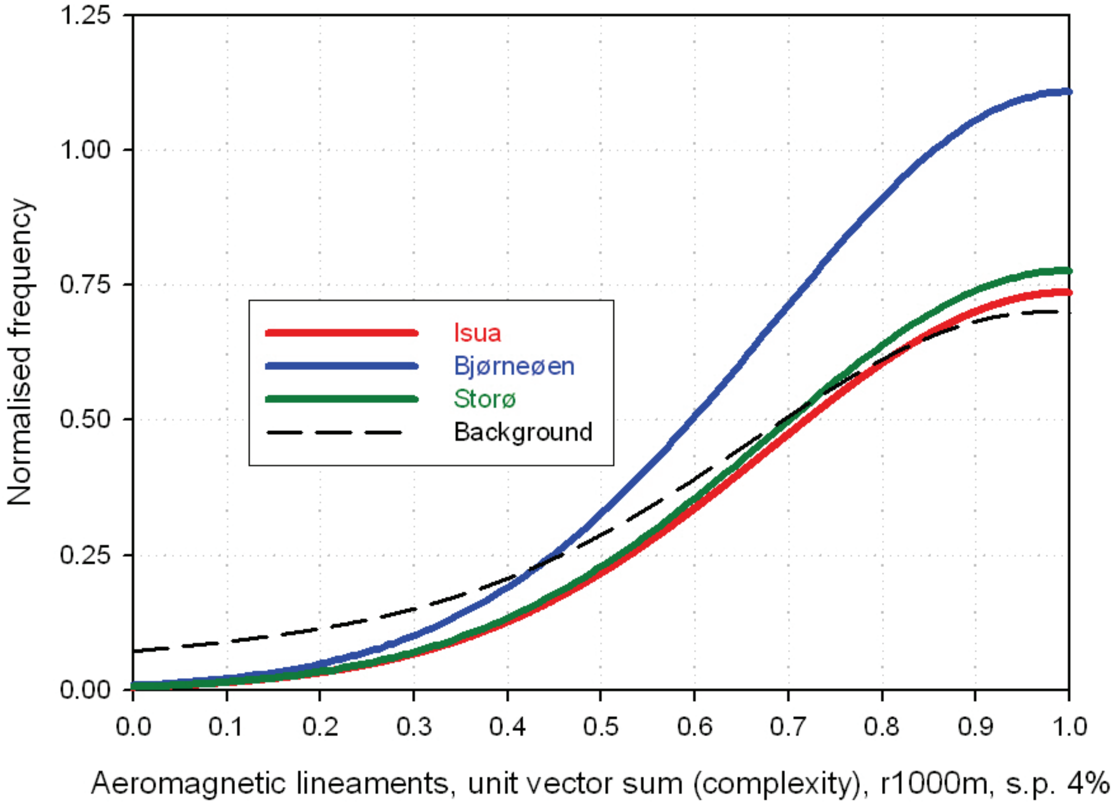

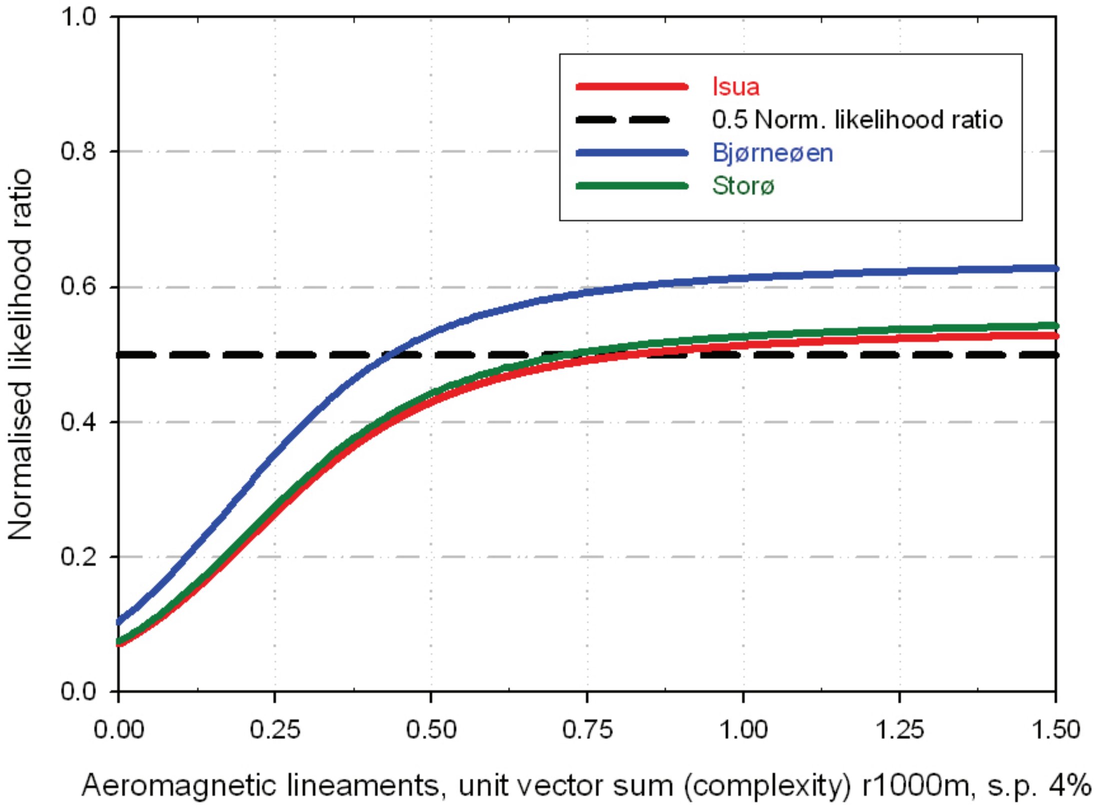

Aeromagnetic lineaments, unit vector sum (complexity), 25-50%, r1000m,
spread parameter 4%

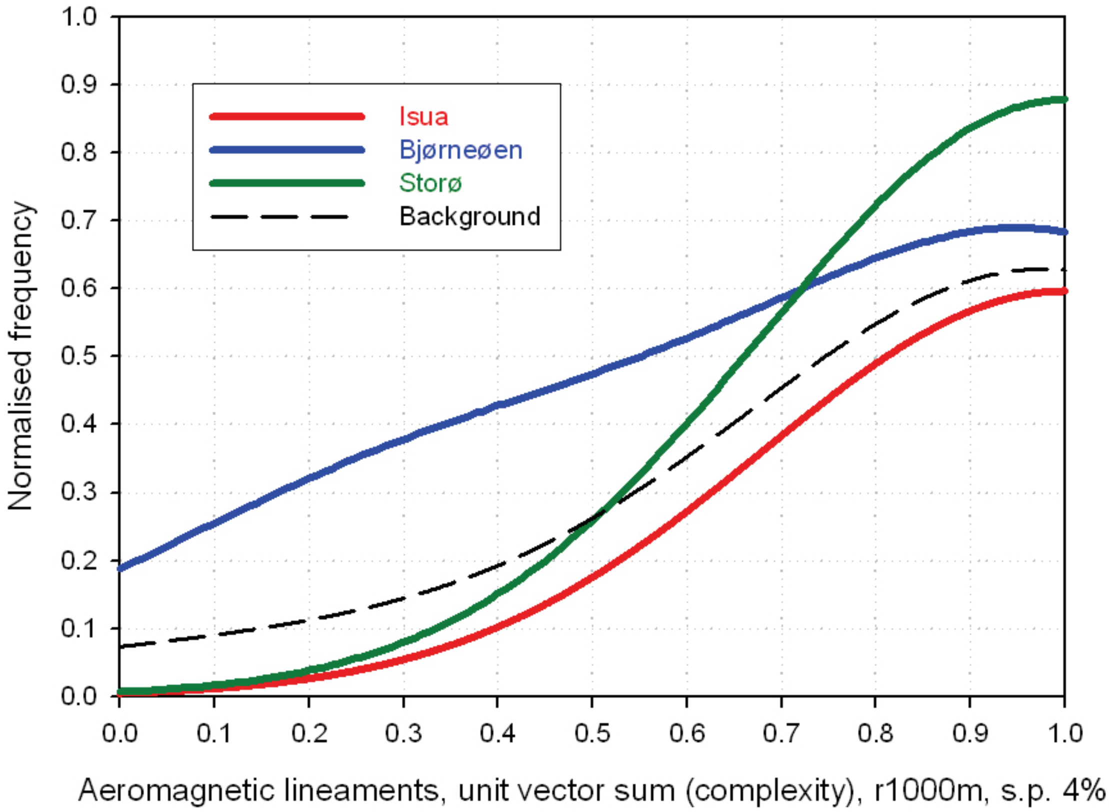

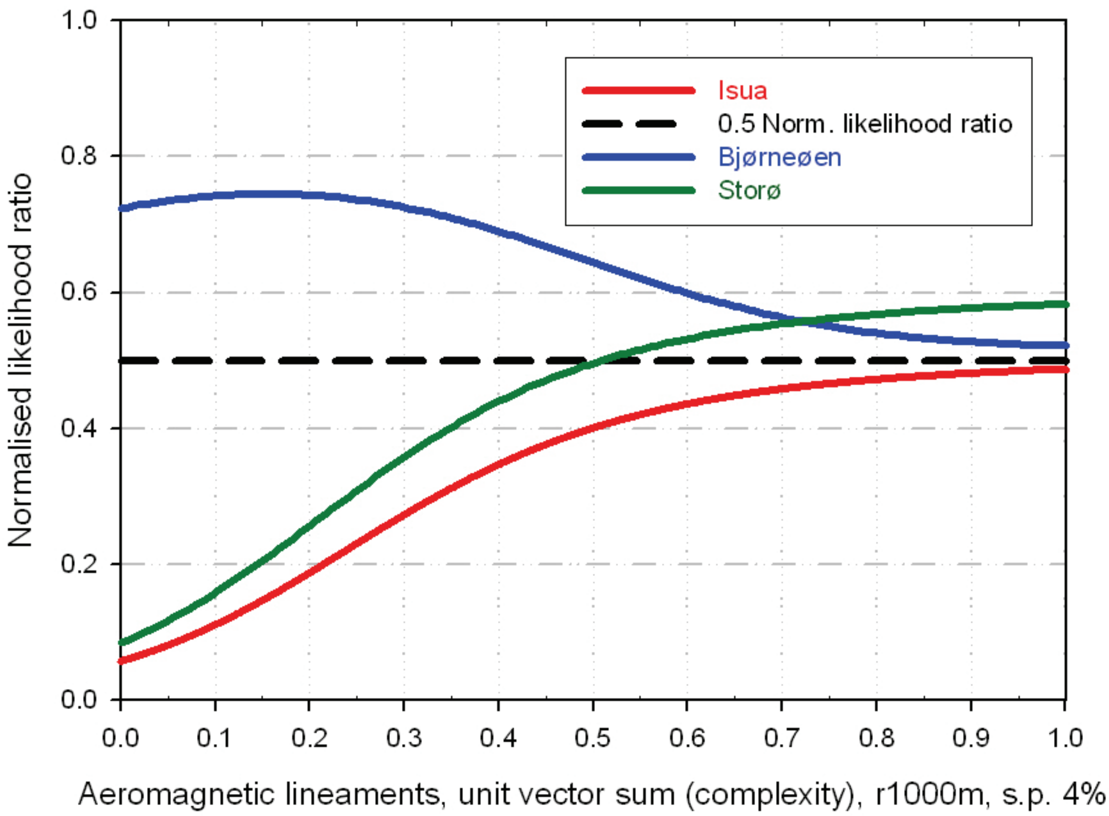

Aeromagnetic lineaments, unit vector sum (complexity), 50-75%, r1000m,
spread parameter 4%

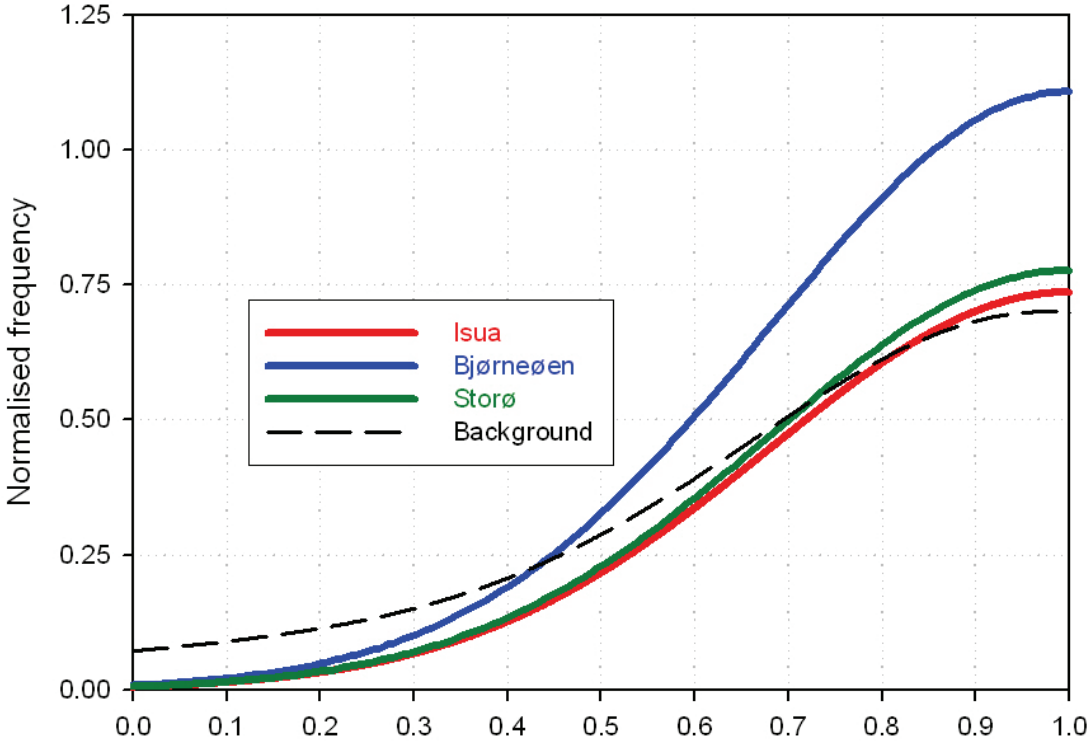

Aeromagnetic lineaments, unit vector sum (complexity), r1000m, s.p. 4%

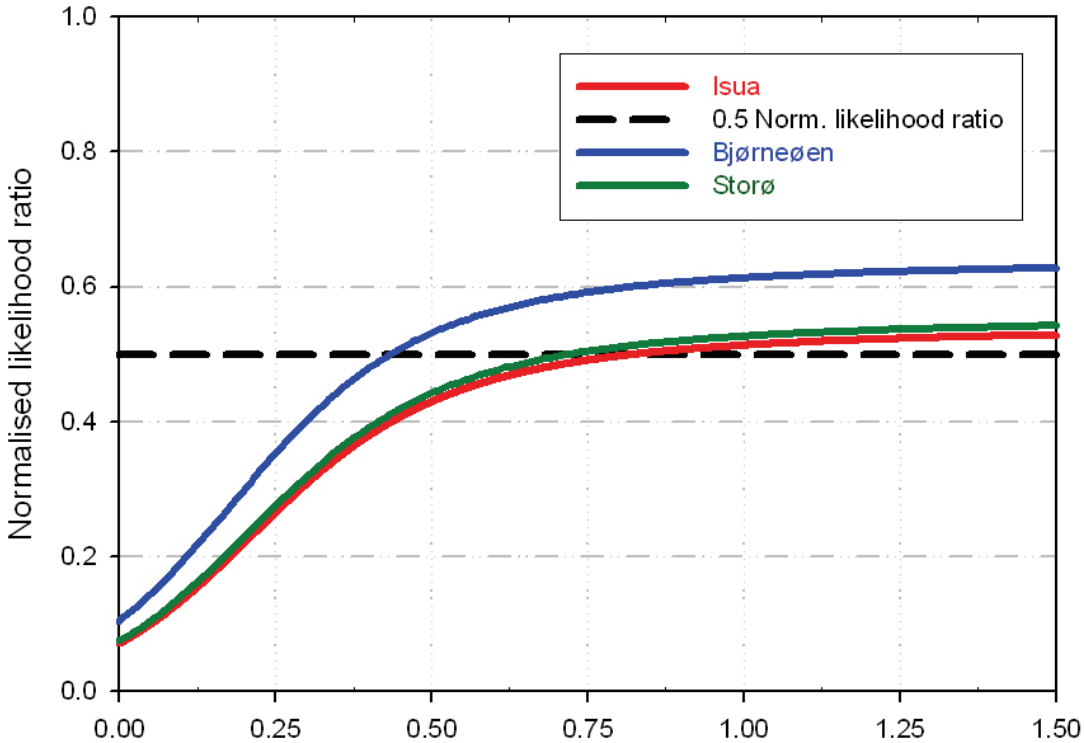

Aeromagnetic lineaments, unit vector sum (complexity) r1000m, s.p. 4%

Aeromagnetic lineaments, unit vector sum (complexity), 75-100%, r1000m,
spread parameter 4%

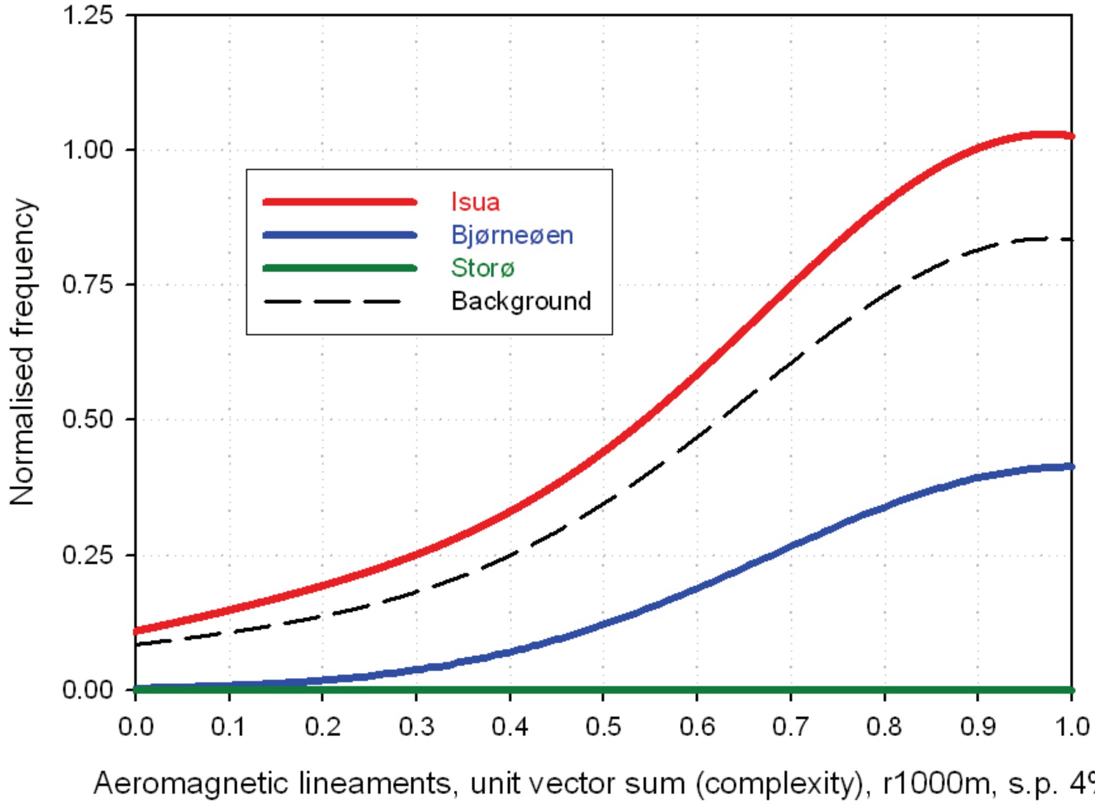

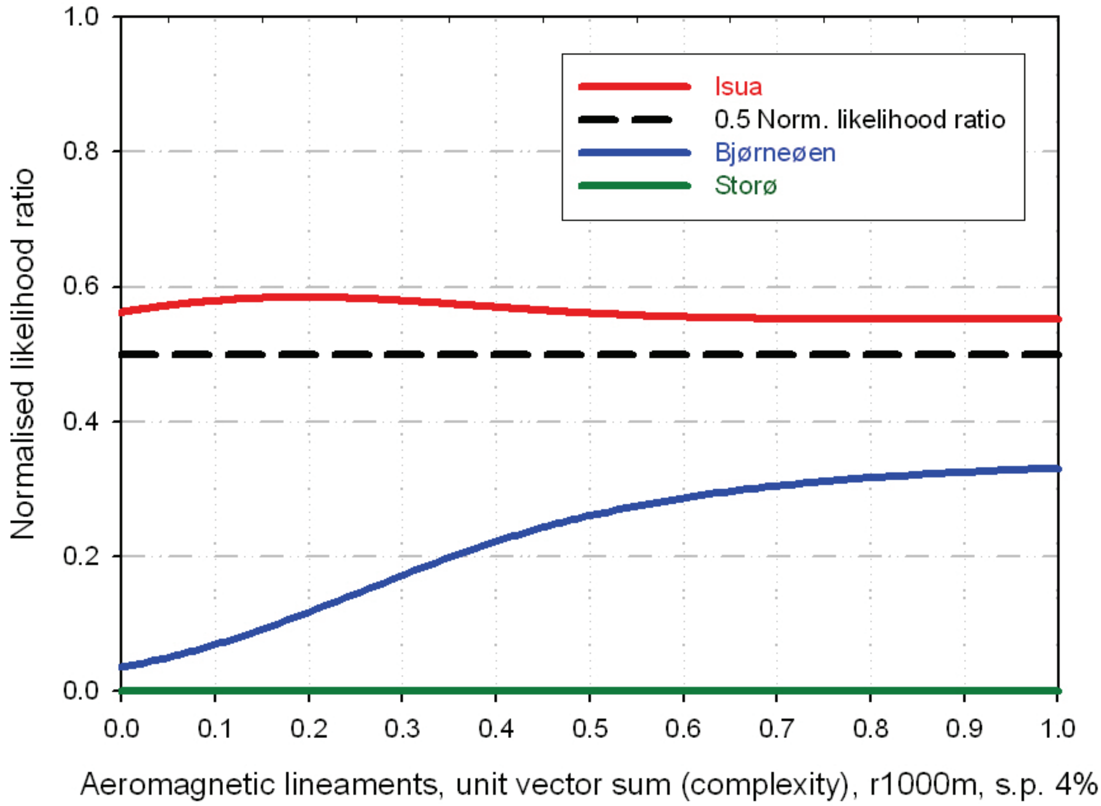

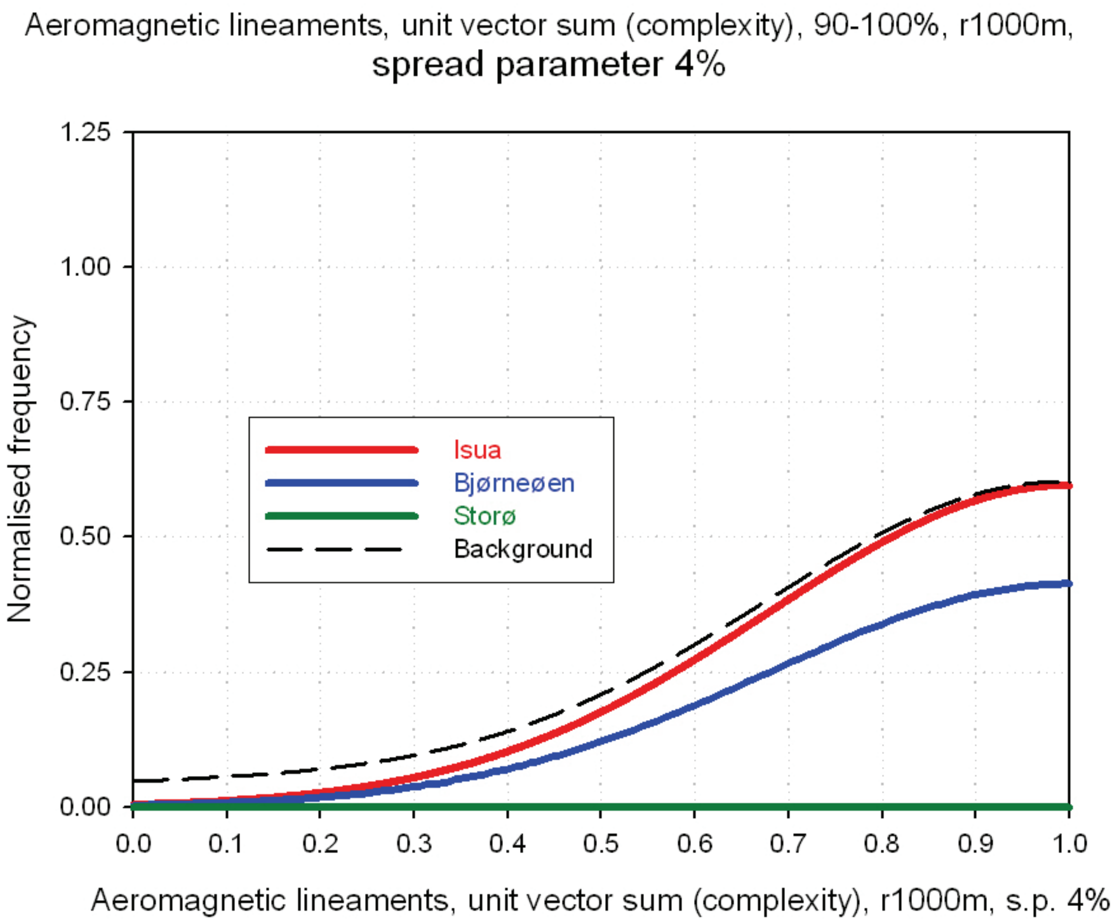
Aeromagnetic lineaments, unit vector sum (complexity), 90-100%, r1000m,
spread parameter 4%
Normalised frequency
1.25
1.00
0.75
0.50
0.25
0.00
Isua
Bjørneøen
Storø
Background
0.0
0.1
0.2
0.3
0.4
0.5
0.6
0.7
0.8
0.9
1.0
Aeromagnetic lineaments, unit vector sum (complexity), r1000m, s.p. 4%

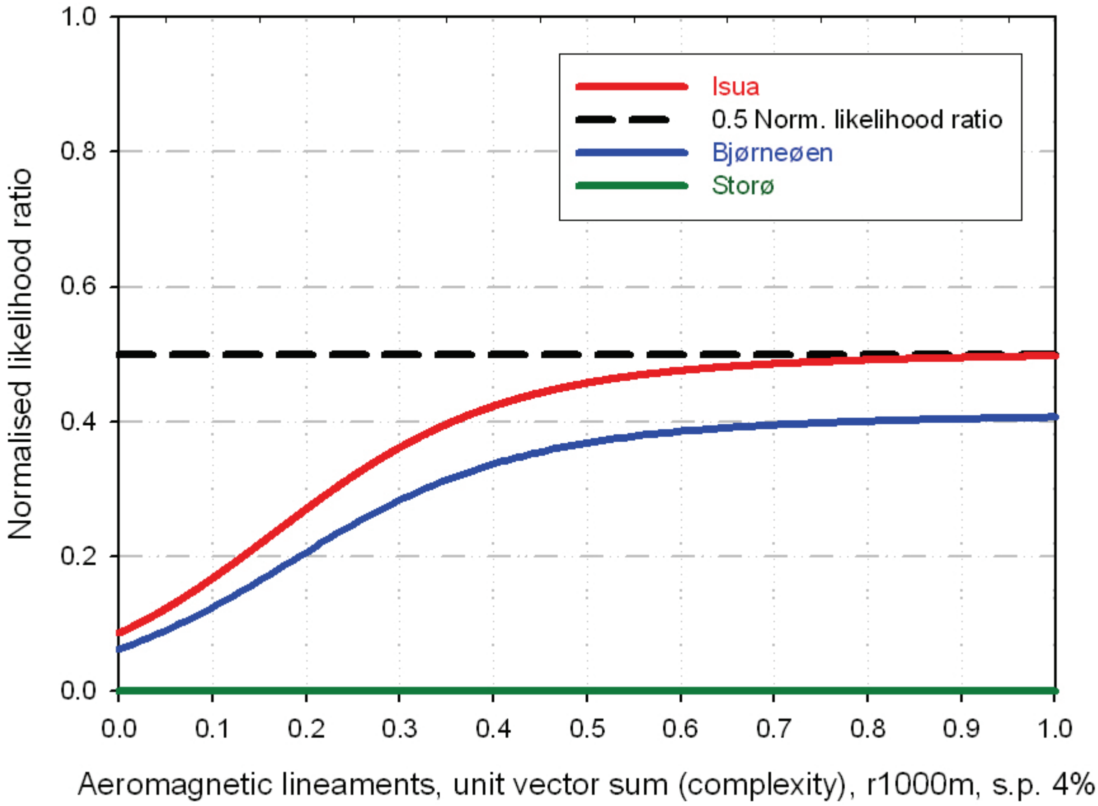
Normalised likelihood ratio
1.0
0.8
0.6
0.4
0.2
0.0
Isua
0.5 Norm. likelihood ratio
Bjørneøen
Storø
0.0
0.1
0.2
0.3
0.4
0.5
0.6
0.7
0.8
0.9
1.0
Aeromagnetic lineaments, unit vector sum (complexity), r1000m, s.p. 4%